THE UNIVERSITY
of EDINBURGH

Interference Mitigation Techniques for Optical Attocell Networks

Zhe Chen

A thesis submitted for the degree of Doctor of Philosophy.
The University of Edinburgh.
September 2016

Abstract

The amount of wireless data traffic has been increasing exponentially. This results in the shortage of radio frequency (RF) spectrum. In order to alleviate the looming spectrum crisis, visible light communication (VLC) has emerged as a supplement to RF techniques. VLC uses light emitting diodes (LEDs) for transmission and employs photodiodes (PDs) for detection. With the advancement of the LED technology, LEDs can now fulfil two functions at the same time: illumination and high-speed wireless communication. In a typical indoor scenario, each single light fixture can act as an access point (AP), and multiple light fixtures in a room can form a cellular wireless network. We refer to this type of networks as 'optical attocell network'. This thesis focuses on interference mitigation in optical attocell networks.

Firstly, the downlink inter-cell interference (ICI) model in optical attocell networks is investigated. The conventional ray-tracing channel model for non-line-of-sight (NLOS) path is studied. Although this model is accurate, it leads to time-consuming computer simulations. In order to reduce the computational complexity, a simplified channel model is proposed to accurately characterise NLOS ICI in optical attocell networks. Using the simplified model, the received signal-to-interference-plus-noise ratio (SINR) distribution in optical attocell networks can be derived in closed-form. This signifies that no Monte Carlo simulation is required to evaluate the user performance in optical attocell networks.

Then, with the knowledge of simplified channel model, interference mitigation techniques using angle diversity receivers (ADRs) are investigated in optical attocell networks. An ADR typically consists of multiple PDs with different orientations. By using proper signal combining schemes, ICI in optical attocell networks can be significantly mitigated. Also, a novel double-source cell configuration is proposed. This configuration can further mitigate ICI in optical attocell networks in conjunction with ADRs. Moreover, an analytical framework is proposed to evaluate the user performance in optical attocell networks with ADRs.

Finally, optical space division multiple access (SDMA) using angle diversity transmitters is proposed and investigated in optical attocell networks. Optical SDMA can exploit the available bandwidth resource in spatial dimension and mitigate ICI in optical attocell networks. Compared with optical time division multiple access (TDMA), optical SDMA can significantly improve the throughput of optical attocell networks. This improvement scales with the number of LED elements on each angle diversity transmitter. In addition, the upper bound and the lower bound of optical SDMA performance are derived analytically. These bounds can precisely evaluate the performance of optical SDMA systems. Furthermore, optical SDMA is shown to be robust against user position errors, and this makes optical SDMA suitable for practical implementations.

Declaration of originality

I hereby declare that the research recorded in this thesis and the thesis itself was composed and originated entirely by myself in the Department of Electronics and Electrical Engineering at The University of Edinburgh.

Zhe Chen

Acknowledgements

This thesis is dedicated to my family. Without them, this thesis won't have been possible. I would like to deliver my faithful love to my wife, Chen Li, for her support and patience. I would like to express my inexplicable gratitude to my parents, Qinging Liu and Jianci Chen, for their devotion and selfless care. My deepest gratitude belongs to my grandmother, Huifen Zhang, for her unconditioned love in the past 27 years.

I offer my sincerest gratitude to my supervisor, Professor Harald Haas, for his support, patience and valuable advice throughout my PhD. His enthusiasm for research and novel ideas have greatly inspired me.

My sincere thanks go to Dr. Tsonev and Dr. Basnayaka for their generous help and insightful comments.

Also, I would like to thank my colleagues in UPVLC project. Their support and encouragement helped me to go through all those difficulties.

Last but not least, I would like to thank my friends and colleagues in IDCOM. Their support and encouragement gave me wonderful experiences and precious memories.

Contents

List of figures

List of tables

Acronyms and abbreviations

ACO-OFDM	asymmetrically clipped optical orthogonal frequency division multiplexing
ADC	analogue-to-digital converter
ADR	angle diversity receiver
AM	amplitude modulation
AP	access point
APD	avalanche photodiode
ASE	area spectral efficiency
AWGN	additive white Gaussian noise
A/D	analogue-to-digital
BER	bit error ratio
CDF	cumulative distribution function
CPC	compound parabolic concentrator
CSI	channel state information
DAC	digital-to-analog converter
DC	direct current
DCO-OFDM	DC biased optical orthogonal frequency division multiplexing
DD	direct detection
DSL	digital subcarrier line
DSP	digital signal processor
D/A	digital-to-analogue
EGC	equal gain combining
EHF	extremely high frequency
EMI	electromagnetic interference
E/O	electrical-to-optical
FFR	fractional frequency reuse
FFT	fast Fourier transform
FM	frequency modulation
FOV	field-of-view
FPGA	field-programmable gate array

GSM	generalised spatial modulation
GSSK	generalised space shift keying
ICI	inter-cell interference
IEEE	Institute of Electrical and Electronics Engineers
IF	infrared radiation
IFFT	inverse fast Fourier transform
IM	intensity modulation
IM/DD	intensity modulation and direct detection
ISI	inter-symbol interference
LD	laser diode
LED	light-emitting diode
LOS	line-of-sight
MAC	medium access control
MIMO	multiple-input and multiple-output
ML	maximum likelihood
MRC	maximum ratio combining
NLOS	non-line-of-sight
OFDM	orthogonal frequency division multiplexing
OFDMA	orthogonal frequency division multiple access
OOK	on-off keying
OPC	optimum combining
OWC	optical wireless communications
O/E	optical-to-electrical
O-OFDM	optical orthogonal frequency division multiplexing
PAM	pulse width modulation
PD	photodiode
PDF	probability density function
PIN	p-intrinsic-n
PLC	power-line communication
PM	phase modulation
PPM	pulse position modulation
PSD	power spectral density
PWM	pulse width modulation
P/S	parallel-to-serial

QAM	quadrature amplitude modulation
RCLED	resonant-cavity light emitting diodes
RF	radio frequency
RGB	red-green-blue
RMS	root-mean-square
RR	round-robin
SBC	select best combining
SDMA	space division multiple access
SINR	signal-to-interference-plus-noise ratio
SNR	signal-to-noise ratio
SM	spatial modulation
SPAD	single-photon avalanche diode
SSK	space shift keying
S/P	serial-to-parallel
TDMA	time division multiple access
TIA	transimpedance amplifier
VNI	visual networking index
VL	visible light
VLC	visible light communications
VLCC	visible light communication consortium
WDM	wavelength-division multiplexing

Nomenclature

$*$	complex conjugate
$A_{\text{eff}}^{\text{bare}}$	effective signal collection area of a PD (considering incidence angle)
A_{eff}	effective signal collection area of a PD (without considering incidence angle)
A_{p}	physical area of a PD
α'	attenuation factor
α	tilted angle
ΔA	the area of the reflection surface element
b	index of the desired AP
$b_{\text{des}}^{(k)}$	the desire AP of user k
B	modulation bandwidth
B_{DC}	DC bias shift of DCO-OFDM
$\mathcal{B}_{\text{inter}}^{(b,k)}$	the set of interfering APs for user k according to the selected AP b
$\otimes$	mathematical convolution
τ	responsivity of a PD
$d_{q,\text{tx}}$	the distance between the optical transmitter and the q^{th} reflecting surface element
d_{e}	the distance between the actual position and the estimated position
$\text{E}[\cdot]$	statistical expectation operation
$f_{\gamma_{\text{dB}}}(\gamma_{\text{dB}})$	the PDF of SINR γ_{dB}
$f_{\text{I}}(\gamma_{\text{dB}})$	the PDF of SINR γ_{dB} in region I
$f_{\text{II}}(\gamma_{\text{dB}})$	the PDF of SINR γ_{dB} in region II
$f_{\text{overall}}(\gamma_{\text{dB}})$	the PDF of SINR γ_{dB} within the entire cell
$f_{\text{SBC}}(\gamma_{\text{dB}})$	the PDF of SINR γ_{dB} when SBC scheme is used
$F(\gamma)$	the CDF of SINR γ
$F(\gamma_{\text{dB}})$	the CDF of SINR γ_{dB}
$F_{\text{I}}(\gamma_{\text{dB}})$	the CDF of SINR γ_{dB} in region I
$F_{\text{II}}(\gamma_{\text{dB}})$	the CDF of SINR γ_{dB} in region II
$F_{\text{overall}}(\gamma_{\text{dB}})$	the CDF of SINR γ_{dB} within the entire cell
$F_{\text{SBC}}(\gamma_{\text{dB}})$	the CDF of SINR γ_{dB} when SBC scheme is used
$F_{\text{EGC,edge}}(\gamma_{\text{dB}})$	the CDF of SINR γ_{dB} at cell edge when EGC scheme is used

$F_{\mathrm{EGC,centre}}(\gamma_{\mathrm{dB}})$	the CDF of SINR γ_{dB} at cell centre when EGC scheme is used
$F_{\mathrm{MRC}}(\gamma_{\mathrm{dB}})$	the CDF of SINR γ_{dB} when MRC scheme is used
$F_{\mathrm{OPC}}(\gamma_{\mathrm{dB}})$	the CDF of SINR γ_{dB} when OPC scheme is used
$g(\psi)$	the concentrator gain corresponding to incidence angle ψ
$g_{\mathrm{h(opt)}}$	optical path gain
$\gamma_{(b,k)}$	the SINR of the user k that establish a link with its source AP b
γ_{min}	the minimum SINR
γ_{max}	the maximum SINR
γ_0	the user SINR at the cell centre ($r = 0$)
γ_{I}	the user SINR at the boundary of scenario I ($r = R_{\mathrm{I}}$)
$\gamma_{\mathrm{SBC}}(r)$	the SINR of a user when SBC scheme is used
$\gamma_{\mathrm{SBC,side}}(r)$	the SINR of a user when side PD is chosen.
$\gamma_{\mathrm{EGC,centre}}(r)$	the SINR of a user at cell centre when EGC scheme is used
$\gamma_{\mathrm{EGC,edge}}(r)$	the SINR of a user at cell edge when EGC scheme is used
$\gamma_{\mathrm{MRC}}(r)$	the SINR of a user when MRC scheme is used
$\gamma_{\mathrm{OPC}}(r)$	the SINR of a user when OPC scheme is used
$\gamma_{\mathrm{0,SBC}}$	the user SINR at the cell centre when SBC scheme is used
$\gamma_{\mathrm{II,SBC}}$	the user SINR at the boundary of scenario I when SBC scheme is used
$\gamma_{\mathrm{0,EGC}}$	the user SINR at the cell centre when EGC scheme
$\gamma_{\mathrm{I,EGC}}$	the user SINR at the boundary of scenario I when EGC scheme is used
$I_{k,c}$	the index of the source LED element for active user k
Γ	SINR distribution of active users
$h(t)$	channel response
h	the height of a room
H	channel gain
H_{overall}	the overall DC gain
$H_{\mathrm{2nd_reflection}}$	the DC gain of second order reflection NLOS link
H_{pos}	the channel gain between the positive AP and the optical receiver
H_{neg}	the channel gain between the negative AP and the optical receiver
ΔH	the difference between H_{pos} and H_{neg}
H_{s}	channel gain between reflector S and point O
H'_{s}	channel gain between reflector S and point W
$H_{\mathrm{s}'}$	channel gain between reflector S' and point O
$H'_{\mathrm{s}'}$	channel gain between reflector S' and point W

H_{src}	the channel gain from source AP to an optical receiver
H_{inter}	the channel gain from interfering AP to an optical receiver
$H_{a,p}$	the channel gain between the AP a and the PD p
i	the index of the optical APs in the vicinity
I	the total number of maximum light reflections taken into account in a propagation model
I_{PD}	generated photocurrent at a wavelength λ
$I_{0,h}$	the intensity density of the reflected light on point O
$I_{r,h}$	the intensity density of an arbitrary point on the ceiling
$\mathcal{I}_{\mathrm{NLOS}}$	the total electrical power of NLOS interference
$\mathbf{I}$	identity matrix
k_{B}	Boltzmann's constant
k_{o}	the index of time domain signal
k	the index of an active user
K	the total number of active users
$L_{1,p}$	the first part of NLOS path
$L_{i,p}$	the second part of NLOS path
L_{d}	the distnace between the cell centre and the AP
λ	wavelength of light
λ_{min}	the minimum wavelength of incident light
λ_{max}	the maximum wavelength of incident light
l_{o}	the index of input bit
l_{s}	the horizontal distance between cell centre O and a reflector S
m	Lambertian index
m_{o}	the index of OFDM subcarrier
M	the number of PDs on an ADR
n_{ref}	refractive index
N	the total number of LED elements on an angle diversity transmitter
N_0	noise spectral density
N_{shot}	one-sided PSD of shot noise spectral density
N_{thermal}	thermal noise spectral density
$\bar{N}_{\mathrm{a}}$	the average number of the active LED elements
$N(t)$	instantaneous noise signal
$n(k_{\mathrm{o}})$	AWGN noise from receiver front-ends

Ω_{TDMA}	the spectral efficiency of the optical TDMA
$\bar{\Omega}_{\mathrm{SDMA}}$	the average spectral efficiency of the optical SDMA
$\bar{\Omega}_{\mathrm{SDMA,est}}$	the estimated average spectral efficiency of the optical SDMA
$\bar{\Omega}_{\mathrm{single}}$	the average spectral efficiency of only a single LED element
$\Omega_{\mathrm{downward}}$	the spectral efficiency of the downward LED element
$\bar{\Omega}_{\mathrm{downward}}$	the average spectral efficiency of the downward LED element
Ω_{LB}	the lower bound of the average spectral efficiency in an optical cell
Ω_{UB}	the upper bound of the average spectral efficiency in an optical cell
P_{tx}	optical power from an transmitter
P_{rx}	the received power of information signal
$P(\lambda)$	optical light power at a wavelength λ
$\bar{P}_{\mathrm{am}}$	the average received power of ambient light
$P(\Gamma < \gamma)$	the probability of SINR distribution Γ is less than γ
P_{oe}	the probability that a neighbouring LED element is occupied
P_0	the probability that no LED element is occupied
φ_{A}	azimuth angle
ϕ	irradiance angle
Φ_{tx}	transmitter semi-angle at half power
Φ_{ref}	reflecting material emission semi-angle at half power
q_{elec}	the charge of one electron
Q	the total number of reflecting elements
r	the horizontal distance between an active user and cell centre
r'	horizontal distance between point W and point O
R	responsivity of a PD
R_0	radiant intensity
R_{TIA}	TIA resistor
R_1	the radius of the desired cell
R_{I}	the radius of region I
R_{II}	the radius of region II
R_{cell}	the radius of an optical cell
$\mathbf{R}_{nn}$	interference-plus-noise correlation matrix
$\mathrm{rect}(\cdot)$	rectangular function
ρ	the reflectivity of a reflecting material
ρ_p	the reflectivity of the reflecting element p
ρ_q	the reflectivity of the reflecting element q

ρ_{floor}	the reflectivity of floor
ρ_{ceiling}	the reflectivity of ceiling
s_k	the index of the PD of user k
$s_{k,\text{los}}$	the index of the PD that can establish LOS link with the source AP
S'	a reflector
$S_{\text{inst}}(t)$	instantaneous input optical power
S_{sum}	the received optical power from positive and negative AP
S_{wall}	the area of wall
SNR_{elec}	electrical SNR
ψ	incidence angle
Ψ_{fov}	the FOV of an optical receiver (concentrator)
σ_{e}	the standard variance of the position error
$T_{\text{s}}(\psi)$	is the signal transmission of an optical filter corresponding to incidence angle ψ
T_{K}	device temperature in Kelvin
$\bar{S}$	average input optical power
$\mathbf{u}_{\text{src}}^{b}$	the signal received from the source AP b
$\mathbf{u}_{\text{b}'}$	the set of interference signals
w_p	the weight of the PD p
$\mathbf{w}$	a vector which contains the different weight factors
x	the coordinates on x-axis of an active user
θ_{P}	polar angle
y	the coordinates on y-axis of an active user
$Y(t)$	instantaneous output current
η	throughput gain
z	represents the number of LED elements that is not occupied
ζ	user density

$(x_{\text{tx}}, y_{\text{tx}}, h)$	the coordinates of an optical transmitter in a reflection model
$(0, y_{\text{w}}, z_{\text{w}})$	the coordinates of a point on the wall in a reflection model
$(x_{\text{rx}}, y_{\text{rx}}, 0)$	the coordinates of an optical receiver in a reflection model
(x_c, y_c, h)	the coordinates of an angle diversity transmitter

Chapter 1
Introduction

1.1 Motivation

In recent years, the emergence of mobile devices such as smart phones has dramatically changed our daily life. These devices enables a wide range of multimedia services which require high speed data transmission. As the number of mobile devices increases, the amount of wireless data traffic increases accordingly and it exhibits an exponential growth. For instance, the latest data provided by Cisco shows that overall mobile data traffic is expected to reach 24.3 exabytes per month by 2019 [2]. In order to fulfil the growing data demand, advanced techniques such as multiple-input multiple-output (MIMO) [3–11], and orthogonal frequency division multiplexing (OFDM) [12–18] have been developed for radio frequency (RF). Although these techniques effectively exploit the RF communication capacity, it is predicted that the increasing demand in mobile communication cannot be satisfied [19].

The deficiency of spectrum resource is a key factor that limits the capacity of wireless communication. Contemporary wireless communication exhaustively exploits the RF spectrum in the range up to 10 GHz. In an attempt to alleviate the looming spectrum crunch, the unregulated parts of the electromagnetic spectrum are explored to expend communication bandwidth.

Recently, researchers focus on the spectrum ranging from 30-300 GHz [20–23]. This region is referred to as the extremely high frequency (EHF) or millimetre wave band with wavelength ranging from 1 to 10 mm. Millimetre-wave communication is very promising due to its relatively high availability. Some millimetre-wave communication systems managed to achieve multi-gigabit data rate [24, 25]. However, millimetre-wave communication operates at very high frequency band. This means that the design of front-end device for millimetre-wave communication is challenging.

Infrared radiation (IR) is also studied for high speed communication in addition to the conventional RF spectrum [1, 26–29]. Infrared emitters and detectors are capable of high speed transmission and their cost is considerably low. IR cannot penetrate opaque objects which means that the co-channel interference between different rooms separated by opaque walls is zero. This makes the IR favourable for short-range implementations [30–34]. However, high speed Infrared transmission requires relatively high transmit power which is strictly limited by eye-safety regulation.

According to the DIN 5031 standard, the wavelength of the visible radiation spectrum is between 400 nm and 800 nm. This spectrum can be perceived by human eyes and it is commonly

referred to as visible light spectrum. We refer to the communication using visible light spectrum as visible light communication (VLC). The total usable bandwidth in VLC is about 375 THz which is more than 3000 times higher than the RF spectrum below 10 GHz [55]. With the development of light emitting diode (LED) technology, LEDs can now fulfil two functions at the same time: illumination and high speed wireless data communication. This means that VLC enables the transformation of conventional lighting infrastructures into high speed wireless networks. The advantages of VLC are as follows: a) compared with RF, VLC operates in an unregulated part of the electromagnetic spectrum; b) since visible light (VL) cannot penetrate walls, VLC can transmit wireless data more securely within a confined area; c) VLC is intrinsically safe to use in electromagnetic interference (EMI) sensitive environments [35–38], such as aircraft, hospitals and oil refineries.

In terms of point-to-point link, VLC shows a great potential to achieve high transmission speeds. Khalid *et al.* demonstrated a 1 Gb/s link over a commercial white phosphor-coated LED [39]. A breakthrough in optical wireless transmission speed is reported in [40]. A data rate of 3 Gb/s is achieved with the use of 50-μm Gallium Nitride μLED. Recently, μLED-based VLC system is demonstrated to provide a data rate of over 10 Gb/s with the use of wavelength division multiplexing [41].

Apart from exploring unregulated communication spectrum, dense spectrum reuse can further boost the area spectral density. If a single transmitter serves a large number of users in a multi-user system, high transmission power is required. This is because the users far from the desired transmitter experience significant signal attenuation. Hence, this type of system is not energy efficient. Instead of using a single transmitter with high power, several low-power transmitters in a cellular configuration are used to serve different users. These low-power transmitters are deployed in different locations and are named access points (APs). Compared with a single transmitter system, this type of configuration can provide much higher power efficiency and expand the system bandwidth by efficient frequency reuse [42–46].

The most effective way of improving the performance of cellular networks is to reduce the inter-site distance between each AP in the system. In the past 25 years, the network spectral efficiency of cellular systems has increased by two orders of magnitude. The concept of heterogeneous networks has been introduced [47–51]. A typical heterogeneous network consists of different cell layers such as microcells, picocells and femtocells. The deployment of femtocells enables intensive frequency reuse which provides higher mobile data capacity. However, such

cell configuration will introduce new intra-cell and intercell interference. This means the cell size of femtocells is restricted to avoid compromising frequency reuse gain.

Using VLC can further reduce the cell size. Compared with RF, LEDs with limited transmission angle are much easier to be designed which provide illumination within more confined regions [52–54]. Due to the confined coverage of LEDs, an optical cell has a smaller size than a RF cell. An optical cellular network facilitates higher frequency reuse and, therefore, higher data density than small-cell RF wireless networks. In 2013, Haas put forward the concept of LiFi networks in [55]. This type of network can be developed based on the existing lighting infrastructures. Multiple light fixtures in a room function as optical APs. Haas referred to this type of network as *optical attocell network* [55]. In [56], optical attocell networks show a significant improvement when compared with RF femtocell. Nearly three orders of magnitude area spectral efficiency (ASE) improvement has been achieved in a $5 \times 2.5 \times 3$ m office.

In order to fulfil illumination requirements, light fixtures are usually placed close to each other. This type of deployment can achieve high spectral efficiency by dense spatial reuse. However, when optical APs are too close to each other and transmit independent signals, inter-cell interference (ICI) at cell edge is inevitable. This limits the performance of optical attocell networks. In terms of the ICI mitigation, the existing methods are based on the coordination of light signals from neighbouring APs. In [57–59], different ICI mitigation methods are put forward such as, the busy burst approach, joint transmission and fractional frequency reuse (FFR). Based on scheduling information, ICI can be effectively mitigated, especially at the cell edge.

In this thesis, in order to have a insightful understanding of ICI in optical attocell networks, the channel modelling of ICI is studied. Conventional ray-tracing model requires a huge amount of computational resource since it considers high order light reflections in optical attocell networks. Also, in the conventional ray-tracing model, light reflecting surfaces are split into small light reflectors. The calculation of non-line-of-sight (NLOS) channels using these small light reflectors are time-consuming. Hence, in order to reduce the computational complexity, a simplified model is proposed to estimate NLOS ICI in optical attocell networks.

Inspired by compound eyes of insects, the concept of angular diversity has been implemented in the design of optical receivers in VLC. A typical angle diversity receiver (ADR) consists of multiple photodiodes (PDs) pointing to different directions. It can precisely capture the desired light signals without losing coverage. This feature is favourable in optical attocell networks,

since it can be used to eliminate the interference from other cells. Hence, ADRs are proposed in optical attocell networks and different signal combining schemes are considered and evaluated.

The multiple access scheme, space division multiple access (SDMA), is favourable since APs with more concentrated beams introduce less ICI. Also, SDMA facilitates spatial reuse within cells which can further improve data density. In RF, directional narrow beams are generated by carefully changing the amplitude and phase of the signals transmitted by an antenna array. In comparison, a LED has an inherent feature of confined field-of-view (FOV). This characteristic facilitates the generation of directional light beams. Therefore, optical SDMA using angle diversity transmitters is proposed and evaluated in optical attocell networks.

1.2 Contribution

This thesis focuses on characterising and mitigating ICI in optical attocell networks. A simplified ICI model, novel ICI mitigation schemes and an advanced multiple access scheme that can mitigate ICI are proposed and analysed both numerically and theoretically. The accuracy of the theoretical models is validated by Monte Carlo simulations.

Firstly, a simplified model is proposed by only considering second-order light reflections. A new method of evaluating NLOS reflections is also introduced in the simplified model. With the use of the simplified model, the signal-to-interference-plus-noise ratio (SINR) distribution of indoor optical attocell networks can be derived analytically in closed-form. Results show that the simplified model has a close match with the conventional NLOS ray-tracing model. The simplified model can be applied to different scenarios, such as optical attocell networks using angle diversity receivers and angle diversity transmitters. Part of the work on the simplified model led to the publication of [60].

With the knowledge of ICI modelling, interference mitigation techniques using ADRs are investigated in optical attocell networks. Four signal combining schemes are considered for ADRs: select best combining (SBC), equal gain combining (EGC), maximum ratio combining (MRC) and optimum combining (OPC). Also, a novel double-source cell configuration which exploits the benefit of ADRs is proposed. In specific, to the best of the author's knowledge, OPC is firstly proposed in an VLC system. Results show that an ADR can greatly improve the system performance in comparison with a single-PD receiver. Also, when double-source cell configuration is implemented, additional improvement can be obtained. A criteria for selecting transmission

mode is proposed for double-source cell configuration. Furthermore, an analytical framework is proposed for analysing optical attocell networks using ADRs. Analytical models for different scenarios including line-of-sight (LOS) and NLOS propagation are derived and the accuracy of the models has been validated by Monte Carlo simulations. The work conducted on ADRs and double-source cell configuration has led to the publication of [61–63].

Another method to mitigate ICI in optical attocell networks is optical SDMA with angle diversity transmitters. In this work, optical SDMA is realised by using angle diversity transmitters. The results show that optical SDMA significantly outperforms optical time division multiple access (TDMA) in terms of ASE. It is found that this improvement scales with the number of elements on each angle diversity transmitter. In addition, the upper and lower bound of the performance of optical SDMA is derived analytically. These bounds can be used to estimate the performance of SDMA systems. The study is also extended to consider the user position errors. Monte-Carlo simulations show that the system is robust to user position errors. This means optical SDMA is practical to implement. Part of the work conducted on optical SDMA using angle diversity transmitters has led to the publication of [64, 65].

1.3 Thesis Layout

The rest of the thesis is organised as follows. Chapter 2 introduces the fundamental knowledge of front-end VLC system and the concepts of optical attocell networks.

Chapter 3 investigates the downlink modelling of NLOS interference. The proposed simplified ICI model is introduced in detail. The accuracy of the model is evaluated numerically and theoretically.

Chapter 4 investigates the interference mitigation techniques using an ADR in optical attocell networks. Firstly, the principle of four signal combination schemes are introduced. Also, a novel double-source cell configuration is proposed for ADRs. Furthermore, an analytical framework is put forward to analyse optical attocell networks using ADRs. Analytical models for different scenarios including LOS and NLOS propagation are derived and the accuracy of the models has been validated by Monte Carlo simulations.

Chapter 5 proposes a new multiple access scheme, optical SDMA, in optical attocell networks. Optical SDMA is realised by using angle diversity transmitters. In addition, the upper and

lower bound of the performance of SDMA system are derived analytically. Finally, the study is extended by considering the user position errors.

Chapter 6 summaries the key results of this thesis. Some conclusions are derived based on these results. Moreover, limitations and future work are listed in this chapter.

1.4 Summary

The VLC spectrum is three orders of magnitude larger than the entire RF spectrum. This is very promising to solve the shortage of communication spectrum in RF. Since LEDs have a confined coverage area, they are very suitable for implementing in small cell wireless networks. By exploiting the existing visible light infrastructure, optical attocell networks can provide high data density. This thesis provides insight into ICI mitigation techniques in optical attocell networks. In this chapter, motivation, main contributions and the outline of this thesis are listed.

Chapter 2
Background

2.1 Introduction

The need for communication between one person to another never stops. When people are close to each other, voice and gestures are used to exchange information which leads to the emergence of language. When the distance between people becomes longer, voice and gestures are no longer capable of conveying messages. Then, visible light becomes a competitive candidate to send messages [66]. The use of sunlight, fire and smoke signalling can be dated back to two thousand years ago. For example, in ancient Greece, warriors used their polished shields to reflect sunlight to signal in the battlefield. Also, according to Roman records, polished metal plates were used to transmit signals to a distant place by reflecting sunlight. In China, fire beacons were built on the Great Wall in order to indicate the invasion of enemies. Similarly, Romans and American Indians used smoke to signal their presence in hostile territory [67]. Before recent decades, lighthouses had been the first choice for the ships near shore to avoid potential threat.

In early 19th century, a wireless solar telegraph named 'heliograph' was equipped in US military. Heliograph uses the flashes of reflected sunlight to send Morse code. These signals are generated by momentarily spinning the mirror, or by deliberately shielding the beam with a specifically designed shutter. Also, signal lamps were often used in the navy to send visual signals to other ships typically in the format of Morse code. The earliest example of advanced visible light communication (VLC) technology was put forward and demonstrated by Alexander Graham Bell. This demonstration is named 'photophone' which uses reflected sunlight on a vibrating mirror and a selenium photo cell to transmit voice via a visible light beam [68].

The invention of laser and laser diodes stimulated the development of optical communication [69, 70]. In 1970s, low loss optical fibres were developed as a medium for transmitting information using laser. Also, optical fibre amplifiers and in-fibre Bragg gratings were invented in 1980s and 1990s. These inventions are the basis of the current high-speed infrastructures of Internet. The development of optical fibre technology results in the advancement in optical front-end elements, such as light emitting diode (LED)s, laser diodes, p-intrinsic-n (PIN) diodes and avalanche photodiode (APD) etc. These components have attracted researchers to consider optical communication in wireless aspect which leads to the modern VLC.

The first optical wireless system was proposed by Gfeller and Bapst in 1979 [71]. In this work, both line-of-sight (LOS) and diffusive optical channels were studied and transmission

speeds up to 1 Mbps was proved to be feasible if optical transmission power was sufficient. Since that work, a lot of following studies have been performed which gives a deeper understanding of VLC systems [1, 31, 72, 73]. An VLC system implementing white LED was proposed by Komine and Nakagawa [74, 75]. LEDs in this VLC system are directly linked together by the mains-power cable and the data exchange between them is realised by power-line communication (PLC). In the recent years, high speed demonstrations using LEDs have been developed. A μLED-based VLC demonstration can provide a data rate of over 10 Gb/s [41] by using wavelength division multiplexing. This significant transmission speed improvement shows a great potential in VLC technology. In 2013, Haas put forward the concept of optical attocell network in [55]. Since then, a lot of researches have been conducted on optical attocell networks [56–59, 76, 77]. The results show that an optical attocell network can achieve three orders of magnitude system performance improvement when compared with radio frequency (RF) femtocell. The standardisation of VLC was first driven by Visible Light Communication Consortium (VLCC) in Japan [78]. In 2011, an Institute of Electrical and Electronics Engineers (IEEE) standard 802.15.7 "IEEE standard for Local and Metropolitan Area Networks, Part 15.7: Short-Range Wireless Optical Communication Using Visible Light" was introduced [79]. In 2014, IEEE P802.15.7r1 task group was formed to write a revision to IEEE 802.15.7-2011 [80]. A number of VLC options are proposed in the revision which includes: a) optical camera communications which use the flash lights, displays and image sensors as front-end devices; b) LED-ID which use LEDs for identification purpose; c) LiFi which is high-speed, bidirectional wireless network using visible light.

2.2 VLC Links

The fundamental concepts of the VLC links are discussed in this section, which includes the classification of VLC links, channel characteristic of front-end components, source of noise, propagation model and modulation schemes.

2.2.1 The Design of VLC Links

The classification of VLC links is illustrated in Figure 2.1. There are two criteria to classify VLC links [1]. The first one depends on the degree of directionality of transmitters and receivers. Following this criteria, there are three types of links, directed links, nondirected links

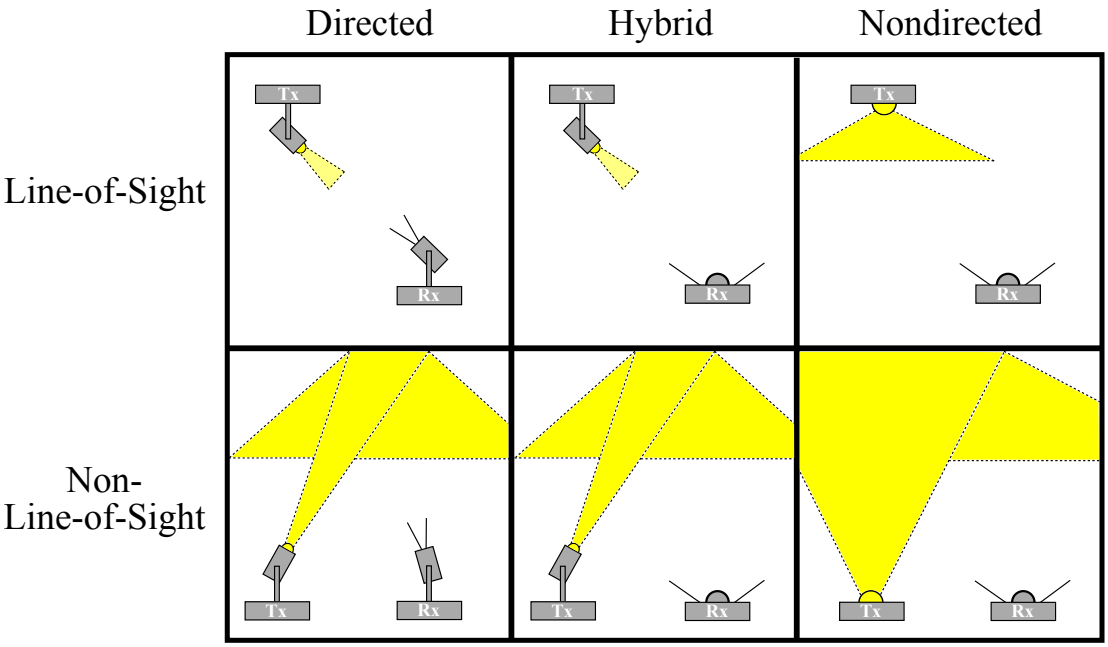

Figure 2.1: *Classification of VLC links [1].*

and hybrid links. In a directed link, transmitters and receivers are highly directional. This means the alignment between transmitters and receivers is important to ensure link quality. Such links are very useful when high speed or energy efficient transmission is required. In a nondirected link, the half power semi-angle of transmitters and the field-of-view (FOV) of receivers are wide. This means precise calibration is not necessary. This type of links is very suitable to systems that require ubiquitous coverage and mobility. Hybrid link is the combination of the directed link and nondirected link. In this system, transmitters and receivers are of different degrees of directionality. This type of links is very useful when a system requires the trade-off between transmission speed and mobility.

The second criteria to classify VLC links is the way of establishing data transmission between transmitters and receivers. According to this criteria, there are two types of links, LOS links and non-line-of-sight (NLOS) links. LOS means that there is a continuous signal path between a transmitter and a receiver without blocking by opaque objects. In the NLOS case, light signals from a transmitter require one or multiple reflections to reach a receiver. On the one hand, the use of LOS links can maximise the received signal-to-noise ratio (SNR) while minimising the effect of multi-path distortion. On the other hand, NLOS link design is robust to the blockage by opaque objects, which is suitable to fulfil the requirement of ubiquitous coverage.

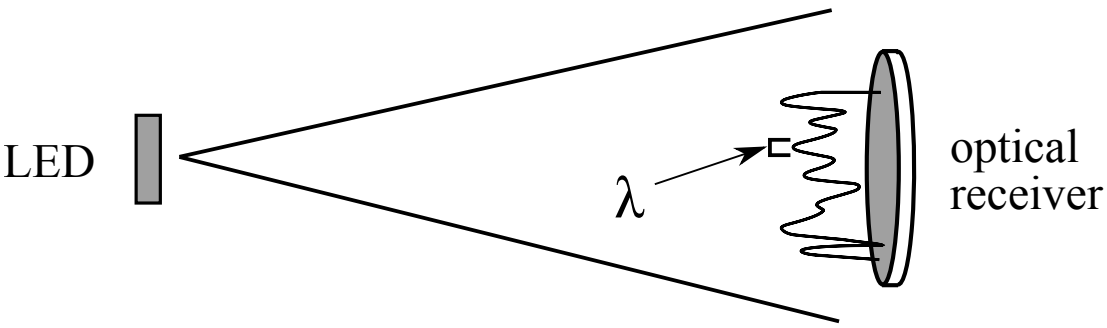

Figure 2.2: *A VLC IM/DD link. The wavelength of visible light is denoted as λ.*

2.2.2 IM/DD (Intensity Modulation/Direct Detection) Channels

In RF wireless system, modulation techniques include the coherent modulation of amplitude, phase and frequency and also the combination of them [81–84]. An RF receiver usually consists of one or more antennas and the received signals are down-converted by heterodyne or homodyne detection techniques. This involves the use of local oscillator and a mixer. The voltage of the output electrical signals is linear with the amplitude of the received carrier electric field.

Unlike RF, conventional light sources, including LEDs, are incoherent sources. This means that these sources cannot generate a beam of photons with the same frequency and constant phase difference. This is because, in a incoherent light source, the transitions between energy levels in an atom is a completely random process and there is no control over when an atom will lose energy in the form of radiation. In a typical VLC system, since LEDs are incoherent light source, it is difficult to capture a stable carrier. Therefore, optical receivers for coherent detection cannot be used. Hence, intensity modulation (IM) is a preferable modulation technique in VLC. IM is a form of modulation that the instantaneous power of the carrier is in accordance with the waveform of modulating signals. In order to capture IM signals, a practical detection technique named direct detection (DD), is used. In DD, a photodiode (PD) proportionally converts the received instantaneous optical power to a current.

In RF, the magnitude and phase of received signals exhibit spatial variation. This is referred to as fading. Since the length of RF antennas is usually smaller than the wavelength of received signal, the variation of fading is often modelled as a random process. In VLC, as the width and length of an photodetector are much longer than visible light wavelength, the variant fading

within an optical receiver can be averaged (see in Figure 2.2). Therefore, in VLC, channel fading is usually deterministic.

Based on a typical intensity modulation and direct detection (IM/DD) baseband channel model [1], the instantaneous output current of a PD is:

$$Y(t) = RS_{\text{inst}}(t) \otimes h(t) + N(t), \tag{2.1}$$

where $\otimes$ denotes mathematical convolution; $S_{\text{inst}}(t)$ represents the instantaneous optical power; R represents the responsivity of a PD; $h(t)$ is the channel impulse response; $N(t)$ represents the instantaneous noise signal. Since $S_{\text{inst}}(t)$ is instantaneous optical power, it cannot be negative:

$$S_{\text{inst}}(t) \geq 0. \tag{2.2}$$

The optical power in this thesis is defined as the variance of optical power at a transmitter end. Hence, the optical power P_{tx} is given by:

$$P_{\text{tx}} = \lim_{T\to\infty} \sqrt{\frac{1}{2T}\int_{-T}^{T} (S(t) - \bar{S})^2 \mathrm{d}t}, \tag{2.3}$$

where $\bar{S}$ is given by:

$$\bar{S} = \lim_{T\to\infty} \frac{1}{2T}\int_{-T}^{T} S(t)\mathrm{d}t. \tag{2.4}$$

With this definition, the transmitted optical power also depends on the modulation format of the symbol.

Also, the received electrical SNR of the baseband channel can be represented as:

$$\gamma = \frac{\left(RP_{\text{tx}}H\right)^2}{N_0 B}. \tag{2.5}$$

where H is channel direct current (DC) gain

$$H = \int_{-\infty}^{\infty} h(t)\mathrm{d}t \tag{2.6}$$

and B is the modulation bandwidth and N_0 is the noise spectral density. Here, it is assumed that thermal noise is the dominant noise in the system. The detailed discussion of other form of noise is presented later in Sec.2.2.4. Also, it can be observed from (2.5) and (2.3) that SNR of

the system varies with different modulation techniques. For example, if the modulation index of a VLC system is defined as I_{mod}, $S(t)$ will be:

$$S(t) = I_{\mathrm{mod}} S_{\mathrm{AC}}(t) + S_{\mathrm{DC}}, \tag{2.7}$$

where $S_{\mathrm{AC}}(t)$ is the AC component and S_{DC} is the DC component. Then, (2.3) can be rewritten as:

$$P_{\mathrm{tx}} = I_{\mathrm{mod}} \lim_{T\to\infty} \sqrt{\frac{1}{2T}\int_{-T}^{T} \big(S_{\mathrm{AC}}(t)\big)^2 \mathrm{d}t}. \tag{2.8}$$

It can be observed that P_{tx} is proportional to I_{mod}. Also, according to (2.6), γ is proportional to I_{mod}^2.

In this thesis, it is also assumed that the symbol duration of the system is much longer than the duration of channel impulse response. Hence, the performance of VLC system is characterised on the basis of channel DC gain instead of time-dispersive channel gain.

2.2.3 Optical Front-end Elements

Figure 2.3 illustrates a typical transmission link of VLC. All necessary front-end elements are demonstrated and they can be categorised as transmitter front-end and receiver front-end.

2.2.3.1 Transmitter Front-end

As illustrated in Figure 2.3, a transmitter front-end usually consists of a digital signal processor (DSP) and a digital-to-analog converter (DAC). The function of a DSP is to convert input information bits into digital signals. In practice, this work can be accomplished through a field-programmable gate array (FPGA). The obtained digital signals are then fed into DAC, which ends up with analogue current signals. Recently, a design of an energy efficient high-speed DAC for driving LED is presented in [85]. This design achieves 1 Gb/s sampling rate with a electrical efficiency of 67%. After the DAC, analogue current signals are forward to the light source. Currents signals are converted into optical light of different intensity.

In a VLC system, LEDs are commonly used as optical sources. In particular, a LED is the most favourable transmitter front-end since it is widely used for the purpose of illumination [78, 86–89]. Depending on the material and techniques of fabrication, LEDs have different

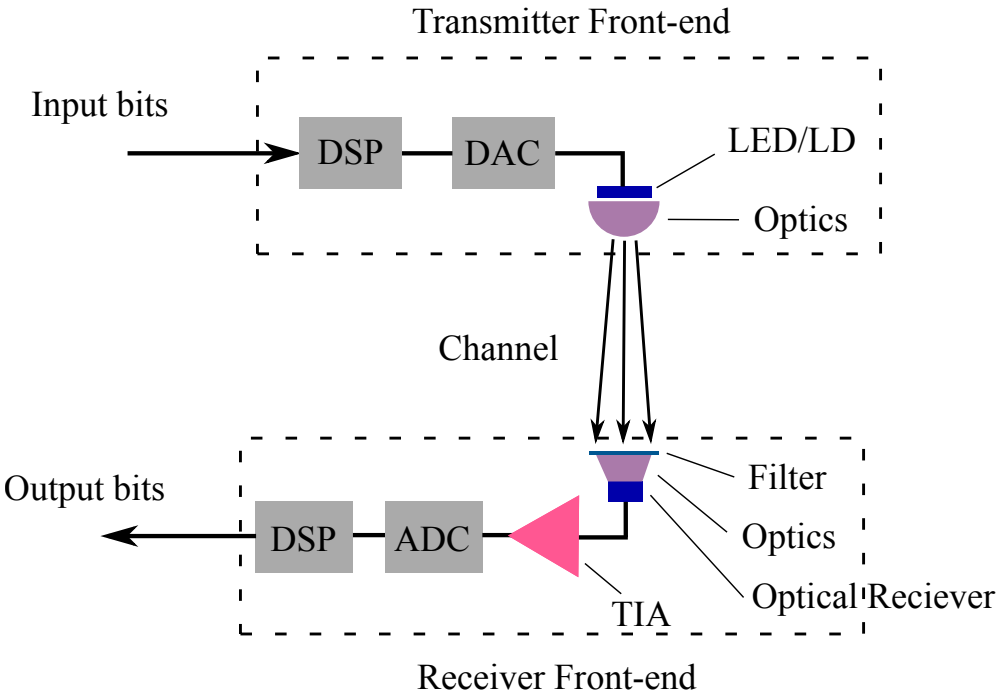

Figure 2.3: *A typical VLC transmission link. The commonly used front-end devices of the transmitters and receivers are presented.*

colours and power efficiencies. In general, there are two types of commercial white LEDs. The first type is red-green-blue (RGB) LED. This LED yields white optical light by blending three colour components which are generated by different set of devices [40, 90]. The other type of LEDs that can generate white light is a blue LED chip covered by a yellow-phosphor coating. The emission of narrow blue spectrum can be absorbed and efficiently re-emitted by phosphor coating. The emitted light has a wide emission profile across the entire visible light spectrum [39, 40]. The limiting factor of using this type of LEDs is that the absorption and re-emission time of phosphor is slow. Therefore, the 3-dB bandwidth of these LEDs is about 2 MHz [40, 91]. In order to expand the modulation bandwidth, a blue filter is used to remove the slow signal components from phosphor. As a result, the 3-dB modulation bandwidth up to 20 MHz has been obtained using phosphor-coated commercial LED [39, 91]. Carrier lifetime and innate junction capacitance are the most important factors that limits the modulation speed of the LED [40, 92–94]. The lifetime of the carrier can be decreased by increasing the current density within the junction. The most efficient way of increasing the current density is to reduce the size of a LED. To this end, a Gallium Nitride based LED, named μLED, is designed which can provide a modulation bandwidth over 400 MHz [92]. Also, based on μLED, a

demonstration is designed which reaches a data rate over 1 Gb/s [95]. A drawback of μLED is that, the current efficiency drops when the current density increases. This is due to the issue of heat generation [96]. When current level is high, extra current input will generate more heat instead of optical output.

In general, the emission from an optical transmitter can be modelled as a Lambertian pattern. The radiant intensity using a generalised Lambertian model is given as [1]:

$$R_0 = \frac{(m+1)}{2\pi} \cos^m \phi, \tag{2.9}$$

where R_0 is the radiant intensity; ϕ is the irradiance angle; m is the Lambertian index which can be represented as:

$$m = -\frac{\ln 2}{\ln(\cos \Phi_{\mathrm{tx}})}, \tag{2.10}$$

where Φ_{tx} is the transmitter semi-angle at half power. By changing Φ_{tx}, the radiant pattern can be changed.

2.2.3.2 Receiver Front-end

At the receiver end, the received light signals are converted to the electric signals with the use of optical detectors. A number of devices can be used as optical detectors, such as imaging sensors [97–99], solar cell panels [100–102] and also LEDs [103, 104]. These devices can work under different circumstances in various applications. However, the long response time of these devices significantly restricts their communication bandwidth. Therefore, in order to realise high-speed VLC, PDs are preferable since they can provide wider communication bandwidth [78, 105].

In general, PDs are classified into three types according to their operation mode. The first type is PIN diode. A PIN diode consists of a wide undoped intrinsic semiconductor region between a positive-type semiconductor and an negative-type semiconductor region. With proper reverse bias, a PIN diode can exploit the energy from the electron and hole pairs created by photons. The current generated by PIN diode is approximately linear to the energy of received photons. The second type of PD is APD. APD is a specially designed PD which applies a high reverse bias (typically 20-200 V). Due to the avalanche effect, more than 100 internal current gain can be achieved. This feature makes an APD very suitable to the environment that light intensity is expected to be low. Although an APD can achieve a high current gain, it is very vulnerable to

ambient shot noise as well as the internal excess noise, which is introduced in the multiplication process [1]. Multiplication process means the multiplication of the number of initial, optically generated charge carriers in APD. This process amplifies photocurrent in APD. The light energy captured by an APD increases when the area of a device increases. However, the transit times of the device also scales with its area. This means that there is always a trade-off between the received energy and receiver bandwidth. The third type of PD is single-photon avalanche diode (SPAD). Similar to APD, SPAD exploit the avalanche effect of a reverse biasing of p-n junction. Unlike APD, the reverse bias of a SPAD is designed to be well above the breakdown voltage of an p-n junction. This operation is named as Geiger mode which can achieve a gain up to 10^6 [106, 107]. The gain of a SPAD is so high that even a single photon can trigger a current pulse. The intensity of a SPAD output signal is acquired by counting the number of pulses within a measurement time slot. Since the gain of a SPAD is very high, it is preferable to be used in the environment of extremely low light levels. However, there are two limitation restricting the use of a SPAD in high-speed application of VLC. Firstly, the gain of a SPAD is so high that it can be easily saturated. Hence, proper filter is required to reject ambient light when environment light level is high. Secondly, the operation of pulse counting makes a SPAD highly nonlinear [108]. This means that the received signals will be affected by non-linear effect.

In high-speed VLC application, such as wavelength division multiplexing system, bandpass filters are required to exclude unnecessary colour components (see Figure 2.3). Bandpass filters usually consist of multiple thin dielectric layers which exploit the phenomenon of optical interference [109]. The bandwidth of optical filter is required to be larger than the bandwidth of the desired signals so that the received optical power can be maximised. Also, the transmission spectrum of a typical bandpass filter is shifted when the incident angle changes [1]. Therefore, a filter must be carefully placed if it is on wide FOV receiver.

Typically, the received power of a PD is proportional to the physical area of it. If the physical area of a PD increases, it can capture more optical power and be more robust to movement and rotation. However, it is expensive to increase the size of a PD. Moreover, large physical area results in a slow switching time which reduces the receiver bandwidth. Hence, it is of vital importance to find a way to collect more light energy without compromising the bandwidth of a PD. A method of increasing the effective area of a PD is the use of an optical concentrator. Usually, there are two main types of concentrators: imaging concentrators and non-imaging

concentrators. Imaging concentrators collect light signals and project the original image of the optical transmitter on a PD. They are favourable to use in a multiple-input multiple-output (MIMO) configuration. This is because, with the use of imaging concentrator, optical links from different LEDs can be well separated. This significantly improves the capacity of each optical channel and reduces the complexity of detection [38, 95, 110]. The use of non-imaging concentrators aim for optimising the transmission of light radiation from an optical transmitter to a PD. Unlike imaging concentrators, nonimaging concentrators focus all light energy to a small area, which means that it can no longer separate different optical channels and be applicable to a MIMO configuration [111]. Instead, nonimaging concentrators can effectively collect light energy and achieve higher gain. Typically, an effective signal collection area is [1]:

$$A_{\text{eff}}^{\text{bare}} = A_{\text{p}} \cos\psi \times \text{rect}(\frac{\pi}{2}), \tag{2.11}$$

where A_{p} is the physical area of a PD; ψ is the incidence angle; $\text{rect}(\cdot)$ represents a rectangular function. With a concentrator and a filter, the effective area becomes [1]:

$$A_{\text{eff}}^{\text{bare}} = A_{\text{p}} T_s(\psi) g(\psi) \cos\psi \times \text{rect}(\Psi_{\text{fov}}), \tag{2.12}$$

where $T_s(\psi)$ is the signal transmission of an optical filter corresponding to incidence angle ψ; Ψ_{fov} is the FOV of an optical receiver and $g(\psi)$ is the concentrator gain. With the use of nonimaging concentrators, there is a trade-off between FOV and gain. Ideally, a nonimaging concentrator has a gain [112] of

$$g(\psi) = \frac{n_{\text{ref}}^2}{\sin^2 \Psi_{\text{fov}}} \text{rect}(\Psi_{\text{fov}}), \tag{2.13}$$

where n_{ref} is the internal refractive index. In Figure 2.4, three types of nonimaging concentrators are illustrated. The first one is a hemisphere lens optical nonimaging concentrator with a planar longpass filter on the top a PD Figure 2.4(a). For this concentrator, $\Psi_{\text{fov}} \approx \frac{\pi}{2}$ and $g(\psi) \approx n^2$ over the entire FOV. In some scenarios, when a bandpass filter is required, a planar filter is no longer suitable. As the incidence angle of the concentrator changes, the filter passband shifts. This leads to the design of another type of concentrators which is illustrated in Figure 2.4(b). For this concentrator, a bandpass filter is bonded on the outer surface of the hemisphere concentrator. The change of the incidence angle of the concentrator will not have a great impact on the filter passband [1]. Therefore, with this type of design, an optical receiver can achieve wide FOV and narrow bandwidth at the same time. The third type of nonimaging

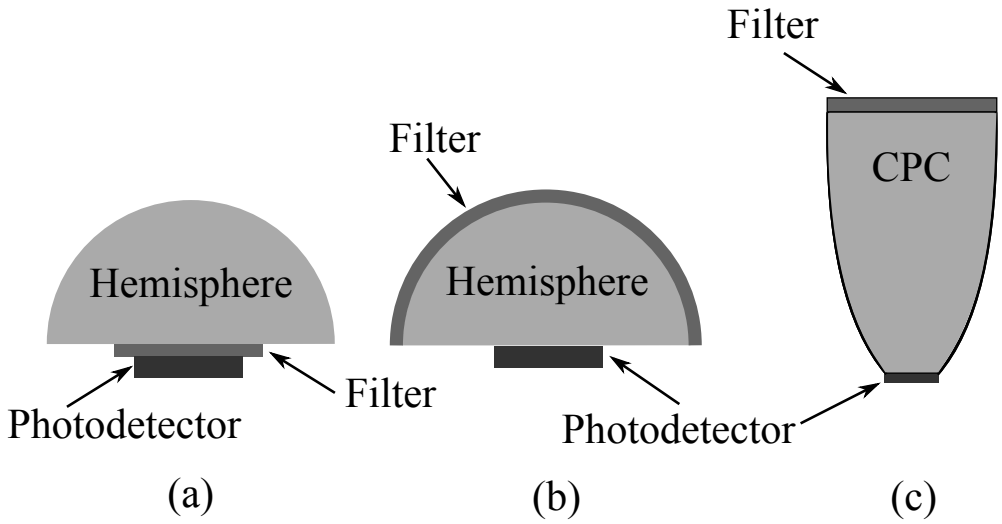

Figure 2.4: *Different types of nonimaging optical concentrator. (a) hemisphere with planar optical filter; (b) hemisphere with hemispherical optical filter; (c) CPC with planar optical filter.*

concentrator is named compound parabolic concentrator (CPC), which is illustrated in Figure 2.4(c). This concentrator can achieve a much higher gain compared with the hemisphere concentrator at the cost of a narrower FOV. The representation of concentrator gain of CPC is similar to (2.13). In this design, planar optical bandpass filter can be used at different FOV. The drawback of CPC is its excessive length, especially when Ψ_{fov} is small. Some researches have been done to deal with this issue [113]. In this thesis, CPC concentrator is used in all scenarios, as it has a cut-off effect for the light signal outside its FOV which is beneficial to the interference cancellation.

After passing an optical filter and concentrator, light signals are converted to electric signals by PDs. One important parameter here is responsivity τ. It is a ratio of the generated photocurrent to the incident light power at a given wavelength. The responsivity over the desired bandwidth can be represented as:

$$\tau = \int_{\lambda_{\min}}^{\lambda_{\max}} \tau(\lambda)\mathrm{d}\lambda = \int_{\lambda_{\min}}^{\lambda_{\max}} \frac{I_{\mathrm{PD}}(\lambda)}{P(\lambda)}\mathrm{d}\lambda, \tag{2.14}$$

where $I_{\mathrm{PD}}(\lambda)$ is the generated photocurrent at a wavelength λ and $P(\lambda)$ is the optical light power at a wavelength λ; $\lambda_{\max}$ is the maximum wavelength of incident light; $\lambda_{\min}$ is the minimum wavelength of incident light.

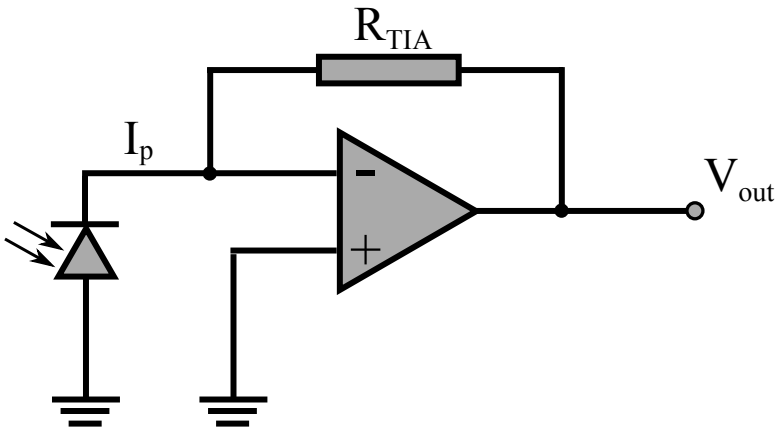

Figure 2.5: *A typical transimpedance amplifier. R_{TIA} represents the feedback resistor in an amplifier configuration. I_{p} is the photo-diode current. V_{out} is the output voltage.*

The received electric analogue signals are fed to analogue-to-digital converter (ADC), where digital signals can be obtained. Finally, these digital signals will pass another DSP which decodes and generates output information bits.

2.2.4 Noise Sources

In a high speed VLC communication system, one of the most important limiting factors of transmission speed is noise. Noise is usually introduced at receiver front-ends which can significantly degrade system performance. Typically, there are two different types of noise: thermal noise and shot noise.

Thermal noise is another noise from receiver front-ends. It is mainly introduced at the transimpedance amplifier (TIA) stage. A typical TIA is illustrated in Figure 2.5. An PD captures optical power from light sources and generates current I_{p}. This current is transferred to output voltage V_{out} by TIA. In this type of TIA, the resistor R_{TIA} dominates the thermal noise which can be modelled as additive white Gaussian noise (AWGN). Hence, for this type of configuration the power spectral density (PSD) of this thermal noise can be calculated as [114, 115]:

$$N_{\mathrm{thermal}} = \frac{4k_{\mathrm{B}}T_{\mathrm{K}}}{R_{\mathrm{TIA}}} \left[\frac{\mathrm{A}^2}{\mathrm{Hz}}\right], \tag{2.15}$$

where k_{B} is the Boltzmann's constant, which is $1.38\times10^{-23}[J/K]$; $T_{\mathrm{K}}[\mathrm{K}]$ is the device temperature in Kelvin; R_{TIA} is the TIA resistor. The thermal noise contribution not only depends on

the configuration of TIA, but also relates to the modulation bandwidth. For high speed transmission, when modulation bandwidth exceeds a few hundred MHz, the thermal noise from other components in the TIA need to be consider as described in [114, 115].

Shot noise is a type of electronic noise which can be modelled by a Poisson process. It originates from the discrete nature of electric charge and it is also relevant to the particle nature of light. There are a lot of sources that generates shot noise. This includes ambient light from sun light, street light, incandescent and fluorescent lamps [71]. Although these sources emit light without any modulation, they provide large optical power than the desired communication signal. This means after passing through a PD, there is a large DC photocurrent that causes shot noise. The DC component in communication signal can be easily removed by using a proper signal processing technique. However, the shot noise introduced by DC component cannot be eliminated. Hence, the one-sided PSD of shot noise can be represented as:

$$N_{\text{shot}} = 2q_{\text{elec}}\tau\bar{P}_{\text{rx}}\left[\frac{\text{A}^2}{\text{Hz}}\right], \tag{2.16}$$

where q_{elec} is the charge of one electron which is 1.602×10^{-19} C and $\bar{P}_{\text{rx}}$ is the average received optical power. Not only external light source causes shot noise, the light signal from the desired link can generate shot noise as well. This happens specially in the condition that the lighting fixtures have the dual functionality of illumination and communication. When a VLC system use an APD as optical receiver, the issue of shot noise must be carefully considered. When shot noise is small enough, an APD can provide high SNR performance since the effect of thermal noise overcome the effect of shot noise and will not affect by the high internal gain. However, when shot noise is large, it can be significantly amplified by the avalanche effect of APD and overcome the effect of thermal noise. Thus, in this case, both desired signals and shot noise are simultaneously amplified by APD which degrades SNR performance of an receiver.

Finally, the overall noise generated by receiver front-ends can be represented as the combination of APD shot noise and thermal noise from the TIA, which is given as:

$$N_0 = N_{\text{shot}} + N_{\text{thermal}}, \tag{2.17}$$

where N_{shot} and N_{thermal} can be directly added since they are AWGN and uncorrelated. In a typical indoor scenario, thermal noise is greater than shot noise.

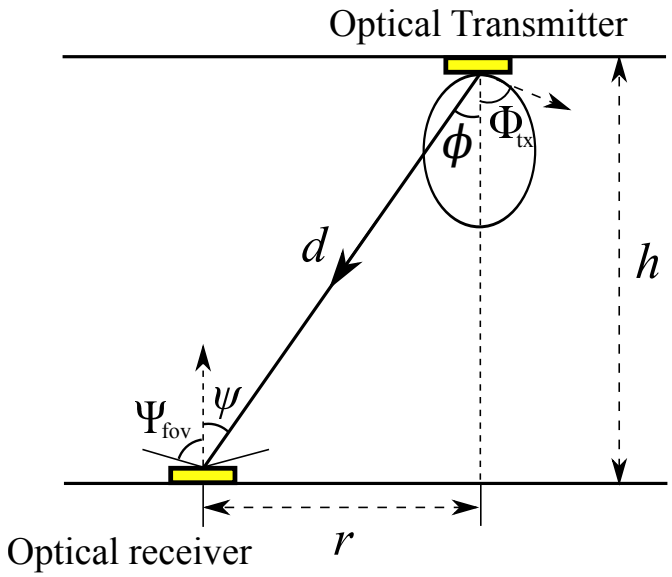

Figure 2.6: *The geometry of a LOS link.*

2.2.5 Propagation Models

In order to study a VLC system, the most important thing is to characterise an optical channel and determine its DC gain. The DC gain of the optical channel can be characterised by ray tracing model instead of statistic model. This is because, in VLC, the distance of light propagation and the size of transmitter and receiver front-ends are significantly larger than the wavelength of visible light. Hence, diffraction will not occur in this scenario which guarantees the accuracy of the ray-tracing model.

2.2.5.1 LOS Link

In LOS links (directed, hybrid or nondirected), the DC gain can be accurately computed. The geometry of a LOS link is illustrated in Figure 2.6, where an optical transmitter and an optical receiver are placed in a room with a height of h and the horizontal distance between them is r. The channel DC gain can be calculated by [1]:

$$H_0 = \frac{(m+1)A_{\text{eff}}}{2\pi d^2}\cos^m(\phi)\cos(\psi)\text{rect}\left(\frac{\psi}{\Psi_{\text{fov}}}\right), \tag{2.18}$$

where d is the distance between an optical transmitter and an optical receiver; Ψ_{fov} is the FOV of the optical receiver; m is the Lambertian order of the optical transmitter and is a function of the

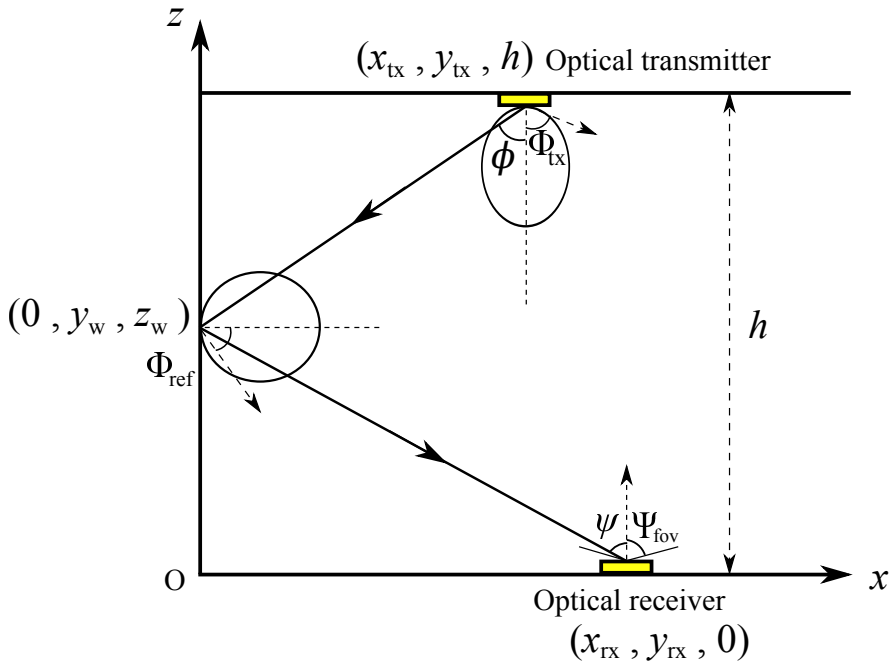

Figure 2.7: *The geometry of a first order reflection NLOS link.* $(x_{\mathrm{tx}}, y_{\mathrm{tx}}, h)$ *are the coordinates of an optical transmitter.* $(0, y_{\mathrm{w}}, z_{\mathrm{w}})$ *are the coordinates of a point on the wall.* $(x_{\mathrm{rx}}, y_{\mathrm{rx}}, 0)$ *are the coordinates of an optical receiver.*

transmitter half-intensity radiation angle Φ_{tx} as $m = -1/\log_2(\cos(\Phi_{\mathrm{tx}}))$; ϕ is the irradiance angle of the optical transmitter; ψ is the incidence angle the optical receiver; $\mathrm{rect(x)}$ represents the rectangular function. The effective signal collection area A_{eff} is given as:

$$A_{\mathrm{eff}} = A_{\mathrm{p}} G \frac{n_{\mathrm{ref}}^2}{\sin^2(\Psi_{\mathrm{fov}})}, \tag{2.19}$$

where n_{ref} is the refractive index of the receiver optics; A_{p} is the physical area of a PD; T_{s} is the signal transmission gain of the optical filter.

2.2.5.2 NLOS Link

In NLOS directed and non-directed links, the transmitted power reaches the optical receivers through reflections. The geometry of a first order reflection NLOS link is illustrated in Figure 2.7. First order reflection means that the entire light path from a transmitter to a receiver experiences one reflection. Most of the materials used in a building are effective reflectors, which have the reflectivity within $0.6 - 0.9$ [1]. Therefore, these materials can be deemed as

Lambertian reflectors. This means reflecting materials absorb the incident light energy and reflect them as Lambertian pattern. The intensity of reflected light is proportional to the cosine of irradiance angle and it is independent to the incidence angle of incoming light. In a second order reflection NLOS link, the channel gain can be calculated as [1]:

$$H_{\mathrm{2nd-reflection}} = \frac{\rho T_s A_{\mathrm{eff}} x_{\mathrm{tx}}^2 x_{\mathrm{rx}}^2}{\pi^2} \iint\limits_{S_{\mathrm{wall}}} \frac{[x_{\mathrm{rx}}^2 + (y_{\mathrm{rx}} - y_{\mathrm{w}})^2 + z_{\mathrm{w}}^2]^{-2}}{(x_{\mathrm{tx}}^2 + (y_{\mathrm{tx}} - y_{\mathrm{w}})^2 + (h - z_{\mathrm{w}})^2)^2} \mathrm{d}x_{\mathrm{w}} \mathrm{d}y_{\mathrm{w}}, \quad (2.20)$$

where ρ is the reflectivity of a reflecting material; $(x_{\mathrm{tx}}, y_{\mathrm{tx}}, h)$ is the the coordinates of an optical transmitter; $(0, y_{\mathrm{w}}, z_{\mathrm{w}})$ is the coordinates of a point on the wall; $(x_{\mathrm{rx}}, y_{\mathrm{rx}}, 0)$ is the coordinates of an optical receiver; S_{wall} is the area of the wall.

As the second-order reflection model is described, the next step is to generalise it to higher order reflections. In order to derive this model, all of the smooth reflection surfaces are divided into a number of small reflecting surface elements [116]. Each element collects the energy of the light signal incident on its surface and re-emits a fraction of the collected light determined by the reflection coefficient of the surface material.

In a generalised model, a NLOS link can be divided into three parts. The first part is the light path from an optical transmitter to the q^{th} reflecting surface element. The optical channel gain for this path can be calculated as:

$$L_{1,q} = \frac{(m+1)\Delta A}{2\pi d_{q,\mathrm{tx}}^2} \cos^m(\phi) \cos(\psi), \quad (2.21)$$

where ΔA is the area of the reflecting surface element. The distance between the optical transmitter and the q^{th} reflecting surface element is denoted as $d_{q,\mathrm{tx}}$. Equation (2.21) provides a method to calculate the power distribution on the reflecting walls due to a single-point source. The incident light is absorbed by each reflection element and re-emitted with a Lambertian pattern, and the intensity is determined by the reflection coefficient ρ. Therefore, the power on each reflecting surface element after the i^{th} light reflection can be derived.

Hence, in the second part of the NLOS path, the optical channel gain is described as:

$$L_{i,p} = \sum_{q=1}^{Q} \frac{\rho_q (m_{\mathrm{ref}} + 1) \cos^{m_{\mathrm{ref}}}(\phi) \cos(\theta) \Delta A}{2\pi d_{p,q}^2} L_{i-1,q}, \quad (2.22)$$

where i represents the number of the light reflections and $d_{p,q}$ is the distance between the

reflecting element p and the reflecting element q. The total number of reflecting elements is Q. The reflectivity of the reflecting element q is ρ_q; m_{ref} is the Lambertian order of the reflecting element, which is a function of the reflecting material emission semi-angle at half power Ψ_{ref} as $m_{\text{ref}} = 1/\log_2(\cos(\Psi_{\text{ref}}))$. For most surfaces, $\Psi_{\text{ref}} = 60^{\text{o}}$.

The third part of the NLOS link is the light path from the reflecting elements to an optical receiver. The optical channel gain for this path can be represented as:

$$H_i = \sum_{p=1}^{Q} L_{i,p} \frac{\rho_p (m_{\text{ref}} + 1) \Delta A}{2\pi d_{\text{rx,p}}^2} \cos^{m_{\text{ref}}}(\phi) \cos(\psi) \text{rect}\left(\frac{\psi}{\Psi_{\text{fov}}}\right), \tag{2.23}$$

where $d_{\text{rx,p}}$ is the distance between the q^{th} reflecting surface element and the optical receiver; the reflection coefficient of the reflecting element p is ρ_p.

Finally, the overall DC gain is the sum of the LOS component and the NLOS components:

$$H_{\text{overall}} = H_0 + \sum_{i=1}^{I} H_i, \tag{2.24}$$

where I is the total number of maximum light reflections taken into account in a propagation model.

2.2.6 Modulation Schemes

As discussed in Section 2.2.2, since light signal generated by LEDs are incoherent, the only feasible way to convey information is to use IM/DD. Unlike RF, the modulation signals in VLC must be real and positive. This means some modulation scheme in RF requires modification before applying to VLC.

2.2.6.1 Single Carrier Modulation

Real single carrier modulation scheme can be adapted to VLC from RF without major modification. These modulation schemes include on-off keying (OOK), pulse position modulation (PPM), pulse width modulation (PWM) and unipolar pulse amplitude modulation (PAM). The detail of these modulation schemes is introduced as follows.

OOK

OOK is the simplest way of modulation by representing digital data using "1s" and "0s". In terms of OOK implementation, two specific optical output power levels, $P_{\mathrm{H,OOK}}$ and $P_{\mathrm{L,OOK}}$, are defined. $P_{\mathrm{H,OOK}}$ is the higher optical power which represents "1" and $P_{\mathrm{L,OOK}}$ is the lower optical power which represents "0". Usually, $P_{\mathrm{H,OOK}}$ and $P_{\mathrm{L,OOK}}$ are chosen to maximise their difference. Since there is no issue of non-linearity, $P_{\mathrm{H,OOK}}$ can be the maximum possible optical output power and $P_{\mathrm{L,OOK}}$ can be 0.

PPM

PPM is a way of modulation by varying the position of the pulses in a time interval T. The way of generating pulses in PPM is similar to that of OOK. If M_{PPM} possible positions are used in one time interval, $\log_2(M_{\mathrm{PPM}})$ bits can be represented within a time interval T.

PWM

PWM is a way of modulation by varying the pulse width in a time interval T. If M_{PWM} possible positions can be used in one time interval, $\log_2(M_{\mathrm{PWM}})$ bits can be represented within a time interval T. PPM is very useful in VLC system due to its flexibility of adjusting illumination condition. With the help of variable pulse position modulation (VPPM) [117], illumination with dimming control and communication can be realised simultaneously in VLC.

PAM

PAM is a way of modulation by encoding messages in the amplitude of a series of signal pulses. If a PAM symbol has M_{PAM} possible amplitudes, $\log_2(M_{\mathrm{PAM}})$ bits can be represented by one PAM symbol. Unlike RF, VLC can only use positive optical output power. This means that only unipolar PAM can be implemented.

The advantages of single carrier modulation techniques are: i) compared with multiple carrier modulation, single carrier modulation techniques can achieve better performance in flat channels; ii) compared with multiple carrier modulation techniques, single carrier modulation techniques are simple to implement and of low complexity; iii) compared with multiple carrier modulation techniques, single carrier modulation techniques experience less impact from non-

linear distortion at an optical transmitter. This is because these modulation techniques are time domain based which can be easily shaped and constrained in a desired range.

2.2.6.2 Multiple Carrier Modulation

Compared with single carrier modulation, multiple carrier modulation offers higher data rates. Multiple carrier modulation generally includes discrete multitone (DMT) and orthogonal frequency division multiplexing (OFDM). At high data rates, the information signal is affected by inter-symbol interference (ISI) when passing through a dispersive optical channel. Also, when the off-the-shelf components are used, extra ISI is generated. This results in limited modulation bandwidth and the main limiting factor of the communication rate [39, 40, 90]. Moreover, the frequency response of realistic channel is usually non-flat in high frequency region. This means that the use of modulation bandwidth in non-flat region requires appropriate equalisation techniques. For single carrier modulation, equalisation in non-flat channel requires sophisticated digital filter. Hence, multiple carrier modulation, especially OFDM is favourable in this scenario. The advantage of using OFDM are: i) it enables simple equalisation using single-tap equaliser in the frequency domain; ii) as the entire available bandwidth is split into multiple narrowband subcarriers, it is possible to adaptively allocate information bits and energy to individual subcarriers according to their channel properties. This can effectively exploit the communication resources; iii) OFDM technique can be directly used as a multiple access scheme at the medium access control (MAC) level, where different subcarriers of OFDM can be effectively allocated to different users [118].

Since a VLC system uses IM/DD, the way of generating OFDM signals need to be modified. Conventional OFDM subcarriers are modulated by M-quadrature amplitude modulation (QAM) signals. As a result, the time domain signals are complex and bipolar. To make the time domain signals real, Hermitian symmetry is required to impose in the block of symbols before inverse fast Fourier transform (IFFT). To make the time domain signals unipolar, two different methods are proposed in a typical VLC system, which are denoted as DC biased optical orthogonal frequency division multiplexing (DCO-OFDM) and asymmetrically clipped optical orthogonal frequency division multiplexing (ACO-OFDM), respectively. Details of DCO-OFDM and ACO-OFDM are introduced in the following parts.

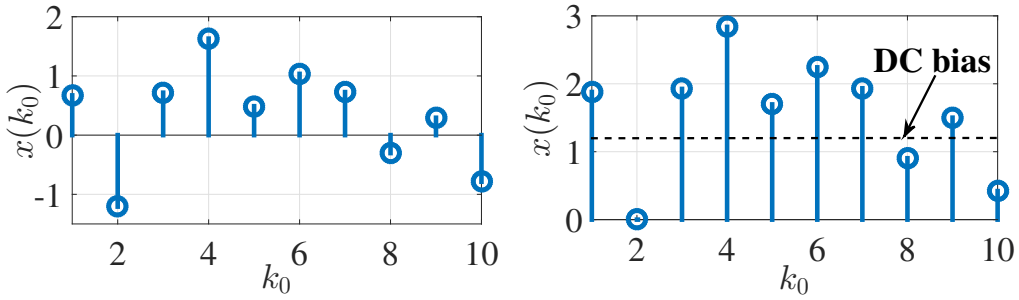

(a) Bipolar time domain signal. (b) Biased time domain signal.

Figure 2.8: *DCO-OFDM signal generation. The cyclic prefix is not illustrated.*

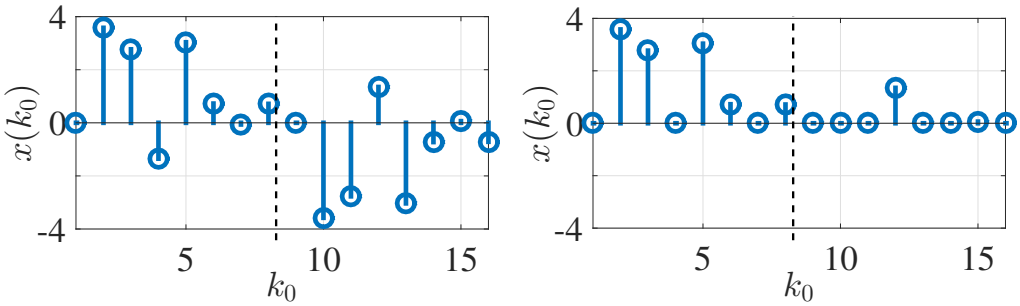

(a) Time domain signal before clipping. (b) Time domain signal after clipping.

Figure 2.9: *ACO-OFDM signal generation. The cyclic prefix is not illustrated.*

2.2.6.3 DCO-OFDM

In DCO-OFDM, a positive DC bias is added to the bipolar time domain signal [119]. Then, the non-negative value of the biased signal is clipped so that the time domain signal becomes unipolar. An example of DCO-OFDM time domain signal is illustrated in Figure 2.8. With the use of DCO-OFDM, unipolar time domain OFDM signal can be generated straightforwardly. The need for DC bias results in the waste of transmission power. However, in the perspective of downlink, the addition of DC bias is beneficial since it provides illumination.

2.2.6.4 ACO-OFDM

In order to generate energy efficient unipolar OFDM signal that can avoid adding DC bias, ACO-OFDM is proposed [119–123]. Only impose the information bits on odd-indexed subcarriers, ACO-OFDM can inherently generate unipolar signal without DC bias by exploiting the properties of Fourier transform (see Figure. 2.9).

Compared with DCO-OFDM, ACO-OFDM sacrifices half of the spectral efficiency to make the time domain signal unipolar. In return, ACO-OFDM is more energy efficient than DCO-OFDM.

2.3 Optical Attocell Networks

With the implementation of cellular networks, RF technology managed to serve a large number of users with high service quality. Compared with a single transmitter, cellular networks can provide higher power efficiency and also higher spectral efficiency by means of frequency reuse [42, 124–130]. Due to the limitation of available communication bandwidth, the most effective way to improve the performance of cellular networks is to reduce the inter-site distance between each access point (AP) in the system. A femtocell is usually referred to as a low power, low cost, plug-and-play AP which is small in cell size. The deployment of femtocells introduces new intra-cell and intercell interference, which degrades the system performance.

VLC is very suitable in small-cell system since the coverage area of a LED is intrinsically limited. In order to provide high speed broadband service with wide coverage, networked VLC system, namely optical attocell network, is required. As the visible light spectrum does not interfere with RF, the existing RF cellular network will not be affected by optical APs. This means, with the use of optical cells, the total throughput of the heterogeneous network can be further improved. Unlike RF transmitters that are usually omnidirectional, optical transmitters are intrinsically directional. The transmitted light of an AP can be strictly confined within a limited region. Also, as visible light cannot penetrate wall, physically there is no co-channel interference between the neighbouring rooms. With these features, optical attocell networks can be deployed in extremely high density. Interestingly, the high-density deployment of lighting infrastructures already exists in order to fulfil the illumination requirement. According to the recent study [56], up to three orders of magnitude throughput improvement can be obtained by optical attocell networks when compared with RF femtocell.

2.3.1 Interference Mitigation

In an optical attocell network, inter-cell interference (ICI) is inevitable since APs are placed close to each other. This can significantly compromise the system performance. In order to mitigate ICI, three methods were studied. The first one is joint transmission [58]. In this method,

data transmitted from the adjacent APs are cooperated to avoid ICI at cell edge. Results show that this method can achieve better cell edge signal-to-interference-plus-noise ratio (SINR) and improve the system throughput. However, a drawback of joint transmission systems is that they require extra signalling overhead. The second interference mitigation technique is fractional frequency reuse (FFR) [59]. By using FFR, cells are partitioned into spatial regions with different frequency reuse factors. Since adjacent regions use different frequency band, ICI can be effectively avoided. Hence, the cell edge user SINR and spectral efficiency of optical attocell networks are significantly improved. The third ICI mitigation method is busy burst signalling [57]. For this method, a busy burst signal will be broadcast if a user intend to receive data in the following frame. In optical attocell networks, a busy burst signal is generated to indicate the neighbouring cells to avoid data transmission while the desired AP is transmitting. By using this method, each AP in the system can acquire the knowledge of interference without central supervision. Results show that busy burst approach can improve the system performance without compromising the user throughput at cell edge.

2.3.2 Multiple User Access Schemes

In optical attocell networks, it is of vital importance to have multiple access schemes to facilitate users to get access to APs. In this part, three different multiple user access schemes, time division multiple access (TDMA), space division multiple access (SDMA) and orthogonal frequency division multiple access (OFDMA) are introduced.

2.3.2.1 TDMA

In an optical TDMA scenario, a single-element transmitter is functioned as an AP. All active users share the same bandwidth resource in their corresponding optical cell. Information for different users is transmitted in different time slots. Only one of the active users can be served in each time slot. Therefore, the received SINR of an active user k can be expressed as:

$$\gamma_k = \frac{\left(\tau P_{\mathrm{tx}} H_{\hat{b},k}\right)^2}{N_0 B + \sum_{b' \neq \hat{b}} \left(\tau P_{\mathrm{tx}} H_{b',k}\right)^2}, \tag{2.25}$$

where τ is the responsivity of the PD; P_{tx} is the optical power transmitted by an AP and is assumed to be the same for all APs; $H_{\hat{b},k}$ is the channel attenuation between user k and the

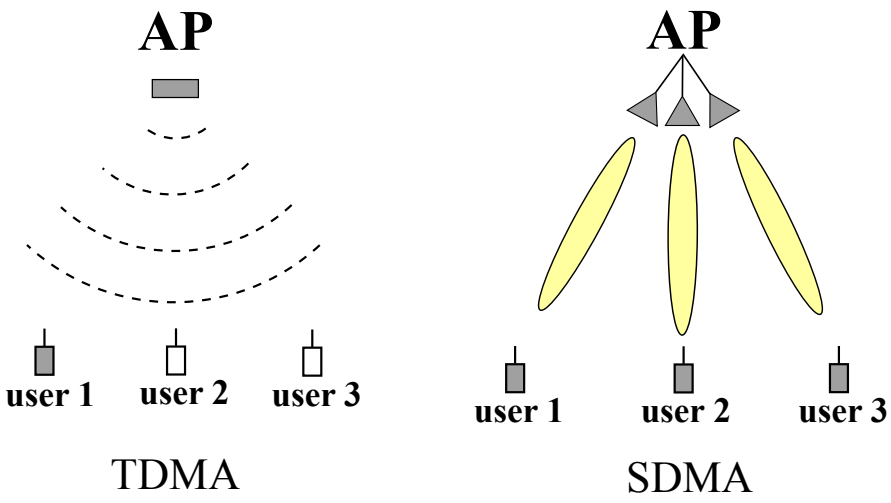

Figure 2.10: *The difference between TDMA and SDMA. On the left is a TDMA scenario. Only user 1 is served within a time slot. On the right is a SDMA scenario. Four users are served simultaneously within one time slot.*

desired AP $\hat{b}$; $\sum_{b' \neq \hat{b}} \left(rP_{\mathrm{t}}H_{b',k}\right)^2$ represents the interference signal from interfering APs; N_0 is the additive white Gaussian noise (AWGN) power spectral density; B is the optical communication bandwidth. If a simple round-robin (RR) scheduler is used, the spectral efficiency of the optical TDMA system is as follows:

$$\Omega_{\mathrm{TDMA}} = \frac{1}{K}\sum_{k=1}^{K}\log_2(1+\gamma_k), \tag{2.26}$$

where K is the total number of the active users.

2.3.2.2 SDMA

Unlike TDMA, SDMA is multiple access scheme that supports simultaneous transmission to different active users. SDMA was initially implemented in RF communication [131]. As illustrated in Figure 2.10, in a TDMA scenario, an AP consists of a single-element transmitter which has wide transmission pattern. Only one user can be served within a time slot. Unlike TDMA, the AP in SDMA system consists of multiple LED elements which can generate multiple directional narrow light beams simultaneously. Hence, more than one active user can be served within a single time slot. By exploiting the location information of active users, the interference between these narrow beams can be significantly mitigated. Therefore, SDMA is able to offer

superior performance in comparison with TDMA. Detailed analysis of optical SDMA and the comparison between optical TDMA and optical SDMA are discussed in Chapter 5.

2.3.2.3 OFDMA

In an optical OFDMA scenario, the entire modulation bandwidth is divided into a number of subcarriers by the operations of IFFT. This can be done by either DCO-OFDM or ACO-OFDM. Multiple access is achieved by allocating subsets of the subcarriers to different users. The received SINR of a subcarrier i_{o} is:

$$\gamma(i_{\mathrm{o}}) = \frac{\left(\tau P_{\mathrm{tx}} H_{\hat{b}}(i_{\mathrm{o}})\right)^2}{N_0 B + \sum_{b' \neq \hat{b}} \left(\tau P_{\mathrm{tx}} H_{b'}(i_{\mathrm{o}})\right)^2}, \tag{2.27}$$

where $H_{\hat{b}}(i_{\mathrm{o}})$ is the channel gain of the desired AP $\hat{b}$; $H_{b'}(i_{\mathrm{o}})$ represents the channel gain from interfering AP b'. The spectral efficiency of the optical OFDMA system is as follows:

$$\Omega_{\mathrm{OFDMA}} = \frac{1}{I_{\mathrm{sub}}} \sum_{i_{\mathrm{o}}=1}^{I_{\mathrm{sub}}} \log_2\left(1 + \gamma(i_{\mathrm{o}})\right), \tag{2.28}$$

where I_{sub} is the total number of the OFDMA subcarriers.

2.4 Summary

In this chapter, a brief history of VLC and the fundamental concepts for VLC link-level design are introduced. These concepts include: the classification for VLC links, IM/DD channel, the characteristic of transmitter and receiver front-end elements and the noise source in VLC links. With these fundamental concepts, both LOS and NLOS optical channels are modelled. In order to increase the spectral efficiency of VLC links, modulation schemes including single carrier and multi-carrier modulation are introduced.

In addition, the concept of optical attocell networks is presented. Also, interference mitigation schemes and multiple access schemes for optical attocell networks are also discussed.

Chapter 3
Channel Modelling for Optical Attocell Networks

3.1 Introduction

In an optical attocell network, inter-cell interference (ICI) consists of two parts: line-of-sight (LOS) and non-line-of-sight (NLOS) ICI. Conventionally, both LOS and NLOS ICI are characterised by ray tracing model [1]. In order to mitigate the LOS ICI, one of the most effective ways is to use angle diversity receiver (ADR) as optical receivers [132]. An ADR consists of multiple directional photodiode (PD) with narrow field-of-view (FOV). With the use of signal combining schemes, an angle diversity receiver can reject LOS ICI from the cell in the vicinity without losing the coverage. In terms of NLOS ICI, since light interference can be reflected by walls, ceilings and floors, even a narrow FOV optical receiver fails to exclude it. Hence, NLOS ICI is inevitable at receiver side. The estimation of the NLOS ICI is of significant importance as it limits the upper bound of the system performance in optical attocell networks.

In this section, a simplified model was proposed to evaluate NLOS ICI in optical attocell networks. This model is based on the assumption that the symbol duration of the system is much longer than the duration of channel impulse response. Therefore, direct current (DC) channel gain instead of time dispersive channel gain is taken into account. In this model, only second order light reflections are considered. Also a novel way of estimating light reflection is introduced. This model significantly simplifies the calculation of NLOS reflections. With this model, the analytical result of signal-to-interference-plus-noise ratio (SINR) distribution in optical attocell networks can be represented as closed-form. The results of Monte Carlo simulations verify the accuracy of the analytical model.

The rest of the chapter is organized as follows. In section 3.2, conventional propagation model for light transmission in optical attocell networks is introduced and discussed in this section. Section 3.3 describes the simplified NLOS propagation model. The analytical derivation of the SINR distribution in attocell network is given in Section 3.4. The analytical and numerical results are presented and discussed in Section 3.6. Finally, conclusions are given in Section 3.7.

3.2 Conventional Ray-tracing Model

The channel DC gain of LOS path in this optical attocell network can be calculated by (2.18) in Chapter 2. The conventional way of calculating the channel gain is that, all of the smooth reflection surfaces are divided into a number of small reflecting surface elements [116]. Each

element collects the energy of the light signal incident on its surface and re-emits a fraction of the collected light determined by the reflection coefficient of the surface material. As mentioned in Chapter 2, a NLOS link can be divided into three parts which can be calculated by (2.21), (2.22), (2.23) and (2.24).

3.2.1 The SINR Statistics Evaluation

The service quality of optical attocell networks can be determined by considering the SINR statistics of received SINR. This metric includes the level of received SINR and the cumulative distribution function (CDF) distribution of received SINR. Therefore, in order to evaluate the performance of an optical receiver using a conventional ray-tracing model, the received SINR of the optical receiver need to be determined. First, a desired access point (AP) need to be chosen to maximize the received SINR of the optical receiver. The desire AP for the k-th user, $\hat{b}$, can be chosen as:

$$\hat{b} = \underset{b}{\operatorname{argmax}} \left(H_{b,k} \right). \tag{3.1}$$

where, b is the index of an AP. The $H_{b,k}$ is the channel gain from AP b to user k. Then, the received SINR of the user is:

$$\gamma = \frac{\left(RP_{\mathrm{tx}} H_{\hat{b},k} \right)^2}{N_0 B + \sum_{b' \neq \hat{b}} \left(RP_{\mathrm{tx}} H_{b',k} \right)^2} \tag{3.2}$$

where R is the optical to electric conversion efficiency; P_{tx} is the average electric power of an AP; b' represents the index of interfering AP; N_0 is the noise spectral density; B is the modulation bandwidth. There is no frequency selective fading in a VLC system since the PD area is much larger than the wavelength of the optical signal. Therefore, it is assumed that all APs exhibit similar frequency responses which are determined by the electrical and optical components used.

With the representation of the received SINR, the CDF of the received SINR in optical attocell networks is:

$$F(\gamma) = P(\gamma < \Gamma). \tag{3.3}$$

where Γ is the threshold of the received SINR.

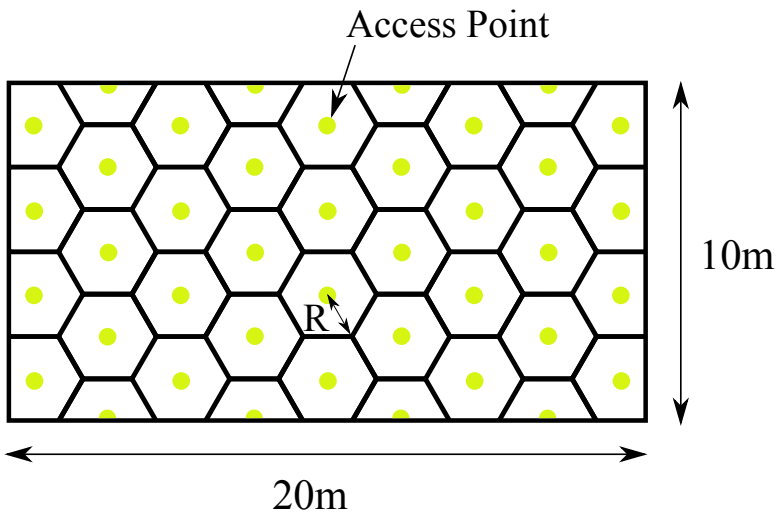

Figure 3.1: *The layout of a hexagonal optical attocell network.*

3.2.2 Simulation and Discussion

In this thesis, hexagonal optical attocell network is chosen since hexagonal configuration provides the optimised performance in terms of system capacity and illumination [133]. The layout of a hexagonal optical attocell network is illustrated in Figure 3.1. The parameters of hexagonal optical attocell network is consistent with the parameters in [133]: the optical attocell network is deployed in a typical $20 \times 11 \times 4$ m office with 40 light emitting diode (LED) on the ceiling. Each LED is placed in the centre of a hexagonal cell and the radius of the cell, R_{cell}, is 3 m. Single-element optical receivers are used in this scenario and they are all assumed to be placed at a desktop height of 1 m. Also, the FOV of the each PD is identical, which is 30^{o}. Transmission power of each optical AP, P_{tx} is 1 W. The half power semi-angle of an optical transmitter is 40^{o}. The physical area of an optical receiver is 1cm^2. Also, up to fourth order multipath reflections are taken into account. Matlab with parallel computation module is used to perform the Monte Carlo simulation.

In the simulation, active users in the attocell network are assumed to be uniformly distributed in the entire office. By varying the position of the active users across all possible locations in the room and estimating the respective achievable SINR, the CDF of the SINR for the active users can be determined, which is shown in Figure 3.2.

The distribution of the SINR are split into two different parts: high SINR region and low SINR region. This is due to the cut-off effect of optical receiver FOV. The users in region 1 (Fig-

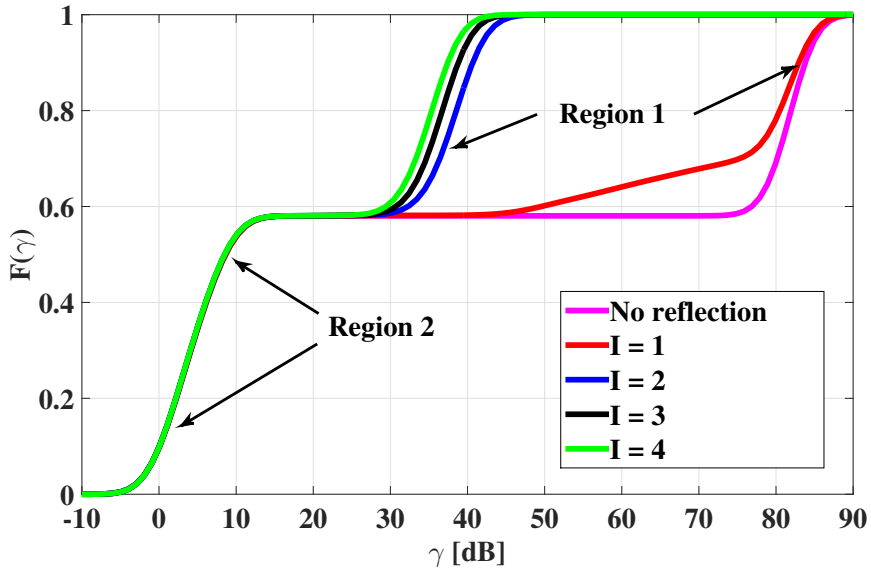

Figure 3.2: *The CDF of the SINR for the single-PD receiver when FOV is* 30^{o}*. The SINR of users in Region 1 corresponds to the high SINR part. The SINR of users in Region 2 corresponds to the low SINR part.* I *is the total number of maximum light reflections taken into account in a propagation model.*

ure 3.4) are near the cell centre and are free from LOS ICI. This is because optical receivers with limited FOV can reject LOS ICI from neighbouring cells. This means that they can achieve higher SINR than the cell-edge users in region 2 where user performance affects by LOS ICI. Compared with the performance where there is no light reflection ($I = 0$), the SINR performance only slightly degrades when the first order reflection ($I = 1$) is considered. This is because the first order reflection can only reach the optical receiver via the walls. In most parts of the room, the first order reflection can be easily rejected by the optical receiver with limited FOV. Only users at the edge of the room can be affected by the interfering signal from the first order reflection. However, when both the first and second order reflections are taken into account, the SINR performance in the high SINR part dramatically decreases. This is because all users can receive the second order reflected interfering signals through the reflection off the ceiling. When higher-order reflections are considered, the SINR performance degrades slightly. This is because the magnitude of high-order reflected light decays significantly due to the power loss of reflection. Therefore, it is notable that the second order light reflection is the dominant NLOS ICI component in the optical attocell networks.

Unlike the first order reflection, the power of the second or higher-order reflected interfering

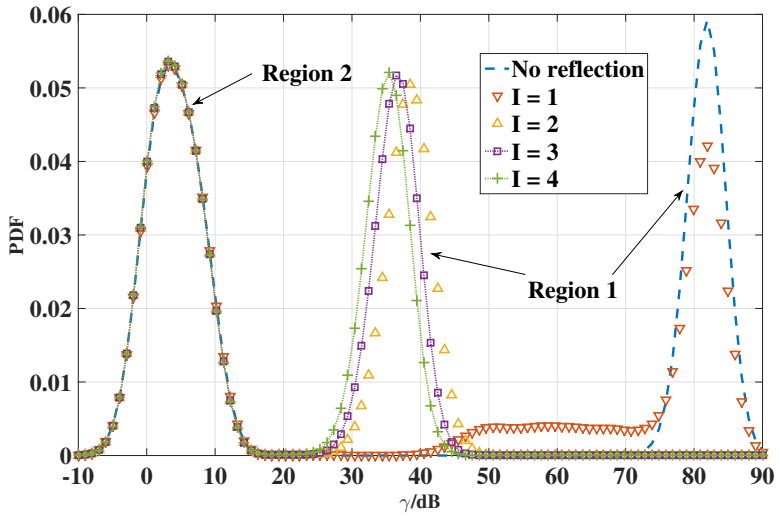

Figure 3.3: *The PDF of the SINR for the single-PD receiver when FOV is* 30^{o}.

signal is spread over the entire ceiling area which means it is impossible to totally eliminate it by only adjusting the FOV of the receiver. Furthermore, since the power of the reflected interfering signal is proportional to the transmission power of the optical APs, the reflected interfering signal will always constrain the upper limit of the SINR performance especially when high transmitted optical power or a low-noise receiver is used. Therefore, it is of vital importance to analytically model the reflected ICI, especially for the users in region 1 where NLOS ICI dominates.

Fig. 3.3 shows the characteristic of SINR distribution in the PDF perspective. It can be observed that the PDF of user SINR is clustered in three different SINR regions. The region with the lowest SINR corresponds to the users that experience LOS interference. The region with the highest SINR corresponds to the users that experience no-interference. This only happens when up to first order reflection is taken into account. If higher order reflections are considered, SINR drops as users will experience NLOS interference from light reflections.

3.3 Simplified NLOS Propagation Model

In the analytical model, a 7-cell configuration is considered, as is shown in Figure 3.5. The cell in the centre is the desired cell and the six interfering cells are in the vicinity of the desired cell. As discussed in the last section, the users in cell centre are mainly affected by NLOS ICI which

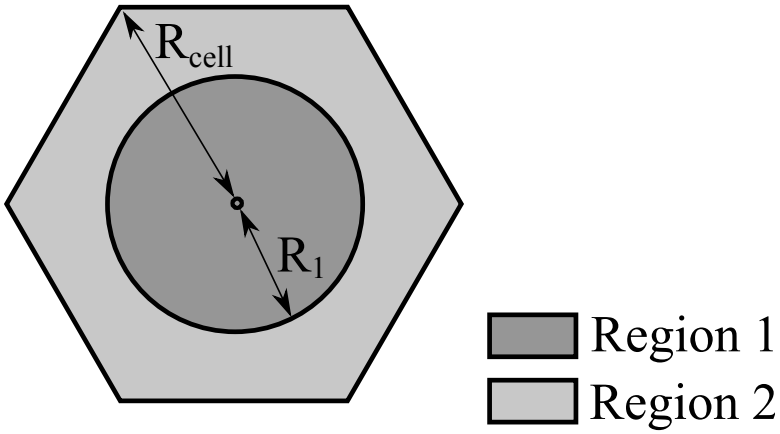

Figure 3.4: *The layout of a hexagonal optical cell.*

is dominated by second order reflection. Hence, in order to focus on NLOS ICI, all users are assumed to be distributed within the centre of the desired cell with a radius of R_1.

In the conventional model, the computation complexity of the NLOS path is high. This is because high-order reflections are taken into account in conventional ray-tracing models. However, this is unnecessary in optical attocell networks. As illustrated in Figure 3.6, the FOV of the optical receiver is designed to be narrow enough to block the LOS interference ($O \rightarrow C$) from cells in the vicinity. Furthermore, the narrow FOV optical receiver also blocks the first-order reflections ($O \rightarrow D \rightarrow C$) which are reflected by walls. Second-order reflections are the only dominant inter-cell interference occurred because the other high-order reflections attenuates significantly, thus are negligible. Hence, only the second-order reflections (point $O \rightarrow A \rightarrow B \rightarrow C$) are assumed in the simplified model. Usually, the propagation path of the second order reflection can be divided into two parts as part I (point $O \rightarrow A \rightarrow B$) and part II (point $B \rightarrow C$).

3.3.1 NLOS Path I

For this path, light signals are considered to be transmitted from an optical transmitter at point O on the ceiling, reflected by the floor and transmitted back to the ceiling (see Figure 3.7). The optical power density of the reflected light at point O, $\mathcal{I}_0$, has the maximum value and can be

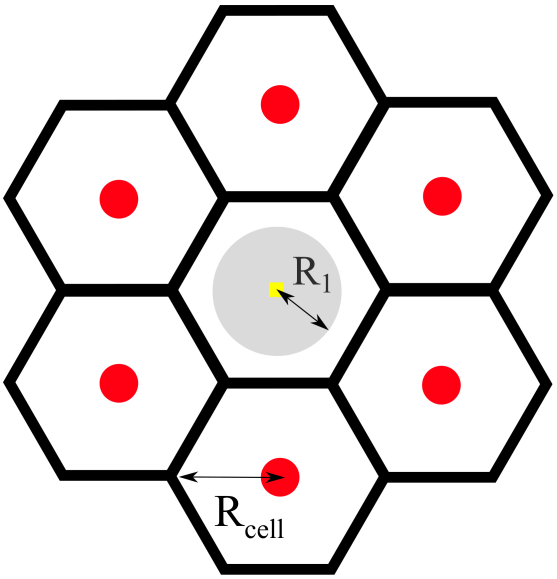

Figure 3.5: *The layout of the simplified attocell network.*

presented as:

$$\mathcal{I}_0 = \frac{C(m+1)(n+1)}{4\pi^2 h^{-(m+n+2)}} \iint_{\text{floor}} \frac{dxdy}{(x^2+y^2+h^2)^{(m+n+6)/2}}. \tag{3.4}$$

Here, x, y in (3.4) can be replaced by ϕ, φ, respectively. The mathematical relationship between them is as follows:

$$\begin{cases} x = h\tan(\phi)\cos(\varphi) \\ y = h\tan(\phi)\sin(\varphi), \end{cases} \tag{3.5}$$

where ϕ is the angle of irradiance and φ is the azimuth angle. Then, the intensity density at point O can be calculated in closed-form:

$$\begin{aligned} \mathcal{I}_0 &= \frac{C(m+1)(n+1)}{4\pi^2 h^4} \int_0^{2\pi} \int_0^{\pi/2} \cos(\phi)^{m+n+6} J d\phi d\varphi \\ &= \frac{C(m+1)(n+1)}{2\pi h^2 (m+n+4)}, \end{aligned} \tag{3.6}$$

where the coefficient $C = \rho_{\text{floor}}\rho_{\text{ceiling}}P_{\text{tx}}$; and the reflection coefficient of the floor and ceiling are ρ_{floor} and ρ_{ceiling}, respectively; also, J is the Jacobian determinant of the coordinate conversion which can be represented as:

$$J = \det\left(\left[\frac{\partial x}{\partial \phi} \frac{\partial x}{\partial \varphi}; \frac{\partial y}{\partial \phi} \frac{\partial y}{\partial \varphi} \right] \right). \tag{3.7}$$

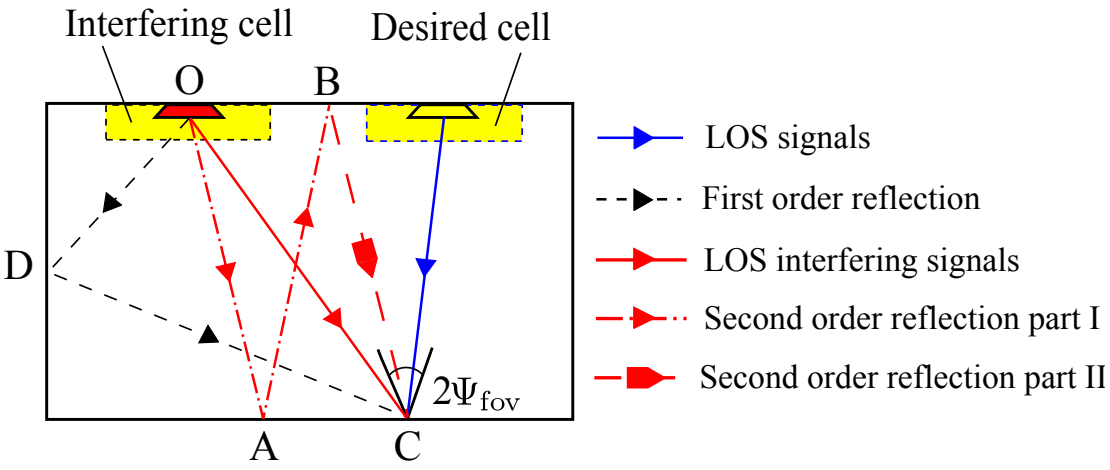

Figure 3.6: *The signal propagation model in an optical attocell network.*

In the simplified model, instead of reflecting by the entire floor, all light energy is assumed to be concentrated and reflected by two points, S and S', shown in Figure 3.8. It is also assumed that the intensity density at point O is identical to that in the conventional ray-tracing model. The intensity density of the reflected light reaches its peak at point O and attenuates at the other locations on the ceiling. The attenuation of the light signals depends on v, which is the horizontal distance between the desired point W and the start point O. Also, the attenuation depends on the attenuation factor, α'. Any two points on the ceiling have the same intensity density of the reflected light if their distances to O are the same. Hence, for an arbitrary point on the ceiling, the intensity density can be represented as:

$$\begin{aligned}\mathcal{I}_v &= 0.5\mathcal{I}_0\left(\frac{H'_{\text{s}}}{H_{\text{s}}}\right)^{\alpha'/2} + 0.5\mathcal{I}_0\left(\frac{H'_{\text{s}'}}{H_{\text{s}'}}\right)^{\alpha'/2} \\ &= \frac{0.5\mathcal{I}_0(h^2+l_{\text{s}}^2)^{\alpha'}}{(h^2+(v+l_{\text{s}})^2)^{\alpha'}} + \frac{0.5\mathcal{I}_0(h^2+l_{\text{s}}^2)^{\alpha'}}{(h^2+(v-l_{\text{s}})^2)^{\alpha'}},\end{aligned} \tag{3.8}$$

where, H_{s}, $H_{\text{s}'}$, H'_{s} and $H'_{\text{s}'}$ are four different channel gains from reflectors S and S$'$ to the ceiling (see Figure 3.8); h is the height of the room; l_{s} is the horizontal distance between point O and point S. Since the energy spread of a transmitter scales with its transmitter semi-angle, a heuristic equation is used to determine l_{s}, which is:

$$l_{\text{s}} = h\tan(\Phi_{\text{tx}}). \tag{3.9}$$

The attenuation factor, α', is chosen to minimise the difference between the intensity density

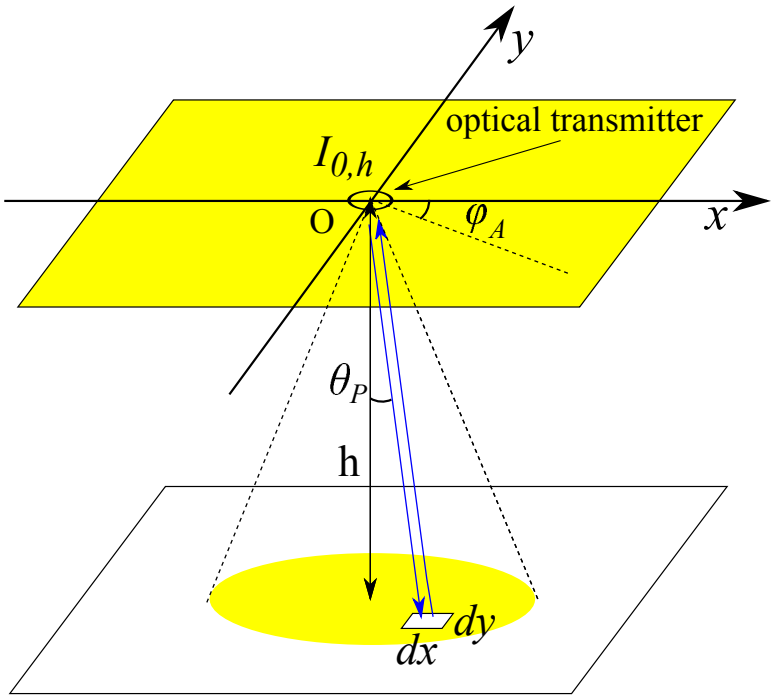

Figure 3.7: *The conventional signal propagation model for NLOS path I.*

of the proposed simplified model, $\mathcal{I}_{n_s\Delta v}$, and the intensity density of the conventional model, $\hat{\mathcal{I}}_{n_s\Delta v}$, which is represented as:

$$\alpha' = \underset{\alpha'}{\operatorname{argmin}} \sum_{n_s=1}^{N_s} \left| \mathcal{I}_{n_s\Delta v} - \hat{\mathcal{I}}_{n_s\Delta v} \right|, \tag{3.10}$$

where Δv is the step size; n_s is the index of step size; N_s is the total number of steps. The value of α' is more accurate when the step size Δv is smaller and N_s is greater. The estimated α' at different transmitter semi-angle is presented in Figure 3.9. Note that only a few points of α need to be calculated and a fourth-order polynomial is used for interpolation, which is:

$$\alpha' = -1.88 \times 10^{-8}\Phi_{tx}^4 + 4.80 \times 10^{-6}\Phi_{tx}^3 - 2.68 \times 10^{-4}\Phi_{tx}^2 + 0.0098\Phi_{tx} + 2.02. \tag{3.11}$$

Considering the simplified NLOS model, the optical power density of an arbitrary point on the ceiling, $\mathcal{I}_v$, can be calculated in closed-form using (3.8). As a result, the simplified model significantly reduces the computational complexity in comparison with the conventional ray-tracing model.

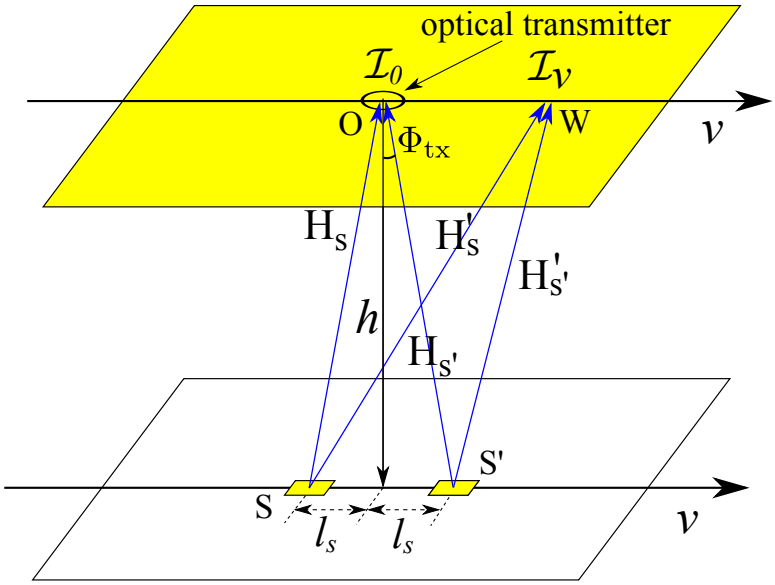

Figure 3.8: *The simplified propagation model for NLOS path I.*

3.3.2 NLOS Path II

For this path, the reflected light from the ceiling is transmitted to an optical receiver, as shown in Figure 3.10. Due to the limitation of the receiver FOV, only the reflected light within the grey area on the ceiling can be captured by the receiver. For optical receivers with narrow FOV, the optical power intensity of the reflected light in the grey area can be assumed as constant. In a 7-cell optical attocell network, NLOS ICI is generated by the six neighbouring APs. The distance between an interfering AP and the desired cell centre is $\sqrt{3}R_{\text{cell}}$. Therefore, the total NLOS ICI can be calculated as:

$$\begin{aligned} \mathcal{I}_{\text{NLOS}} &= 6\left[\int_0^{h\tan(\Psi_{\text{single}})} R\mathcal{I}_v 2\pi r' H(r')\mathrm{d}r'\right]^2 \\ &= 6\left[R\mathcal{I}_v A_{\text{eff}}\sin^2(\Psi_{\text{single}})\right]^2\Big|_{v=\sqrt{3}R_{\text{cell}}}. \end{aligned} \tag{3.12}$$

By using the proposed simplified NLOS model, the NLOS ICI received by an optical receiver can be calculated in closed-form by (3.12).

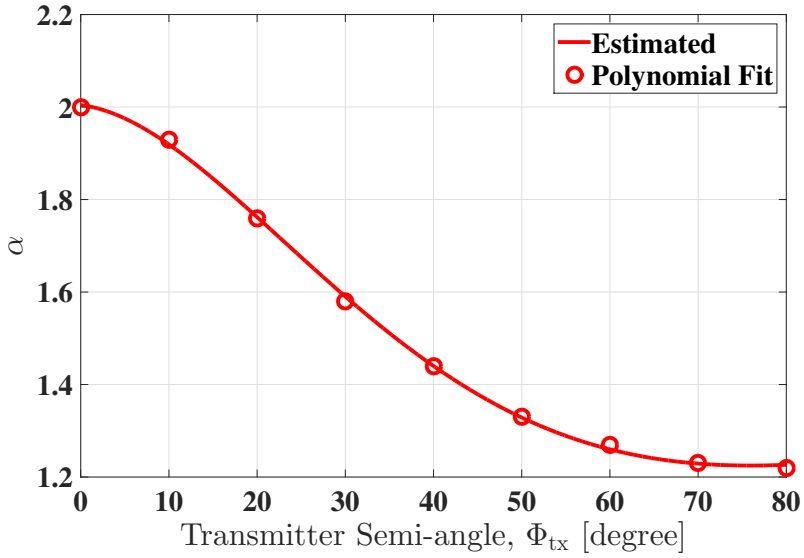

Figure 3.9: *The value of attenuation factor α at different transmitter semi-angle.*

3.4 Theoretical Derivation of the SINR Distribution of NLOS Interference

In this section, the CDF of the SINR of an optical attocell network is derived analytically. All users are assumed to be located within the central area of the desired cell, which is illustrated in Figure 3.5. The radius of the area is R_1. The horizontal distance between an active user and the desired cell centre is represented as r. The user location follows a uniform distribution and the PDF of r can be represented as:

$$f_r(r) = \frac{2r}{R_1^2}. \tag{3.13}$$

By considering the geometry relationship between the parameters: $d = h/\cos(\phi), \cos(\phi) = h/\sqrt{h^2 + r^2}, \psi = \phi$, (2.18) can be expressed as:

$$H(r) = \frac{(m+1)A_{\text{eff}}}{2\pi h^2} \left(\frac{h}{\sqrt{h^2 + r^2}} \right)^{m+3}. \tag{3.14}$$

Since an optical attocell network is usually interference limited [133], the signal-to-interference

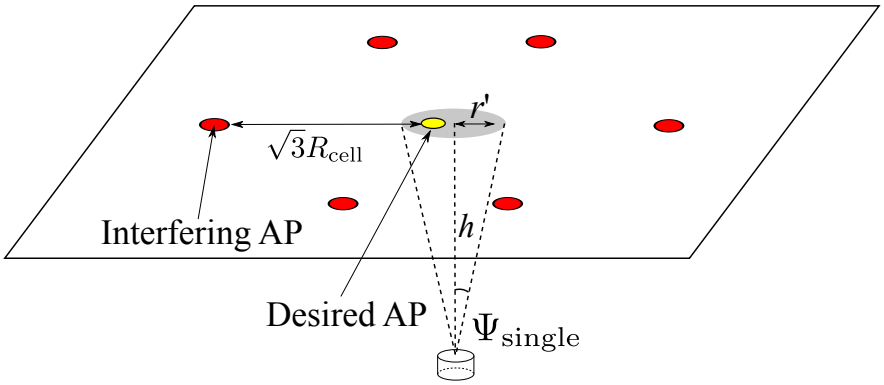

Figure 3.10: *The simplified propagation model for NLOS path II. Yellow spot represents the desire AP and red spots represent interfering APs.*

ratio (SIR) can be represented as:

$$\gamma(r) = \frac{\left(RP_{\text{tx}}H(r)\right)^2}{I_{\text{NLOS}} + N_0 B} \approx \frac{\left(RP_{\text{tx}}H(r)\right)^2}{I_{\text{NLOS}}}. \tag{3.15}$$

Considering the relationship $\gamma_{\text{dB}} = 10\log_{10}(\gamma)$ and probability density transform rule, the PDF of SIR γ_{dB} can be generated as:

$$f_{\gamma_{\text{dB}}}(\gamma_{\text{dB}}) = \frac{h^2 \ln 10}{10(m+3)R_1^2} \exp\left(-\frac{(\gamma_{\text{dB}} + \gamma_{\max})\ln 10}{10(m+3)}\right), \tag{3.16}$$

where $\gamma_{\max}$ is the maximum achievable SIR which exists at the cell centre which can be represented as:

$$\gamma_{\max} = 20\log_{10}\left(\frac{RP_{\text{tx}}(m+1)A_{\text{eff}}}{2\pi h^2}\right) - 10\log_{10}(I_{\text{NLOS}}). \tag{3.17}$$

The CDF of the SIR of an optical receiver in the optical attocell network can be represented in closed-form:

$$\begin{aligned} F(\gamma_{\text{dB}}) &= \int_{\gamma_{\min}}^{\gamma_{\text{dB}}} f(\gamma_{\text{dB}})\mathrm{d}\gamma_{\text{dB}} \\ &= -\frac{h^2}{R_1^2}\exp\left(-\frac{(\gamma_{\text{dB}} + \gamma_{\max})\ln 10}{10(m+3)}\right) + \frac{h^2}{R_1^2}\exp\left(-\frac{(\gamma_{\min} + \gamma_{\max})\ln 10}{10(m+3)}\right), \end{aligned} \tag{3.18}$$

where $\gamma_{\min}$ is the minimum achievable SIR which exists at the cell edge:

$$\gamma_{\min} = 10\log_{10}\left(\frac{\left(RP_{\text{tx}}H(R_1)\right)^2}{I_{\text{NLOS}}}\right). \tag{3.19}$$

Cell radius, R_{cell}	3 m
Responsivity, R	1 A/W
Room height, h	4 m
Surface half-intensity radiation angle, Φ_{ref}	60°
Refractive index, n_{ref}	1.5
Transmission Power of an AP, P_{tx}	1 W
Modulation Bandwidth, B	20 MHz
AWGN spectral density, N_0	10^{-21}A/Hz
Step size, Δv	0.05 m
Total step number, N_{s}	200

Table 3.1: *Simulation Parameters*

3.5 Computational Complexity

In terms of the computational complexity, the nondirected model described in [31] calculates the channel gain by dividing reflection surface into small pieces. This means that the computational complexity of this model depends on the size of the room and the area of each reflect element, ΔA. The total area of reflection surface is defined as A_{total}. Hence, according to [31], the computational complexity of the nondirected model is represented as $\mathcal{O}(n_{\text{elem}}^{i})$, where i is the reflection order and n_{elem} is the total number of reflection elements which can be calculated as $n_{\text{elem}} = \dfrac{A_{\text{total}}}{\Delta A}$.

In comparison, as discussed in the previous section, our proposed simplified model can be calculated in closed-form. That means the computational complexity of this simplified method does not depend on the size of the room. The computational complexity of the proposed model can be represented as $\mathcal{O}(1)$, which is of less computational complexity.

3.6 Results and Discussion

In this section, the CDF results using conventional ray-tracing method and the proposed simplified model are presented. The CDF results using a ray tracing technique is obtained by Monte-Carlo simulation and the CDF results using the proposed simplified model is generated analytically according to (3.18). In both scenarios, a 7-cell optical attocell network is assumed. Four different transmitter semi-angles are considered, which are 15^{o}, 30^{o}, 45^{o} and 60^{o}, respectively. All other parameters are presented in Table. 3.1.

The comparison between the CDF of SINR using ray-tracing and the the proposed simplified

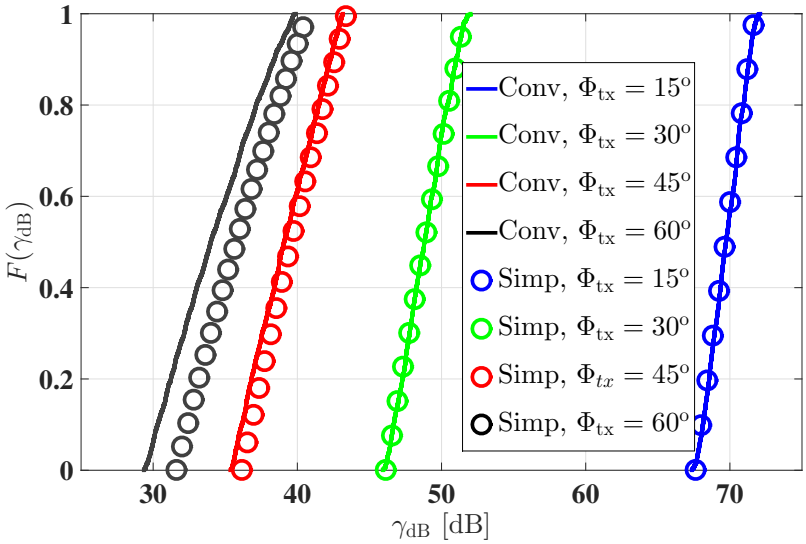

Figure 3.11: *The CDF of the SINR at the optical receiver in terms of different transmitter semi-angle Φ_{tx}. 'Conv' denotes the CDF results obtained by conventional ray-tracing model. 'Simp' denotes the CDF results generated by the simplified model.*

model is presented in Figure 3.11. There is a close agreement between the proposed simplified model and the conventional ray-tracing model, especially when the transmitter semi-angle of the optical receiver is small. The difference between the proposed simplified model and the ray-tracing model becomes greater when the transmitter semi-angle is large. This is because, for NLOS path I, the simplified model is nearly identical to the conventional ray-tracing model when the transmitter semi-angle is considerably small. The accuracy of the model decreases when the transmitter semi-angle increases. However, from an application perspective, optical attocell networks with smaller cell size can provide higher data density. In the small cell scenario, smaller transmitter semi-angle is preferred since it can effectively avoid inter-cell interference. This means that the proposed simplified NLOS propagation model is valid in most of the realistic scenarios and provide accurate closed-form performance estimation in optical attocell networks.

3.7 Summary

In this chapter, the conventional ray-tracing model for optical attocell networks is introduced. While achieving high accuracy, the ray-tracing model is of high computational complexity. In order to address this issue, a simplified model for NLOS propagation is proposed for evaluating

the performance of optical attocell networks. In comparison with the ray-tracing model, the simplified model only considers second-order reflections. Also, a new method for estimating light reflections is introduced. By implementing the simplified model, the SINR distribution of optical attocell networks can be derived analytically in closed-form which significantly reduces the calculation complexity in comparison with ray-tracing technique. By comparing the results of using the conventional ray-tracing model and the proposed simplified model, the accuracy of the simplified model is validated. Apart from optical attocell networks with single-element receiver, the proposed model can also be applied to the optical attocell networks that use angle diversity receivers and angle diversity transmitters.

Chapter 4
Interference Mitigation Techniques using Angle Diversity Receiver

4.1 Introduction

In this chapter, a novel inter-cell interference (ICI) mitigation technique which employs angle diversity receivers (ADRs) is proposed in optical attocell networks. The ADR in the proposed technology consists of multiple narrow field-of-view (FOV) photodiodes (PDs) with different orientations. This type of optical receiver can achieve a large coverage area without introducing extra ambient light and interference light. In [134–137], a single link from an optical transmitter to an ADR is investigated. The results show an improvement in terms of signal-to-noise ratio (SNR), transmission speed and coverage. In this work, four different signal combining schemes namely select best combining (SBC), the equal gain combining (EGC), maximum ratio combining (MRC) and optimum combining (OPC), are proposed for ADRs in optical attocell networks. Also, a novel double-source cell configuration consisting two transmission modes is designed which is shown to provide further improvements to system performance. A criteria of selecting transmission modes in double-source cell configuration is also determined. Finally, an analytical framework for evaluating the performance of an ADR in a hexagonal optical attocell network is introduced. It is further shown that the analytical results accurately predict and evaluate the performance of optical attocell networks.

The remainder of this chapter is organised as follows. Section 4.2 discusses the design of optical angle diversity receivers. Four different signal combining schemes for ADR are discussed in Section 4.3. The concepts of the optical double-source cell are introduced in Section 4.4. Theoretical analysis of the optical attocell networks are discussed in Section 4.5. The results and discussions are presented in Section 4.6. Finally, conclusions of the topic are given in Section 4.7.

4.2 Optical Angle Diversity Receivers

Three types of optical receivers are considered in optical attocell networks. For the purpose of fairness, the parameters of these optical receivers are chosen to make the overall coverage area of each optical receiver equal. The first type is a single-PD receiver with only one upward-pointing PD with a FOV of Φ_{single}. The second type is an ADR with 9 PDs. 9 PDs are chosen to ensure the angle diversity receiver has the same FOV with the single PD receiver. As shown in Figure 4.1, this ADR consists of an upward pointing PD which is surrounded by a ring of 8 PDs. The third type is an ADR with 20 PDs as shown in Figure 4.2. This ADR has an

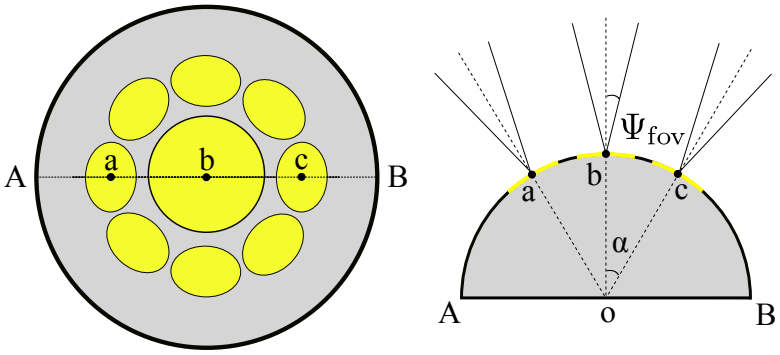

Figure 4.1: *The illustration of an ADR (9 PDs).*

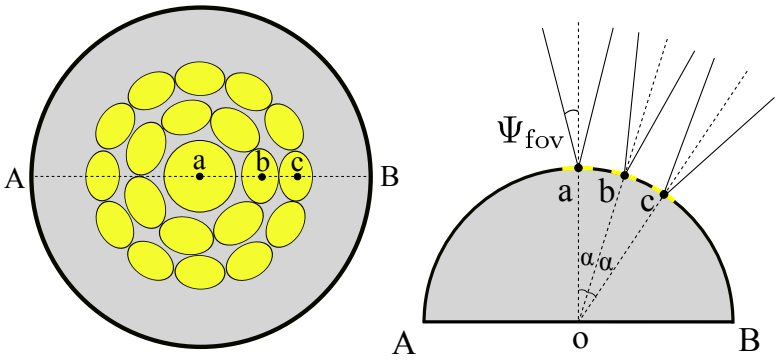

Figure 4.2: *The illustration of an ADR (20 PDs).*

upward-pointing PD which is surrounded by two rings of PDs. The number of PDs in each ring is 7 and 12, respectively. This can also ensure the FOV of the angle diversity receiver is similar to the single-PD receiver. Each PD on an ADR has the same FOV, Ψ_{ADR}. In addition, as shown in Figure 4.1 and Figure 4.2, α is defined as the tilted angle between the neighbouring rings. The tilted angle, α is designed so that the overlap between the coverage area of each PD is minimised. As a result, the ADR has a strong ability to separate different light sources. The coverage area of a single-PD receiver (S1) and the coverage area of each ADR (S2,S3) are illustrated in Figure 4.3.

In optical attocell networks, ICI can be reduced by increasing the number of PDs on an optical receiver, especially when PDs point to a different directions. The reasons for this are twofold. Firstly, since the overall coverage area of each optical receiver is identical, the optical receiver with more PDs can have a narrower FOV for each PD. A narrow FOV PD can effectively reject the line-of-sight (LOS) ICI. Secondly, due to the dispersive nature of light reflections, a

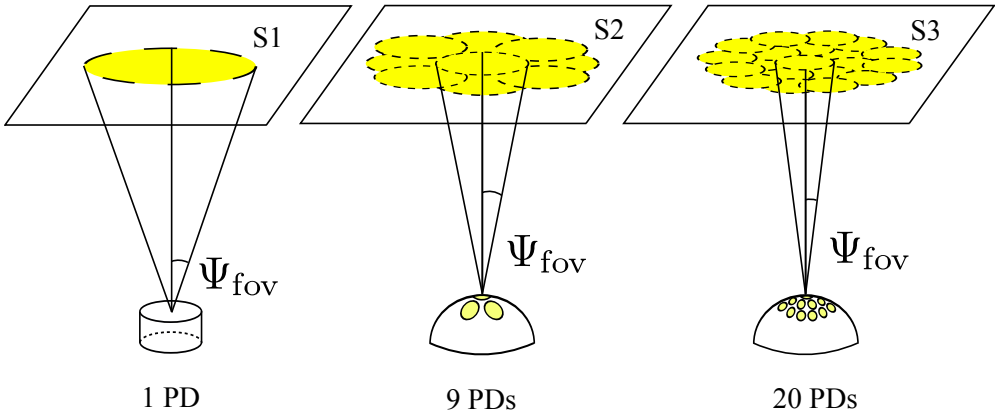

Figure 4.3: *The coverage area of each type of optical receivers on the ceiling. The overall coverage area of an ADR is the union of the individual coverage areas of each PD on that ADR. The coverage area of the single-PD receiver is defined by the only PD.*

narrow FOV PD can significantly mitigate the non-line-of-sight (NLOS) ICI because it collects less light from reflections. Secondly, as the number of individual detector elements on a receiver increases, the granularity of the receiver increases. This results in the better capability of suppressing ICI.

4.3 Signal Combining Schemes for ADR

An ADR consists of multiple PD elements with different orientations. It can significantly mitigate ICI if proper signal combining schemes are used. Therefore, four popular signal combining schemes in radio frequency (RF), namely SBC, EGC, MRC and OPC, are adapted and implemented to the proposed ADRs. The detail of these signal combining schemes are described later in this section.

Similar to RF [138], it is assumed that a user chooses an access point (AP) that provides the strongest signal as:

$$a_{\mathrm{d}} = \underset{a}{\operatorname{argmax}} \sum_{p=1}^{N_{\mathrm{PD}}} \left| H_{a,p} \right|^2. \tag{4.1}$$

The ADR combines the received signals from its PDs. According to [1], the signal-to-interference-

plus-noise ratio (SINR) of the desired user after signal combining is given by:

$$\gamma = \frac{\left(\sum_{p=1}^{N_{\mathrm{PD}}} RP_{\mathrm{tx}} w_p H_{a_{\mathrm{d}},p}\right)^2}{\sum_{p=1}^{N_{\mathrm{PD}}} w_p^2 N_0 B + \sum_{a=1,a\neq a_{\mathrm{d}}}^{N_{\mathrm{AP}}} \left(RP_{\mathrm{tx}} \sum_{p=1}^{N_{\mathrm{PD}}} w_p H_{a,p}\right)^2}, \tag{4.2}$$

where w_p is the weight of the PD p; N_0 is the additive white Gaussian noise (AWGN) power spectral density; B is the communication bandwidth; P_{tx} is the transmission power of an optical AP. If N_{PD} is set to be 1, (4.2) represents the SINR of an user with a single-PD receiver.

In different combining schemes, the weights are evaluated differently, and requires the knowledge of channel state information (CSI) at the ADR. In this study, CSI is assumed as channel direct current (DC) gain, H, and usually ADR acquires CSI through pilot sequences.

4.3.1 SBC scheme

In SBC, only the signal from the PD which has the highest received SNR is selected. All the signals from other PDs are discarded. The index of the desired PD is determined by:

$$p_{\mathrm{d}} = \underset{p}{\mathrm{argmax}} \frac{\left(RP_{\mathrm{tx}} H_{a_{\mathrm{d}},p}\right)^2}{N_0 B}. \tag{4.3}$$

The weight of PDs is:

$$w_p = \begin{cases} 1 & p = p_{\mathrm{d}} \\ 0 & \text{otherwise.} \end{cases} \tag{4.4}$$

The weight of PDs is determined by the knowledge of CSI. According to (4.3), only the knowledge of CSI from the desired cell to a user is required. The knowledge of CSI from the other interfering APs to the user is unnecessary. In terms of the circuit design, a switch is required for selecting the signals from the desired PD.

4.3.2 EGC scheme

The EGC is a simple signal combining scheme in which signals from all PDs are combined with equal weights giving $w_p = 1$.

The EGC requires only a simple adder for the combining circuit. No knowledge of CSI from any AP to a user is required for signal combining. Since optical power from multiple PDs is added up, the received optical power using EGC is higher than the optical power using SBC. However, as the signal from each PD is equally weighted, co-channel interference cannot be suppressed effectively which could result in poor overall SINR performance.

4.3.3 MRC scheme

In MRC, weights w_p, are proportional to the SNR [139] on each PD, which is:

$$w_p = \frac{\left(RP_{\mathrm{tx}}H_{a_{\mathrm{d}},p}\right)^2}{N_0B}. \tag{4.5}$$

Here, $H_{a_{\mathrm{d}},p}$ can be determined by pilot sequence and N_0B can be determined at the optical detector by setting all optical APs to transmit constant light. It is notable that, since the symbol duration is expected to be long enough, the time difference caused by the geometry of an angle diversity receiver can be negligible. That means the signals can be regarded as coherent.

Similar to SBC, MRC only requires knowledge of CSI from the desired AP to a user. For circuit design, a multiplier and an adder are necessary for combining the received signals. With a proper weight on each PD, MRC should boost the desired signal components and attenuates ICI and noise components which should result in a high overall SINR.

4.3.4 OPC scheme

If there is no ICI, MRC can provide the optimum SNR [140]. However, in the proposed optical attocell network, both LOS and NLOS ICI components from the neighbouring APs can be received. The correlation between interference terms at different PDs significantly affects the performance of MRC. As a consequence, OPC is considered. OPC was initially used in RF scenario [140] and is firstly proposed for an visible light communication (VLC) system. It mitigates ICI by considering an interference-plus-noise correlation matrix which can significantly suppress the correlated interference. In OPC, weights are calculated as follows:

$$\mathbf{w} = \xi\mathbf{R}_{nn}^{-1}\mathbf{u}_{a_{\mathrm{d}}}, \tag{4.6}$$

where the signals received from the desired AP $\mathbf{u}_{a_\mathrm{d}}$ is:

$$\mathbf{u}_{a_\mathrm{d}} = [RP_\mathrm{tx}H_{a_\mathrm{d},1}, RP_\mathrm{tx}H_{a_\mathrm{d},2}, \cdots, RP_\mathrm{tx}H_{a_\mathrm{d},N_\mathrm{PD}}]^T; \tag{4.7}$$

and a vector with the different weight is represented as:

$$\mathbf{w} = [w_1, w_2, \cdots, w_{N_\mathrm{PD}}]^T; \tag{4.8}$$

ξ is a scaling factor; the interference-plus-noise correlation matrix, $\mathbf{R}_{nn}$, is given by:

$$\mathbf{R}_{nn} = N_0 B\mathbf{I} + \sum_{a \neq a_\mathrm{d}} \left[\mathbf{u}_a \mathbf{u}_a^T\right]. \tag{4.9}$$

In (4.9), $\mathbf{I}$ is the identity matrix and $\mathbf{u}_a$ is the signals received from AP a:

$$\mathbf{u}_a = [RP_\mathrm{tx}H_{a,1}, RP_\mathrm{tx}H_{a,2}, \cdots, RP_\mathrm{tx}H_{a,N_\mathrm{PD}}]^T. \tag{4.10}$$

Compared with MRC, OPC not only requires knowledge of CSI from the desired AP to a user, but also the knowledge of CSI from all other interfering APs to the user in order to estimate the interference-plus-noise correlation matrix. However, by exploiting the correlation of interference received each PD, OPC can suppress the correlated interference and this is expected to achieve better SINR performance compared with MRC.

4.4 Double-source Optical Cell

The existing optical attocell has a single AP at each cell centre. Although common, this configuration cannot fully exploit the spatial diversity of ADRs since only a single transmitter element can be used in each cell. Hence, in this section, we increase the number of optical transmitters in each cell and propose a novel double-source cell configuration to further improve the performance of ADRs. As shown in Figure 4.4, in each double-source cell, there are two APs which are termed as the 'positive AP' and the 'negative AP'. The time domain signal transmitted by the 'positive AP' and the 'negative AP' are denoted as $S(t)$ and $S'(t)$, respectively. The dynamic range of them is from 0 to S_H.

In terms of illumination, when the distance between the 'positive AP' and the 'negative AP' is

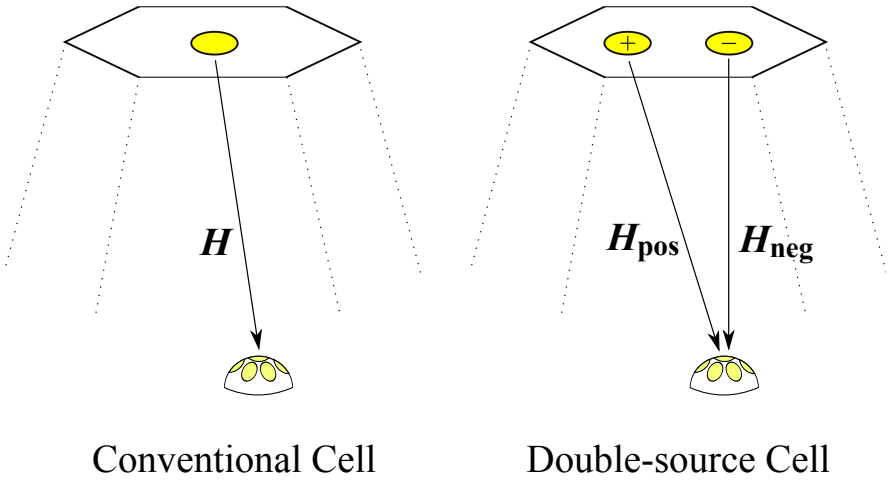

Figure 4.4: *The layout of a conventional optical cell and a double-source optical cell.*

small, the illumination condition of double source cell configuration is similar to that of single-cell configuration. However, when the distance between the 'positive AP' and the 'negative AP' is large, illumination condition will be different and might not meet the indoor illumination requirement. In this case, extra dummy light source can be added in the system to compensate the illumination.

4.4.1 Mode A

Two data transmission modes, mode A and mode B, are defined in double-source cell configuration. In mode A, the relationship between $S'(t)$ and $S(t)$ is represented as:

$$S'(t) = S_{\mathrm{H}} - S(t). \tag{4.11}$$

Since transmission power of an optical AP is defined as the standard deviation of the optical signal, the transmission power of the 'positive AP' and the 'negative AP' is obtained as:

$$\mathrm{P}_{\mathrm{tx,pos}} = \sqrt{\mathbb{E}\left[(S(t) - \mathbb{E}[S(t)])^2\right]}, \tag{4.12}$$

$$\begin{aligned}\mathrm{P}_{\mathrm{tx,neg}} &= \sqrt{\mathbb{E}\left[(S'(t) - \mathbb{E}[S'(t)])^2\right]} \\ &= \sqrt{\mathbb{E}\left[(S_{\mathrm{H}} - S(t) - \mathbb{E}[S_{\mathrm{H}} - S(t)])^2\right]} \\ &= \sqrt{\mathbb{E}\left[(S(t) - \mathbb{E}[S(t)])^2\right]}. \end{aligned} \tag{4.13}$$

Since the transmission power of the 'positive AP' and the 'negative AP' is the same, it is simply denoted as P_{tx}. Furthermore, the transmit power, P_{tx} is assumed to be the same for all APs. As we assume that the symbol duration of the system is much longer than the duration of channel impulse response, channel gain is regarded as non-time-dispersive and is represented by channel DC gain. Therefore, for a single optical cell, the received optical signal at a PD is represented as:

$$S_{\mathrm{sum}}(t) = S(t)H_{\mathrm{pos}} + S'(t)H_{\mathrm{neg}}. \tag{4.14}$$

Therefore, the received optical power at a PD is:

$$\begin{aligned}\mathrm{P}_{\mathrm{rx}} &= \sqrt{\mathbb{E}\left[(S_{\mathrm{sum}}(t) - \mathbb{E}[S_{\mathrm{sum}}(t)])^2\right]} \\ &= \sqrt{\mathbb{E}\left[(S(t)(H_{\mathrm{pos}} - H_{\mathrm{neg}}) - \mathbb{E}[S(t)(H_{\mathrm{pos}} - H_{\mathrm{neg}})])^2\right]} \\ &= \sqrt{\mathbb{E}\left[(S(t) - \mathbb{E}[S(t)])^2\right]}\,|H_{\mathrm{pos}} - H_{\mathrm{neg}}| \\ &= \mathrm{P}_{\mathrm{tx}}\Delta H, \end{aligned} \tag{4.15}$$

where H_{pos} is the channel gain between the 'positive AP' and the optical receiver and H_{neg} is the channel gain between the 'negative AP' and the optical receiver; ΔH denotes the difference between H_{pos} and H_{neg}.

It can be observed from (4.15) that the received signal power is scaled by the channel gain difference, ΔH. Generally, the desired cell is close to a receiver and the interfering cells are much farther. As illustrated in Figure 4.5, a receiver is underneath its desired cell and the channel gain difference ΔH of a PD is large. This is because, the PD has little chance to simultaneously receive LOS signals from the two APs due to the narrow FOV. Therefore, only one of H_{pos}, and H_{neg} appears in the LOS channel gain. Since the difference between LOS and NLOS channel gain is significant, the received optical signal is enhanced. It is also shown in Figure 4.5, a receiver is far from an interfering cell. The channel gains, H_{pos} and H_{neg} are both NLOS channel gains. The difference between them is small which means the received interference is attenuated. Hence, this configuration can effectively boost the signal from the desired cell and suppress the interference. Moreover, the double-source cell configuration is

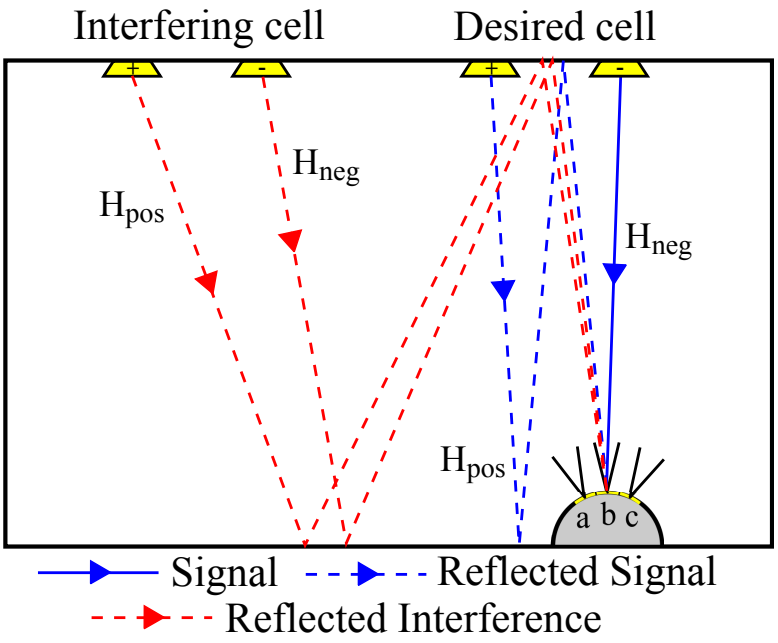

Figure 4.5: *The benefit of implementing a double-source cell configuration.*

easy to implement, since the signal from the 'negative AP' is simply an inverted version of the signal from the 'positive AP'. A practical differential light emitting diode (LED) driver for double-source cell configuration has been made and achieved high energy efficiency [85]. A prototype of a VLC system with double source cell configuration is subjected to future work.

4.4.2 Mode B

Transmission mode A can effectively suppress interference. However, mode A requires an optical receiver that has the ability to separate the signals from the 'positive AP' and 'negative AP' in the desired cell. If a receiver cannot distinguish them, the SINR performance of it will be significantly degraded, especially at the cell centre. In order to facilitate the receivers that cannot distinguish the signals from the 'positive AP' and 'negative AP' in their desired cells, another transmission mode, mode B, is proposed. In mode B, the relationship between $S(t)$ and $S'(t)$ is represented as:

$$S'(t) = S(t). \tag{4.16}$$

This means both APs transmit identical signals which is in the fashion of repetition coding. In order to optimise the system performance in double-source cell configuration, a criteria for transmission mode selection is necessary. Simulations and discussions on this criteria are pre-

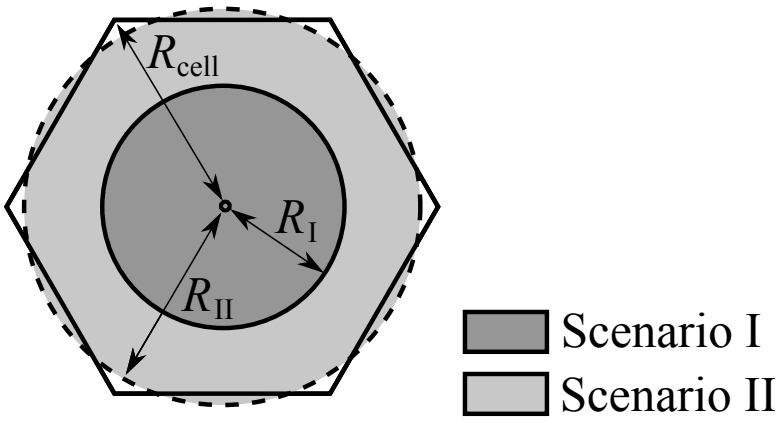

Figure 4.6: *The region of scenario I and scenario II for analysing a single-PD receiver. The region of scenario I is a circle with a radius of R_{I}. The region of scenario II is a circle ring.*

sented in Section 4.6.

4.5 Theoretical Performance for Different Types of Optical Receivers

In this section, a theoretical approach for analysing the performance of angle diversity receivers in optical attocell networks is presented. For simplicity, only the desired AP and the interfering APs in the vicinity of the desired cell are considered. Also, hexagonal cells are assumed. The proposed simplified model described in Chapter 3.3 is used for calculating NLOS interference.

4.5.1 SINR Statistic of Single-PD Receiver

The service quality in optical attocell networks is determined by the statistics of the received SINR. In this study, the distribution, especially the cumulative distribution function (CDF) of the SINR is derived to evaluate the performance of optical attocell networks. The simplified NLOS propagation model proposed in Chapter 3 is applied in the evaluation. Depending on the position of active users, the analysis at a single-PD receiver can be separated into the analysis of two scenarios, scenario I (cell centre) and scenario II (cell edge), as shown in Figure 4.6. For simplicity, the boundaries of scenario I and II are approximated as circles. The area of the approximated circle is equivalent to that of the original region, where $R_{\text{II}} \approx 0.91 R_{\text{cell}}$.

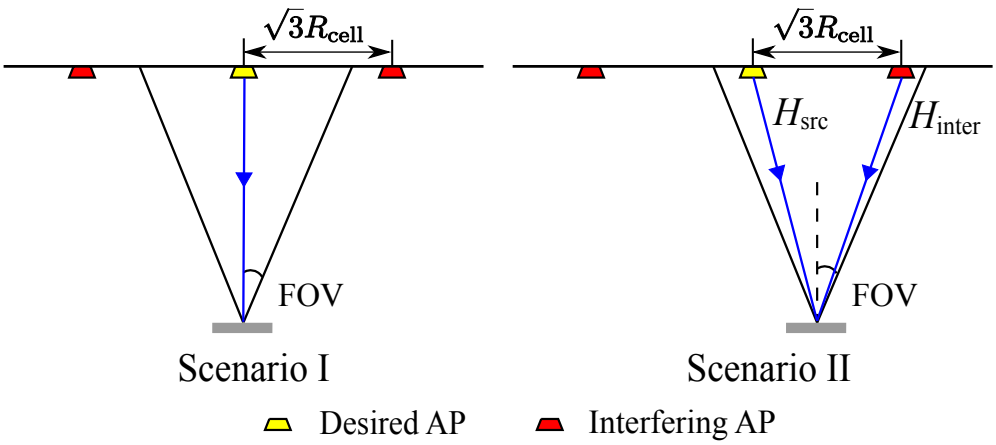

Figure 4.7: *The layout of scenario I and scenario II.*

4.5.1.1 Scenario I

As shown in Figure 4.6, users are uniformly distributed at the cell centre. There is no LOS ICI from the neighbouring optical cells (see Figure 4.7). The horizontal distance between an active user and its desired cell centre is defined as r. The probability density function (PDF) of r is given as:

$$f_{\text{I}}(r) = \frac{2r}{R_{\text{I}}^2}, \quad (0 \leq r \leq R_{\text{I}}) \tag{4.17}$$

where R_{I} is the radius of the circular region of scenario I. By considering the geometry relationship between the parameters: $d = h/\cos(\phi), \cos(\phi) = h/\sqrt{h^2 + r^2}, \psi = \phi$, (3.14) can be expressed as:

$$H(r, \Psi_{\text{single}}) = \frac{(m+1)A_{\text{eff}}(\Psi_{\text{single}})}{2\pi h^2} \left(\frac{h}{\sqrt{h^2 + r^2}} \right)^{m+3}, \tag{4.18}$$

where Ψ_{single} is the FOV of a single-PD receiver. Assuming that an attocell network is an interference limited system, the signal-to-interference ratio (SIR) can be represented as follows:

$$\gamma(r) = \frac{\left(RP_{\text{tx}} H(r, \Psi_{\text{single}}) \right)^2}{\mathcal{I}_{\text{NLOS}}(\Psi_{\text{single}}) + N_0 B} \approx \frac{\left(RP_{\text{tx}} H(r, \Psi_{\text{single}}) \right)^2}{\mathcal{I}_{\text{NLOS}}(\Psi_{\text{single}})}. \tag{4.19}$$

Defining that $\gamma_{\mathrm{dB}} = 10\log_{10}(\gamma)$, the PDF of SIR γ_{dB} can be rewritten as follows:

$$f_{\mathrm{I}}(\gamma_{\mathrm{dB}}) = \begin{cases} \dfrac{h^2 \ln 10}{10(m+3)R_{\mathrm{I}}^2} e^{-\frac{(\gamma_{\mathrm{dB}}+\gamma_{0,\mathrm{dB}})\ln 10}{10(m+3)}} & \gamma_{\mathrm{I,dB}} \leq \gamma_{\mathrm{dB}} \leq \gamma_{0,\mathrm{dB}} \\ 0 & \text{otherwise,} \end{cases} \tag{4.20}$$

where $\gamma_{0,\mathrm{dB}}$ is the maximum SIR at the cell centre ($r = 0$), which is represented as follows:

$$\gamma_{0,\mathrm{dB}} = 10\log_{10}\left(\frac{(RP_{\mathrm{tx}}H(0,\Psi_{\mathrm{single}}))^2}{\mathcal{I}_{\mathrm{NLOS}}(\Psi_{\mathrm{single}})}\right); \tag{4.21}$$

and $\gamma_{\mathrm{I,dB}}$ is the minimum SIR at the boundary of the region of scenario I ($r = R_{\mathrm{I}}$):

$$\gamma_{\mathrm{I,dB}} = 10\log_{10}\left(\frac{(RP_{\mathrm{tx}}H(R_{\mathrm{I}},\Psi_{\mathrm{single}}))^2}{\mathcal{I}_{\mathrm{NLOS}}(\Psi_{\mathrm{single}})}\right). \tag{4.22}$$

The closed-form CDF of the SIR for the scenario I is:

$$F_{\mathrm{I}}(\gamma_{\mathrm{dB}}) = \begin{cases} 0 & \gamma_{\mathrm{dB}} < \gamma_{\mathrm{I,dB}} \\ \dfrac{h^2}{R_{\mathrm{I}}^2}\left(-10^{-\frac{(\gamma_{\mathrm{dB}}+\gamma_{0,\mathrm{dB}})}{10(m+3)}} + 10^{-\frac{(\gamma_{\mathrm{I}}+\gamma_{0,\mathrm{dB}})}{10(m+3)}}\right) & \gamma_{\mathrm{I,dB}} \leq \gamma_{\mathrm{dB}} \leq \gamma_{0,\mathrm{dB}} \\ 1 & \gamma_{\mathrm{dB}} > \gamma_{0,\mathrm{dB}}. \end{cases} \tag{4.23}$$

4.5.1.2 Scenario II

As shown in Figure 4.6, users are uniformly distributed at the cell edge. LOS interference from the neighbouring cell can be received (see Figure 4.7). The PDF of r in scenario II can be represented as follows:

$$f_{\mathrm{II}}(r) = \frac{2r}{R_{\mathrm{II}}^2 - R_{\mathrm{I}}^2}, \quad (R_{\mathrm{I}} \leq r \leq R_{\mathrm{II}}), \tag{4.24}$$

where R_{II} is the outer radius of the region of scenario II.

In this scenario, LOS ICI can be received by users. Since the magnitude of the LOS ICI is a few orders of magnitude higher than the NLOS ICI and noise [133], NLOS ICI and noise are

assumed to be negligible. Hence, the SINR of the system can be approximated as follows:

$$\gamma(r) = \frac{\left(RP_{\mathrm{tx}}H_{\mathrm{src}}(r)\right)^2}{\left(RP_{\mathrm{tx}}H_{\mathrm{inter}}(r)\right)^2} = \left(\frac{h^2+r^2}{h^2+(\sqrt{3}R_{\mathrm{cell}}-r)^2}\right)^{-(m+3)}, \tag{4.25}$$

where $H_{\mathrm{src}}(r)$ is the link from desired AP to optical receiver; $H_{\mathrm{inter}}(r)$ is the link from interfering AP to optical receiver. The CDF of the SINR for the scenario II is:

$$F_{\mathrm{II}}(\gamma_{\mathrm{dB}}) = \begin{cases} 0 & \gamma_{\mathrm{dB}} < 0 \\ \dfrac{h^2+\tilde{r}}{R_{\mathrm{II}}^2-R_{\mathrm{I}}^2}\left(-10^{\frac{-\gamma_{\mathrm{dB}}}{10(m+3)}}+10^{\frac{-\gamma'_{\mathrm{dB}}}{10(m+3)}}\right) & 0 \le \gamma_{\mathrm{dB}} \le \gamma'_{\mathrm{dB}} \\ 1 & \gamma_{\mathrm{dB}} > \gamma'_{\mathrm{dB}}, \end{cases} \tag{4.26}$$

where $\tilde{r} = \sqrt{3}R_{\mathrm{cell}} - (R_{\mathrm{I}}+R_{\mathrm{II}})/2$ and consequently γ'_{dB} yields:

$$\gamma'_{\mathrm{dB}} = -10(m+3)\log_{10}\left(\frac{h^2+R_I^2}{h^2+(\sqrt{3}R_{\mathrm{cell}}-R_{\mathrm{I}})^2}\right). \tag{4.27}$$

4.5.1.3 Overall Theoretical Performance

Based on the results for scenario I and scenario II, the CDF of the SINR of a single-PD receiver in an optical attocell network can be derived. The PDF of r is given as:

$$f_{\mathrm{overall}}(r) = \frac{2r}{R_{\mathrm{II}}^2}, \quad (0 \le r \le R_{\mathrm{II}}), \tag{4.28}$$

where r is the radius of the polar coordinates of the user distribution.

When $0 < r \le R_{\mathrm{I}}$, the PDF of the SINR, γ_{dB}, can be derived and is similar to (4.20):

$$f_{\mathrm{overall}}(\gamma_{\mathrm{dB}}) = \frac{h^2\ln 10}{10(m+3)R_{\mathrm{II}}^2}e^{-\frac{(\gamma_{\mathrm{dB}}+\gamma_0)\ln 10}{10(m+3)}} = \frac{R_{\mathrm{I}}^2}{R_{\mathrm{II}}^2}f_{\mathrm{I}}(\gamma_{\mathrm{dB}}). \tag{4.29}$$

Similarly, when $R_{\mathrm{I}} < r \le R_{\mathrm{II}}$, the PDF of the SINR, γ_{dB}, can be calculated as follows:

$$f_{\mathrm{overall}}(\gamma_{\mathrm{dB}}) = \frac{R_{\mathrm{II}}^2-R_{\mathrm{I}}^2}{R_{\mathrm{II}}^2}f_{\mathrm{II}}(\gamma_{\mathrm{dB}}). \tag{4.30}$$

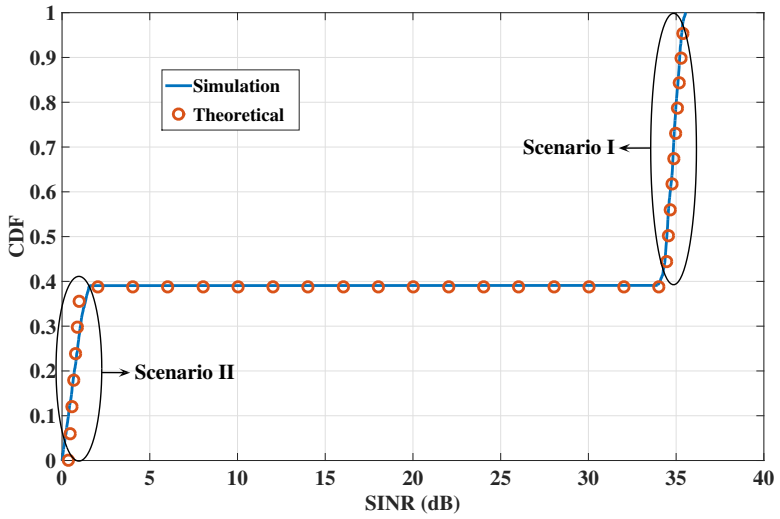

Figure 4.8: *The CDF of the received SINR when single-PD receivers are used. Solid line represents the simulation result and the round markers represents the theoretical result.*

Cell radius, R_{cell}	1.5 m
Transmission power, P_{tx}	1 W
The height of the room, h	3 m
Responsivity, r	0.5 A/W
The gain of the optical filter, G	1
Refractive index, n	1.5
Transmitter half-intensity radiation angle, θ_{tx}	25°
The physical area of a PD, A_{p}	5 mm^2
Modulation Bandwidth, B	20 MHz
AWGN spectral density, N_0	1×10^{-21}A^2 /Hz

Table 4.1: *Simulation Parameters*

Consequently, the CDF of the SINR yields:

$$\begin{aligned} F_{\text{overall}}(\gamma_{\text{dB}}) &= \int_{-\infty}^{\gamma_{\text{dB}}} f_{\text{overall}}(\gamma_{\text{dB}})\mathrm{d}\gamma_{\text{dB}} \\ &= \int_{-\infty}^{\gamma_{\text{dB}}} \frac{R_{\text{I}}^2}{R_{\text{II}}^2} f_{\text{I}}(\gamma_{\text{dB}}) + \frac{R_{\text{II}}^2 - R_{\text{I}}^2}{R_{\text{II}}^2} f_{\text{II}}(\gamma_{\text{dB}})\mathrm{d}\gamma_{\text{dB}} \\ &= \frac{R_{\text{I}}^2}{R_{\text{II}}^2} F_{\text{I}}(\gamma_{\text{dB}}) + \frac{R_{\text{II}}^2 - R_{\text{I}}^2}{R_{\text{II}}^2} F_{\text{II}}(\gamma_{\text{dB}}). \end{aligned} \tag{4.31}$$

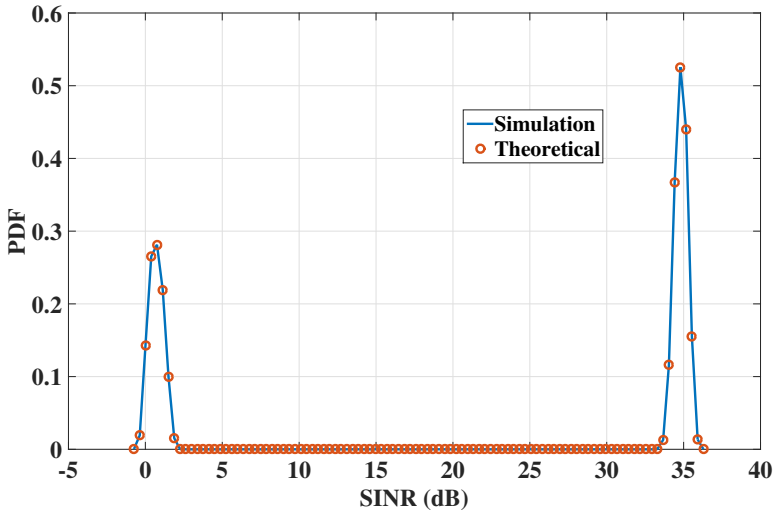

Figure 4.9: *The PDF of the received SINR when single-PD receivers are used. Solid line represents the simulation result and the round markers represents the theoretical result.*

4.5.1.4 Results for Single-PD Receivers

Both Monte Carlo simulation and theoretical results are performed in a 7-cell configuration. For Monte Carlo simulation, up to fourth order reflections are considered. Simulation parameters are listed in Table 4.1. The simulation and theoretical results of using a single-PD receiver is presented in Figure 4.8. The CDF of the SINR consists of two parts, the high SINR part and the low SINR part. The high SINR part corresponds to scenario I. Since users are distributed in cell centre, the limited FOV can reject the LOS interference from neighbouring cells which means only NLOS interference is presented. This results in a high received SINR. The low SINR part corresponds to scenario II. Strong LOS ICI at the cell edge results in low received SINR. It is notable that there is a sharp separation between the low SINR and high SINR part. This is because of the cut-off effect from the FOV-limited optical receiver. The reason of sharp rises in CDF can be explained by Figure 4.9. Figure 4.9 shows the PDF distribution of user SINR. It can be observed that the variance of SINR is very small. This is because the radius of optical cell is small in comparison with the height of the room. Therefore, the change of horizontal distance between the desired AP and its corresponding receiver does not significantly change the user SINR. Finally, the theoretical results show a close match to the simulation results which verifies the accuracy of the theoretical model. This figure clearly shows that the neglect of noise does not impact the accuracy of the theoretical results. This is because intercell interference is the limiting factor which is a few orders of magnitudes higher than noise [133].

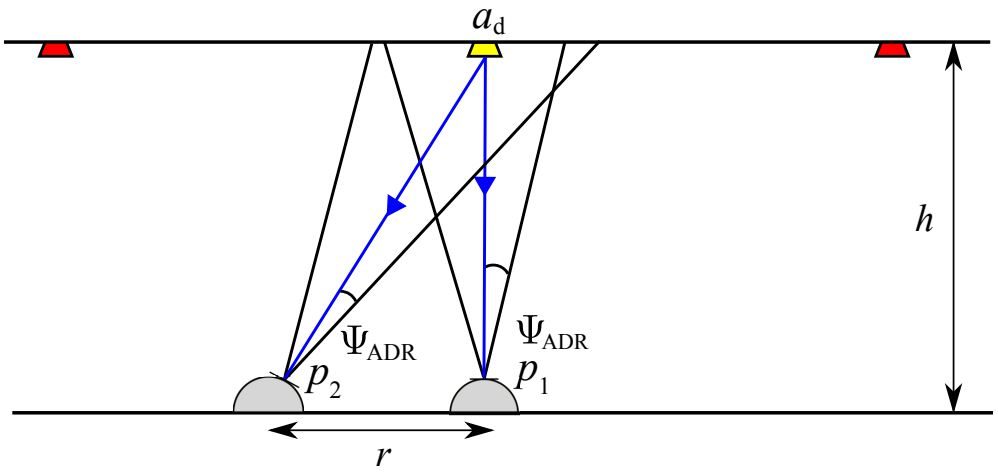

Figure 4.10: *The generalisation of scenario I. The desire AP a_{d} is represented in yellow; the interfering AP s are represented in red.*

4.5.2 SINR Statistics of Angle Diversity Receiver

The theoretical tools developed for analysing single-PD receivers can be generalised to ADRs. For simplicity, it is assumed that each PD on an ADR covers a different direction and there is no overlap between the aperture of each PD. This means that one PD can establish at most one LOS link with a desired AP.

4.5.2.1 SBC

As shown in Figure 4.10, a user in the cell centre selects the upward pointing PD, p_1 to achieve the best SINR performance. The SIR of the user can be derived as follows:

$$\gamma_{\mathrm{SBC,centre}}(r) = \frac{\left(RP_{\mathrm{tx}}H(r,\Psi_{\mathrm{ADR}})\right)^2}{\mathcal{I}_{\mathrm{NLOS}}(\Psi_{\mathrm{ADR}})}, \tag{4.32}$$

where Ψ_{ADR} is the FOV of PDs on an ADR; $\mathcal{I}_{\mathrm{NLOS}}(\Psi_{\mathrm{ADR}})$ is the NLOS interference received by p_1. A user at the cell edge selects PD, p_2 to achieve the best SIR, and the SIR of the user is:

$$\gamma_{\mathrm{SBC,edge}}(r) = \frac{\left(RP_{\mathrm{tx}}H(r,\Psi_{\mathrm{ADR}})\right)^2}{\mathcal{I}'_{\mathrm{NLOS}}(\Psi_{\mathrm{ADR}})}, \tag{4.33}$$

where $\mathcal{I}'_{\mathrm{NLOS}}$ is the NLOS interference received by p_2. According to [141], when p_1 and p_2 have identical FOV, $\mathcal{I}_{\mathrm{NLOS}}(\Psi_{\mathrm{ADR}}) = \mathcal{I}'_{\mathrm{NLOS}}(\Psi_{\mathrm{ADR}})$. This means the SIR of the optical

receiver can be represented by (4.32) in both cell centre and cell edge area. Therefore, the PDF of the SIR, γ_{dB}, can be calculated by:

$$f_{\mathrm{SBC}}(\gamma_{\mathrm{dB}}) = \int_0^{0.91R_{\mathrm{cell}}} 10\log_{10}\left(\gamma_{\mathrm{SBC,centre}}(r)\right) f_{\mathrm{overall}}(r)\mathrm{d}r. \tag{4.34}$$

This can be simplified as follows:

$$f_{\mathrm{SBC}}(\gamma_{\mathrm{dB}}) = \begin{cases} \dfrac{h^2 \ln 10}{10(m+3)R_{\mathrm{II}}^2} e^{-\frac{(\gamma_{\mathrm{dB}}+\gamma_0)\ln 10}{10(m+3)}} \\ \qquad\qquad \gamma_{\mathrm{II,SBC}} \leq \gamma_{\mathrm{dB}} \leq \gamma_{0,\mathrm{SBC}} \\ 0 \qquad\qquad \text{otherwise,} \end{cases} \tag{4.35}$$

where $\gamma_{0,\mathrm{SBC}}$ is the SIR at $r = 0$:

$$\gamma_{0,\mathrm{SBC}} = 10\log_{10}\left(\frac{(RP_{\mathrm{tx}}H(0,\Psi_{\mathrm{ADR}}))^2}{\mathcal{I}_{\mathrm{NLOS}}(\Psi_{\mathrm{ADR}})}\right), \tag{4.36}$$

and $\gamma_{\mathrm{II,SBC}}$ is the SIR at $r = R_{\mathrm{II}}$:

$$\gamma_{\mathrm{II,SBC}} = 10\log_{10}\left(\frac{(RP_{\mathrm{tx}}H(R_{\mathrm{II}},\Psi_{\mathrm{ADR}}))^2}{\mathcal{I}_{\mathrm{NLOS}}(\Psi_{\mathrm{ADR}})}\right). \tag{4.37}$$

The CDF of the SIR of SBC scheme can be determined as follows:

$$F_{\mathrm{SBC}}(\gamma_{\mathrm{dB}}) = \begin{cases} 0 \qquad\qquad \gamma_{\mathrm{dB}} < \gamma_{\mathrm{II,SBC}} \\ \dfrac{h^2}{R_{\mathrm{II}}^2}\left(-10^{-\frac{\gamma_{\mathrm{dB}}+\gamma_{0,\mathrm{SBC}}}{10(m+3)}} + 10^{-\frac{\gamma_{\mathrm{II,SBC}}+\gamma_{0,\mathrm{SBC}}}{10(m+3)}}\right) \\ \qquad\qquad \gamma_{\mathrm{II,SBC}} \leq \gamma_{\mathrm{dB}} \leq \gamma_{0,\mathrm{SBC}} \\ 1 \qquad\qquad \gamma_{\mathrm{dB}} > \gamma_{0,\mathrm{SBC}}. \end{cases} \tag{4.38}$$

4.5.2.2 EGC

In cell centres, the received signal of a user using EGC is similar to that of SBC. This is because, as discussed in the assumption, only one of the PDs can receive the LOS signal from the desired cell. However, since the weights of all PDs are identical, the received NLOS ICI increases when the number of PDs on the receiver increases. Therefore, the SIR can be approximated as

follows:

$$\gamma_{\mathrm{EGC,centre}}(r) \approx \frac{\left(RP_{\mathrm{tx}}H(r,\Psi_{\mathrm{ADR}})\right)^2}{M^2\mathcal{I}_{\mathrm{NLOS}}(\Psi_{\mathrm{ADR}})}. \tag{4.39}$$

Similarly, the SIR of cell edge users can also be approximated as follows:

$$\gamma_{\mathrm{EGC,edge}}(r) = \frac{\left(RP_{\mathrm{tx}}H_{\mathrm{src}}(r,\Psi_{\mathrm{ADR}})\right)^2}{\left(RP_{\mathrm{tx}}H_{\mathrm{inter}}(r,\Psi_{\mathrm{ADR}})\right)^2}. \tag{4.40}$$

Similar to the derivation in Section 4.5.1, the CDF of SIR, γ_{dB} in EGC can be approximated as follows:

$$F_{\mathrm{EGC}}(\gamma_{\mathrm{dB}}) \approx \frac{R_{\mathrm{I}}^2}{R_{\mathrm{II}}^2}F_{\mathrm{EGC,centre}}(\gamma_{\mathrm{dB}}) + \frac{R_{\mathrm{II}}^2 - R_{\mathrm{I}}^2}{R_{\mathrm{II}}^2}F_{\mathrm{EGC,edge}}(\gamma_{\mathrm{dB}}), \tag{4.41}$$

where $F_{\mathrm{EGC,edge}}(\gamma_{\mathrm{dB}}) = F_{\mathrm{II}}(\gamma_{\mathrm{dB}})$ and $F_{\mathrm{EGC,centre}}(\gamma_{\mathrm{dB}})$ is:

$$F_{\mathrm{EGC,centre}}(\gamma_{\mathrm{dB}}) = \begin{cases} 0 & \gamma_{\mathrm{dB}} < \gamma_{\mathrm{I,EGC}} \\ \dfrac{h^2}{R_{\mathrm{I}}^2}\left(-10^{-\frac{(\gamma_{\mathrm{dB}}+\gamma_{0,\mathrm{EGC}})}{10(m+3)}} + 10^{-\frac{(\gamma_{\mathrm{I,EGC}}+\gamma_{0,\mathrm{EGC}})}{10(m+3)}}\right) & \\ & \gamma_{\mathrm{I,EGC}} \le \gamma_{\mathrm{dB}} \le \gamma_{0,\mathrm{EGC}} \\ 1 & \gamma_{\mathrm{dB}} > \gamma_{0,\mathrm{EGC}}. \end{cases} \tag{4.42}$$

Here, $\gamma_{0,\mathrm{EGC}}$ is the SIR at the cell centre ($r = 0$):

$$\gamma_{0,\mathrm{EGC}} = 10\log_{10}\left(\frac{(RP_{\mathrm{tx}}H(0,\Psi_{\mathrm{single}}))^2}{M^2\mathcal{I}_{\mathrm{NLOS}}(\Psi_{\mathrm{ADR}})}\right); \tag{4.43}$$

and γ_{I} is the SIR at the boundary of scenario I ($r = R_{\mathrm{I}}$):

$$\gamma_{\mathrm{I,EGC}} = 10\log_{10}\left(\frac{(RP_{\mathrm{tx}}H(R_{\mathrm{I}},\Psi_{\mathrm{single}}))^2}{M^2\mathcal{I}_{\mathrm{NLOS}}(\Psi_{\mathrm{ADR}})}\right). \tag{4.44}$$

4.5.2.3 MRC

In MRC, different weights will be allocated to different PDs according to their SIR. Therefore, the SIR of a user when using MRC can be represented as:

$$\gamma_{\mathrm{MRC}} = \frac{\left(RP_{\mathrm{tx}}\sum_{p=1}^{N_{\mathrm{PD}}} w_p H_{a_{\mathrm{d}},p}\right)^2}{\mathcal{I}_{\mathrm{NLOS,MRC}}}, \tag{4.45}$$

where $\mathcal{I}_{\mathrm{NLOS,MRC}}$ is NLOS ICI when MRC is used. According to the assumption that only one of the PD can establish LOS link to the source AP, it can be concluded that:

$$w_{p_\mathrm{d}} \gg w_{p\neq p_\mathrm{d}}. \tag{4.46}$$

The LOS links have the highest SIR, and thus contributes the most to the received signal. Therefore, (4.45) can be approximated as follows:

$$\begin{aligned}\gamma_{\mathrm{MRC}}(r) &\approx \frac{\Big(RP_{\mathrm{tx}}w_{p_\mathrm{d}}H(r,\Psi_{\mathrm{ADR}})\Big)^2}{w_{p_\mathrm{d}}^2\mathcal{I}_{\mathrm{NLOS}}(\Psi_{\mathrm{ADR}})} \\ &= \frac{\Big(RP_{\mathrm{tx}}H(r,\Psi_{\mathrm{ADR}})\Big)^2}{\mathcal{I}_{\mathrm{NLOS}}(\Psi_{\mathrm{ADR}})}.\end{aligned} \tag{4.47}$$

After the approximation, (4.47) and (4.32) are identical. Hence, the CDF of the SIR for MRC is: $F_{\mathrm{MRC}}(\gamma_{\mathrm{dB}}) = F_{\mathrm{SBC}}(\gamma_{\mathrm{dB}})$.

4.5.2.4 OPC

OPC mitigates NLOS ICI by exploiting CSI of NLOS ICI. The SINR of OPC can be calculated as follows:

$$\gamma_{\mathrm{OPC}} = \frac{\Big(\sum_{p=1}^{N_{\mathrm{PD}}} Rw_pP_{\mathrm{tx}}H_{a_\mathrm{d},p}\Big)^2}{\mathcal{I}_{\mathrm{NLOS,OPC}} + \sum_{p=1}^{N_{\mathrm{PD}}} w_p^2N_0B}, \tag{4.48}$$

where $\mathcal{I}_{\mathrm{NLOS,OPC}}$ is NLOS ICI. Similar to MRC, the SINR of OPC can be further approximated as follows:

$$\gamma_{\mathrm{OPC}}(r) \approx \frac{\Big(RP_{\mathrm{tx}}w_{p_\mathrm{d}}H(r,\Psi_{\mathrm{ADR}})\Big)^2}{\mathcal{I}_{\mathrm{NLOS,OPC}} + \sum_{p=1}^{N_{\mathrm{PD}}} w_p^2N_0B}. \tag{4.49}$$

The proof of (4.49) is provided in Appendix A.1. Since the NLOS ICI can be effectively suppressed in OPC, an upper bound of the OPC can be established:

$$\gamma_{\mathrm{OPC,UB}}(r) = \frac{\Big(RP_{\mathrm{tx}}H(r,\Psi_{\mathrm{ADR}})\Big)^2}{N_0B} > \gamma_{\mathrm{OPC}}(r). \tag{4.50}$$

The proof of (4.50) is provided in Appendix A.1. The CDF of the SIR for the upper bound, $F_{\mathrm{OPC,UB}}(\gamma_{\mathrm{dB}})$ is as follows:

$$F_{\mathrm{OPC,UB}}(\gamma_{\mathrm{dB}}) = \begin{cases} 0 & \gamma_{\mathrm{dB}} < \gamma_{\mathrm{II,OPC}} \\ \dfrac{h^2}{R_{\mathrm{II}}^2}\left(-10^{-\frac{(\gamma_{\mathrm{dB}}+\gamma_{0,\mathrm{OPC}})}{10(m+3)}} + 10^{-\frac{(\gamma_{\mathrm{II,OPC}}+\gamma_{0,\mathrm{OPC}})}{10(m+3)}}\right) & \\ & \gamma_{\mathrm{II,OPC}} \leq \gamma_{\mathrm{dB}} \leq \gamma_{0,\mathrm{OPC}} \\ 1 & \gamma_{\mathrm{dB}} > \gamma_{0,\mathrm{OPC}}, \end{cases} \tag{4.51}$$

where $\gamma_{\mathrm{II,OPC}}$ can be represented as follows:

$$\gamma_{\mathrm{II,OPC}} = 10\log_{10}\left(\frac{\left(RP_{\mathrm{tx}}H(R_{\mathrm{II}}, \Psi_{\mathrm{ADR}})\right)^2}{N_0 B}\right), \tag{4.52}$$

and $\gamma_{0,\mathrm{OPC}}$ can be represented as follows:

$$\gamma_{0,\mathrm{OPC}} = 10\log_{10}\left(\frac{\left(RP_{\mathrm{tx}}H(0, \Psi_{\mathrm{ADR}})\right)^2}{N_0 B}\right). \tag{4.53}$$

4.5.3 SINR Statistics of Double-source Cell Configuration

In double-source cell configuration, the distance between two APs in the same cell is designed in such a way that no PD on an ADR can simultaneously receive LOS light signals from two APs in the desired cell. Defining the distance as d_{double}, this relationship can be represented as:

$$d_{\mathrm{double}} \geq 2h\tan(\Phi_{\mathrm{fov}}). \tag{4.54}$$

In this section, the SINR performance of ADR in double-source cell configuration using mode A is analysed. Since 'positive AP' and 'negative AP' are close to their cell centre, the LOS channel gain of them is calculated by (5.12).

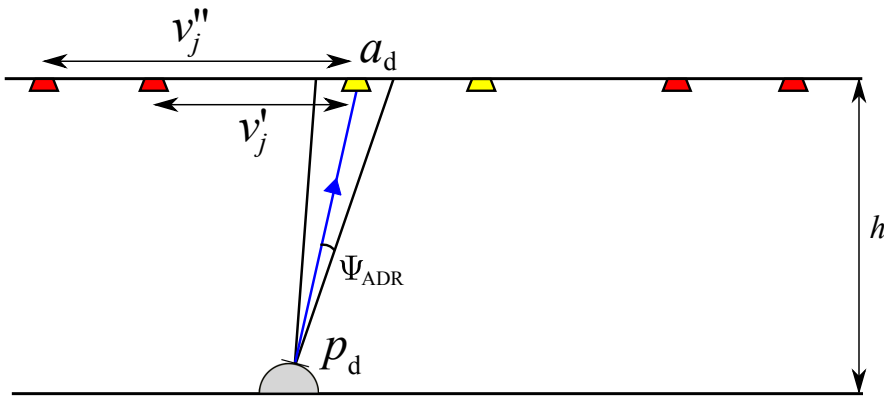

Figure 4.11: *The SBC in double source cell configuration.*

4.5.3.1 SBC

As illustrated in Figure 4.11, the ADR using SBC choose one AP to establish a LOS link. Similar to (4.32), the SINR of a user can be approximated as follows:

$$\gamma_{\mathrm{SBC}}^{\mathrm{double}}(r) = \frac{\left(\frac{1}{2}P_{\mathrm{tx}}RH(r,\Psi_{\mathrm{ADR}})\right)^2}{\mathcal{I}_{\mathrm{NLOS,SBC}}^{\mathrm{double}}(\Psi_{\mathrm{ADR}})}. \tag{4.55}$$

According to (4.15) and (3.12), the total NLOS interference, $\mathcal{I}_{\mathrm{NLOS,SBC}}^{\mathrm{double}}(\Psi_{\mathrm{ADR}})$, for a double-source cell configuration can be represented as follows:

$$\mathcal{I}_{\mathrm{NLOS,SBC}}^{\mathrm{double}}(\Psi_{\mathrm{ADR}}) = A_{\mathrm{eff}}^2 R^2 \sin^2(\Psi_{\mathrm{ADR}}) \sum_j \left| I_{v_j'} - I_{v_j''} \right|^2, \tag{4.56}$$

where j is the index of an interfering optical cell; v_j' represents the distance from the desired AP to a 'positive AP' in cell j; v_j'' represents the distance from the desired AP to a 'negative AP' in cell j. The CDF of the SINR when SBC is used in double source cell configuration can be derived using a method similar to the analysis of single source cell configuration in Section 4.5.1.

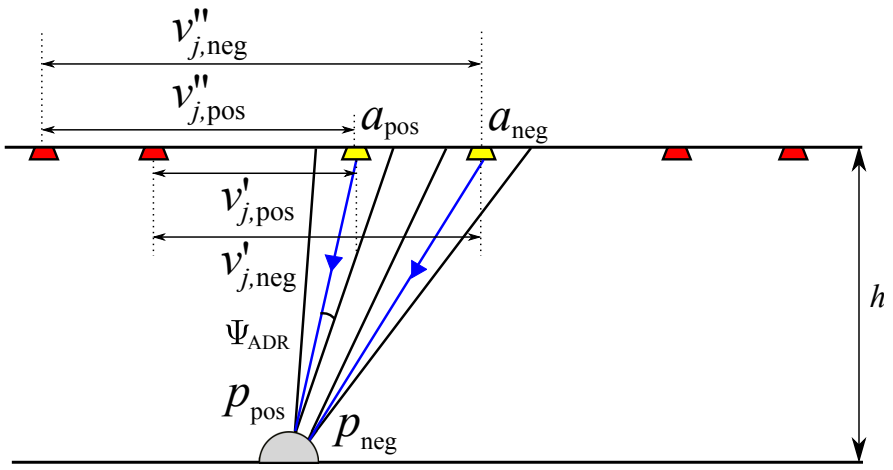

Figure 4.12: *The MRC scheme in double source cell configuration.*

4.5.3.2 MRC

As illustrated in Figure 4.12, ADR using MRC can establish two LOS links with both 'positive AP' and 'negative AP'. The SINR of an active user can therefore be calculated as:

$$\gamma_{\text{MRC}}^{\text{double}} = \frac{\left(\frac{1}{2}RP_{\text{tx}}\left(w_{p_{\text{pos}}}H_{a_{\text{pos}},p_{\text{pos}}} + w_{p_{\text{neg}}}H_{a_{\text{neg}},p_{\text{neg}}}\right)\right)^2}{\mathcal{I}_{\text{NLOS,MRC}}^{\text{double}}(\Psi_{\text{ADR}})}, \tag{4.57}$$

where $\mathcal{I}_{\text{NLOS,MRC}}^{\text{double}}(\Psi_{\text{ADR}})$ is the power of NLOS ICI in double source cell configuration when MRC is used. Since the distance between 'positive AP' and 'negative AP' in the desired cell is much smaller than the cell cell size and the transmission power of them is the same, the relationship between the channel gain $H_{a_{\text{pos}},p_{\text{pos}}}$ and $H_{a_{\text{neg}},p_{\text{neg}}}$ is:

$$H_{a_{\text{pos}},p_{\text{pos}}} \approx H_{a_{\text{neg}},p_{\text{neg}}}. \tag{4.58}$$

According to (4.5) and (4.58), the relationship between the weights of PDs is:

$$w_{p_{\text{pos}}} \approx w_{p_{\text{neg}}}. \tag{4.59}$$

To this end, (4.57) can be approximated as follows:

$$\gamma_{\text{MRC,double}}(r) \approx \frac{\left(RP_{\text{tx}}H(r,\Psi_{\text{ADR}})\right)^2}{\mathcal{I}'^{\text{double}}_{\text{NLOS,MRC}}(\Psi_{\text{ADR}})}, \tag{4.60}$$

where $\mathcal{I}'^{\text{double}}_{\text{NLOS,MRC}}(\Psi_{\text{ADR}})$ is represented as follows:

$$\mathcal{I}'^{\text{double}}_{\text{NLOS,MRC}}(\Psi_{\text{ADR}}) = A_{\text{eff}}^2 R^2 \sin^2(\Psi_{\text{ADR}}) \sum_j \left(\left| \mathcal{I}_{v'_{j,\text{pos}}} - \mathcal{I}_{v''_{j,\text{pos}}} \right| + \left| \mathcal{I}_{v'_{j,\text{neg}}} - \mathcal{I}_{v''_{j,\text{neg}}} \right| \right)^2, \tag{4.61}$$

where $v'_{j,\text{pos}}$ is the horizontal distance between a 'positive AP' in interfering cell j and the 'positive AP' in the desired cell; $v'_{j,\text{neg}}$ is the horizontal distance between a 'positive AP' in the interfering cell j and the 'negative AP' in the desired cell; $v''_{j,\text{pos}}$ is the horizontal distance between a 'negative AP' in interfering cell j and the 'positive AP' in the desired cell; $v''_{j,\text{neg}}$ is the horizontal distance between a 'negative AP' in the interfering cell j and the 'negative AP' in the desired cell.

4.5.3.3 OPC

Similar to MRC, the LOS signals of OPC are captured by two PDs that can establish LOS links with desired APs. Therefore, the SINR of OPC in double-source cell configuration can be determined as follows:

$$\gamma^{\text{double}}_{\text{OPC}} = \frac{\left(\frac{1}{2} R P_{\text{tx}} \left(w_{p_{\text{pos}}} H_{a_{\text{pos}},p_{\text{pos}}} + w_{p_{\text{neg}}} H_{a_{\text{neg}},p_{\text{neg}}} \right) \right)^2}{\mathcal{I}^{\text{double}}_{\text{NLOS,OPC}} + \sum_{p=1}^{N_{\text{PD}}} w_p^2 N_0 B}, \tag{4.62}$$

where $\mathcal{I}^{\text{double}}_{\text{NLOS,OPC}}$ is the NLOS interference component of OPC. The SINR of OPC in double-source cell configuration can be approximated as follows:

$$\gamma^{\text{double}}_{\text{OPC}}(r) \approx \frac{\left(\frac{1}{2} R P_{\text{tx}} \left(w_{p_{\text{pos}}} + w_{p_{\text{neg}}} \right) H(r, \Psi_{\text{ADR}}) \right)^2}{\mathcal{I}^{\text{double}}_{\text{NLOS,OPC}} + \sum_{p=1}^{N_{\text{PD}}} w_p^2 N_0 B}. \tag{4.63}$$

Similar to single-source cell configuration, the upper bound of the OPC in double-source cell configuration is represented as follows:

$$\gamma^{\text{double}}_{\text{OPC,UB}}(r) = \frac{\left(R P_{\text{tx}} H(r, \Psi_{\text{ADR}}) \right)^2}{2 N_0 B} > \gamma^{\text{double}}_{\text{OPC}}(r). \tag{4.64}$$

The proof for (4.64) is provided in Appendix A.2. By comparing (4.50) and (4.64), it is notable that the noise level is doubled when double-source configuration is used. This is because that

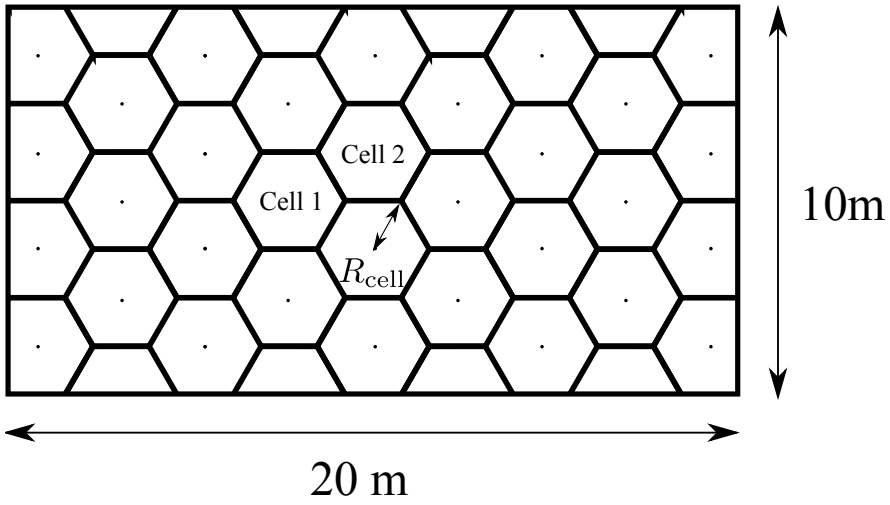

Figure 4.13: *The layout of a* $20 \times 10 \times 4$ m *room implementing an optical attocell network.*

two PDs in an ADR are used to receive LOS signals which doubles the noise from amplifier circuit. Therefore, when double-source cell configuration is used, the SINR performance of OPC is expected to degrade by 3 dB.

4.6 Results and Discussions

In this section, both numerical Monte-Carlo simulation and theoretical results are evaluated. As illustrated in Figure 4.13, numerical simulation is performed in a $20 \times 10 \times 4$ m room and up to fourth-order reflections are considered. As a baseline, the performance of the single-PD receiver is evaluated. The FOV of the single-PD receiver Ψ_{single} is set as 22^{o} which can avoid ICI at the desired cell centre. ADRs are designed to have the equivalent FOV to single-PD receiver. For the ADR with 9 PDs, α and Ψ_{ADR} are set to be 8.5^{o} and 15.5^{o}, respectively. For the ADR with 20 PDs, α and Ψ_{ADR} are set to be 6^{o} and 10.5^{o}, respectively. These chosen parameters guarantee the equal coverage area of all optical receivers. In the double source cell configuration, the distance between the APs in the desired cell are chosen so that an ADR can distinguish the light signals from these APs. Therefore, when the 9-PD receiver is used, the distance between APs in the same cell is set as 0.7 m. When the 20-PD receiver is used, the distance is set as 0.5 m. The reflection coefficients of the walls, the ceiling, and the floor are 0.8, 0.8 and 0.2, respectively [142]. For fairness, the optical transmission power of the AP in the conventional single-source cell configuration is 1 W, and the optical transmission power of

Responsivity, r	0.5 A/W
The gain of the optical filter, G	1
Refractive index, n	1.5
Transmitter half-intensity radiation angle, θ_{tx}	25°
The physical area of a PD, A_{p}	$5\ \mathrm{mm}^2$
Modulation Bandwidth, B	20 MHz
AWGN spectral density, N_0	$1 \times 10^{-21}\mathrm{A}^2$/Hz

Table 4.2: *Simulation Parameters*

the APs in the double-source cell configuration is set to 0.5 W. Other simulation parameters are presented in Table 4.2. For the theoretical results, a seven-cell configuration with second-order reflection is assumed and the other parameters are identical.

The CDF of the SINR for the indoor attocell network can be determined by varying the position of the optical receiver across all of the possible locations and estimating the respective received SINR.

4.6.1 Convention Single-source Cell Configuration

Figure 4.14 shows the SINR performance for the single-source cell configuration when the ADR with 9 PDs is used. The SINR performance of 9-PD ADR is similar to the single-PD receiver when EGC is used. This is because, for the high SINR region in the cell centre, NLOS interference from all PDs is added together which is equivalent to a single large FOV receiver. For the low SINR region in the cell edge, the EGC cannot suppress the LOS interference from the neighbouring cell which results in the same SINR performance with the single-PD receiver. The theoretical result closely matches the trend of the numerical result for EGC. In some sections of the graph, there are 6 dB gaps between the numerical and theoretical results. This is because, in the numerical simulation, LOS signal might be captured by two different PDs simultaneously at some positions which doubles the received optical power.

By using SBC, the SINR performance of 9-PD ADR is significantly better than the single-PD receiver. This is because, the SBC chooses the PD that provides the highest channel gain. Due to the narrow FOV, this PD is free from LOS ICI. This means that the SBC can successfully avoid LOS ICI at cell edge. From (3.12), it is notable that the NLOS ICI decreases when the FOV of a PD decreases. Since the FOV of the selected PD is narrower than the single-

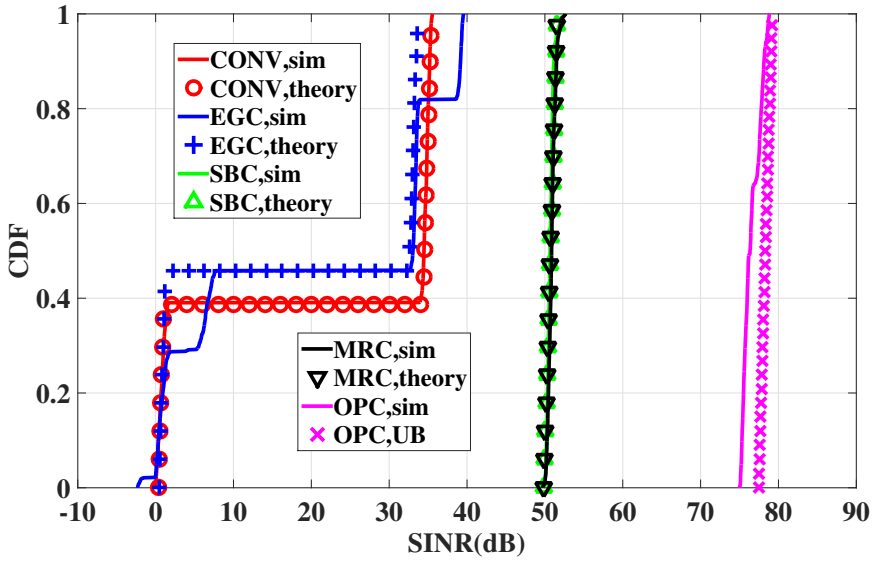

Figure 4.14: *The CDF of the achieved SINR at* 9*-PD ADR in conventional cell configuration when different signal combining scheme is implemented. The simulation and theoretical results are denoted by 'sim','theory', respectively. The upper bound is denoted as 'UB'.*

PD receiver, the NLOS interference is significantly mitigated compared to single-PD receiver. Also, the numerical result closely match the theoretical result, which proves the accuracy of the model.

The performance of the MRC technique is, as expected, nearly identical to the SBC methods. Due to the diffusive NLOS propagation path, the received interference signals are correlated in each PD and the MRC is unable to suppress this interference. Therefore, the performance of the MRC is not optimal.

As shown in Figure 4.14, the OPC scheme has the best SINR performance among all signal combining schemes. By using the interference-plus-noise correlation matrix, the OPC can generate the best weights for the ADR. These weights can effectively suppress the correlated NLOS interfering signal. Result shows that the OPC achieve over 20 dB improvement over the SBC and MRC schemes. Also, the numerical result of OPC is close to the theoretical upper bound. This shows that OPC can significantly suppress the ICI.

Figure 4.15 shows the SINR performance for the single-source cell configuration when the ADR with 20 PDs is used. In terms of EGC performance, the trend of the SINR performance

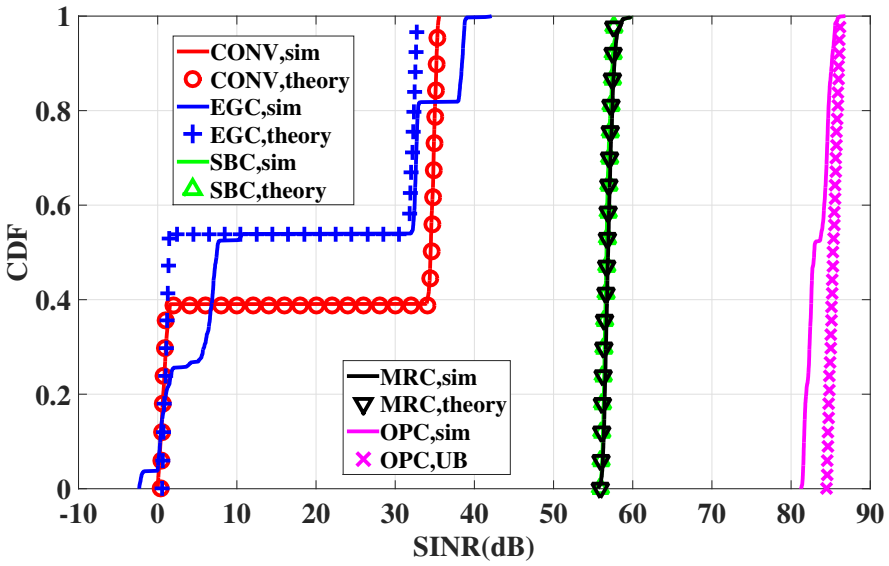

Figure 4.15: *The CDF of the achieved SINR at* 20*-PD ADR in conventional cell configuration when different signal combining schemes are implemented. The simulation and theoretical results are denoted by 'sim','theory', respectively. The upper bound is denoted as 'UB'.*

is similar to the scenario with 9-PD receiver. This is because, the overall coverage area of the ADR remains unchanged when the number of receiver elements increases. In terms of the SBC and MRC techniques, the SINR performance of the 20-PD ADR exhibits a 5 dB improvement over the 9-PD ADR system. This is because each PD on the 20-PD ADR has a narrower FOV. A narrower FOV means less NLOS ICI can be captured. Therefore, the overall SINR performance improves. In terms of the OPC, ICI from other cells is significantly suppressed. The main factor affects the system performance is the magnitude of the received power. Since the receiver element on 20-PD ADR has a narrower FOV and higher concentration gain than the 9-PD ADR, the 20-PD ADR can capture stronger light signals. Therefore, 20-PD ADR performs better than 9-PD ADR when OPC is used.

In summary, in single-source cell configuration, the OPC performs the best in comparison with the other signal combining schemes. However, this signal combining scheme requires the knowledge of CSI not only from the desired cell but also from all other interfering cells. Moreover, ADRs using SBC and MRC can achieve better SINR performance than single-PD receivers by simply using the knowledge of CSI from the desired cell.

In the engineering perspective, as shown in Table 4.3, EGC is not recommended for implemen-

Schemes	Performance	CSI knowledge	Recommendation
EGC	Worst	No	Not recommended
SBC	Sub-optimal	Desired AP	for systems with limited CSI estimation capability
MRC	Sub-optimal	Desired AP	for systems with limited CSI estimation capability
OPC	Optimal	All APs	for the systems aiming for best SINR performance without concerning the expense of CSI estimation

Table 4.3: *Summaries for signal combining schemes*

tation, since its SINR performance is similar to the performance using single-PD receiver. SBC and MRC can significantly improve the SINR performance which is very suitable for the systems with limited CSI estimation capability. OPC is recommended for the system that aiming for best SINR performance without concerning the expense of CSI estimation.

4.6.2 Double-Source Configuration

In this section, the performance of the SBC, MRC, and OPC techniques are evaluated in the double-source cell configuration using transmission mode A.

Figure 4.16 shows the SINR performance for both the single-source cell and the double-source cell configurations when 9 PDs ADRs are used. In terms of the SBC, the SINR performance improves significantly when double-source cell configuration is implemented. This is because the NLOS ICI has been significantly mitigated when the signals from two APs in the same interfering cells combine destructively. Also, there is a close match between the theoretical result and numerical result. In terms of MRC, the SINR is nearly identical to the SINR performance of the SBC. This is similar to the performance in single-source cell configuration. It can also be observed that the SINR of the OPC scheme in double-source cell degrades by 3 dB compared with single-source cell. This is consistent with the theoretical analysis in (4.50) and (4.64). Since two PDs are required for OPC to capture light signals in double-source cell, the total noise power is doubled compared with single-source cell.

Figure 4.17 shows the SINR performance for both single-source cell and double-source cell configurations when the ADR composed of 20 PDs is used. Compared with 9-PD receiver, each signal combining scheme achieves at least 5 dB SINR improvement when 20-PD receiver

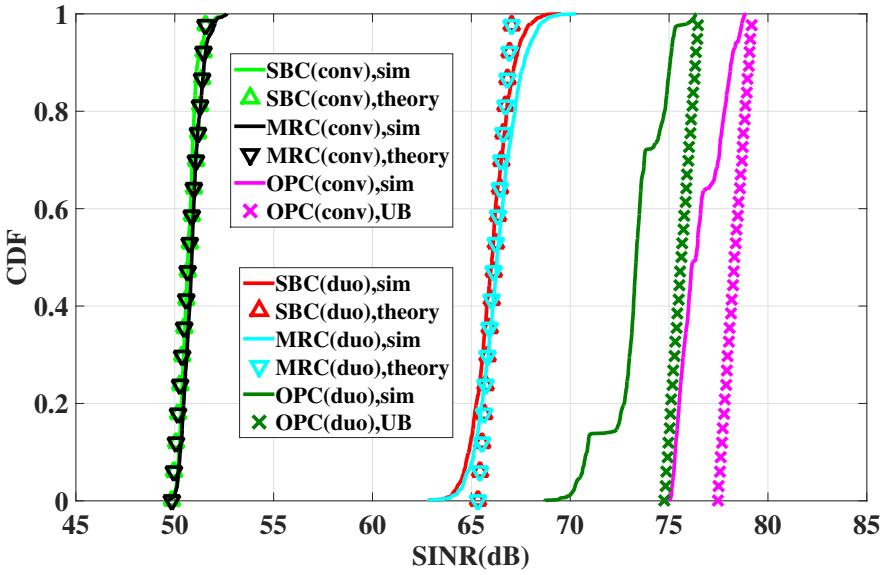

Figure 4.16: *The CDF of the achieved SINR at a* 9*-PD ADR when different signal combining scheme is implemented. The results for the conventional and double-source cell configuration are denoted by 'conv' and 'double', respectively. The upper bound is denoted as 'UB'.*

is used. This is consistent with the results for single-source cell.

In double-source cell configuration, an important observation is that the SINR performance of SBC and MRC is close to the SINR performance of OPC, which can approach the performance of ICI free system. Compared with OPC, SBC and MRC require less knowledge of CSI. Hence, it is more preferable to implement in a practical system.

4.6.3 Transmission Mode Selection

Although double-source cell configuration using mode A shows a significant improvement, it is not optimal in all scenarios. In practical optical attocell cell networks, several factors might affect the performance using mode A: a) some multi-element optical receivers may only support suboptimal signal combining scheme, such as EGC, which means the use of SBC, MRC, or OPC is impossible; b) active users equipped with single-PD receiver will experience significant signal attenuation in cell centre since they cannot distinguish the signals from different APs in the same desired cell; c) when user density is low, only a few APs are active which means the ICI is significantly decreased and the system can be regarded as a noise-limited system. In order to address these issues, transmission mode B (APs in the same cell transmit identical

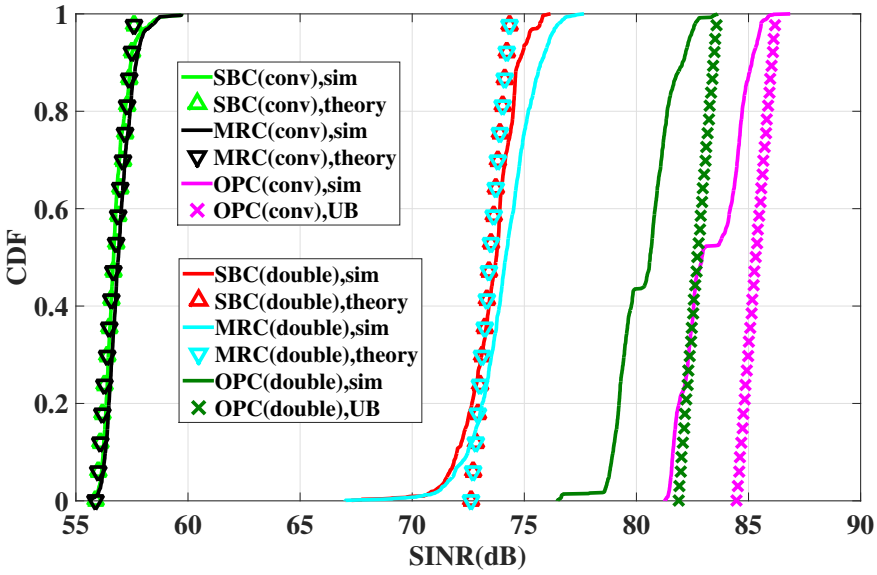

Figure 4.17: *The CDF of the achieved SINR at a* 20*-PD ADR when different signal combining scheme is implemented. The results for the conventional and double-source cell configuration are denoted by 'conv' and 'double', respectively. The upper bound is denoted as 'UB'.*

signals in repetition coding fashion) is used as a complementary transmission mode in double-source attocell networks. In order to determine the selection criteria of the transmission mode, two cases are studied. One case is the interference-limited case. As illustrated in Figure 4.13, only the desired cell (cell 1) and the interfering cell (cell 2) are activated in the room. Only the performance in the desired cell is evaluated. The other case is the noise-limited case. In this case, only one cell (cell 1) in the room is activated and evaluated.

Figure 4.18 shows the SINR performance in cell 1 when one neighbouring interfering cell is active. In terms of single-PD receiver, mode B achieves better performance. This is because single-PD receiver can not separate the signals from the 'positive AP' and the 'negative AP'. This results in a significant attenuation of the received signal power, especially in cell centre. The performance of EGC is similar to the single-PD receiver. As the EGC combines the signals from both 'positive AP' and 'negative AP', the system performance degrades. In terms of the SBC and MRC, the SINR performance significantly improves when mode A is used. This is due to the ICI mitigation by mode A. In terms of OPC, there is no difference between mode A and B. This is because OPC can effectively collect light energy and suppress correlated ICI by adjusting the weight at each PD.

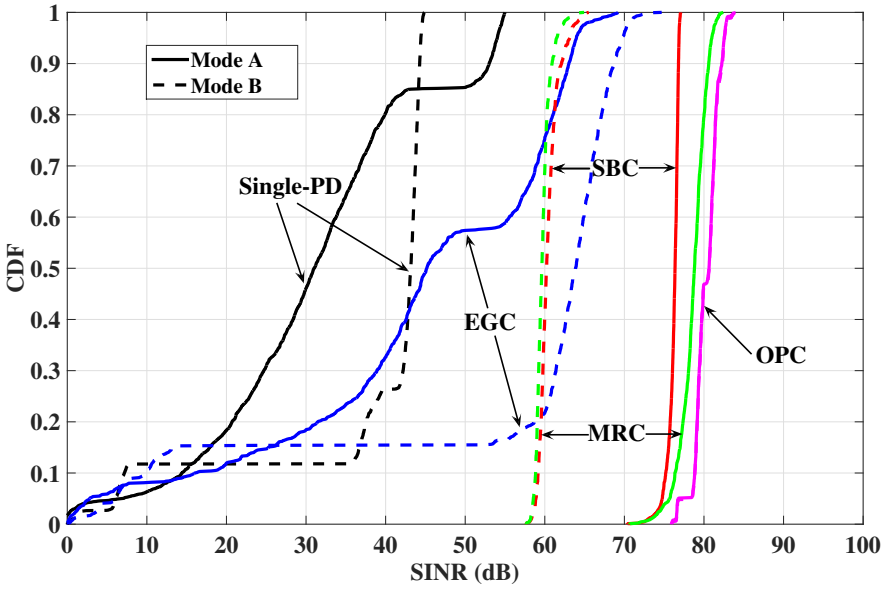

Figure 4.18: *The CDF of the achieved SNR when only one neighbouring cell is active. Two types of optical receivers, single-PD receiver and* 20*-PD receiver, are used. Transmission mode A is represented as solid lines and transmission mode b is represented as dash lines.*

	Single-PD	EGC	SBC	MRC	OPC
Interference	B	B	A	A	A or B
No Interference	B	B	A or B	A or B	A or B

Table 4.4: *The Criteria of Transmission Mode Selection.*

Figure 4.19 shows the CDF of SNR in cell 1 without ICI. In terms of single-PD receiver and EGC, there is a significant improvement when mode B is used. This is because mode B boosts the received signal power of a user. In terms of SBC, since only one of the AP can be used for data transmission, the performance of the mode A and mode B is the same. In terms of the MRC, transmission mode A and transmission mode B are identical since the energy from both APs can be captured in both modes. Finally, the performance of the OPC is identical to the MRC since there is no ICI. The criteria of selecting transmission mode in double-source cell configuration is listed in Table 4.4.

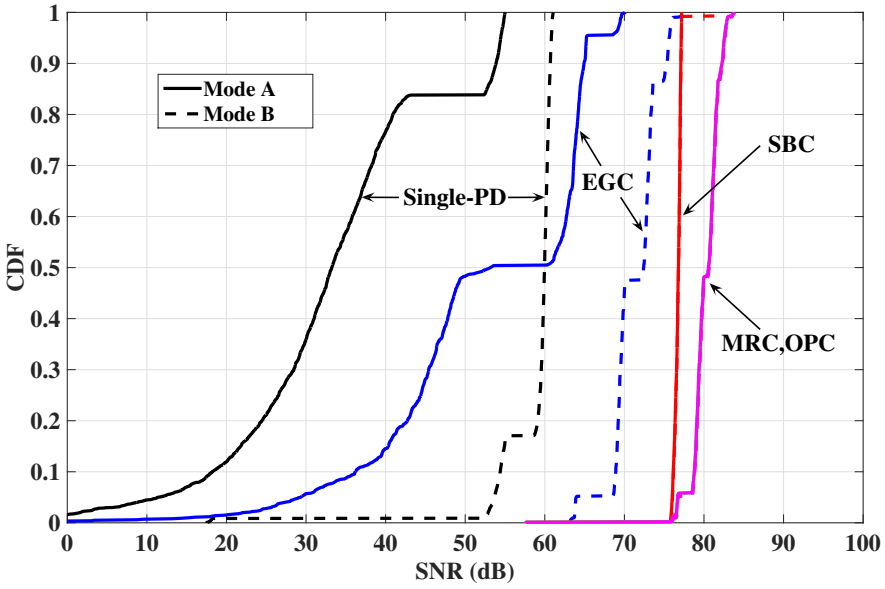

Figure 4.19: *The CDF of the achieved SNR at single-PD receiver and* 20*-PD ADR when no neighbouring cell is active. Two types of optical receivers, single-PD receiver and* 20*-PD receiver, are used. Transmission mode A is represented as solid lines and transmission mode b is represented as dash lines.*

4.7 Summary

This chapter investigates interference mitigation techniques for indoor optical attocell networks with ADRs. Four different signal combining schemes, namely SBC, EGC, MRC and OPC are evaluated. The performance of ADR is also comprehensively compared with conventional single-PD receivers. A novel double-source cell configuration is proposed for the first time for ADR which can further mitigate ICI. Results show that an ADR outperforms a single-PD receiver in terms of the SINR performance. In particular, an ADR using OPC performs the best which approaches the performance of interference-free systems. However, OPC requires the knowledge of CSI from all optical APs in the network. In comparison, MRC and SBC can also provide better performance than single-PD receiver and only the knowledge of CSI from the desired cell is required. Results also show that, SBC and MRC can achieve better SINR performance in mode A double-source cell configuration than in single-source cell configuration. Mode B can provide better performance when single-PD receiver or ADR with EGC are used in double-source cell configuration. The criteria for selecting transmission modes in double-source attocell networks is determined. Moreover, according to the proposed analytical framework, the theoretical performance of optical attocell networks with ADRs is derived in

closed-form. There is a close match between the numerical and theoretical results which proves the accuracy of the analytical model.

Chapter 5
SDMA using Angle Diversity Transmitter in Optical Attocell Networks

5.1 Introduction

In a cellular multi-user system, time division multiple access (TDMA) is a typical multiple access scheme. In TDMA, the data intended for different users is transmitted in different time slots, and occupies the entire system bandwidth in its respective time slot. There are two limitations in TDMA: i) only one user can be served in a single time slot; ii) in a cellular network, a TDMA transmitter radiate signals omni-directionally to provide full cell coverage, this causes strong inter-cell interference (ICI), especially to cell edge users. In order to overcome these limitations, space division multiple access (SDMA) is introduced which adds a spatial dimension to TDMA. SDMA is a well-known method in radio frequency (RF) [143] which has been integrated into 4G communication standards such as LTE and IEEE802.11ac [144]. In SDMA, the transmitter with an antenna array is used to generate spatially separated beams pointing to different active users. In this way, multiple users can be served simultaneously within the same time slot without experiencing strong interference.

Although SDMA shows promising performance in RF, it cannot be directly adopted in visible light communication (VLC). One of the key issues is the transmitter. In RF, directional narrow beams are generated by changing the amplitude and phase of the signals transmitted by an antenna array. However, this approach cannot be implemented straightforwardly to optical attocell network. Since intensity modulation and direct detection (IM/DD) is used, the phase of light signals cannot be changed in VLC. However, an light emitting diode (LED) has an inherent feature of a confined beam. This characteristic can be exploited for generating directional light beams. Therefore, in optical SDMA, an angle diversity transmitter with multiple directional narrow field-of-view (FOV) LED elements is used as the optical transmitter. The angle diversity transmitter can simultaneously serve multiple users at different locations by activating transmitter elements pointing to different directions. In this way, optical SDMA can potentially mitigate ICI in optical attocell network.

In RF, SDMA increases the system spectral efficiency by multiplexing information intended for multiple users using channel state information [143, 145, 146]. The existing approaches to improve the spectral efficiency of VLC networks includes a system consisting of multi-beam transmitters and imaging diversity receivers [97]. However, this system does not support multiple users and its mobility is significantly restricted by the imaging optical receiver. In [61] and [147], an optical attocell network is proposed which can achieve a higher system spectral efficiency by exploiting frequency reuse and different ICI mitigation methods. In [148], optical

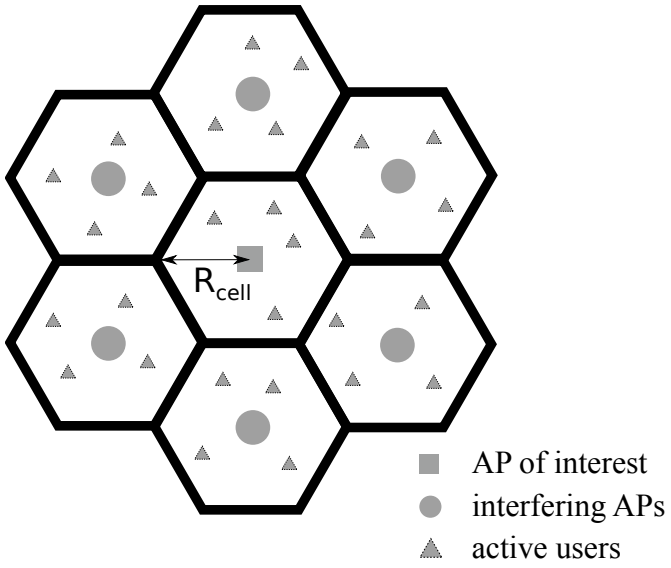

Figure 5.1: *The layout of a 7-cell attocell network.*

SDMA is experimentally realised by using spatial light modulator and results show that SDMA can effectively enhance the received light signal. But this work has limitations: only a single cell is considered which cannot reflect the actual performance of SDMA in a large scale optical attocell network. Therefore, in this section, optical SDMA using angle diversity transmitters for optical attocell network is proposed and analysed.

The rest of this chapter is organised as follows. Section 5.2 introduce the downlink propagation model. The concept of optical TDMA is introduced in Section 5.3. The concept of an optical SDMA system is introduce in Section 5.4 and is divided as follows: Section 5.4.1 introduces the design of angle diversity transmitter; Section 5.4.2 discusses the spatial grouping strategy for angle diversity transmitter; the position error model for each active user in an optical SDMA system is presented in Section 5.4.4. Section 5.5 explains the analytical derivation of the upper and lower bound of an optical SDMA system performance. Section 5.6 confirms the validity of the theoretical result by means of Monte Carlo simulation. Also, both theoretical and simulation results are discussed in this section. Finally, Section 5.7 gives the concluding remarks.

5.2 Propagation Model

The downlink transmission of an optical attocell network is the main focus in this study. A 7-cell optical attocell network is assumed and the performance of the central cell is discussed in order to eliminate cell edge effects in the simulations (see Figure 5.1). LED lighting fixtures constitute optical attocell wireless access points (APs). These APs are assumed to be placed in the ceiling and the optical receivers for all active users are assumed to be placed at the desktop height of $0.85\ \mathrm{m}$. For the optical receiver, a wide FOV photodiode (PD) of 70^{o} is assumed. An optical receiver with a large FOV ensures that line-of-sight (LOS) components dominate rather than non-line-of-sight (NLOS) components which are a few orders of magnitude weaker than LOS components. Therefore, in this section, only the effect of LOS paths of the light fixtures is considered. The direct current (DC) gain of a LOS link can be accurately calculated by (2.18) which is introduced in Chapter 2.

5.3 Optical TDMA

In order to serve multiple users in optical attocell network, a multiple access scheme is necessary. One of the common schemes for multiple user access is TDMA. In a typical optical TDMA scenario, an AP typically consists of only one LED element. All active users share the same bandwidth resource in their corresponding optical cell. Information for different users is transmitted in different time slots. Therefore, the received signal-to-interference-plus-noise ratio (SINR) of an active user k can be expressed as follows:

$$\gamma_k = \frac{\left(RP_{\mathrm{tx}}H_{(\hat{b},k)}\right)^2}{N_0B + \sum_{b'\neq\hat{b}}\left(RP_{\mathrm{tx}}H_{(b',k)}\right)^2}, \tag{5.1}$$

where R is the responsivity of the PD; P_{tx} is the optical power transmitted by an AP and is assumed to be the same for all APs; $H_{(\hat{b},k)}$ is the channel attenuation between user k and the desired AP $\hat{b}$; $\sum_{b'\neq\hat{b}}\left(rP_{\mathrm{t}}H_{(b',k)}\right)^2$ represents the interference signal from interfering APs; N_0 is the additive white Gaussian noise (AWGN) power spectral density; B is the optical communication bandwidth.

If a simple round-robin (RR) scheduler is used, the spectral efficiency of the optical TDMA

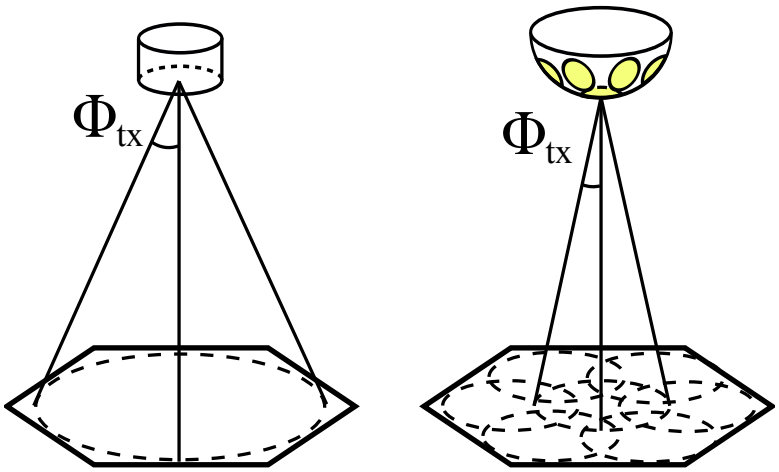

Figure 5.2: *The layout of the optical TDMA scenario with a conventional single-element optical transmitter (left) and the layout of the optical SDMA scenario with an angle diversity optical transmitter (right).*

system is as follows:

$$\Omega_{\mathrm{TDMA}}(k) = \frac{1}{K}\sum_{k=1}^{K}\log_2(1+\gamma_k), \tag{5.2}$$

where K is the total number of the active users.

The optical TDMA systems described here have two main disadvantages. Firstly, users in the system are successively assigned to different time slots. Only one user can be served in each time slot. This strategy significantly limits the overall performance of the system since the available bandwidth cannot be effectively shared and this limits the user data rate granularity. Secondly, the conventional single-element optical transmitter requires a large half intensity radiation angle to achieve full light and signal coverage. As a consequence, ICI in the system could significantly increase and the overall system performance is then compromised.

5.4 Optical SDMA

In order to overcome the disadvantages of optical TDMA systems, a multiple access scheme SDMA (as described in Chapter 2.3.2) is introduced to support parallel transmissions.

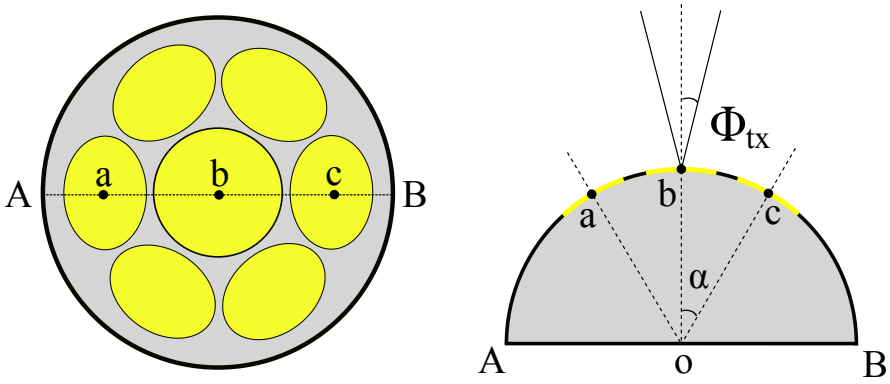

Figure 5.3: *The layout of a* 7*-element angle diversity transmitter.*

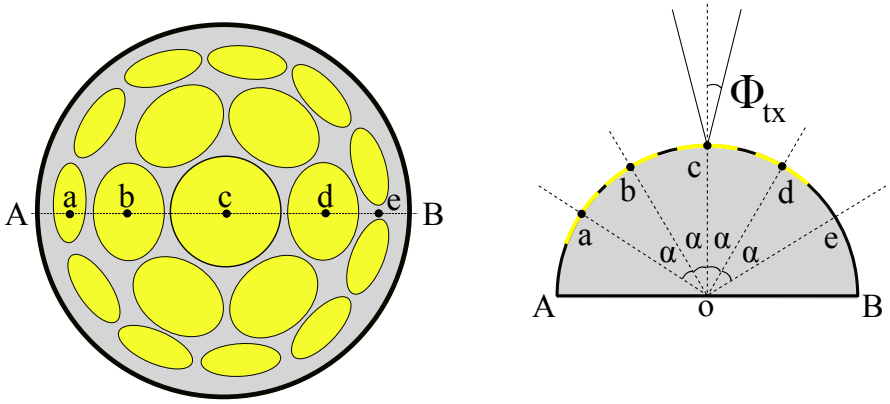

Figure 5.4: *The layout of a* 19*-element angle diversity transmitter.*

5.4.1 Angle Diversity Transmitter

In order to deploy SDMA in VLC, an optical transmitter which can generate parallel narrow beams of light is required. Hence, a multi-element angle diversity transmitter is introduced. The layout of the angle diversity transmitter is given in Figure 5.2. Multiple narrow-FOV LED elements are mounted on a semi-sphere base. Each of the elements points in a different direction which achieve the same coverage area as the conventional single-element optical transmitter.

The angle diversity transmitter considered in this study consists of several LEDs. The first LED is installed at the centre of a semi-sphere base. Then, rings of LEDs are installed around the central LED with increasing radius. In this study, three types of angle diversity transmitters (7-element, 19-element and 37-element) are considered. The layout of these angle diversity transmitters are illustrated in Figure 5.3-5.5. Here, α is the angle between each neighbouring

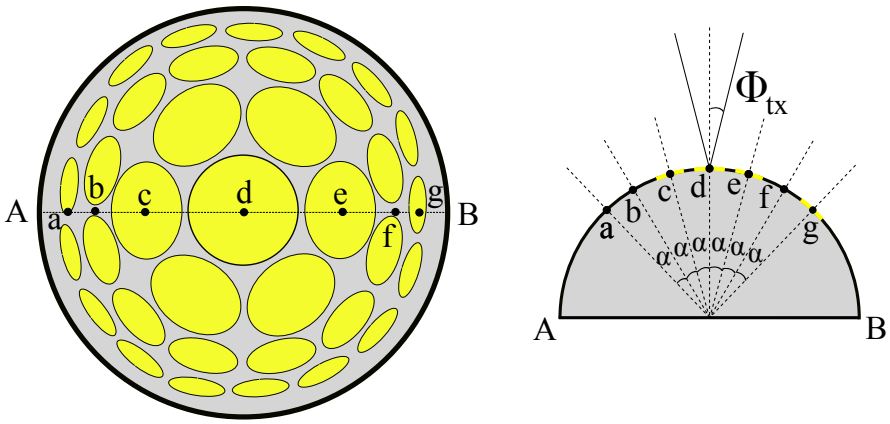

Figure 5.5: *The layout of a* 37*-element angle diversity transmitter.*

rings of LEDs.

In RF, the realisation of narrow beam transmitters requires multiple RF chains and complex beam-steering algorithms. In VLC, by exploiting an angle diversity transmitter, narrow beam optical signals can be generated, and complex algorithms for beamforming can be avoided. The parallel directional transmissions can be realised by activating the LEDs that cover only the areas occupied by active users. The remaining LEDs which are not used for communication generate constant light to provide room illumination. Therefore, an angle diversity transmitter can provide both uniform illumination while communicating to multiple users.

The use of an angle diversity transmitter can effectively mitigate the ICI in an optical attocell network. As shown in Figure 5.6, in a snapshot of an optical TDMA system, user 3 and user 5 are active and are served by APs in cell 1 and cell 2, respectively. Since the transmitter semi-angle for the single-element transmitter is large, both user 3 and user 5 experience strong ICI. For the identical snapshot in an optical SDMA system, all users can be served by spot beams. Since active LEDs only cover the areas of active users, ICI can be significantly mitigated.

It is notable that the beam angle of an angle diversity transmitter is narrow. This means that this type of systems require accurate user position information for beam alignment. The detailed discussion of the impact of user position information is in Sec.5.4.4.

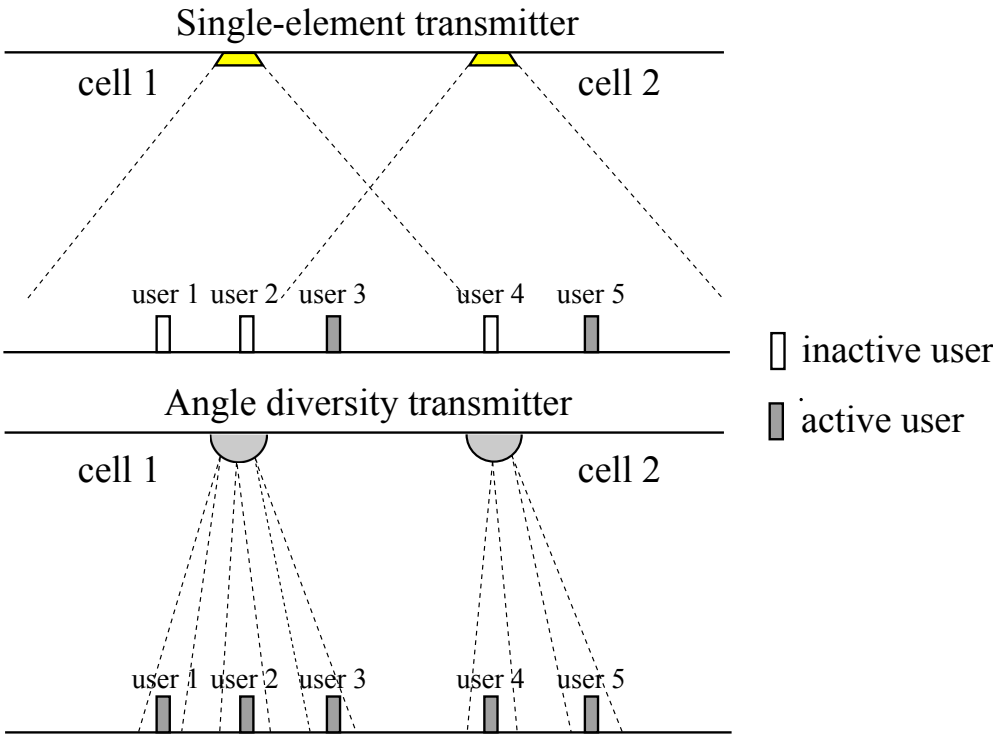

Figure 5.6: *Single-element versus angle diversity transmitter: the figure on the top illustrates optical TDMA. The figure at the bottom illustrates optical SDMA. Cell* 1 *and cell* 2 *are two neighbouring cells in an optical attocell network.*

5.4.2 Spatial Grouping

In an attocell network, it is assumed that each active user connects to the AP that provides the best signal strength. In each optical cell, active users are served by different LED elements of the angle diversity transmitter. In optical SDMA, these active users cannot be assigned to arbitrary LED elements since some users might be spatially close to each other which results in overlapping beams and high mutual interference. Therefore, in the absence of adaptive beamforming, a proper spatial grouping strategy is essential to achieve high spectral efficiency in an optical SDMA system with a fixed grid of beams.

The most important part of the spatial grouping strategy is to determine the source LED element for each active user. The geometry of an optical cell is given in Figure 5.7. The coordinates of the angle diversity transmitter c is (x_c, y_c, h) and the coordinates of an active user k is $(x_k, y_k, 0)$; $v_{k,c}$ is the vector from the angle diversity transmitter c to an active user k; $v_{m,c}$ is the normal vector of the LED element m on the angle diversity transmitter c; and $\theta_{k,m,c}$ is the angle between the vector $v_{k,c}$ and vector $v_{m,c}$. The source LED element of active user k is

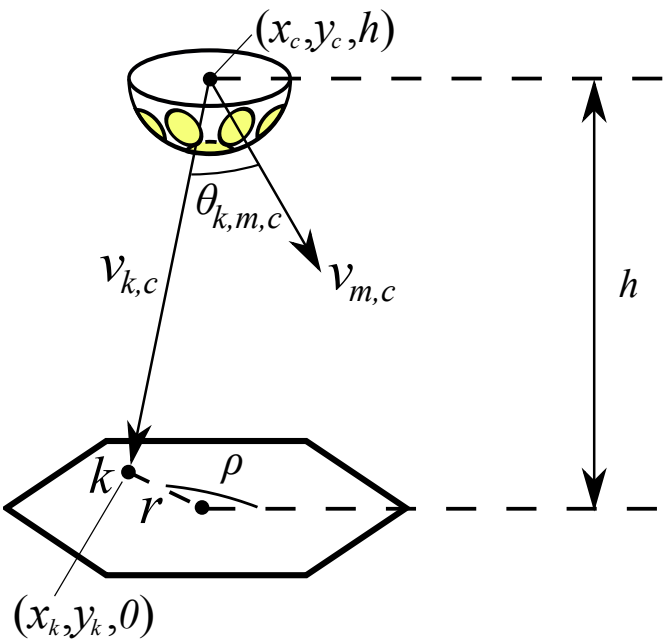

Figure 5.7: *The geometry of an optical cell. The position of the active user k can be represented by polar coordinate $(r\cos(\rho), r\sin(\rho))$.*

chosen to minimise the angle $\theta_{k,m}$. The index of the source LED element for active user k can be described as follows:

$$I_{k,c} = \min_{m} \theta_{k,m,c}, \quad (c = \hat{c}) \tag{5.3}$$

where $\hat{c}$ is the desired cell for active user k; $\theta_{k,m,c}$ can be represented as:

$$\theta_{k,m} = \arccos\left(\frac{\overrightarrow{v}_{k,c} \cdot \overrightarrow{v}_{m,c}}{\|\overrightarrow{v}_{k,c}\|\|\overrightarrow{v}_{m,c}\|}\right). \tag{5.4}$$

When the source LED element for each active user is determined, it is able to determine which LED elements on the angle diversity transmitter are active. In some situations, some active users could be spatially close. This means that more than one active user will be allocated to the same LED element. In order to serve multiple users with one LED element, a TDMA scheme outlined in Section 5.3 is required. Also, RR scheduling is assumed.

An example of resource allocation in optical SDMA is illustrated in Figure 5.8. Three LED elements are active. User $1, 2$, are allocated to element 1. These two users equally share the resource. User $3, 4, 5$, are allocated to element 3. Three users equally share the bandwidth resource. User 6 is allocated to element 5. Since there is only one user in that beam, user 6

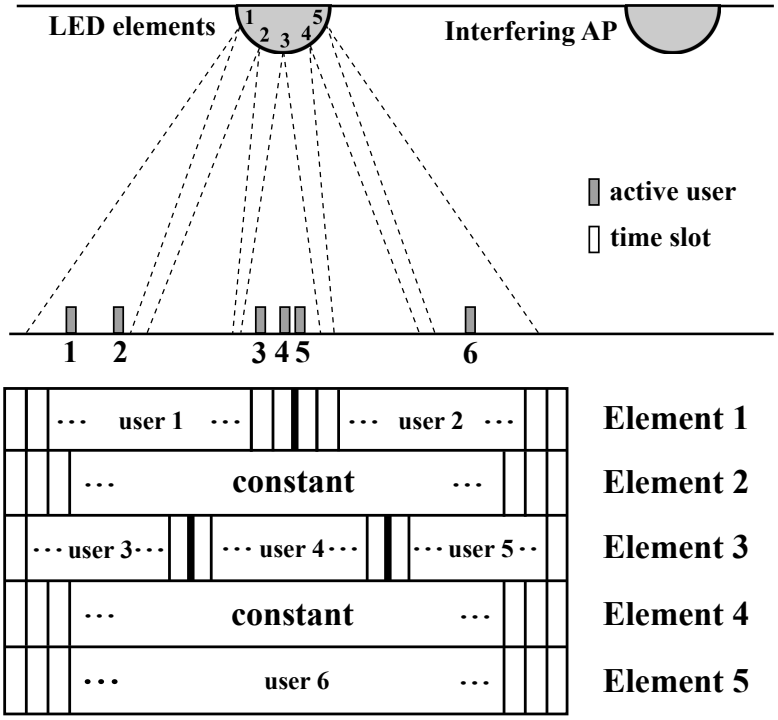

Figure 5.8: *An example frame of resource allocation in optical SDMA.*

uses the entire bandwidth continuously. The other two elements 2 and 4 are inactive, since no users are required to be served by them. Therefore, these LED elements do not carry intensity modulation (IM) signals and provide constant light output for illumination.

5.4.3 Performance Evaluation

In order to evaluate the SINR performance for each active user, interference is a key factor to be considered. In this scenario, interference consist of two parts: intra-cell interference and ICI. Intra-cell interference originates from the active LED elements in the desired optical cell. ICI is the interference generated by the active LED elements in the other optical cells. Hence, the SINR of active user k can be expressed as:

$$\gamma_k = \frac{\left(RP_{\mathrm{tx}}H_{k,m,\hat{c}}\right)^2}{N_0B + \sum\limits_{m' \neq m}\left(RP_{\mathrm{tx}}H_{k,m',\hat{c}}\right)^2 + \sum\limits_{c'}\sum\limits_{\hat{m}}\left(RP_{\mathrm{tx}}H_{k,\hat{m},c'}\right)^2}, \tag{5.5}$$

where $H_{k,m,\hat{c}}$ is the channel attenuation between the desired LED element m and an active user k in the desired cell $\hat{c}$; $\sum\limits_{m' \neq m}\left(RP_{\mathrm{tx}}H_{k,m'}\right)^2$ represents the intra-cell interference; and m' is the

index of active LED elements in the desired cell; $\sum_{c'} \sum_{\hat{m}} \left(RP_{\text{tx}}H_{k,\hat{m},c'}\right)^2$ represents the ICI; $\hat{m}$ is the index of active LED elements in each interfering cell; c' is the index of the interfering cell.

In optical SDMA, active users in each optical cell equally share the bandwidth resource. Therefore, the spectral efficiency of the optical SDMA can be calculated as follows:

$$\Omega_{\text{SDMA}} = \sum_{k}^{K} \frac{1}{g_k} \log_2(1+\gamma_k), \tag{5.6}$$

where g_k is the total number of active users served by the desired LED element of active user k; K is the total number of active users in an optical cell.

The relative positions of active users in the optical cells can significantly affect the spectral efficiency of the system. In this study, the spectral efficiency gain is used to evaluate the performance of an SDMA system. This metric uses the system performance of the TDMA system as the baseline. The gain is defined as:

$$\eta = \frac{\Omega_{\text{SDMA}}}{\Omega_{\text{TDMA}}}. \tag{5.7}$$

For the purpose of fairness, in both scenarios, the following simulation parameters are set to be identical: i) total transmission power; ii) total number of active users; and iii) the position of active users. Therefore, the spectral efficiency gain is purely from the implementation of the angle diversity transmitter and the resource allocation strategy.

5.4.4 The model of position errors

As discussed in the previous section, the spatial grouping strategy depends on the position information of active users. This means position information is crucial to the operation of the optical SDMA system. However, the position information is not always accurate due to the limitation of the optics. When different indoor positioning techniques and devices [149], [150] are used, the position errors vary accordingly. In this section, the model of the inaccurate position estimation is introduced.

Assume that the coordinate of the actual position of an active user k is (x_k, y_k) and the estimated

position is (x'_k, y'_k). The relationship between (x_k, y_k) and (x'_k, y'_k) can be represented as:

$$\begin{cases} x'_k = x_k + e_k \\ y'_k = y_k + e'_k \end{cases} \tag{5.8}$$

where both e_k and e'_k follow a zero-mean normal distribution $\mathcal{N}(0, \sigma_e^2)$ [151]; and σ_e is the standard variance. For each active user, e_k and e'_k are independent and identically distributed. The distance between the actual position and the estimated position can be represented as:

$$d_e = \sqrt{(x_k - x'_k)^2 + (y_k - y'_k)^2}. \tag{5.9}$$

Here, according to [152], d_e follows Rayleigh distribution and the mean value of d_e is:

$$\mathbb{E}[d_e] = \sqrt{\frac{\pi}{2}}\sigma_e. \tag{5.10}$$

In the optical SDMA, the result of user grouping is affected by the position errors. Some users could be allocated to suboptimal optical cells and this results in an increased intra-cell interference. Therefore, by considering position errors of active users, the system performance of optical SDMA is degraded.

5.5 Theoretical Analysis of Optical SDMA

A theoretical framework to analyse the performance of an optical SDMA is presented in this section. In the system model, the SINR of each active user is dependent on both the position of the desired user and the position of interfering users. Hence, exact performance analysis seems to be complex, but an insightful upper and lower bound for the average spectral efficiency are derived here. They can be used to closely estimate the actual performance of an optical SDMA system.

5.5.1 An Upper Bound for the SDMA System Performance

From (5.5) and (5.6), it is interesting to note that the performance of an SDMA system is limited by three factors: noise, intra-cell interference and ICI. Firstly, the best-case scenario of the SDMA system is considered. In the best-case scenario, it is assumed that all LED elements

used in the system are with different colours and optical receivers can perfectly distinguish these colours. Therefore, intra-cell interference and ICI are assumed to be negligible. In this scenario, an upper bound for the SDMA system performance can be obtained. The derivation of the upper bound is presented as follows.

In an optical cell, each LED element on the angle diversity transmitter independently serves users at different locations. The spectral efficiency within an optical cell is equal to the sum of the spectral efficiencies of each active LED elements. Since each LED element points into a different direction, the average spectral efficiency for each active LED element is different. An active LED element can achieve the highest average spectral efficiency when it points vertically downward. This is because the active users served by this LED element are closest to the angle diversity transmitter and have the strongest channel gain. The average spectral efficiency of an active LED element pointing vertically downward is derived as follows.

For simplicity, the service region of the downward LED element is approximated as a circle. Assuming R_{cell} is the radius of the hexagonal cell, the radius of the approximated circle can be determined by: $R \approx 0.91R_{\text{cell}}$. Also, it is assumed that the active users within this circular region are uniform distributed. Assuming r is the horizontal distance between an active user and the centre of its service region, the probability density function (PDF) of r can therefore be given as:

$$f_r(r) = \frac{2r}{R^2} \quad (0 \leq r \leq R), \tag{5.11}$$

where R is the radius of the service region. By considering the geometry relationship between the parameters $d = h/\cos(\phi), \cos(\phi) = h/\sqrt{h^2 + r^2}, \psi = \phi$, (3.14) can be expressed as:

$$H(r) = \frac{(m+1)A_{\text{eff}}}{2\pi h^2} \left(\frac{h}{\sqrt{h^2 + r^2}} \right)^{m+3}. \tag{5.12}$$

Due to the noise-limited characteristic of the system, the signal-to-noise ratio (SNR) can be represented as:

$$\gamma(r) = \frac{\Big(RP_{\text{tx}}H(r)\Big)^2}{N_0 B}. \tag{5.13}$$

In this scenario, (5.6) is modified as follows:

$$\Omega_{\text{downward}} = \sum_{k}^{K'} \frac{1}{g_k} \log_2(1 + \gamma_k), \tag{5.14}$$

where K' is the total number of active users within the service region of the downward LED element. Since all users in this scenario are served by the downward LED element, $g_k = K'$. Also, there is no mutual interference between users. Therefore, γ_k for all k is independently and identically distributed. Therefore, the average spectral efficiency of the downward LED element can be represented as follows:

$$\begin{aligned}\bar{\Omega}_{\text{downward}} &= \mathbb{E}\left[\sum_{k}^{K'} \frac{1}{g_k} \log_2(1+\gamma_k)\right] \\ &= \sum_{k}^{K'} \frac{1}{K'} \mathbb{E}_r \left[\log_2(1+\gamma(r))\right] \\ &= \mathbb{E}\left[\log_2(1+\gamma(r))\right] \\ &= \int_0^R \log_2(1+\gamma(r)) f_r(r) \mathrm{d}r.\end{aligned} \tag{5.15}$$

Note that the average spectral efficiency is independent of the number of users served by the vertically downward pointing LED element, K'.

Since the average spectral efficiency of the other LED elements is less than the average spectral efficiency in the downward element, the average spectral efficiency in the entire optical cell, Ω_{SDMA}, can be bounded by $\bar{\Omega}_{\text{downward}}$:

$$\bar{\Omega}_{\text{SDMA}} \leq \bar{N}_{\text{a}} \bar{\Omega}_{\text{downward}} = \Omega_{\text{UB}}, \tag{5.16}$$

where $\bar{N}_{\text{a}}$ is the average number of the active LED elements; Ω_{UB} is the upper bound of the average spectral efficiency in an optical cell.

In an optical SDMA system, $\bar{N}_{\text{a}}$ is not a fixed number. This number depends on the total number of LED elements on an angle diversity transmitter and also the total number of active users in the optical cell. For example, if there is only one active user, $\bar{N}_{\text{a}}$ is always 1. However, when there are significant number of active users in an optical cell, $\bar{N}_{\text{a}}$ is approximately equal to the total number of LED elements on the angle diversity transmitter. According to [153], $\bar{N}_{\text{a}}$ can be calculated by:

$$\bar{N}_{\text{a}} = N - N(1 - 1/N)^K, \tag{5.17}$$

where N is the total number of LED elements on an angle diversity transmitter; and K is the number of users within an optical cell. The result of $\bar{N}_a$ is presented in Figure 5.9. Note that

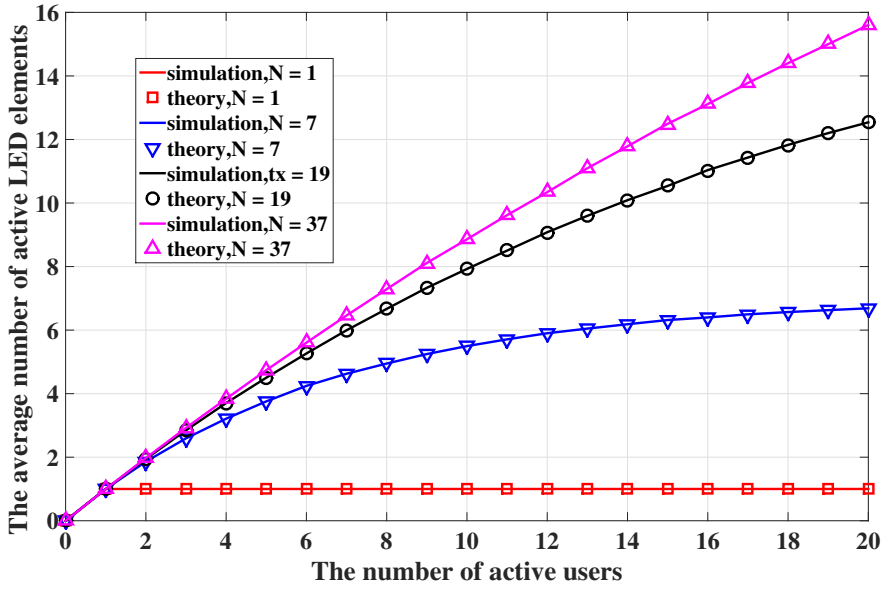

Figure 5.9: *The average number of active LED elements for different number of active users and LED elements.*

$\bar{N}_a$ increases when there are more active users in an optical cell. Also the maximum value of $\bar{N}_a$ is clipped by the number of LED elements on an angle diversity transmitter. The simulation result closely matches the theoretical result which proves the accuracy of the probability model.

5.5.2 A Lower Bound for the SDMA System Performance

After considering the best-case scenario, the worst-case scenario is now considered. In the worst-case scenario, the inactive LED element in an optical cell is no longer transmitting constant light signals. Instead, random light signals are transmitted. In this scenario, the intra-cell interference and ICI are maximised. Also, the intra-cell interference and ICI of an active user is independent of the position of other users. Therefore, a lower bound of the SDMA system performance can be obtained. The derivation of the lower bound is presented as follows.

In this scenario, the representation of the user position PDF is identical to the previous scenario, (5.11). The system is assumed to be interference limited and the intra-cell interference dominates the interference components. Therefore, the signal-to-interference ratio (SIR) can be represented as:

$$\gamma_k = \frac{\left(RP_{\text{tx}}H_{k,m,\hat{c}}\right)^2}{\sum_{m' \neq m}\left(RP_{\text{tx}}H_{k,m',\hat{c}}\right)^2}, \tag{5.18}$$

where the channel attenuation, $H_{k,m,\hat{c}}$, can be modelled as follows:

$$H_{k,m,\hat{c}} = \frac{(\lambda+1)A_{\text{eff}}}{2\pi d_{k,\hat{c}}^2} \cos^{\lambda}(\phi_{k,m,\hat{c}}) \cos(\psi_{k,\hat{c}}) \times \text{rect}\left(\frac{\psi_{k,\hat{c}}}{\Psi_{\text{fov}}}\right), \tag{5.19}$$

and the channel attenuation, $H_{k,m',\hat{c}}$, can be represented as follows:

$$H_{k,m',\hat{c}} = \frac{(\lambda+1)A_{\text{eff}}}{2\pi d_{k,\hat{c}}^2} \cos^{\lambda}(\phi_{k,m',\hat{c}}) \cos(\psi_{k,\hat{c}}) \times \text{rect}\left(\frac{\psi_{k,\hat{c}}}{\Psi_{\text{fov}}}\right), \tag{5.20}$$

and (5.18) can be rewritten as follows:

$$\gamma_k = \frac{\left(\cos(\phi_{k,m,\hat{c}})\right)^2}{\sum_{m' \neq m} \left(\cos(\phi_{k,m',\hat{c}})\right)^2}, \tag{5.21}$$

where $(r\cos\rho, r\sin\rho, 0)$ is the coordinate of the user k; $\cos\phi_{k,m,c}$ is represented by:

$$\cos\phi_{k,m,c} = \left(\frac{\overrightarrow{v}_{k,c} \cdot \overrightarrow{v}_{m,c}}{\|\overrightarrow{v}_{k,c}\| \|\overrightarrow{v}_{m,c}\|}\right) = \frac{rp_{m,c}\cos\rho + rq_{m,c}\sin\rho - hw_{m,c}}{\sqrt{r^2+h^2}}, \tag{5.22}$$

where $\overrightarrow{v}_{m,c} = (p_{m,c}, q_{m,c}, w_{m,c})$ is defined as a normalised direction vector where $p_{m,c}^2 + q_{m,c}^2 + w_{m,c}^2 = 1$.

Considering (5.21) and (5.22), the spectral efficiency of the optical SDMA system with only a single activated LED element can be denoted as follows:

$$\Omega(r,\rho) = \log_2(1+\gamma(r,\rho)). \tag{5.23}$$

Using the flower model described in [154] and [133], $\Omega(r,\rho)$ in (5.23) can be further simplified as $\Omega'(r,\rho)$. Since all transmitters are active and interfering transmitters are symmetrically located, the magnitude of the interference term can be approximated by the flower model as the combination of sine waves. The derivation and representation of $\Omega'(r,\rho)$ is provided in Appendix B.2. The result of $\Omega'(r,\rho)$ is shown in Figure 5.10. Note that the flower model approximation accurately matches the exact model.

The average spectral efficiency of the optical SDMA system with only a single activated LED

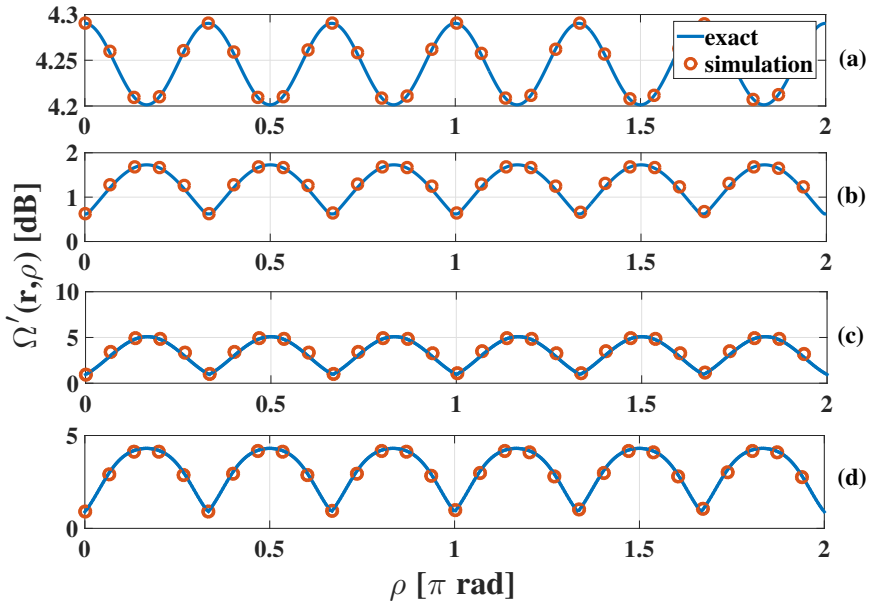

Figure 5.10: *The exact and approximation result of* $\Omega'(r,\rho)$. *In (a),* $N = 7$, $r = 0.5$ m. *In (b),* $N = 7$, $r = 1$ m. *In (c),* $N = 7$, $r = 1.5$ m. *In (d),* $N = 19$, $r = 1.5$ m.

element is:

$$\begin{aligned}\bar{\Omega}_{\text{single}} &= \mathbb{E}_r\left[\Omega'(r,\rho)\right] \\ &= \int_0^R \int_0^{2\pi} \Omega'(r,\rho) f_r(r) \mathrm{d}\rho \mathrm{d}r \\ &= \int_0^R \Omega''(r) f_r(r) \mathrm{d}r,\end{aligned} \tag{5.24}$$

where the representation of $\Omega''(r)$ is provided as follows.

For 7-element transmitter, the cell area can be divided into two parts: the area that is served by the central LED and area that is served by the outer ring of LEDs. For the former scenario, $0 \leq r < h\tan(\frac{\alpha}{2})$,

$$\Omega'(r,\rho) = \frac{\Omega(r,0^{\text{o}}) + \Omega(r,\frac{\pi}{6})}{2} + \frac{\Omega(r,0) - \Omega(r,\frac{\pi}{6})}{2}\cos(6\rho). \tag{5.25}$$

For the latter scenario, $h\tan(\frac{\alpha}{2}) \leq r \leq R$.

$$\Omega'(r,\rho) = \Omega(r,\frac{\pi}{6}) + \Omega(r,0) - \Omega(r,\frac{\pi}{6})|\sin(3\rho)|. \tag{5.26}$$

The representation of $\Omega''(r)$ for the transmitters with more transmitter elements is listed in Appendix B.3.

Similar to (5.16), the lower bound of the average spectral efficiency for the entire cell is scaled with $\bar{N}_a$:

$$\Omega_{\mathrm{LB}} = \bar{N}_a \bar{\Omega}_{\mathrm{single}}. \tag{5.27}$$

5.5.3 The Estimation of the SDMA System Performance

The upper bound, Ω_{UB} in (5.16), can be regarded as the performance of a SDMA system with no interference. That means each user in the system experiences no interference from neighbouring LED elements. The lower bound, Ω_{LB} in (5.27), can be regarded as the performance of a SDMA system with full interference. For instance, in the context of Figure 5.1, each user experiences interference from all 6 neighbouring LED elements. However, the interference experienced by a typical user in SDMA attocell networks varies significantly. For instance, a SDMA deployment such as shown in Figure 5.1 may experience interference from a varied number of LEDs from 0 to 6. In this section, the analysis in Section 5.5.1 and Section 5.5.2 is extended to estimate the performance of SDMA systems more accurately. Let the average spectral efficiency of a typical user with z interfering LEDs be denoted as Ω_z, $z = 0, 1, ..., 6$. From the definition of Ω_{UB} and Ω_{LB}, it is clear that $\Omega_0 = \Omega_{\mathrm{UB}}$ and $\Omega_6 = \Omega_{\mathrm{LB}}$. Hence, Ω_z, $z = 1, ..., 6$ can be expressed as:

$$\Omega_z = \log_2\left(1 + \frac{\mathcal{S}}{z\mathcal{I}}\right) \approx \log_2\left(\frac{\mathcal{S}}{z\mathcal{I}}\right) = \Omega_{\mathrm{LB}} + \log_2\left(\frac{6}{z}\right), \tag{5.28}$$

where $\mathcal{S}$ represents the signal term which is identical to the numerator in (5.18), and $\mathcal{I}$ is the interference term which is identical to the denominator in (5.18). By assuming the probability of occurrence of each scenario as P_z, the estimated average spectral efficiency of the SDMA scheme is given as:

$$\Omega_{\mathrm{SDMA,est}} = \sum_{z=0}^{6} P_z \Omega_z \tag{5.29}$$

The method of calculating P_z is described as follows. Note that P_z is dependent on the user density in the attocell network. If user density is low, P_0 would be very high since users tend to be well separated. If user density is high, P_0 would be very low since most of the users are

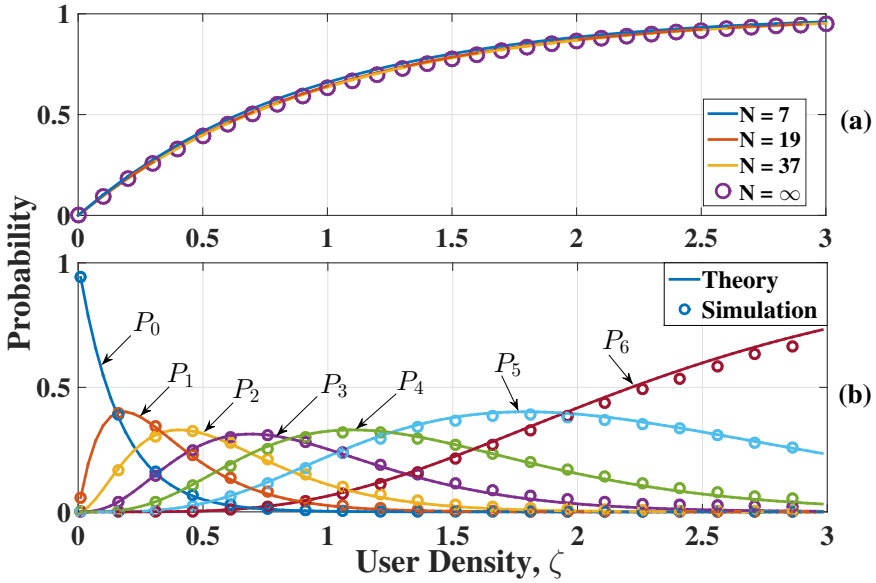

Figure 5.11: *(a) The result of P_{oe} for different number of N. (b) The result of P_z when $N = 37$.*

clustered. Let the user density, ζ, is defined as:

$$\zeta = \frac{K}{N}. \tag{5.30}$$

According to (5.17), the probability that a neighbouring LED element is occupied can be represented as:

$$P_{\text{oe}} = \frac{\bar{N}_{\text{a}}}{N} = 1 - (1 - 1/N)^{\zeta N}. \tag{5.31}$$

If N is large, P_{oe} can be calculated as:

$$\lim_{N\to\infty} P_{\text{oe}} = 1 - \lim_{N\to\infty} (1 - 1/N)^{\zeta N} = 1 - e^{-\zeta}. \tag{5.32}$$

The proof of (5.32) is provided in Appendix B.1. The result of P_{oe} for different N is presented in Figure 5.11 (a). It can be observed that the difference between the result, P_{oe}, for different values of N is very small. Therefore, it is assumed that $P_{\text{oe}} = 1 - e^{-\zeta}$ regardless of the value of N.

In order to derive P_z, consider the scenario when $z = 0$. In this scenario, none of the 6 LED

Responsivity, R	0.5 A/W
The gain of the optical filter, G	1
Refractive index, n	1.5
PD area, A_{p}	$0.1\mathrm{cm}^2$
AWGN spectral density, N_0	1×10^{-21}A/Hz
The radius of an optical cell, R_{cell}	3 m

Table 5.1: *Simulation Parameters*

elements in the vicinity is occupied. Hence, P_0 can be evaluated as:

$$P_0 = \binom{6}{0} (P_{\mathrm{oe}})^0 (1 - P_{\mathrm{oe}})^6. \tag{5.33}$$

Similarly, P_z can be evaluated as:

$$P_z = \binom{6}{z} (P_{\mathrm{oe}})^z (1 - P_{\mathrm{oe}})^{6-z}. \tag{5.34}$$

The result of P_z when $N = 37$ is shown in Figure 5.11 (b). The theoretical and simulation results match very closely, which proves the accuracy of the theoretical model. Substituting the result for P_z in (5.34) into (5.29) yields the estimated average spectral efficiency.

5.6 Results and Discussions

The performance of the optical SDMA system is simulated and evaluated in this section. In particular, the average spectral efficiency of the system and the cumulative distribution function (CDF) of the spectral efficiency gain are illustrated and discussed. Moreover, the system performance is also evaluated when position errors of active users are considered.

5.6.1 Simulation Setup

In the simulation, both the optical TDMA scheme and the optical SDMA scheme are considered. The optical TDMA system is used as a benchmark system. In the optical TDMA scenario, the half-intensity radiance angle of single-element transmitter is assumed to be 60^{o}. For the 7-element angle diversity transmitter, $\alpha = 20^{\mathrm{o}}$, $\Phi_{\mathrm{tx}} = 17^{\mathrm{o}}$; for the 19-element angle diversity transmitter, $\alpha = 22^{\mathrm{o}}$, $\Phi_{\mathrm{tx}} = 10^{\mathrm{o}}$; for the 37-element angle diversity transmitter,

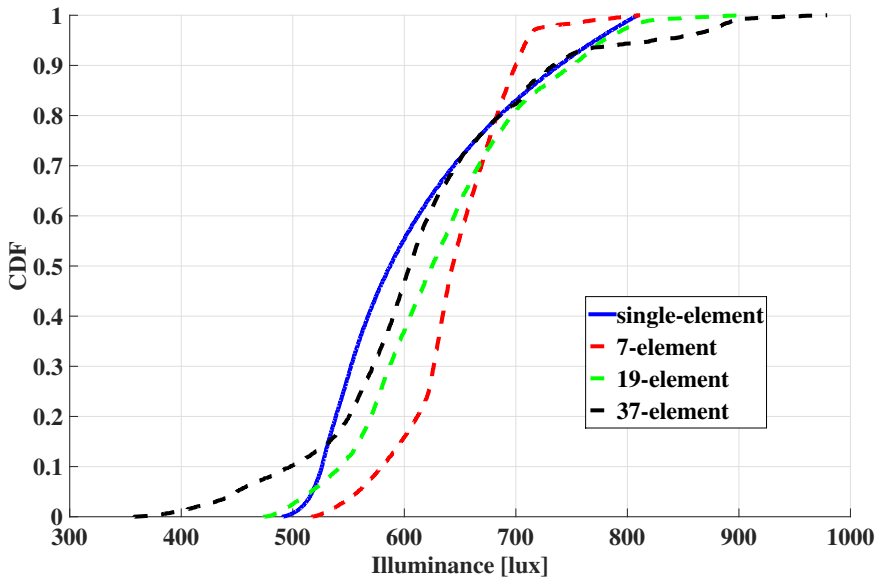

Figure 5.12: *The illuminance distribution for different types of optical transmitters.*

$\alpha = 14.3^{\circ}$, $\Phi_{\text{tx}} = 7^{\circ}$. In the optical SDMA scenario, the parameters of angle diversity transmitters are designed to have similar half-intensity radiance angle with single-element receiver. For the purpose of fairness, the sum transmission power of all LED elements is identical for all types of optical transmitters. The distribution function of illumination for different types of optical transmitters is given in Figure 5.12. This figure is generated by separating an optical cell into small grids and accumulating the value of illuminance in each grid. It is notable that all types of optical transmitters can meet indoor illumination requirement [56] which is $300\text{lux} \leq I_{\text{Illum}} \leq 1500\text{lux}$, where I_{Illum} is the indoor illuminance.

Optical transmitters are assumed to be placed at the centre of each cell at a height of 3 m. The optical receivers for all active users are assumed to be placed at the height of a desk, 0.85 m. The transmission power of an optical transmitter is set as 2 W. Table 5.1 gives the other simulation parameters.

5.6.2 Spectral Efficiency Performance

In the simulation, in order to generate the average spectral efficiency of the optical SDMA system, 100000 snapshots are generated for each number of active users. For each snapshot, it is ensured that active users are spatially uniformly distributed. The sum spectral efficiencies

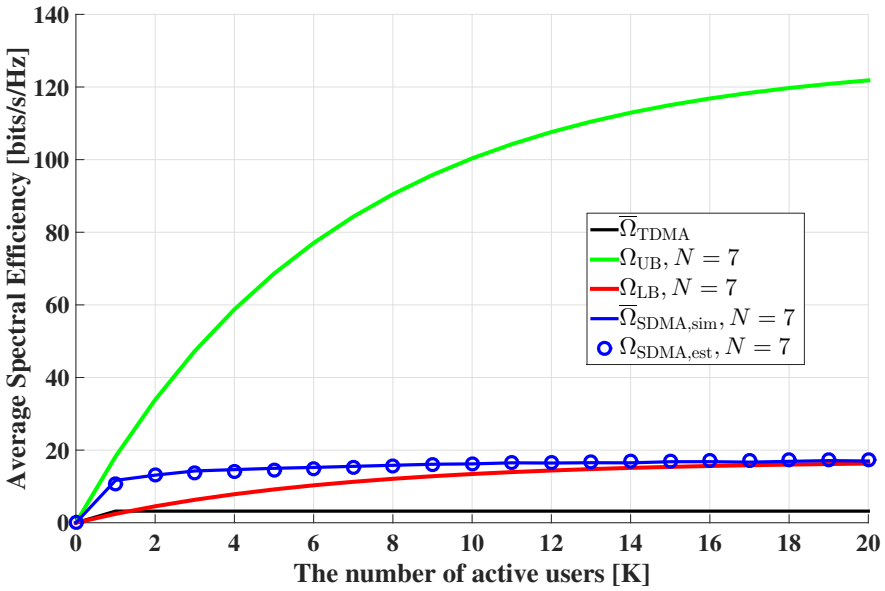

Figure 5.13: *The spectral efficiency of optical attocell network for different number of active users is shown when 7-element angle diversity transmitter is implemented.* $\overline{\Omega}_{\mathrm{SDMA,sim}}$ *represents the simulation result of the actual performance of the optical SDMA system.* $\overline{\Omega}_{\mathrm{SDMA,sim}}$ *represents the estimated theoretical result which is calculated by* (5.29).

of all users in the central optical cell of the 7-cell attocell network is calculated. Finally, the average spectral efficiency is obtained as the average of the sum spectral efficiency over all snapshots. The average spectral efficiencies for the optical TDMA scheme and the optical SDMA scheme are denoted by $\overline{\Omega}_{\mathrm{TDMA}}$ and $\overline{\Omega}_{\mathrm{SDMA}}$, respectively. N denotes the number of LED elements on each angle diversity transmitter.

Figure 5.13 shows the average spectral efficiency of the optical SDMA system when a 7-element angle diversity transmitter is used as the optical transmitter. The simulation results and estimated results of the average spectral efficiency of the optical SDMA system are denoted by $\overline{\Omega}_{\mathrm{SDMA,sim}}$ and $\overline{\Omega}_{\mathrm{SDMA,est}}$, respectively. It is notable that the average spectral efficiency increases when the total number of active users increases. The average spectral efficiency quickly saturates as the number of active users increases.

The upper bound of the system, Ω_{UB}, increases significantly when the number of active users increases. When K is small, $\Omega_{\mathrm{SDMA,sim}}$ is close to Ω_{UB}. This is because users tend to be well-separated in this scenario which results in low intra-cell interference and ICI. When K increases, the gap between $\Omega_{\mathrm{SDMA,sim}}$ and Ω_{UB} increases. This is because the calculation of

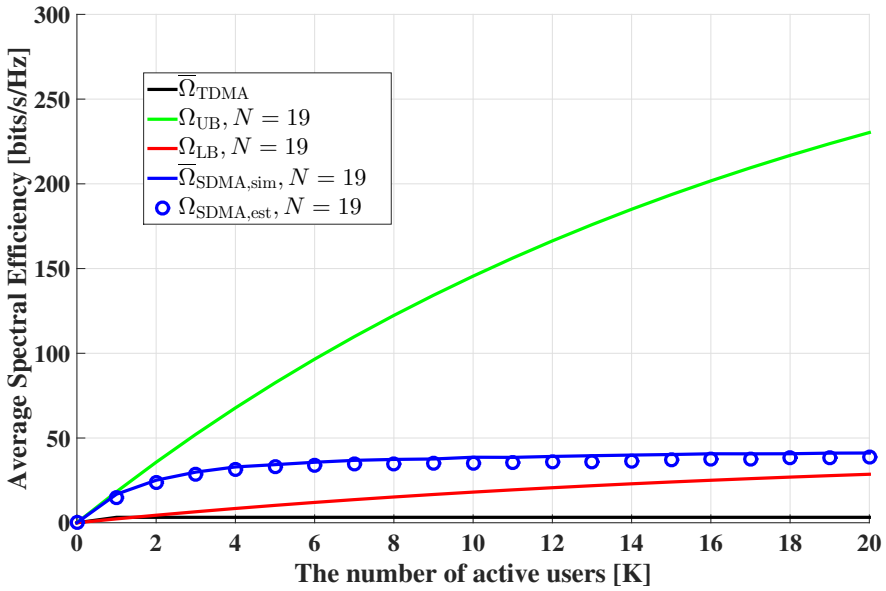

Figure 5.14: *The spectral efficiency of optical attocell network for different number of active users is shown when* 19*-element angle diversity transmitter is implemented.* $\overline{\Omega}_{\mathrm{SDMA,sim}}$ *represents the simulation result of the actual performance of the optical SDMA system.* $\overline{\Omega}_{\mathrm{SDMA,sim}}$ *represents the estimated theoretical result which is calculated by* (5.29).

upper bound considers no intra-cell and ICI.

The lower bound, Ω_{LB}, is calculated assuming all LED elements are active (strong intra-cell interference). When K is small, the actual intra-interference in the system is small. Therefore, $\overline{\Omega}_{\mathrm{SDMA,sim}}$ is a few times larger than Ω_{LB} when K is small. When K is large, Ω_{LB} approaches $\overline{\Omega}_{\mathrm{SDMA}}$. This is because, when there is a considerable number of active users in a cell, all LED elements on angle diversity transmitters are active. This setup is identical to the assumptions for calculating Ω_{LB}.

One important observation is that there is a close match between the simulation result, $\Omega_{\mathrm{LB,sim}}$, and theoretical estimation, $\Omega_{\mathrm{SDMA,est}}$. This validates the accuracy of the theoretical model and the related analysis in Section 5.5.3. Also, this means that the performance of optical SDMA can be well-estimated without complex Monte-Carlo simulations. It can also be observed that the SDMA system significantly outperforms the TDMA system that up to 6 times higher average spectral efficiency can be achieved. The angle diversity transmitter can generate narrow directional light beams which can effectively reduce ICI and enable parallel transmission. This results in the improvement on average spectral efficiency.

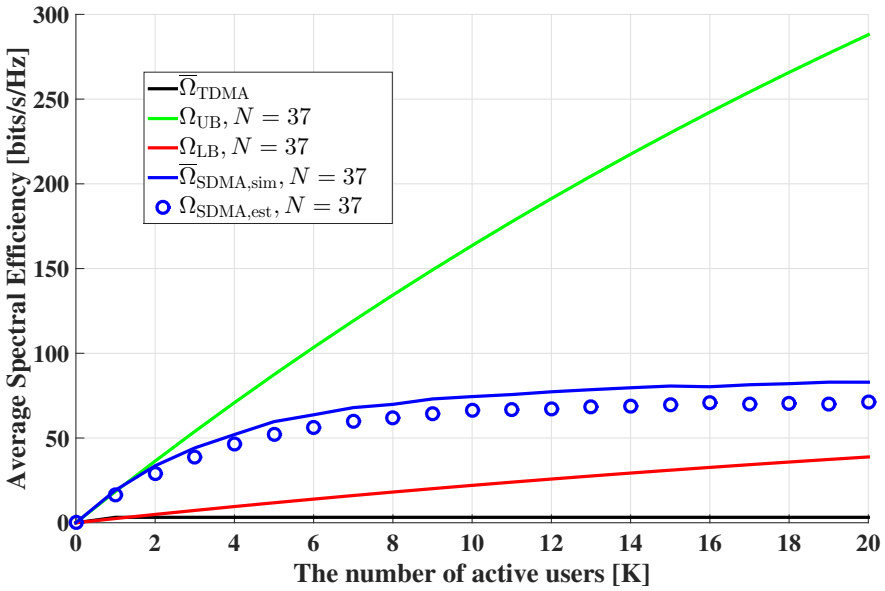

Figure 5.15: *The spectral efficiency of optical attocell network for different number of active users is shown when* 37*-element angle diversity transmitter is implemented.* $\overline{\Omega}_{\mathrm{SDMA,sim}}$ *represents the simulation result of the actual performance of the optical SDMA system.* $\overline{\Omega}_{\mathrm{SDMA,sim}}$ *represents the estimated theoretical result which is calculated by* (5.29).

Figure 5.14 shows the average spectral efficiency of the optical SDMA system when a 19-element angle diversity transmitter is used as the optical transmitter. The trend of the spectral efficiency performance in this scenario is similar to that in the previous scenario. Note that, when compared with TDMA, the SDMA system with a 19-element angle diversity transmitter can achieve up to 17 times higher average spectral efficiency than the TDMA system. When the number of transmitter elements increases further, the average spectral efficiency of the SDMA increases accordingly. Figure 5.15 shows that the SDMA system with a 37-element angle diversity transmitter can achieve up to 26 times higher average spectral efficiency than the TDMA system. This average spectral efficiency gain is obtained at the expense of using the angle diversity transmitter with 36 more LED elements. Also, this spectral efficiency gain requires position information with more accuracy which will be discussed in Sec.5.6.4.

In summary, the theoretical estimation, $\Omega_{\mathrm{SDMA,est}}$, can accurately predict the actual system performance $\overline{\Omega}_{\mathrm{SDMA}}$. The upper bound, Ω_{UB}, can provide a potential system average spectral efficiency when the advanced interference mitigation scheme is implemented (such as multiple colour LED elements to avoid intra-cell interference). Also, the lower bound, Ω_{LB}, describes

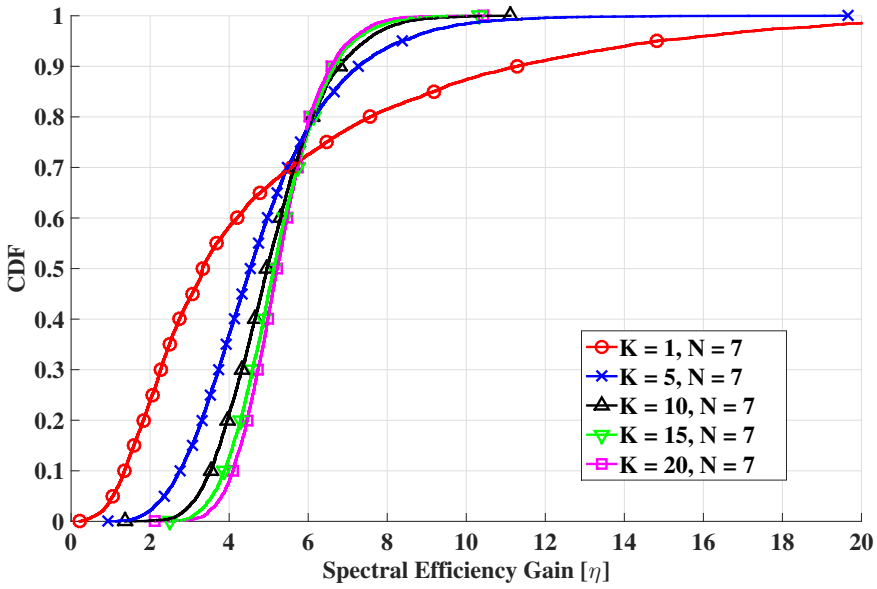

Figure 5.16: *The spectral efficiency gain of the optical SDMA system for different number of active users ($N = 7$).*

the average spectral efficiency of the system when no interference mitigation scheme is taken into account. It is observed that as K increases, the actual SDMA system transfers from a noise-limited system to an interference-limited system.

It is worth pointing out that optical SDMA using angle diversity transmitter requires more engineering work including the circuit design for supplying signals to multiple LED elements and the optics design to generate directed light beams. Also, optical SDMA requires more knowledge of channel state information to ensure the data transmission on each LED element. As optical SDMA requires multiple-element AP, the resource allocation algorithm of optical SDMA is more complex than optical TDMA with single-element APs.

5.6.3 Statistics of the Spectral Efficiency Gain

Figure 5.16 shows the performance of the spectral efficiency gain, η, when a 7-element angle diversity transmitter is used. It is apparent that most of the time η is greater than unity. This means the optical SDMA system significantly outperforms the TDMA system regardless of the position of the active users. The dynamic range of the spectral efficiency gain, η, is large. This is because the throughput gain is strongly related to the position of active users.

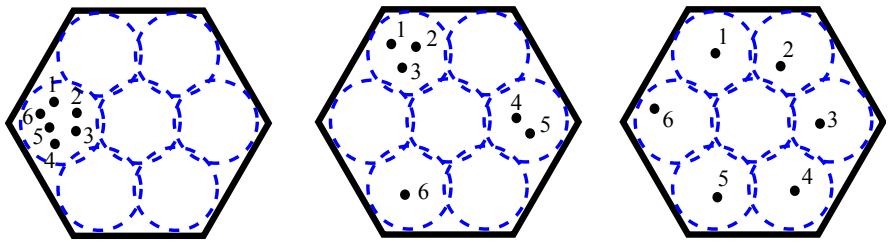

Figure 5.17: *Three typical scenarios for the SDMA system: 1. All active users are close to each other (left); 2. Some of the active users are close to each other (middle); 3. All active users are well-separated (right).*

When there is only one active user in a cell, $K = 1$, η can be very high at some positions. This is because, in a TDMA system, the half-intensity radiation angle of an optical transmitter is large which results in strong cell edge interference. In SDMA systems, this interference can be significantly mitigated, since only one LED element with narrow half-intensity radiation angle is activated at a time. When an active user is at the cell centre, the ICI is not significant in TDMA systems. In that scenario, SDMA cannot significantly improve the system spectral efficiency, which results in lower η. Also, the transmission power of a single link in a SDMA scheme is lower than that in a TDMA scheme. As a result, η may be less than 1.

When there is more than one active user in a cell, $K > 1$, η mainly depends on the relative distance between users. For example, in Figure 5.17, three typical scenarios are illustrated. For the first scenario, all active users are close to each other and within the region that is served by the same transmitter element. In that scenario, the spectrum of one LED element is shared by all users. Therefore, the spectral efficiency gain is achieved only from interference mitigation. For the second scenario, some of the active users are clustered together and three LED elements are activated simultaneously. This means, apart from the spectral efficiency gain from the interference mitigation, approximately three times extra spectral efficiency gain can be achieved by parallel transmissions. For the third scenario, each of the active users are well-separated. In that scenario, approximately six times extra spectral efficiency gain can be achieved from parallel transmission.

Figure 5.18 and 5.19 show the performance of the spectral efficiency gain when 19-element and 37-element angle diversity transmitters are used, respectively. The trend of the results are similar to the previous scenarios where a 7-element angle diversity transmitter is used. The overall spectral efficiency gain increases as the number of transmitter element increases. This

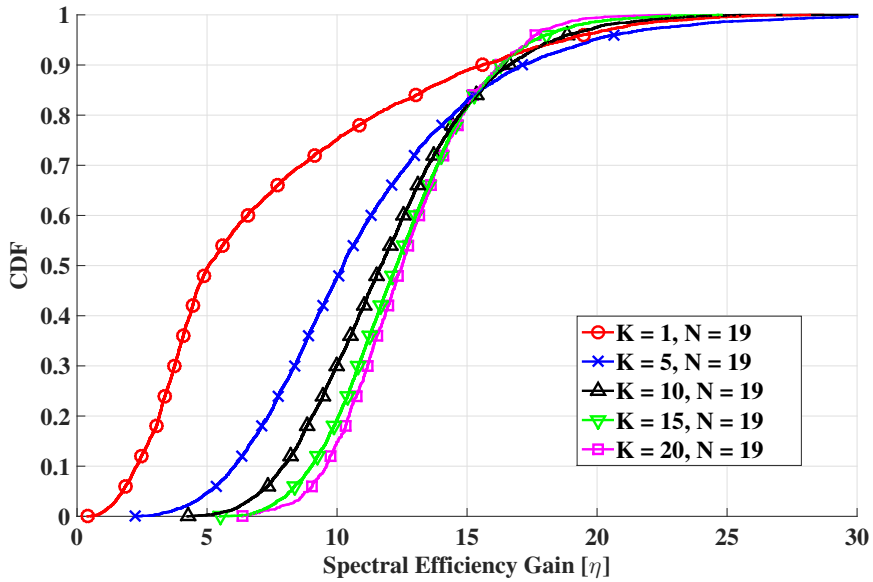

Figure 5.18: *The spectral efficiency gain of the optical SDMA system for different number of active users ($N = 19$).*

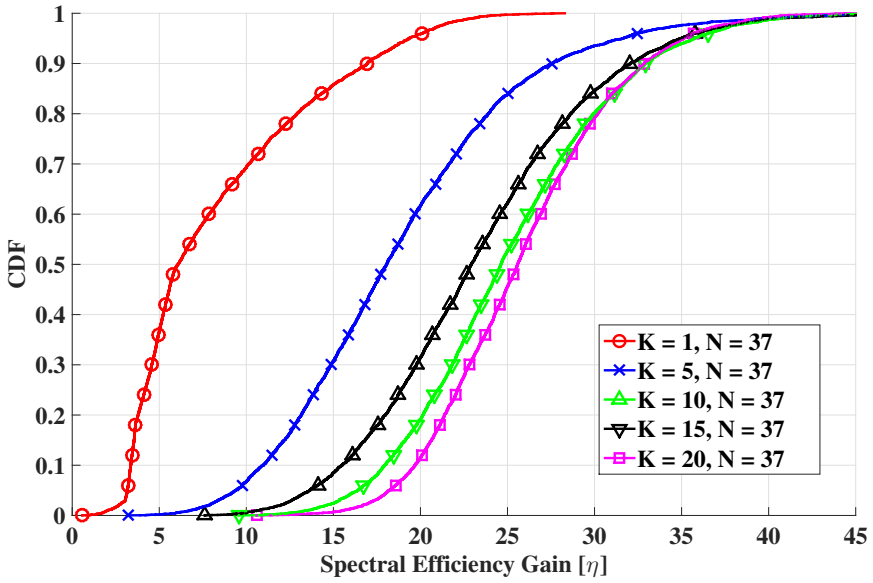

Figure 5.19: *The spectral efficiency gain of the optical SDMA system for different number of active users ($N = 37$).*

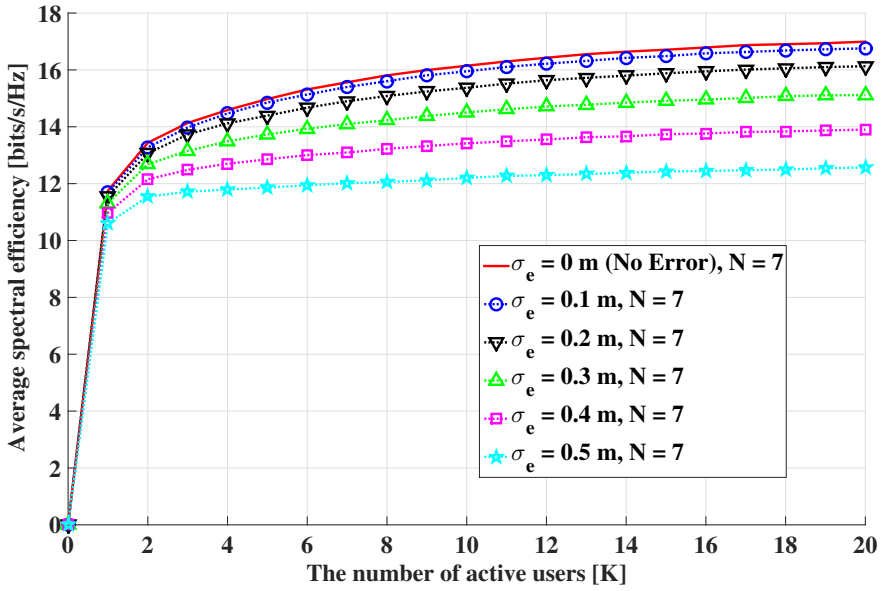

Figure 5.20: *The average spectral efficiency of the optical SDMA system when different standard variance of the position error is considered ($N = 7$).*

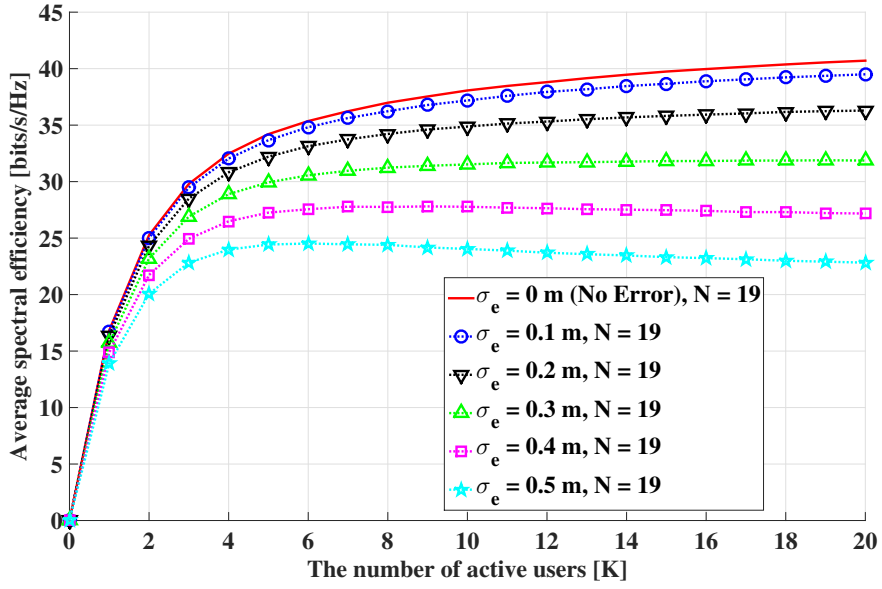

Figure 5.21: *The average spectral efficiency of the optical SDMA system when different standard variance of the position error is considered ($N = 19$).*

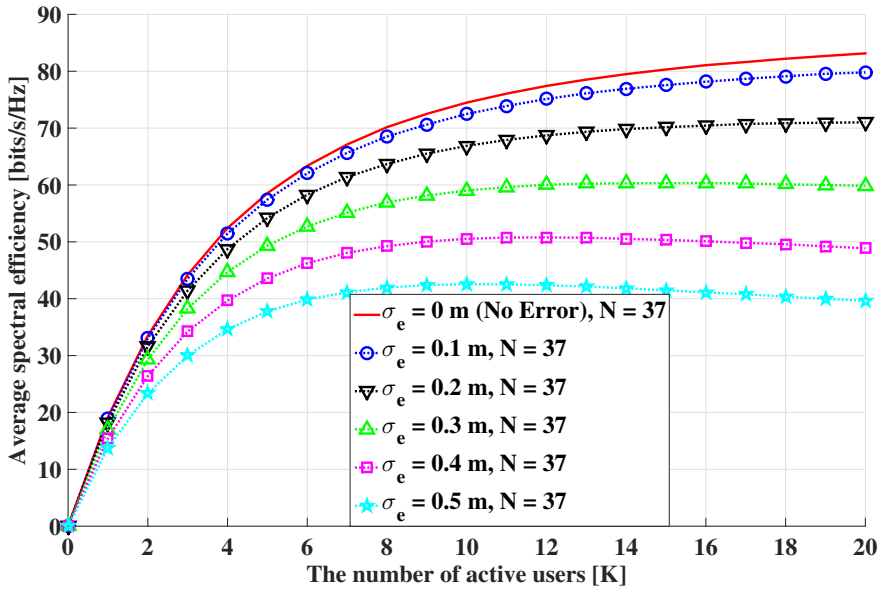

Figure 5.22: *The average spectral efficiency of the optical SDMA system when different standard variance of the position error is considered ($N = 37$).*

is because, when the number of LED elements on an angle diversity transmitter increases, the half-intensity angle of each element decreases accordingly. Narrow half-intensity angle of transmitter elements can effectively mitigate the ICI as well as the intra-cell interference. Also, the optical transmitter with more LED elements has a better ability to separate active users and create more parallel links to them. Hence, it can be concluded that the spectral efficiency gain of a SDMA system is scaled with the number of LED elements on each optical transmitter.

5.6.4 Position Errors

Figure 5.20 shows the average spectral efficiency of the optical SDMA system using 7-element transmitter when different σ_e are considered. According to the characteristics of the normal distribution, 95% of the estimated positions of active users are within two standard deviations ($2\sigma_e$) away from their actual positions. The curve with no markers represents the average spectral efficiency of the SDMA system, when the position information is perfectly known, $\sigma_e = 0$. When σ_e increases to 0.1 m, the average spectral efficiency of the SDMA system decreases only by 1.3% compared with the system with perfect position information. When σ_e is increased to 0.2 m, 0.3 m, 0.4 m and 0.5 m, the performance of the SDMA system decreases by 5%, 11%, 18% and 26%, respectively. When σ_e is large, the position information

for all active users is inaccurate. As a result, incorrect LED elements in each optical cell are activated. This means active users may not be served by their optimal LED element and additional performance penalties are introduced. Therefore, the overall system performance is degraded significantly if the user position errors are large.

Figure 5.21 shows the average spectral efficiency of the optical SDMA system using the 19-element transmitter when different σ_e is considered. When σ_e is 0.1 m, 0.2 m, 0.3 m, 0.4 m and 0.5 m, the performance of the SDMA system decreases 3%, 11%, 22%, 33% and 44%, respectively, compared with the system with perfect position information. For the SDMA system using 37-element transmitter (Figure 5.22), when σ_e are 0.1 m, 0.2 m, 0.3 m, 0.4 m and 0.5 m, the performance of the SDMA system decreases 4%, 14%, 28%, 41% and 52%, respectively, compared with the system with perfect position information. This means that when the number of transmitter elements increases, the SDMA system is more sensitive to position information of the active users. This is because, when the number of LED elements increases, the service area of each LED element is smaller. This means active users may be easily misallocated to the cell in the vicinity when the position information is inaccurate. Therefore, for a fixed σ_e, the SDMA system using more transmitter elements performs worse. It is also notable that the performance of the SDMA system is compromised when σ_e increases. Fortunately, optical attocells are perfect for indoor positioning which has been the first major application. With the use of the-state-of-the-art indoor positioning techniques, an average position error of less than 0.25 m can be often achieved [150]. This means $\mathbb{E}[d_e] = \sqrt{\frac{\pi}{2}}\sigma_e < 0.25$ m and $\sigma_e < 0.2$ m can be obtained. Therefore, the system average spectral efficiency only decreases by 14%. This result is very promising since the optical SDMA is robust to the position error which makes it suitable for practical implementation.

5.7 Summary

In this chapter, an optical attocell network adopting optical SDMA is proposed. In this network, an angle diversity transmitter is equipped in each optical cell and it can serve multiple active users simultaneously. With the use of an angle diversity transmitter, the ICI between optical cells can be significantly mitigated. The results clearly indicate that the optical SDMA system significantly outperforms the optical TDMA benchmark system. In particular, up to 26 times higher average spectral efficiency can be achieved when the transmitter is equipped with 37 LED elements. Also, an upper bound and lower bound of the SDMA system are derived analytically. These bounds can be used and can accurately predict the performance of the SDMA system. In addition, the result of average spectral efficiency gain clearly indicates that the SDMA system outperforms the TDMA system, regardless of the relative positions of the active users. Finally, position errors for the active users are considered. Results shows that the SDMA system is robust to user position errors, and the system performance is only compromised by 14% when the practical state-of-the-art indoor position techniques are used. The results strongly support the suitability of optical SDMA systems for practical implementations.

Chapter 6
Conclusions, Limitations and Future work

6.1 Summary and Conclusions

In this thesis, inter-cell interference (ICI) mitigation techniques in optical attocell networks have been studied. A simplified model for estimating non-line-of-sight (NLOS) ICI has been proposed. The proposed model can significantly reduce the computational complexity of conventional ray-tracing model. Also, in order to mitigate ICI in optical attocell networks, angle diversity receivers (ADRs) with different signal combining schemes have been proposed as receiver front-ends. Moreover, with angle diversity transmitters, optical space division multiple access (SDMA) has been achieved, which also mitigates ICI in optical attocell networks. With the help of the simplified model, a theoretical framework has been proposed. Also, this framework can accurately predict the system performance of optical attocell networks with angle diversity transmitters and ADRs.

In the first main chapter of the thesis, a downlink ICI model in optical attocell networks is investigated and a novel simplified model is proposed for estimating NLOS ICI in optical attocell networks. The results suggest that light reflections have significant impact on the user signal-to-interference-plus-noise ratio (SINR) performance. Specifically, the second order reflections are predominant components in the NLOS ICI. Base on that, a simplified model is proposed to reduce the computational complexity by only considering second-order light reflections. The model is further simplified by introducing a new method of evaluating NLOS light reflections. By using the proposed simplified model, the SINR distribution of optical attocell networks has been derived in closed-form. The simulation results show that the simplified model achieves a close match with the conventional NLOS ray-tracing model. This simplified model can also be applied to other scenarios, such as optical attocell networks with angle diversity receivers and angle diversity transmitters.

In the second main chapter of the thesis, interference mitigation techniques using ADRs are investigated in optical attocell networks. Four different signal combining schemes for ADRs and a novel double-source cell configuration are proposed. The results show that an ADR outperformed a single-PD receiver in terms of SINR performance. In particular, the ADR with optimum combining (OPC) performs the best which approaches interference-free system. However, OPC requires channel state information (CSI) knowledge from all access points (APs). In comparison, maximum ratio combining (MRC) and select best combining (SBC) provide sub-optimal performance by considering the CSI knowledge from the desired AP. Also, double-source cell configuration can further improve the system performance when ADRs are used. A

criteria of selecting transmission mode in double-source cell configuration is determined which improves the system performance in different scenarios. It can also be concluded that when the number of elements on an ADR increases, an ADR is more capable of avoiding ICI which results in better system performance. Furthermore, an analytical framework is proposed for analysing optical attocell networks using ADRs. Analytical models for different scenarios including line-of-sight (LOS) and NLOS propagation are derived and the accuracy of the models have been validated.

In the third main chapter of the thesis, optical SDMA using angle diversity transmitters is studied in optical attocell networks. By using optical SDMA, multiple active users can be simultaneously served at different positions. This can increase the available bandwidth resource and also mitigate ICI in optical attocell networks. The results show that optical SDMA significantly outperforms the conventional optical time division multiple access (TDMA) in terms of system average spectral efficiency. This improvement scales with the number of elements on each angle diversity transmitter. In particular, up to 26 times higher average spectral efficiency can be achieved when a 37-element light emitting diode (LED) transmitter is used. In addition, the upper bound and the lower bound of the performance of optical SDMA systems are derived analytically. These bounds can estimate the performance of SDMA systems. Moreover, the results of average spectral efficiency gain clearly show that the SDMA system outperforms the TDMA system, regardless of the relative positions of the active users. The study is finally extended to account for the user position errors. The system performance is only compromised by up to 14% when the practical state-of-the-art indoor position techniques are used. Monte-Carlo simulation results show that the system is very robust to user position errors. This means that optical SDMA systems are suitable for practical implementation.

6.2 Limitations and Future Work

The results of analytical model presented in Chapter 3 show a close agreement with the Monte-Carlo simulation. However, all the simulation results and analytical results are based on the assumption of flat linear additive white Gaussian noise (AWGN) channel. In future work, the multipath effect from the light reflections will be considered. Also, the bandwidth limitation of transmitter front-ends and receiver front-ends will be considered. Apart from that, the proof-of-concept experiments can be performed to evaluate the accuracy of theoretical model.

In Chapter 4, ADRs are used to mitigate ICI in optical attocell networks. It is assumed that all ADRs are equipped with compound parabolic concentrator (CPC) concentrator. CPC concentrator can provide high concentration gain and precisely limit the field-of-view (FOV) of a photodiode (PD) element. CPC concentrator has strong cut-off effect. If incident light are within the FOV of a concentrator, all optical energy from incident light can be captured. On the contrary, if incident light is out of the FOV, no optical energy can be received from the LOS link. This characteristic is very beneficial for interference mitigation in optical attocell networks since interfering light from the undesired directions can easily be rejected. However, a CPC concentrator has drawbacks: the narrower the FOV of a CPC concentrator, the higher the concentrator gain, but the longer a concentrator will be. In some scenarios, it is impossible to use a narrow FOV CPC due to the limitation of size. Therefore, other types of concentrators also need to be considered. This means further work can be conducted to evaluate the performance of ADRs with other types of concentrators. Also, proof-of-concept experiments could be carried out to validate the theoretical models. In the future work, a prototype network consists of optical cells with ADRs should be developed.

In Chapter 5, optical SDMA using angle diversity transmitters are investigated in optical attocell networks. In this thesis, the analysis of system performance only accounts for 7 optical cells. In future work, more optical cells will be considered. Also, the edge effects and the light reflections from walls will be taken into account. With the help of edge effects, the optical cells close to walls will suffer less ICI since opaque walls can reject interfering light signals from other rooms. However, walls have disadvantages. When users are located at the corner, LOS links may be affected by reflected light from walls. Therefore, edge effect in optical attocell networks should be further investigated when optical SDMA is applied. In future work, the coordination between different optical cells could be considered to further mitigate ICI.

Appendix A
Interference Mitigation Techniques using Angle Diversity Receiver

A.1 The Proof of (4.49) and (4.50)

$$\gamma_{\mathrm{OPC}} = \frac{\tau^2 P_{\mathrm{tx}}^2 \Big(w_{p_{\mathrm{d}}} H_{a_{\mathrm{d}},p_{\mathrm{d}}} + \sum\limits_{p \neq p_{\mathrm{d}}} w_p H_{a_{\mathrm{d}},p} \Big)^2}{\mathcal{I}_{\mathrm{NLOS,OPC}} + \sum_{p=1}^{N_{\mathrm{PD}}} w_p^2 N_0 B}. \tag{A.1}$$

The magnitude of the LOS channel is a few orders of magnitude larger than the NLOS channel. Since only the desired PD a_{d} can establish a LOS link with the desired AP:

$$H_{a_{\mathrm{d}},p_{\mathrm{d}}} \gg H_{a_{\mathrm{d}},p}. \quad (p \neq p_{\mathrm{d}}) \tag{A.2}$$

The SINR of OPC can be approximated as follows:

$$\begin{aligned}
\gamma_{\mathrm{OPC}}(r) &\approx \frac{\Big(\tau P_{\mathrm{tx}} w_{p_{\mathrm{d}}} H(r, \Psi_{\mathrm{ADR}}) \Big)^2}{\mathcal{I}_{\mathrm{NLOS,OPC}} + \sum_{p=1}^{N_{\mathrm{PD}}} w_p^2 N_0 B} \\
&= \frac{\Big(\tau P_{\mathrm{tx}} w_{p_{\mathrm{d}}} H(r, \Psi_{\mathrm{ADR}}) \Big)^2}{\mathcal{I}_{\mathrm{NLOS,OPC}} + \sum\limits_{p \neq p_{\mathrm{d}}} w_p^2 N_0 B + w_{p_{\mathrm{d}}}^2 N_0 B} \\
&< \frac{\Big(\tau P_{\mathrm{tx}} w_{p_{\mathrm{d}}} H(r, \Psi_{\mathrm{ADR}}) \Big)^2}{w_{p_{\mathrm{d}}}^2 N_0 B} \\
&= \frac{\Big(\tau P_{\mathrm{tx}} H(r, \Psi_{\mathrm{ADR}}) \Big)^2}{N_0 B} = \gamma_{\mathrm{OPC,UB}}(r).
\end{aligned} \tag{A.3}$$

A.2 The Proof of (4.64)

The SINR of OPC in double-source cell configuration is represented as follows:

$$\begin{aligned}\gamma_{\mathrm{OPC}}^{\mathrm{double}}(r) &= \frac{\left(\frac{1}{2}\tau P_{\mathrm{tx}}\left(w_{p_{\mathrm{pos}}}+w_{p_{\mathrm{neg}}}\right)H(r,\Psi_{\mathrm{ADR}})\right)^2}{\mathcal{I}_{\mathrm{NLOS,OPC}}^{\mathrm{double}}+\sum_{p=1}^{N_{\mathrm{PD}}} w_p^2 N_0 B} \\ &< \frac{\left(\frac{1}{2}\tau P_{\mathrm{tx}}\left(w_{p_{\mathrm{pos}}}+w_{p_{\mathrm{neg}}}\right)H(r,\Psi_{\mathrm{ADR}})\right)^2}{\left(w_{p_{\mathrm{pos}}}^2+w_{p_{\mathrm{neg}}}^2\right)N_0 B}\end{aligned} \tag{A.4}$$

Since

$$\frac{(w_{p_{\mathrm{pos}}}+w_{p_{\mathrm{neg}}})^2}{w_{p_{\mathrm{pos}}}^2+w_{p_{\mathrm{neg}}}^2}\leq 2, \tag{A.5}$$

the SINR of the double source cell configuration is:

$$\gamma_{\mathrm{OPC}}^{\mathrm{double}}(r) < \frac{\left(\tau P_{\mathrm{tx}}H(r,\Psi_{\mathrm{ADR}})\right)^2}{2N_0 B} = \gamma_{\mathrm{OPC,UB}}^{\mathrm{double}}(r). \tag{A.6}$$

Appendix B
SDMA using Angle Diversity Transmitter in Optical Attocell Networks

B.1 The Proof of (5.32)

In order to calculate (5.32), the limitation of a similar equation is firstly considered:

$$\lim_{N\to\infty} \ln(1-1/N)^{\zeta N} = \lim_{N\to\infty} \zeta N \ln(1-1/N). \tag{B.1}$$

Assuming that $t = 1/N$ and according to the L'Hospital's Rule:

$$\lim_{N\to\infty} \zeta N \ln(1-1/N) = \lim_{t\to 0} \frac{[\zeta \ln(1-t)]'}{[t]'} = -\zeta. \tag{B.2}$$

Hence,

$$\lim_{N\to\infty} (1-1/N)^{\zeta N} = e^{-\zeta}. \tag{B.3}$$

B.2 The Derivation of $\Omega'(r,\rho)$

The average spectral efficiency, $\Omega(r,\rho)$, can be approximated by $\Omega'(r,\rho)$. The procedure is presented as follows.

B.2.1 N = 19

Similarly, for the 19-element transmitter, the cell area can be divided into three parts. When $0 \le r < h\tan(\frac{\alpha}{2})$,

$$\Omega'(r,\rho) = \frac{\Omega(r,0)+\Omega(r,\frac{\pi}{6})}{2} + \frac{\Omega(r,0)-\Omega(r,\frac{\pi}{6})}{2}\cos(6\rho). \tag{B.4}$$

When $h\tan(\frac{\alpha}{2}) \leq r < h\tan(\frac{3\alpha}{2})$,

$$\Omega'(r,\rho) = \Omega(r,\frac{\pi}{6}) + \Omega(r,0) - \Omega(r,\frac{\pi}{6})|\sin(3\rho)|. \tag{B.5}$$

When $h\tan(\frac{3\alpha}{2}) \leq r < R$, $\Omega'(r,\rho) =$

$$\begin{cases} \Omega(r,\frac{\pi}{6}) + \Omega(r,\frac{\pi}{4}) + \left(\Omega(r,\frac{\pi}{6}) - \Omega(r,\frac{\pi}{4})\right)|\cos(6\rho)| \\ \qquad\qquad \text{if} \quad \frac{\pi}{12} + \frac{\pi}{3}u < \rho \leq \frac{\pi}{4} + \frac{\pi}{3}u \\ \Omega(r,0) + \Omega(r,\frac{\pi}{12}) + \left(\Omega(r,0) - \Omega(r,\frac{\pi}{12})\right)|\cos(6\rho)| \\ \qquad\qquad \text{otherwise}, \end{cases} \tag{B.6}$$

where $u = 0, 1, 2, 3, 4, 5$.

B.2.2 N = 37

For the 37-element transmitter, the cell area can be divided into four parts. When $0 \leq r < h\tan(\frac{\alpha}{2})$,

$$\Omega'(r,\rho) = \frac{\Omega(r,0) + \Omega(r,\frac{\pi}{6})}{2} + \frac{\Omega(r,0) - \Omega(r,\frac{\pi}{6})}{2}\cos(6\rho). \tag{B.7}$$

When $h\tan(\frac{\alpha}{2}) \leq r < h\tan(\frac{3\alpha}{2})$,

$$\Omega'(r,\rho) = \Omega(r,\frac{\pi}{6}) + \Omega(r,0) - \Omega(r,\frac{\pi}{6})|\sin(3\rho)|. \tag{B.8}$$

When $h\tan(\frac{3\alpha}{2}) \leq r < h\tan(\frac{5\alpha}{2})$, $\Omega'(r,\rho) =$

$$\begin{cases} \Omega(r,\frac{\pi}{6}) + \Omega(r,\frac{\pi}{4}) + \left(\Omega(r,\frac{\pi}{6}) - \Omega(r,\frac{\pi}{4})\right)|\cos(6\rho)| \\ \qquad\qquad \text{if} \quad \frac{\pi}{12} + \frac{\pi}{3}u < \rho \leq \frac{\pi}{4} + \frac{\pi}{3}u \\ \Omega(r,0) + \Omega(r,\frac{\pi}{12}) + \left(\Omega(r,0) - \Omega(r,\frac{\pi}{12})\right)|\cos(6\rho)| \\ \qquad\qquad \text{otherwise}. \end{cases} \tag{B.9}$$

When $h\tan(\frac{5\alpha}{2}) \leq r < R$, $\Omega'(r,\rho) =$

$$\begin{cases} \Omega(r,\frac{\pi}{12}) + \Omega(r,\frac{\pi}{8}) + (\Omega(r,\frac{\pi}{12}) - \Omega(r,\frac{\pi}{8}))|\cos(12\rho)| \\ \qquad\qquad \text{if} \quad \frac{\pi}{24} + \frac{\pi}{3}u < \rho \leq \frac{\pi}{8} + \frac{\pi}{3}u \\ \Omega(r,\frac{\pi}{6}) + \Omega(r,\frac{5\pi}{24}) + (\Omega(r,\frac{\pi}{6}) - \Omega(r,\frac{5\pi}{24}))|\cos(12\rho)| \\ \qquad\qquad \text{if} \quad \frac{\pi}{8} + \frac{\pi}{3}u < \rho \leq \frac{5\pi}{24} + \frac{\pi}{3}u \\ \Omega(r,\frac{\pi}{4}) + \Omega(r,\frac{7\pi}{24}) + (\Omega(r,\frac{\pi}{4}) - \Omega(r,\frac{7\pi}{24}))|\cos(12\rho)| \\ \qquad\qquad \text{if} \quad \frac{5\pi}{24} + \frac{\pi}{3}u < \rho \leq \frac{7\pi}{24} + \frac{\pi}{3}u \\ \Omega(r,0) + \Omega(r,\frac{\pi}{24}) + (\Omega(r,0) - \Omega(r,\frac{\pi}{24}))|\cos(12\rho)| \\ \qquad\qquad \text{otherwise.} \end{cases} \tag{B.10}$$

B.3 The Representation of $\Omega''(r)$

B.3.1 N = 7

When $0 \leq r < h\tan(\frac{\alpha}{2})$,

$$\Omega''(r) = (\pi+1)\Omega(r,0) + (\pi-1)\Omega(r,\frac{\pi}{6}). \tag{B.11}$$

When $h\tan(\frac{\alpha}{2}) \leq r \leq R$,

$$\Omega''(r) = (2\pi-2)\Omega(r,\frac{\pi}{6}) + 2\pi\Omega(r,0). \tag{B.12}$$

B.3.2 N = 19

When $0 \leq r < h\tan(\frac{\alpha}{2})$,

$$\Omega''(r) = (\pi+1)\Omega(r,0) + (\pi-1)\Omega(r,\frac{\pi}{6}). \tag{B.13}$$

When $h\tan(\frac{\alpha}{2}) \leq r < h\tan(\frac{3\alpha}{2})$,

$$\Omega''(r) = (2\pi-2)\Omega(r,\frac{\pi}{6}) + 2\pi\Omega(r,0). \tag{B.14}$$

When $h\tan(\frac{3\alpha}{2}) \leq r < R$,

$$\begin{aligned}\Omega''(r) = (\pi+1)(\Omega(r,0)+\Omega(r,\frac{\pi}{6}))+(\pi-1)\\ \times(\Omega(r,\frac{\pi}{12})+\Omega(r,\frac{\pi}{4})).\end{aligned} \tag{B.15}$$

B.3.3 N = 37

When $0 \leq r < h\tan(\frac{\alpha}{2})$,

$$\Omega''(r) = (\pi+1)\Omega(r,0)+(\pi-1)\Omega(r,\frac{\pi}{6}). \tag{B.16}$$

When $h\tan(\frac{\alpha}{2}) \leq r < h\tan(\frac{3\alpha}{2})$,

$$\Omega''(r) = (2\pi-2)\Omega(r,\frac{\pi}{6})+2\pi\Omega(r,0). \tag{B.17}$$

When $h\tan(\frac{3\alpha}{2}) \leq r < h\tan(\frac{5\alpha}{2})$,

$$\begin{aligned}\Omega''(r) = (\pi+1)(\Omega(r,0)+\Omega(r,\frac{\pi}{6}))+(\pi-1)\\ \times(\Omega(r,\frac{\pi}{12})+\Omega(r,\frac{\pi}{4})).\end{aligned} \tag{B.18}$$

When $h\tan(\frac{5\alpha}{2}) \leq r < R$,

$$\begin{aligned}\Omega''(r) = \frac{1}{2}(\pi+1)(\Omega(r,0)+\Omega(r,\frac{\pi}{12})+\Omega(r,\frac{\pi}{6})+\Omega(r,\frac{\pi}{4}))\\ +\frac{1}{2}(\pi-1)(\Omega(r,\frac{\pi}{24})+\Omega(r,\frac{\pi}{8})+\Omega(r,\frac{5\pi}{24})+\Omega(r,\frac{7\pi}{24})).\end{aligned} \tag{B.19}$$

Appendix C
Publications

All publications are presented in this appendix.

C.1 Journal Articles

Zhe Chen, Dushyantha A. Basnayaka, Xiping Wu and Harald Haas, "Interference Mitigation Using Angle Diversity Receiver in Indoor Optical Attocell Networks", accepted by Journal of Lightwave Technology.

Zhe Chen, Dushyantha A. Basnayaka, H. Haas, "Space Division Multiple Access for Optical Attocell Network Using Angle Diversity Transmitters", submitted to Journal of Lightwave Technology.

C.2 Conference Papers

Z. Chen, N. Serafimovski and H. Haas, "Angle Diversity for an Indoor Cellular Visible Light Communication System," 2014 IEEE 79th Vehicular Technology Conference (VTC Spring), Seoul, 2014, pp. 1-5. doi: 10.1109/VTCSpring.2014.7022832

Z. Chen, D. Tsonev and H. Haas, "Improving SINR in Indoor Cellular Visible Light Communication Networks," 2014 IEEE International Conference on Communications (ICC), Sydney, NSW, 2014, pp. 3383-3388.

Z. Chen, D. Tsonev and H. Haas, "A Novel Double-source Cell Configuration for Indoor Optical Attocell Networks," 2014 IEEE Global Communications Conference, Austin, TX, 2014, pp. 2125-2130.

Z. Chen, D. Tsonev and H. Haas, "Improved Receivers for Asymmetrically-Clipped Optical OFDM," 2014 IEEE 79th Vehicular Technology Conference (VTC Spring), Seoul, 2014, pp. 1-5.

Z. Chen and H. Haas, "Space Division Multiple Access in Visible Light Communications," 2015 IEEE International Conference on Communications (ICC), London, 2015, pp. 5115-5119.

Z. Chen and H. Haas, "A Simplified Model for Indoor Optical Attocell Networks," 2015 IEEE Summer Topicals Meeting Series (SUM), Nassau, 2015, pp. 167-168.

Z. Chen, D. A. Basnayaka and H. Haas, "Space Division Multiple Access in Optical Attocell Networks," 2016 IEEE Wireless Communications and Networking Conference, Doha, Qatar, 2016, pp. 1-5. [invited]

Space Division Multiple Access for Optical Attocell Network Using Angle Diversity Transmitters

Zhe Chen, *Student Member, IEEE*, Dushyantha A. Basnayaka, *Member, IEEE*, and Harald Haas, *Member, IEEE*

***Abstract*—In this paper, an optical space division multiple access (SDMA) scheme is proposed for optical attocell networks. In the system, the conventional single-element transmitter in each optical cell is substituted by an angle diversity transmitter which can simultaneously serve multiple active users at different positions. The type of configuration can increase the available bandwidth resource and also mitigate inter-cell interference (ICI) in optical attocell networks. The results show that an optical SDMA scheme significantly outperforms the conventional optical time division multiple access (TDMA) scheme. The SDMA scheme improves the average spectral efficiency of the system by a factor of 26 for a 37-element light emitting diode (LED) angle diversity transmitter. In addition, the upper and lower bound of the optical SDMA performance are derived analytically. These bounds can precisely estimate the performance of SDMA systems. Also, the study is extended to take account of user position errors, and Monte-Carlo simulations show that the system is very robust to user position errors.**

***Index Terms*—angle diversity transmitter; visible light communication; space division multiple access; position errors**

I. Introduction

WIRELESS data traffic has increased significantly and shows an exponential increase in the future. It is predicted that mobile data traffic is expected to increase to 24.3 exabytes per month by 2019 [1]. Although there has been technical improvements in radio frequency (RF) systems, it is still a technical challenge to meet such high levels of data traffic. In order to address the limited RF spectrum, visible light communication (VLC) technology has been developed as a potential alternative [2]. VLC enables the transformation of conventional lighting infrastructures into high speed access point (AP). Pioneering research shows that VLC is able to attain extremely high data rates [3], [4]. In particular, a single-colour light emitting diode (LED) can achieve transmission speeds of over 3 Gbps [5]. Taking an important step beyond point-to-point VLC links, high speed bi-directional wireless networking solution using visible light are envisaged. The aim in the future is to carry 25% of the indoor data traffic via VLC networks in the future.

In VLC, a LED and a photodiode (PD) are typically used as the transmitter and the receiver, respectively. The information is modulated in the intensity of a LED, termed intensity modulation (IM). At the receiver, a simple non-coherent energy detector is used to recover the information, and this is termed direct detection (DD). The advantages of VLC technology are as follows: i) VLC operates in an unregulated part of the electromagnetic spectrum which means that no license are required for the spectrum resource; ii) since visible light cannot penetrate opaque objects, VLC can transmit wireless data within a specific confined area more securely; iii) VLC is intrinsically safe to use in electromagnetic interference (EMI) sensitive environments [6], such as aircraft, hospitals and oil refineries.

Cellular networks can achieve high data density by harnessing the frequency reuse gains. Compared with RF cells, optical cells are considerably smaller due to the confined coverage of LEDs [7]. An optical cellular network facilitates higher frequency reuse and, therefore, higher data density than small-cell RF wireless networks. Results shows that an optical cellular network significantly outperforms RF femtocell systems [8]. In a typical indoor scenario, each lighting fixture becomes an AP, and can serve multiple users. This type of network is referred to as an optical attocell network [9].

In cellular multi-user systems, time division multiple access (TDMA) is typically used. In TDMA, the data intended for different users is transmitted in different time slots, and occupies the entire system bandwidth in its respective time slot. TDMA has two limitations: i) only one user can be served in a time slot and therefore this does not effectively exploit the available bandwidth; and ii) the transmitter radiates signals omni-directionally to provide full cell coverage, and this causes strong inter-cell interference (ICI), especially to cell-edge users. In order to overcome these limitations, a spatial dimension is added to the conventional TDMA system. In RF, a well-known method is space division multiple access (SDMA) [10] which has been integrated to the 4G communication standards such as LTE and IEEE 802.11ac [11]. In SDMA, an antenna array is used at the transmitter to generate multiple narrow beams pointing towards different active users. In this way, multiple users can be served simultaneously within the same time slot.

Although SDMA shows promising performance in RF, it cannot be directly adopted in VLC. One of the main issues is the transmitter. In RF, directional narrow beams are generated by changing the amplitude and phase of the signals transmitted by an antenna array. However, this approach cannot be implemented straightforwardly in VLC because VLC uses intensity modulation and direct detection (IM/DD). However, in VLC, LEDs have an inherent feature of a confined field-of-view (FOV). This characteristic can be exploited for generating directional light beams. Therefore, in optical SDMA, an angle diversity transmitter which consists of multiple directional narrow FOV LED elements is used as the optical transmitter.

Professor Haas acknowledges support from the Engineering and Physical Sciences Research Council (EPSRC) under Established Career Fellowship grant EP/K008757/1.

Zhe Chen, Dushyantha A. Basnayaka and Harald Haas are with the Institute for Digital Communications, Li-Fi Research and Development Centre, the University of Edinburgh, Edinburgh, UK, EH9 3JL. (e-mail: z.chen@ed.ac.uk; d.basnayaka@ed.ac.uk; h.haas@ed.ac.uk)

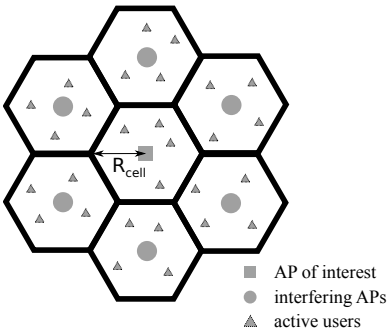

Fig. 1. The layout of a 7-cell attocell network.

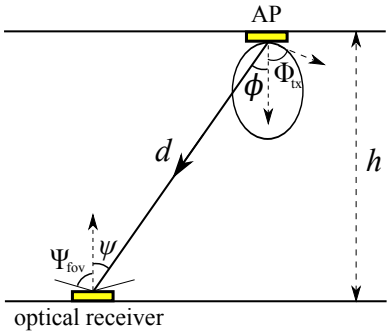

Fig. 2. LOS propagation model.

By activating different transmitter elements, the angle diversity transmitter can simultaneously serve multiple users at different locations.

In previous research, it has been shown that SDMA is an effective scheme which can significantly improve the performance of a RF system [10]. In RF, SDMA increases the system spectral efficiency by multiplexing information intended for multiple users using channel state information [12], [13]. The existing approaches to improve the spectral efficiency of VLC networks includes a system consisting of multi-beam transmitters and imaging diversity receivers [14]. However, this system does not support multiple users and its mobility is significantly restricted by the imaging optical receiver. In [15] and [16], an optical attocell network is proposed which can achieve a higher system spectral efficiency by exploiting frequency reuse and different ICI mitigation methods. However, to the authors' best knowledge, there is little research that exploits the transmitter spatial diversity at a system level. Therefore, in this study, optical SDMA using angle diversity transmitters for an optical attocell network is proposed and systematically analysed.

The remainder of this paper is organised as follows. The system model which includes light propagation, optical TDMA, optical SDMA and position errors is given in Section II. The theoretical analysis of the optical SDMA system is presented in Section III. Numerical and theoretical results are compared and discussed in Section IV. Finally, conclusions are given in Section V.

II. System Model

This study focuses on the downlink transmission of a VLC system. A 7-cell attocell network is assumed and the performance of the cell in the centre is considered in order to eliminate cell edge effects in the simulations (see Fig. 1). LED lighting fixtures are the APs. These APs are assumed to be placed in the ceiling and the optical receivers for all active users are assumed to be placed at a desktop height of 0.85 m. For the optical receiver, a wide FOV PD of 70^{o} is assumed. An optical receiver with a large FOV ensures that line-of-sight (LOS) components dominate rather than non-line-of-sight (NLOS) components which are a few orders of magnitude weaker than LOS components. Therefore, in this study, only the effect of LOS paths of the light fixtures is considered.

A. LOS Propagation Model

A typical LOS link from an AP to an active user is shown in Fig. 2. The direct current (DC) gain of the LOS link can be accurately calculated as follows [17]:

$$H_0 = \frac{(n+1)A_{\text{eff}}}{2\pi d^2}\cos^n(\phi)\cos(\psi)\text{rect}\left(\frac{\psi}{\Psi_{\text{fov}}}\right), \quad (1)$$

where d is the distance between an AP and its corresponding receiver; Ψ_{fov} is the FOV of the optical receiver; n is the Lambertian order of the LED elements; n is also a function of the transmitter half-intensity radiation angle Φ_{tx} as $n = -1/\log_2(\cos(\Phi_{\text{tx}}))$; ϕ is the angle of irradiance; ψ is the angle of light incidence at the receiver; $\text{rect}(\cdot)$ is a unit step function. The effective signal collection area A_{eff} is given as:

$$A_{\text{eff}} = A_{\text{p}}G\frac{n_{\text{ref}}^2}{\sin^2(\Psi_{\text{fov}})}, \quad (2)$$

where n_{ref} is the refractive index of the receiver optics; A_{p} is the physical area of the optical receiver; G is the signal transmission gain of the optical filter.

B. Optical TDMA

In order to serve multiple users in each optical cell, a multiple access scheme is required. TDMA is assumed to be the most common scheme for multi-user access. In a typical optical TDMA scenario, a single-element optical transmitter is adapted as an AP. All active users share the same spectrum in their corresponding optical cell. Information for different users is transmitted in different time slots of identical length. In each time slot, only one of the active users can be served. Therefore, the received signal-to-interference-plus-noise-ratio (SINR) of the active user k can be expressed as:

$$\gamma_k = \frac{\left(\tau P_{\text{tx}}H_{(\hat{b},k)}\right)^2}{N_0B + \sum_{b'\neq\hat{b}}\left(\tau P_{\text{tx}}H_{(b',k)}\right)^2}, \quad (3)$$

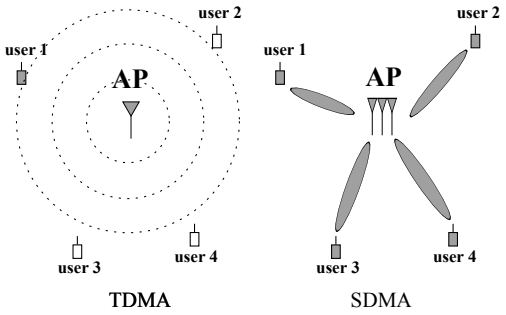

Fig. 3. The difference between TDMA and SDMA. On the left is a TDMA scenario. Only user 1 is served within a time slot. On the right is a SDMA scenario. Four users are served simultaneously within one time slot.

where τ is the responsivity of the PD; P_{tx} is the optical power transmitted by an AP and is assumed to be the same for all APs; $H_{(\hat{b},k)}$ is the channel attenuation between user k and the desired AP $\hat{b}$; $\sum_{b' \neq \hat{b}} \left(rP_{\text{t}}H_{(b',k)}\right)^2$ represents the interference signal from interfering APs; N_0 is the additive white Gaussian noise (AWGN) power spectral density; B is the optical communication bandwidth.

Assuming a simple Round Robin (RR) scheduler, the spectral efficiency of the optical TDMA system is as follows:

$$\Omega_{\text{TDMA}}(k) = \frac{1}{K}\sum_{k=1}^{K}\log_2(1+\gamma_k), \tag{4}$$

where K is the total number of the active users.

The optical TDMA systems described here have two main disadvantages. Firstly, users in the system are successively assigned to different time slots. Only one user can be served in each time slot. This significantly limits the overall performance of the system since the available bandwidth cannot be effectively shared, and this also limits the user data rate granularity. Secondly, the conventional single-element optical transmitter requires a large half intensity radiation angle to achieve full light and signal coverage. As a consequence, ICI in the system could significantly increase and the overall system performance is then compromised.

C. Optical SDMA

In order to overcome the disadvantages of optical TDMA systems, a multiple access scheme that supports parallel transmissions, SDMA, is introduced. SDMA was initially implemented in RF communication [18]. As illustrated in Fig. 3, in a TDMA scenario, an AP consists of a single-element transmitter which generates an omni-directional signal. Only one user can be served within a time slot. Unlike TDMA, the SDMA AP consists of an antenna array which can generate multiple directional narrow beam signals simultaneously. Hence, more than one active user can be served within a single time slot. By exploiting the location information of active users, the interference between these narrow beams can be significantly mitigated. Therefore, in comparison with TDMA, SDMA is able to offer superior performance.

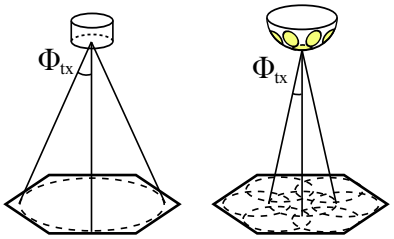

Fig. 4. The layout of the optical TDMA scenario with a conventional single-element optical transmitter (left) and the layout of the optical SDMA scenario with an angle diversity optical transmitter (right).

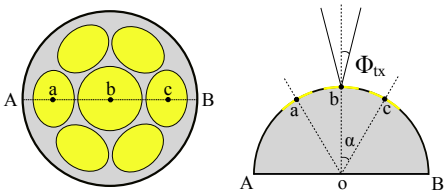

Fig. 5. The layout of a 7-element angle diversity transmitter.

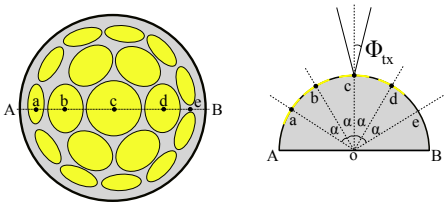

Fig. 6. The layout of a 19-element angle diversity transmitter.

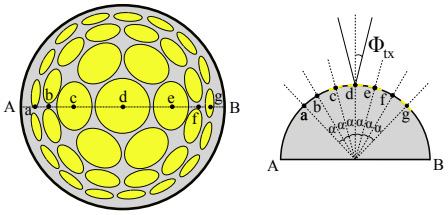

Fig. 7. The layout of a 37-element angle diversity transmitter.

1) Angle Diversity Transmitter: In order to deploy SDMA in VLC, an optical transmitter which can generate parallel narrow beam lights is required. Hence, a multi-element angle diversity transmitter is introduced. The layout of the angle diversity transmitter is given in Fig. 4. Multiple narrow-beam LED elements are mounted on a semi-sphere base. Each of the elements points in a different direction. The combine coverage area of all LED elements on an angle diversity transmitter is identical to the conventional single-element optical transmitter.

The angle diversity transmitter considered in this study consists of several LEDs. The first LED is installed at the

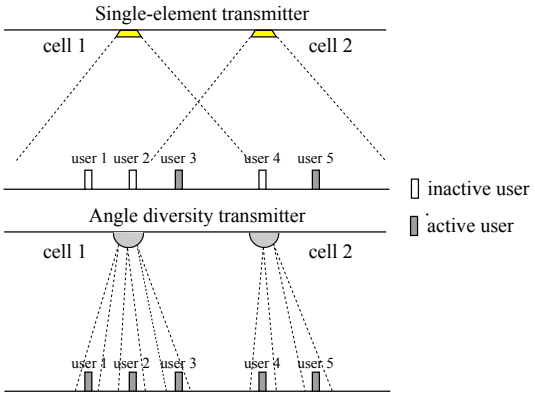

Fig. 8. Single-element versus angle diversity transmitter: the figure on the top illustrates optical TDMA. The figure at the bottom illustrates optical SDMA. Cell 1 and cell 2 are two neighbouring cells in an optical attocell network.

centre of a semi-sphere base. Then, rings of LEDs are installed around the central LED with increasing radius. In this study, three types of angle diversity transmitters (7-element, 19-element and 37-element) are considered. The layout of these angle diversity transmitters are illustrated in Fig. 5-7. Here, α is the angle between each neighbouring rings of LEDs.

In RF, the realisation of narrow beam transmitters requires multiple RF chains and complex beam-steering algorithms. In VLC, by using an angle diversity transmitter, narrow beam optical signals can be generated, and complex algorithms for beamforming can be avoided. The parallel directional transmissions can be realised by activating the LEDs that cover only the areas occupied by active users. The remaining LEDs which are not participating for communication generate constant light to provide room illumination. Therefore, an angle diversity transmitter can provide both uniform illumination and data communicating to multiple users.

The use of an angle diversity transmitter can effectively mitigate the ICI in an optical attocell network. As shown in Fig. 8, in a snapshot of an optical TDMA system, user 3 and user 5 are active and are served by APs in cell 1 and cell 2, respectively. Since the transmitter semi-angle for the single-element transmitter is large, both user 3 and user 5 experience strong ICI. For the identical snapshot in an optical SDMA system, all users can be served by directional beams. Since active LEDs only cover the areas of active users, ICI can be significantly mitigated.

2) Spatial Grouping: In an attocell network, it is assumed that each active user connects to the closest optical access point. In each optical cell, active users are served by different LED elements of the angle diversity transmitter. In optical SDMA, these active users cannot be assigned to arbitrary LED elements since some users might be spatially close to each other which results in overlapping beams and high co-channel interference. Therefore, in the absence of adaptive beamforming, a spatial grouping strategy is essential to achieve high spectral efficiency in an optical SDMA system with a fixed grid of beams.

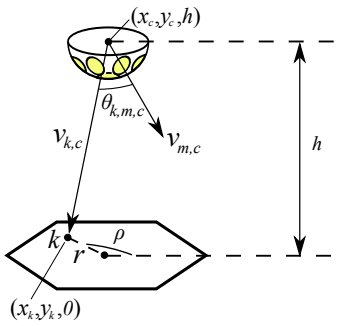

Fig. 9. The geometry of an optical cell. The position of the active user k can be represented by polar coordinate $(r\cos(\rho), r\sin(\rho))$.

The most important part of the spatial grouping strategy is to determine the source LED element for each active user. The geometry of an optical cell is given in Fig. 9. The coordinates of the angle diversity transmitter c is (x_c, y_c, h) and the coordinates of an active user k is $(x_k, y_k, 0)$; $v_{k,c}$ is the vector from the angle diversity transmitter c to an active user k; $v_{m,c}$ is the normal vector of the LED element m on the angle diversity transmitter c; and $\theta_{k,m,c}$ is the angle between the vector $v_{k,c}$ and vector $v_{m,c}$. The source LED element of active user k is chosen to minimise the angle $\theta_{k,m}$. The index of the source LED element for active user k can be given as:

$$I_{k,c} = \min_{m} \theta_{k,m,c}, \quad (c = \hat{c}) \tag{5}$$

where $\hat{c}$ is the desired cell for active user k; $\theta_{k,m,c}$ can be represented as:

$$\theta_{k,m} = \arccos\left(\frac{\overrightarrow{v}_{k,c} \cdot \overrightarrow{v}_{m,c}}{\|\overrightarrow{v}_{k,c}\|\|\overrightarrow{v}_{m,c}\|}\right). \tag{6}$$

When the source LED element for each active user is determined, it is able to determine which LED elements on the angle diversity transmitter are active. In some situations, some active users could be spatially close. This means that more than one active user will be allocated to the same LED element. In order to serve multiple users with one LED element, a TDMA scheme outlined in Section II-B is required. Also, RR scheduling is assumed.

An example of resource allocation in optical SDMA is illustrated in Fig. 10. Three LED elements are active. User $1, 2$, are allocated to element 1. These two users equally share the resource. User $3, 4, 5$, are allocated to element 3. Three users equally share the bandwidth resource. User 6 is allocated to element 5. Since there is only one user in that beam, user 6 uses the entire bandwidth continuously. The other two elements 2 and 4 are inactive, since no users are required to be served by them. Therefore, these LED elements do not carry IM signals and generate only constant light for illumination.

3) Performance Evaluation: In order to evaluate the SINR performance for each active user, interference is a key factor to be considered. In this scenario, interference consist of two parts: intra-cell interference and ICI. Intra-cell interference

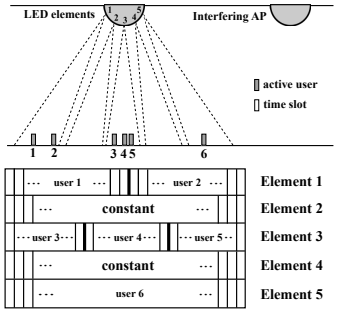

Fig. 10. An example frame of resource allocation in optical SDMA.

originates from the active LED elements in the desired optical cell. ICI is the interference generated by the active LED elements in the other optical cells. Hence, the SINR of active user k can be expressed as:

$$\gamma_k = \frac{\left(\tau P_{\mathrm{tx}} H_{k,m,\hat{c}}\right)^2}{N_0 B + \sum\limits_{m' \neq m} \left(\tau P_{\mathrm{tx}} H_{k,m',\hat{c}}\right)^2 + \sum\limits_{c'} \sum\limits_{\hat{m}} \left(\tau P_{\mathrm{tx}} H_{k,\hat{m},c'}\right)^2}, \tag{7}$$

where $H_{k,m,\hat{c}}$ is the channel attenuation between the desired LED element m and an active user k in the desired cell $\hat{c}$; $\sum\limits_{m' \neq m} \left(\tau P_{\mathrm{tx}} H_{k,m'}\right)^2$ represents the intra-cell interference; and m' is the index of active LED elements in the desired cell; $\sum\limits_{c'} \sum\limits_{\hat{m}} \left(\tau P_{\mathrm{tx}} H_{k,\hat{m},c'}\right)^2$ represents the ICI; $\hat{m}$ is the index of active LED elements in each interfering cell; c' is the index of the interfering cell.

In optical SDMA, active users in each optical cell equally share the bandwidth resource. Therefore, the spectral efficiency of the optical SDMA can be calculated as:

$$\Omega_{\mathrm{SDMA}} = \sum_{k}^{K} \frac{1}{g_k} \log_2(1 + \gamma_k), \tag{8}$$

where g_k is the total number of active users served by the desired LED element of active user k; K is the total number of active users in an optical cell.

The relative positions of active users in the optical cells can significantly affect the spectral efficiency of the system. In this study, the spectral efficiency gain is used to evaluate the performance of an SDMA system. This metric uses the system performance of the TDMA system as the baseline. The gain is defined as:

$$\eta = \frac{\Omega_{\mathrm{SDMA}}}{\Omega_{\mathrm{TDMA}}}. \tag{9}$$

For the purpose of fairness, in both scenarios, the following simulation parameters are set to be identical: i) total transmission power; ii) total number of active users; and iii) the position of active users. Therefore, the spectral efficiency gain is obtained from the implementation of the angle diversity transmitter and the resource allocation strategy.

D. The model of position errors

As previously discussed, the spatial grouping strategy depends on the position information of active users. Thus, position information is crucial to the operation of the optical SDMA system. However, the position information is not always accurate due to the limitation of the indoor positioning techniques. When different indoor positioning techniques and devices [19], [20] are used, the position errors vary accordingly. In this section, a model for the inaccurate position estimation is introduced.

Assume that the coordinate of the actual position of an active user k is (x_k, y_k), and the estimated position is (x'_k, y'_k). The relationship between (x_k, y_k) and (x'_k, y'_k) can be represented as:

$$\begin{cases} x'_k = x_k + e_k \\ y'_k = y_k + e'_k \end{cases} \tag{10}$$

where both e_k and e'_k follow a zero-mean normal distribution $\mathcal{N}(0, \sigma_e^2)$ [21], and σ_e is the standard variance. For each active user, e_k and e'_k are independent and identically distributed. The distance between the actual position and the estimated position can be represented as:

$$d_e = \sqrt{(x_k - x'_k)^2 + (y_k - y'_k)^2}. \tag{11}$$

Here, according to [22], d_e follows Rayleigh distribution and the mean value of d_e is:

$$\mathbb{E}[d_e] = \sqrt{\frac{\pi}{2}} \sigma_e. \tag{12}$$

In the optical SDMA, the result of user grouping is affected by the position errors. Some users could be allocated to suboptimal optical cells and this results in an increased intra-cell interference. Therefore, by considering position errors of active users, the system performance of optical SDMA is degraded.

III. Theoretical Analysis of optical SDMA

A theoretical framework to analyse the performance of an optical SDMA is presented in this section. In the system model, the SINR of each active user is dependent on both the position of the desired user and the position of interfering users. Hence, exact performance analysis would be complex, but an insightful upper and lower bound for the average spectral efficiency are derived here. They can be used to closely estimate the actual performance of an optical SDMA system.

A. An Upper Bound for the SDMA System Performance

From (7) and (8), it is notable that the performance of a SDMA system is limited by three factors: noise, intra-cell interference and ICI. Firstly, the best-case scenario of the SDMA system is considered. In the best-case scenario, it is assumed that all LED elements used in the system are of different colours, and optical receivers can perfectly distinguish these colours. Therefore, the intra-cell interference and ICI are totally cancelled. This means the system is noise-limited. In this scenario, an upper bound for the SDMA system

performance can be obtained. The derivation of the upper bound is presented as below.

In an optical cell, each LED element on the angle diversity transmitter independently serves users at different locations. The spectral efficiency within an optical cell is equal to the sum of the spectral efficiencies of each active LED elements. Since each LED element points to different directions, the average spectral efficiency for each active LED element is different. An active LED element can achieve the highest average spectral efficiency when it points vertically downward. This is because the active users served by this LED element are closest to the angle diversity transmitter and have the strongest channel gain. The average spectral efficiency of an active LED element pointing vertically downward is derived as follows.

For simplicity, the service region of the downward LED element is approximated as a circle. Assuming R_{cell} is the radius of the hexagonal cell, the radius of the approximated circle can be determined by: $R \approx 0.91R_{\text{cell}}$. Also, it is assumed that the active users within this circular region are uniform distributed. Assuming r is the horizontal distance between an active user and the centre of its service region, the probability density function (PDF) of r can therefore be given as:

$$f_r(r) = \frac{2r}{R^2} \quad (0 \leq r \leq R), \tag{13}$$

where R is the radius of the service region. By considering the geometry relationship between the parameters $d = h/\cos(\phi), \cos(\phi) = h/\sqrt{h^2+r^2}, \psi = \phi$, (1) can be expressed as:

$$H(r) = \frac{(m+1)A_{\text{eff}}}{2\pi h^2}\left(\frac{h}{\sqrt{h^2+r^2}}\right)^{m+3}. \tag{14}$$

Due to the noise-limited characteristic of the system, the SINR can be represented as:

$$\gamma(r) = \frac{\left(\tau P_{\text{tx}} H(r)\right)^2}{N_0 B}. \tag{15}$$

In this scenario, (8) is modified as:

$$\Omega_{\text{downward}} = \sum_{k}^{K'} \frac{1}{g_k}\log_2(1+\gamma_k), \tag{16}$$

where K' is the total number of active users within the service region of the downward LED element. Since all users in this scenario are served by the downward LED element, $g_k = K'$. Also, there is no mutual interference between users. Therefore, γ_k for all k is independently and identically distributed. Therefore, the average spectral efficiency of the downward LED element can be represented as:

$$\begin{aligned}\bar{\Omega}_{\text{downward}} &= \mathbb{E}\left[\sum_{k}^{K'} \frac{1}{g_k}\log_2(1+\gamma_k)\right] \\ &= \sum_{k}^{K'} \frac{1}{K'}\mathbb{E}_r\left[\log_2(1+\gamma(r))\right] \\ &= \mathbb{E}_r\left[\log_2(1+\gamma(r))\right] \\ &= \int_0^R \log_2(1+\gamma(r)) f_r(r)\mathrm{d}r.\end{aligned} \tag{17}$$

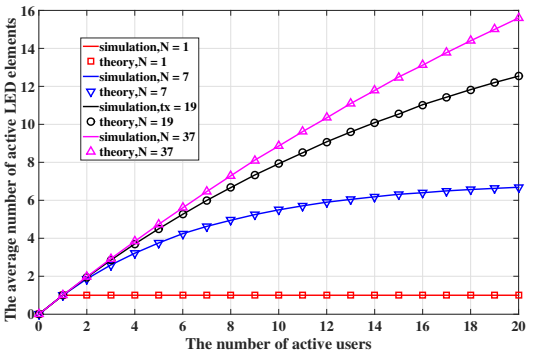

Fig. 11. The average number of active LED elements for different number of active users and LED elements.

Note that the average spectral efficiency is independent of the number of users served by the vertically downward pointing LED element, K'.

Since the average spectral efficiency in the other LED elements is less than the average spectral efficiency in the downward element, the average spectral efficiency in the entire optical cell, Ω_{SDMA}, can be bounded by $\bar{\Omega}_{\text{downward}}$:

$$\bar{\Omega}_{\text{SDMA}} \leq \bar{N}_{\text{a}}\bar{\Omega}_{\text{downward}} = \Omega_{\text{UB}}, \tag{18}$$

where $\bar{N}_{\text{a}}$ is the average number of the active LED elements; Ω_{UB} is the upper bound of the average spectral efficiency in an optical cell.

In an optical SDMA system, $\bar{N}_{\text{a}}$ is not a fixed number. This number depends on the total number of LED elements on an angle diversity transmitter and also the total number of active users in the optical cell. For example, if there is only one active user, $\bar{N}_{\text{a}}$ is always 1. However, when there are significant number of active users in an optical cell, $\bar{N}_{\text{a}}$ is approximately equal to the total number of LED elements on the angle diversity transmitter. According to [23], $\bar{N}_{\text{a}}$ can be calculated by:

$$\bar{N}_{\text{a}} = N - N(1-1/N)^K, \tag{19}$$

where N is the total number of LED elements on an angle diversity transmitter; and K is the number of users within an optical cell. The result of $\bar{N}_a$ is presented in Fig. 11. Note that $\bar{N}_a$ increases when there are more active users in an optical cell. Also the maximum value of $\bar{N}_a$ is limited by the number of LED elements on an angle diversity transmitter. The simulation result closely matches the theoretical result which proves the accuracy of the probability model.

B. A Lower Bound for the SDMA System Performance

After considering the best-case scenario, the worst-case scenario is now considered. In the worst-case scenario, the inactive LED element in an optical cell is no longer transmitting constant light signals. Instead, random light signals are transmitted. In this scenario, the intra-cell interference and ICI are maximised. Also, the intra-cell interference and ICI

of an active user is independent to the position of other users. Therefore, a lower bound of the SDMA system performance can be obtained. The derivation of the lower bound is presented as follows.

In this scenario, the representation of the user position PDF is identical to the previous scenario, (13). The system is assumed to be interference limited and the intra-cell interference dominates the interference components. Therefore, the SINR can be represented as:

$$\gamma_k = \frac{\left(\tau P_{\text{tx}} H_{k,m,\hat{c}}\right)^2}{\sum_{m' \neq m} \left(\tau P_{\text{tx}} H_{k,m',\hat{c}}\right)^2}, \tag{20}$$

where the channel attenuation, $H_{k,m,\hat{c}}$, can be represented as:

$$H_{k,m,\hat{c}} = \frac{(\lambda+1) A_{\text{eff}}}{2\pi d_{k,\hat{c}}^2} \cos^{\lambda}(\phi_{k,m,\hat{c}}) \cos(\psi_{k,\hat{c}}) \times \text{rect}\left(\frac{\psi_{k,\hat{c}}}{\Psi_{\text{fov}}}\right), \tag{21}$$

and the channel attenuation, $H_{k,m',\hat{c}}$, can be represented as:

$$H_{k,m',\hat{c}} = \frac{(\lambda+1) A_{\text{eff}}}{2\pi d_{k,\hat{c}}^2} \cos^{\lambda}(\phi_{k,m',\hat{c}}) \cos(\psi_{k,\hat{c}}) \times \text{rect}\left(\frac{\psi_{k,\hat{c}}}{\Psi_{\text{fov}}}\right), \tag{22}$$

and (20) can be rewritten as:

$$\gamma_k = \frac{\left(\cos(\phi_{k,m,\hat{c}})\right)^2}{\sum_{m' \neq m} \left(\cos(\phi_{k,m',\hat{c}})\right)^2}, \tag{23}$$

where $(r\cos\rho, r\sin\rho, 0)$ is the coordinate of the user k; $\cos\phi_{k,m,c}$ is represented as:

$$\begin{aligned} \cos\phi_{k,m,c} &= \left(\frac{\overrightarrow{v}_{k,c} \cdot \overrightarrow{v}_{m,c}}{\|\overrightarrow{v}_{k,c}\| \|\overrightarrow{v}_{m,c}\|}\right) \\ &= \frac{r p_{m,c} \cos\rho + r q_{m,c} \sin\rho - h w_{m,c}}{\sqrt{r^2 + h^2}}, \end{aligned} \tag{24}$$

where $\overrightarrow{v}_{m,c} = (p_{m,c}, q_{m,c}, w_{m,c})$ is defined as a normalised direction vector where $p_{m,c}^2 + q_{m,c}^2 + w_{m,c}^2 = 1$.

Combined with (23) and (24), the spectral efficiency of the optical SDMA system with only a single activated LED element is given as:

$$\Omega(r,\rho) = \log_2(1 + \gamma(r,\rho)). \tag{25}$$

Using the flower model described in [24] and [25], $\Omega(r,\rho)$ in (25) can be further simplified as $\Omega'(r,\rho)$. Since all transmitters are active and interfering transmitters are symmetrically located, the magnitude of the interference term can be approximated by the flower model as the combination of sine waves. The derivation and representation of $\Omega'(r,\rho)$ is provided in Appendix B. Fig. 12 shows the result of $\Omega'(r,\rho)$. Note that the flower model approximation accurately matches the exact model without approximation.

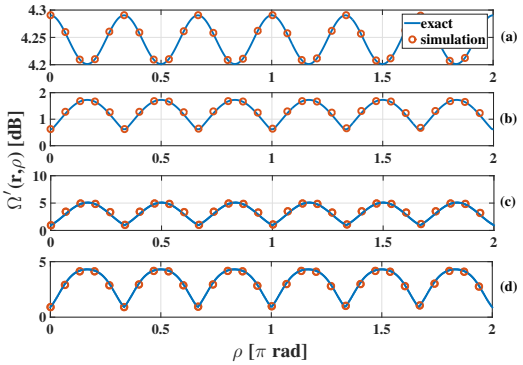

Fig. 12. The exact and approximation result of $\Omega'(r,\rho)$. In (a), $N = 7$, $r = 0.5$ m. In (b), $N = 7$, $r = 1$ m. In (c), $N = 7$, $r = 1.5$ m. In (d), $N = 19$, $r = 1.5$ m.

The average spectral efficiency of the optical SDMA system with only a single activated LED element is:

$$\begin{aligned} \bar{\Omega}_{\text{single}} &= \mathbb{E}_r\left[\Omega'(r,\rho)\right] \\ &= \int_0^R \int_0^{2\pi} \Omega'(r,\rho) f_r(r) \mathrm{d}\rho \mathrm{d}r \\ &= \int_0^R \Omega''(r) f_r(r) \mathrm{d}r, \end{aligned} \tag{26}$$

where the representation of $\Omega''(r)$ is provided in Appendix C.

Similar to (18), the lower bound of the average spectral efficiency for the entire cell is scaled with $\bar{N}_a$:

$$\Omega_{\text{LB}} = \bar{N}_a \bar{\Omega}_{\text{single}}. \tag{27}$$

C. The Estimation of the SDMA System Performance

The upper bound, Ω_{UB} in (18), can be regarded as the performance of a SDMA system with no interference. That means each user in the system experiences no interference from neighbouring LED elements. The lower bound, Ω_{LB} in (27), can be regarded as the performance of a SDMA system with full interference. For instance, in the context of Fig. 1, each user experiences interference from all 6 neighbouring LED elements. However, the interference experienced by a typical user in SDMA attocell networks varies significantly. For instance, a SDMA deployment such as shown in Fig. 1 may experience interference from a varied number of LEDs from 0 to 6. In this section, the analysis in Section III-A and Section III-B is extended to estimate the performance of SDMA systems more accurately. Let the average spectral efficiency of a typical user with z interfering LEDs be denoted as Ω_z, $z = 0, 1, ..., 6$. From the definition of Ω_{UB} and Ω_{LB}, it is clear that $\Omega_0 = \Omega_{\text{UB}}$ and $\Omega_6 = \Omega_{\text{LB}}$. Hence, Ω_z, $z = 1, ..., 6$ can be expressed as:

$$\Omega_z = \log_2\left(1 + \frac{\mathcal{S}}{z\mathcal{I}}\right) \approx \log_2\left(\frac{\mathcal{S}}{z\mathcal{I}}\right) = \Omega_{\text{LB}} + \log_2\left(\frac{6}{z}\right), \tag{28}$$

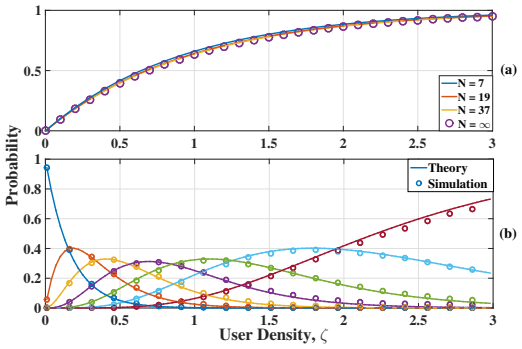

Fig. 13. (a) The result of P_{oe} for different number of N. (b) The result of P_z when $N = 37$.

where $\mathcal{S}$ represents the signal term which is identical to the numerator in (20), and $\mathcal{I}$ is the interference term which is identical to the denominator in (20). By assuming the probability of occurrence of each scenario as P_z, the estimated average spectral efficiency of the SDMA scheme is given as:

$$\Omega_{\text{SDMA,est}} = \sum_{z=0}^{6} P_z \Omega_z. \tag{29}$$

The method of calculating P_z is described as follows. Note that P_z is dependent on the user density in the attocell network. If user density is low, P_0 would be very high since users tend to be well separated. If user density is high, P_0 would be very low since most of the users are clustered. Let the user density, ζ, be defined as:

$$\zeta = \frac{K}{N}. \tag{30}$$

According to (19), the probability that a neighbouring LED element is occupied can be represented as:

$$P_{\text{oe}} = \frac{\bar{N}_{\text{a}}}{N} = 1 - (1 - 1/N)^{\zeta N}. \tag{31}$$

If N is large, P_{oe} can be calculated as:

$$\lim_{N\to\infty} P_{\text{oe}} = 1 - \lim_{N\to\infty} (1 - 1/N)^{\zeta N} = 1 - e^{-\zeta}. \tag{32}$$

The proof of (32) is provided in Appendix A. The result of P_{oe} for different N is presented in Fig. 13 (a). It can be observed that the difference between the result, P_{oe}, for different values of N is very small. Therefore, it is assumed that $P_{\text{oe}} = 1 - e^{-\zeta}$ regardless of the value of N.

In order to derive P_z, consider the scenario when $z = 0$. In this scenario, none of the 6 LED elements in the vicinity is occupied. Hence, P_0 can be evaluated as:

$$P_0 = \binom{6}{0} (P_{\text{oe}})^0 (1 - P_{\text{oe}})^6. \tag{33}$$

Similarly, P_z can be evaluated as:

$$P_z = \binom{6}{z} (P_{\text{oe}})^z (1 - P_{\text{oe}})^{6-z}. \tag{34}$$

TABLE I
SIMULATION PARAMETERS

Responsivity, τ	0.5 A/W
The gain of the optical filter, G	1
Refractive index, n	1.5
PD area, A_{p}	0.1cm^2
AWGN spectral density, N_0	1×10^{-21}A/Hz
The radius of an optical cell, R_{cell}	3 m

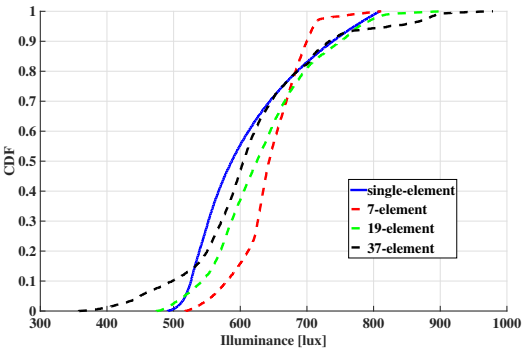

Fig. 14. The illuminance distribution for different types of optical transmitters.

The result of P_z when $N = 37$ is shown in Fig. 13 (b). The theoretical and simulation results agree well and this proves the accuracy of the theoretical model. Substituting the result for P_z in (34) into (29) yields the estimated average spectral efficiency.

IV. Results and Discussions

In this section, the performance of the optical SDMA system is simulated and evaluated. In particular, the average spectral efficiency of the system and the cumulative distribution function (CDF) of the spectral efficiency gain are illustrated and discussed. Also, the system performance is also evaluated when the position errors of active users are considered.

A. Simulation Setup

In the simulation, both the optical TDMA scheme and the optical SDMA scheme are considered. The optical TDMA system is used as a benchmark system. For the optical SDMA scenario, the parameters of angle diversity transmitter are as follows: for the 7-element angle diversity transmitter, $\alpha = 20^{\text{o}}$, $\Phi_{\text{tx}} = 17^{\text{o}}$; for the 19-element angle diversity transmitter, $\alpha = 22^{\text{o}}$, $\Phi_{\text{tx}} = 10^{\text{o}}$; for the 37-element angle diversity transmitter, $\alpha = 14.3^{\text{o}}$, $\Phi_{\text{tx}} = 7^{\text{o}}$. For the optical TDMA scenario, the half-intensity radiance angle of the conventional single-element transmitter is assumed to be 60^{o} which guarantees the same equivalent half-intensity radiance angle for all types of optical transmitters in both scenarios. For the purpose of fairness, the sum transmission power of all LED elements is identical for all types of optical transmitters. The distribution function of illumination for different types

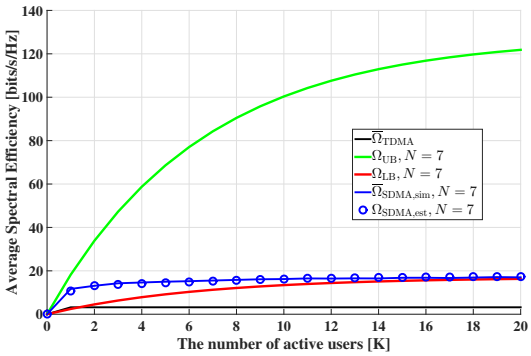

Fig. 15. The spectral efficiency of optical attocell network for different number of active users when a 7-element angle diversity transmitter is implemented. $\overline{\Omega}_{\mathrm{SDMA,sim}}$ represents the simulation result of the actual performance of the optical SDMA system. $\overline{\Omega}_{\mathrm{SDMA,sim}}$ represents the estimated theoretical result which is obtained by (29).

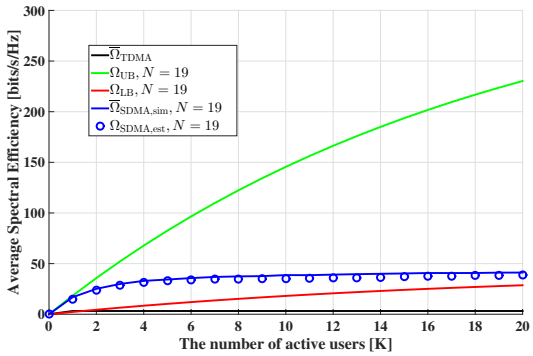

Fig. 16. The spectral efficiency of optical attocell network for different number of active users when a 19-element angle diversity transmitter is implemented. $\overline{\Omega}_{\mathrm{SDMA,sim}}$ represents the simulation result of the actual performance of the optical SDMA system. $\overline{\Omega}_{\mathrm{SDMA,sim}}$ represents the estimated theoretical result which is obtained by (29).

of optical transmitters is given in Fig. 14. This distribution is generated by separating an optical cell into small grids and accumulating the value of illuminance in each grid. It is notable that all types of optical transmitters have similar illumination distribution. This guarantees a fair performance comparison between these optical transmitters.

For both scenarios, optical transmitters are placed at the centre of each cell at a height of 3 m. The optical receiver for all active users are assumed to be placed at the height of a desk, 0.85 m. The transmission power of an optical transmitter is set as 2 W. Table I gives the other simulation parameters.

B. Spectral Efficiency Performance

In the simulation, in order to generate the average spectral efficiency of the optical SDMA system, $100,000$ snapshots are generated for each number of active users. For each snapshot, active users are spatially uniformly distributed. The sum spectral efficiencies of all users in the central optical cell of the 7-cell attocell network is calculated. Finally, the average spectral efficiency is obtained as the average of the sum spectral efficiency over all snapshots. The average spectral efficiencies for the optical TDMA scheme and the optical SDMA scheme are denoted by $\overline{\Omega}_{\mathrm{TDMA}}$ and $\overline{\Omega}_{\mathrm{SDMA}}$, respectively. N denotes the number of LED elements on each angle diversity transmitter.

Fig. 15 shows the average spectral efficiency of the optical SDMA system when a 7-element angle diversity transmitter is used as the optical transmitter. The simulation results and estimated results of the average spectral efficiency of the optical SDMA system are denoted by $\overline{\Omega}_{\mathrm{SDMA,sim}}$ and $\overline{\Omega}_{\mathrm{SDMA,est}}$, respectively. It is notable that the average spectral efficiency increases as the total number of active users increases. Also, the average spectral efficiency quickly saturates as the number of active users increases.

The upper bound of the system, Ω_{UB}, increases significantly when the number of active users increases. When K is small, $\Omega_{\mathrm{SDMA,sim}}$ is close to Ω_{UB}. This is because users tend to be well-separated in this scenario which results in low intra-cell interference and ICI. As K increases, the gap between $\Omega_{\mathrm{SDMA,sim}}$ and Ω_{UB} increases. This is because in the calculation of the upper bound no intra-cell and ICI is considered.

The lower bound, Ω_{LB}, is calculated assuming all LED elements are active (strong intra-cell interference). When K is small, the actual intra-interference in the system is small. Therefore, $\overline{\Omega}_{\mathrm{SDMA,sim}}$ is a few times larger than Ω_{LB} when K is small. When K is large, Ω_{LB} approaches $\overline{\Omega}_{\mathrm{SDMA}}$. This is because, when there is a considerable number of active users in a cell, all LED elements on angle diversity transmitters are active. This setup has the same assumptions as that for calculating Ω_{LB}.

One important observation is that there is a close match between the simulation result, $\Omega_{\mathrm{LB,sim}}$, and theoretical estimation, $\Omega_{\mathrm{SDMA,est}}$. This validates the accuracy of the theoretical model and the related analysis in Section III-C. Also, this means that the performance of optical SDMA can be estimated without the need for complex Monte-Carlo simulations.

It can also be observed that the SDMA system significantly outperforms the TDMA system and up to 6 times higher average spectral efficiency can be achieved. The angle diversity transmitter can generate narrow directional light beams which can effectively reduce ICI and enable parallel transmission. This results in an improved average spectral efficiency.

Fig. 16 shows the average spectral efficiency of the optical SDMA system when a 19-element angle diversity transmitter is used as the optical transmitter. The trend of the spectral efficiency performance in this scenario is similar to that in the previous scenario. Note that, when compared with TDMA, the SDMA system with a 19-element angle diversity transmitter can achieve up to 17 times higher average spectral efficiency than the TDMA system. When the number of transmitter elements increases further, the average spectral efficiency of the SDMA increases accordingly. Fig. 17 shows that the SDMA system with a 37-element angle diversity transmitter

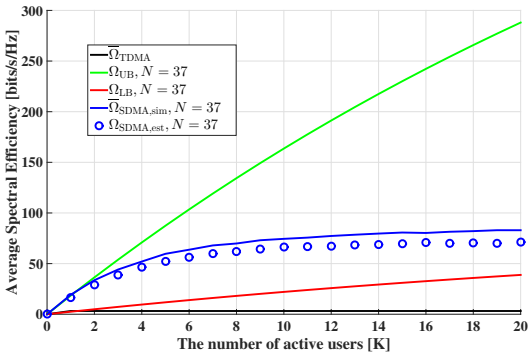

Fig. 17. The spectral efficiency of optical attocell network for different number of active users when a 37-element angle diversity transmitter is implemented. $\overline{\Omega}_{\mathrm{SDMA,sim}}$ represents the simulation result of the actual performance of the optical SDMA system. $\overline{\Omega}_{\mathrm{SDMA,sim}}$ represents the estimated theoretical result which is obtained by (29).

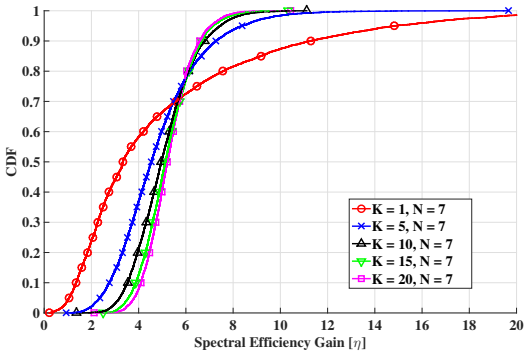

Fig. 18. The spectral efficiency gain of the optical SDMA system for different number of active users ($N = 7$).

can achieve up to 26 times higher average spectral efficiency than the TDMA system.

In summary, the theoretical estimation, $\Omega_{\mathrm{SDMA,est}}$, can accurately predict the actual system performance $\overline{\Omega}_{\mathrm{SDMA}}$. The upper bound, Ω_{UB}, can provide a potential system average spectral efficiency when the advanced interference mitigation scheme is implemented (such as multiple colour LED elements that avoid intra-cell interference). Also, the lower bound, Ω_{LB}, describes the average spectral efficiency of the system when no interefence mitigation scheme is taken into account. It is observed that as K increases, the actual SDMA system transfers from a noise-limited system to an interference-limited system.

C. Statistics of the Spectral Efficiency Gain

Fig. 18 shows the performance of the spectral efficiency gain, η, when a 7-element angle diversity transmitter is used. It is observed that most of the time η is greater than unity. This means the optical SDMA system significantly outperforms

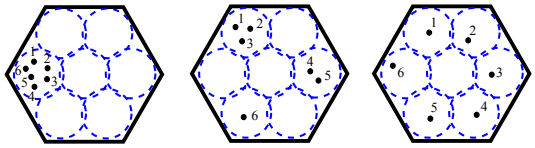

Fig. 19. Three typical scenarios for the SDMA system: 1. All active users are close to each other (left); 2. Some of the active users are close to each other (middle); 3. All active users are well-separated (right).

the TDMA system regardless the position of the active users. The dynamic range of the spectral efficiency gain, η, is large. This is because the throughput gain is strongly related to the position of active users.

When there is only one active user in a cell, $K = 1$, η can be very high at some positions. This is because, in a TDMA system, the half-intensity radiation angle of an optical transmitter is large which results in strong cell edge interference. In SDMA systems, this interference can be significantly mitigated, since only one LED element with narrow half-intensity radiation angle is activated at a time. When an active user is at the cell centre, the ICI is not significant in TDMA systems. In that scenario, SDMA cannot significantly improve the system spectral efficiency, which results in lower η. Also, the transmission power of a single link in a SDMA scheme is lower than that in a TDMA scheme. As a result, η may be less than 1.

When there is more than one active user in a cell, $K > 1$, η mainly depends on the relative distance between users. For example, in Fig. 19, three typical scenarios are illustrated. For the first scenario, all active users are close to each other and within the region that is served by the same transmitter element. In that scenario, the spectrum of one LED element is shared by all users. Therefore, the spectral efficiency gain is achieved only from interference mitigation. For the second scenario, some of the active users are clustered together and three LED elements are activated simultaneously. This means, apart from the spectral efficiency gain from the interference mitigation, approximately three times extra spectral efficiency gain can be achieved by parallel transmissions. For the third scenario, each of the active users are well-separated. In that scenario, approximately six times extra spectral efficiency gain can be achieved using parallel transmission.

Fig. 20 and Fig. 21 show the performance of the spectral efficiency gain when 19-element and 37-element angle diversity transmitters are used, respectively. The trend of the results are similar to the previous scenarios where a 7-element angle diversity transmitter is used. The overall spectral efficiency gain increases as the number of transmitter element increases. This is because, when the number of LED elements on an angle diversity transmitter increases, the half-intensity angle of each element decreases accordingly. Narrow half-intensity angle of transmitter elements can effectively mitigate the ICI as well as the intra-cell interference. Also, the optical transmitter with more LED elements has a better ability to separate active users and create more parallel links to them. Hence, it can be concluded that the spectral efficiency gain of

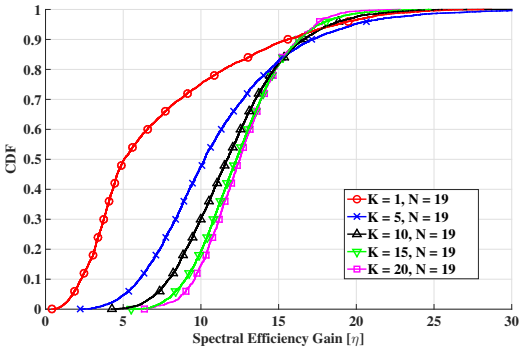

Fig. 20. The spectral efficiency gain of the optical SDMA system for different number of active users ($N = 19$).

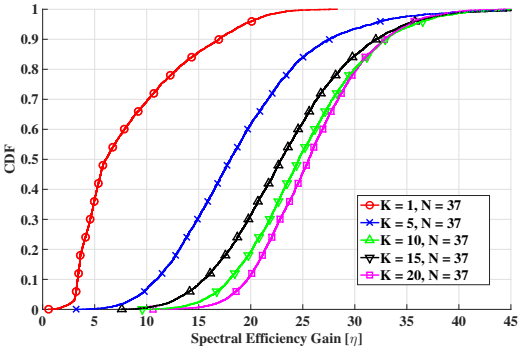

Fig. 21. The spectral efficiency gain of the optical SDMA system for different number of active users ($N = 37$).

a SDMA system is scaled with the number of LED elements on each optical transmitter.

D. Position Errors

Fig. 22 shows the average spectral efficiency of the optical SDMA system using 7-element transmitter when different σ_e are considered. According to the characteristics of the normal distribution, 95% of the estimated positions of active users are within two standard deviations ($2\sigma_e$) away from their actual positions. The curve with no markers represents the average spectral efficiency of the SDMA system, when the position information is perfectly known, $\sigma_e = 0$. When σ_e increases to 0.1 m, the average spectral efficiency of the SDMA system decreases only by 1.3% compared with the system with perfect position information. When σ_e is increased to 0.2 m, 0.3 m, 0.4 m and 0.5 m, the performance of the SDMA system decreases by 5%, 11%, 18% and 26%, respectively. When σ_e is large, the position information for all active users is inaccurate. As a result, incorrect LED elements in each optical cell are activated. This means active users may not be served by their optimal LED element and additional performance penalties

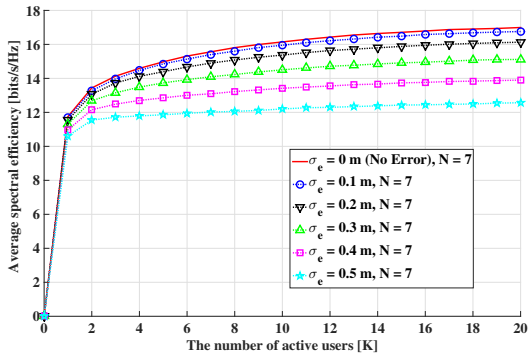

Fig. 22. The average spectral efficiency of the optical SDMA system when different standard variance of the position error is considered ($N = 7$).

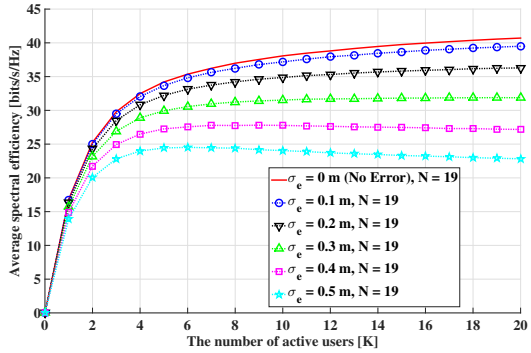

Fig. 23. The average spectral efficiency of the optical SDMA system when different standard variance of the position error is considered ($N = 19$).

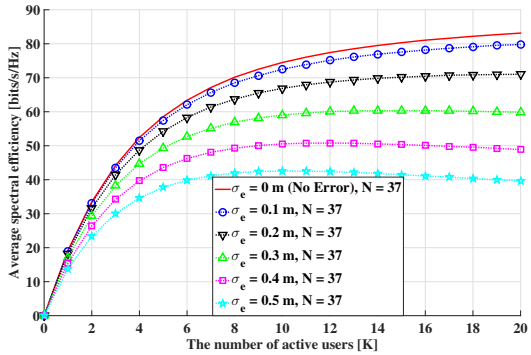

Fig. 24. The average spectral efficiency of the optical SDMA system when different standard variance of the position error is considered ($N = 37$).

are introduced. Therefore, the overall system performance is decreased significantly if the user position errors are large.

Fig. 23 shows the average spectral efficiency of the optical SDMA system using the 19-element transmitter when different

σ_e is considered. When σ_e is 0.1 m, 0.2 m, 0.3 m, 0.4 m and 0.5 m, the performance of the SDMA system decreases 3%, 11%, 22%, 33% and 44%, respectively, compared with the system with perfect position information. For the SDMA system using 37-element transmitter (Fig. 24), when σ_e are 0.1 m, 0.2 m, 0.3 m, 0.4 m and 0.5 m, the performance of the SDMA system decreases 4%, 14%, 28%, 41% and 52%, respectively, compared with the system with perfect position information. This means that when the number of transmitter elements increases, the SDMA system is more sensitive to position information of the active users. This is because, when the number of LED elements increases, the service area of each LED element is smaller. This means active users may be easily misallocated to an adjacent cell when the position information is inaccurate. Therefore, for a fixed σ_e, the SDMA system using more transmitter elements performs worse. It is also notable that the performance of the SDMA system is compromised when σ_e increases. With the use of the-state-of-the-art indoor positioning techniques [20], an average position error of less than 0.25 m can be often achieved. This means $\mathbb{E}[d_e] = \sqrt{\frac{\pi}{2}}\sigma_e < 0.25$ m and $\sigma_e < 0.2$ m can be obtained. Therefore, the system average spectral efficiency only decreases by 14%. This result is very promising since the optical SDMA is robust to position errors and this makes it suitable for practical implementation.

V. Conclusion

In this paper, an optical attocell network adopting optical SDMA is proposed. In this network, an angle diversity transmitter is equipped in each optical cell and can serve multiple active users simultaneously. With the use of an angle diversity transmitter, the ICI between optical cells can be significantly mitigated. The results clearly show that the optical SDMA system significantly outperforms the optical TDMA benchmark system. In particular, up to 26 times higher average spectral efficiency can be achieved when the transmitter is equipped with 37 LED elements. Also, an upper bound and lower bound of the SDMA system are derived analytically. These bounds can accurately predict the performance of the SDMA system. In addition, the result of average spectral efficiency gain clearly shows that the SDMA system outperforms the TDMA system, regardless of the relative positions of the active users. Finally, position errors for the active users are considered. Results shows that the SDMA system is robust to user position errors, and the system performance is only compromised by 14% when the practical state-of-the-art indoor position techniques are used. The results strongly support the suitability of optical SDMA systems for practical implementations.

Appendix

A. The Proof of (32)

Considering a similar limitation:

$$\lim_{N\to\infty} \ln(1-1/N)^{\zeta N} = \lim_{N\to\infty} \zeta N \ln(1-1/N). \tag{35}$$

Assuming that $t = 1/N$ and according to the L'Hospital's Rule:

$$\lim_{N\to\infty} \zeta N \ln(1-1/N) = \lim_{t\to 0} \frac{[\zeta \ln(1-t)]'}{[t]'} = -\zeta. \tag{36}$$

Hence,

$$\lim_{N\to\infty} (1-1/N)^{\zeta N} = e^{-\zeta}. \tag{37}$$

B. The Derivation of $\Omega'(r,\rho)$

The $\Omega(r,\rho)$ can be approximated by $\Omega'(r,\rho)$. The procedure is as follows.

1) N = 7: For the 7-element transmitter, the cell area can be divided into two parts: the area that is served by the central LED and area that is served by the outer ring of LEDs. For the former scenario, $0 \le r < h\tan(\frac{\alpha}{2})$,

$$\Omega'(r,\rho) = \frac{\Omega(r,0^{\mathrm{o}}) + \Omega(r,\frac{\pi}{6})}{2} + \frac{\Omega(r,0) - \Omega(r,\frac{\pi}{6})}{2}\cos(6\rho). \tag{38}$$

For the latter scenario, $h\tan(\frac{\alpha}{2}) \le r \le R$.

$$\Omega'(r,\rho) = \Omega(r,\frac{\pi}{6}) + \Omega(r,0) - \Omega(r,\frac{\pi}{6})|\sin(3\rho)|. \tag{39}$$

2) N = 19: Similarly, for the 19-element transmitter, the cell area can be divided into three parts. When $0 \le r < h\tan(\frac{\alpha}{2})$,

$$\Omega'(r,\rho) = \frac{\Omega(r,0) + \Omega(r,\frac{\pi}{6})}{2} + \frac{\Omega(r,0) - \Omega(r,\frac{\pi}{6})}{2}\cos(6\rho). \tag{40}$$

When $h\tan(\frac{\alpha}{2}) \le r < h\tan(\frac{3\alpha}{2})$,

$$\Omega'(r,\rho) = \Omega(r,\frac{\pi}{6}) + \Omega(r,0) - \Omega(r,\frac{\pi}{6})|\sin(3\rho)|. \tag{41}$$

When $h\tan(\frac{3\alpha}{2}) \le r < R$, $\Omega'(r,\rho) =$

$$\begin{cases} \Omega(r,\frac{\pi}{6}) + \Omega(r,\frac{\pi}{4}) + \left(\Omega(r,\frac{\pi}{6}) - \Omega(r,\frac{\pi}{4})\right)|\cos(6\rho)| \\ \qquad\qquad \text{if} \quad \frac{\pi}{12} + \frac{\pi}{3}u < \rho \le \frac{\pi}{4} + \frac{\pi}{3}u \\ \Omega(r,0) + \Omega(r,\frac{\pi}{12}) + \left(\Omega(r,0) - \Omega(r,\frac{\pi}{12})\right)|\cos(6\rho)| \\ \qquad\qquad \text{otherwise,} \end{cases} \tag{42}$$

where $u = 0, 1, 2, 3, 4, 5$.

3) N = 37: For the 37-element transmitter, the cell area can be divided into four parts. When $0 \le r < h\tan(\frac{\alpha}{2})$,

$$\Omega'(r,\rho) = \frac{\Omega(r,0) + \Omega(r,\frac{\pi}{6})}{2} + \frac{\Omega(r,0) - \Omega(r,\frac{\pi}{6})}{2}\cos(6\rho). \tag{43}$$

When $h\tan(\frac{\alpha}{2}) \le r < h\tan(\frac{3\alpha}{2})$,

$$\Omega'(r,\rho) = \Omega(r,\frac{\pi}{6}) + \Omega(r,0) - \Omega(r,\frac{\pi}{6})|\sin(3\rho)|. \tag{44}$$

When $h\tan(\frac{3\alpha}{2}) \le r < h\tan(\frac{5\alpha}{2})$, $\Omega'(r,\rho) =$

$$\begin{cases} \Omega(r,\frac{\pi}{6}) + \Omega(r,\frac{\pi}{4}) + \left(\Omega(r,\frac{\pi}{6}) - \Omega(r,\frac{\pi}{4})\right)|\cos(6\rho)| \\ \qquad\qquad \text{if} \quad \frac{\pi}{12} + \frac{\pi}{3}u < \rho \le \frac{\pi}{4} + \frac{\pi}{3}u \\ \Omega(r,0) + \Omega(r,\frac{\pi}{12}) + \left(\Omega(r,0) - \Omega(r,\frac{\pi}{12})\right)|\cos(6\rho)| \\ \qquad\qquad \text{otherwise.} \end{cases} \tag{45}$$

When $h\tan(\frac{5\alpha}{2}) \le r < R$, $\Omega'(r,\rho) =$

$$\begin{cases} \Omega(r,\frac{\pi}{12})+\Omega(r,\frac{\pi}{8})+(\Omega(r,\frac{\pi}{12})-\Omega(r,\frac{\pi}{8}))|\cos(12\rho)| \\ \qquad \text{if} \quad \frac{\pi}{24}+\frac{\pi}{3}u < \rho \le \frac{\pi}{8}+\frac{\pi}{3}u \\ \Omega(r,\frac{\pi}{6})+\Omega(r,\frac{5\pi}{24})+(\Omega(r,\frac{\pi}{6})-\Omega(r,\frac{5\pi}{24}))|\cos(12\rho)| \\ \qquad \text{if} \quad \frac{\pi}{8}+\frac{\pi}{3}u < \rho \le \frac{5\pi}{24}+\frac{\pi}{3}u \\ \Omega(r,\frac{\pi}{4})+\Omega(r,\frac{7\pi}{24})+(\Omega(r,\frac{\pi}{4})-\Omega(r,\frac{7\pi}{24}))|\cos(12\rho)| \\ \qquad \text{if} \quad \frac{5\pi}{24}+\frac{\pi}{3}u < \rho \le \frac{7\pi}{24}+\frac{\pi}{3}u \\ \Omega(r,0)+\Omega(r,\frac{\pi}{24})+(\Omega(r,0)-\Omega(r,\frac{\pi}{24}))|\cos(12\rho)| \\ \qquad \text{otherwise.} \end{cases} \tag{46}$$

C. The Representation of $\Omega''(r)$

1) N = 7: When $0 \le r < h\tan(\frac{\alpha}{2})$,

$$\Omega''(r) = (\pi+1)\Omega(r,0)+(\pi-1)\Omega(r,\frac{\pi}{6}). \tag{47}$$

When $h\tan(\frac{\alpha}{2}) \le r \le R$,

$$\Omega''(r) = (2\pi-2)\Omega(r,\frac{\pi}{6})+2\pi\Omega(r,0). \tag{48}$$

2) N = 19: When $0 \le r < h\tan(\frac{\alpha}{2})$,

$$\Omega''(r) = (\pi+1)\Omega(r,0)+(\pi-1)\Omega(r,\frac{\pi}{6}). \tag{49}$$

When $h\tan(\frac{\alpha}{2}) \le r < h\tan(\frac{3\alpha}{2})$,

$$\Omega''(r) = (2\pi-2)\Omega(r,\frac{\pi}{6})+2\pi\Omega(r,0). \tag{50}$$

When $h\tan(\frac{3\alpha}{2}) \le r < R$,

$$\Omega''(r) = (\pi+1)(\Omega(r,0)+\Omega(r,\frac{\pi}{6}))+(\pi-1) \times(\Omega(r,\frac{\pi}{12})+\Omega(r,\frac{\pi}{4})). \tag{51}$$

3) N = 37: When $0 \le r < h\tan(\frac{\alpha}{2})$,

$$\Omega''(r) = (\pi+1)\Omega(r,0)+(\pi-1)\Omega(r,\frac{\pi}{6}). \tag{52}$$

When $h\tan(\frac{\alpha}{2}) \le r < h\tan(\frac{3\alpha}{2})$,

$$\Omega''(r) = (2\pi-2)\Omega(r,\frac{\pi}{6})+2\pi\Omega(r,0). \tag{53}$$

When $h\tan(\frac{3\alpha}{2}) \le r < h\tan(\frac{5\alpha}{2})$,

$$\Omega''(r) = (\pi+1)(\Omega(r,0)+\Omega(r,\frac{\pi}{6}))+(\pi-1) \times(\Omega(r,\frac{\pi}{12})+\Omega(r,\frac{\pi}{4})). \tag{54}$$

When $h\tan(\frac{5\alpha}{2}) \le r < R$,

$$\Omega''(r) = \frac{1}{2}(\pi+1)(\Omega(r,0)+\Omega(r,\frac{\pi}{12})+\Omega(r,\frac{\pi}{6})+\Omega(r,\frac{\pi}{4})) +\frac{1}{2}(\pi-1)(\Omega(r,\frac{\pi}{24})+\Omega(r,\frac{\pi}{8})+\Omega(r,\frac{5\pi}{24})+\Omega(r,\frac{7\pi}{24})). \tag{55}$$

REFERENCES

[1] Cisco Visual Networking Index, "Global Mobile Data Traffic Forecast Update, 2014-2019," White Paper, Feb. 2015. [Online]. Available: http://www.cisco.com/c/en/us/solutions/collateral/service-provider/visual-networking-index-vni/white_paper_c11-520862.html

[2] H. Elgala, R. Mesleh, and H. Haas, "Indoor Optical Wireless Communication: Potential and State-of-the-Art," *IEEE Commun. Mag.*, vol. 49, no. 9, pp. 56–62, Sep. 2011.

[3] A. M. Khalid, G. Cossu, R. Corsini, P. Choudhury, and E. Ciaramella, "1-Gb/s Transmission over a Phosphorescent White LED by Using Rate-adaptive Discrete Multitone Modulation," *IEEE Photon. J.*, vol. 4, no. 5, pp. 1465–1473, Oct 2012.

[4] G. Cossu, A. Wajahat, R. Corsini, and E. Ciaramella, "5.6 Gbit/s Downlink and 1.5 Gbit/s Uplink Optical Wireless Transmission at Indoor Distances," in *2014 European Conference on Optical Communication (ECOC)*, Sep 2014, pp. 1–3.

[5] D. Tsonev, H. Chun, S. Rajbhandari, J. McKendry, S. Videv, E. Gu, M. Haji, S. Watson, A. Kelly, G. Faulkner, M. Dawson, H. Haas, and D. O'Brien, "A 3-Gb/s Single-LED OFDM-Based Wireless VLC Link Using a Gallium Nitride μLED," *IEEE Photon. Technol. Lett.*, vol. 26, no. 7, pp. 637–640, Apr. 2014.

[6] S. Hussain, M. Abdallah, and K. Qaraqe, "Hybrid Radio-visible Light Downlink Performance in RF Sensitive Indoor Environments," in *2014 6th International Symposium on Communications, Control and Signal Processing (ISCCSP)*, May 2014, pp. 81–84.

[7] T. Borogovac, M. Rahaim, and J. B. Carruthers, "Spotlighting for Visible Light Communications and Illumination," in *IEEE Global Communications Conference (GLOBECOM 2010) Workshops*, 6-10 Dec 2010, pp. 1077–1081.

[8] I. Stefan, H. Burchardt, and H. Haas, "Area Spectral Efficiency Performance Comparison between VLC and RF Femtocell Networks," in *IEEE International Conference on Communications (ICC)*, Budapest, Hungary, Jun. 9–13 2013, pp. 1–5.

[9] H. Haas, "High-speed Wireless Networking Using Visible Light," SPIE Newsroom, Apr. 19 2013.

[10] A. J. Paulraj and C. B. Papadias, "Space-time Processing for Wireless Communications," *IEEE Signal Process. Mag.*, vol. 14, no. 6, pp. 49–83, Nov. 1997.

[11] I. P802.11, "IEEE802.11ac: The Next Evolution of Wi-Fi Standards," 2012.

[12] H. Yin and H. Liu, "Performance of Space-division-multiple-access (SDMA) with Scheduling," *IEEE Trans. Wireless Commun.*, vol. 1, no. 4, pp. 611–618, Oct 2002.

[13] K. Huang, J. Andrews, and R. Heath, "Performance of Orthogonal Beamforming for SDMA with Limited Feedback," *IEEE Trans. Veh. Technol.*, vol. 58, no. 1, pp. 152–164, Jan 2009.

[14] P. Djahani and J. M. Kahn, "Analysis of Infrared Wireless Links Employing Multibeam Transmitters and Imaging Diversity Receivers," *IEEE Trans. Commun.*, vol. 48, no. 12, pp. 2077–2088, Dec. 2000.

[15] Z. Chen, N. Serafimovski, and H. Haas, "Angle diversity for an Indoor Cellular Visible Light Communication System," in *IEEE 79th Vehicular Technology Conference*, May 2014.

[16] C. Chen, N. Serafimovski, and H. Haas, "Fractional frequency reuse in optical wireless cellular networks," in *2013 IEEE 24th International Symposium on Personal Indoor and Mobile Radio Communications (PIMRC)*, Sept 2013, pp. 3594–3598.

[17] J. M. Kahn and J. R. Barry, "Wireless Infrared Communications," *Proc. IEEE*, vol. 85, no. 2, pp. 265–298, Feb. 1997.

[18] L. Godara, "Application of Antenna Arrays to Mobile Communications. II. Beam-forming and Direction-of-arrival Considerations," *Proc. IEEE*, vol. 85, no. 8, pp. 1195 –1245, Aug. 1997.

[19] M. geun Moon and S. il Choi, "Indoor Position Estimation Using Image Sensor Based on VLC," in *2014 International Conference on Advanced Technologies for Communications (ATC)*, Oct 2014, pp. 11–14.

[20] M. Yasir, S. Ho, and B. Vellambi, "Indoor Positioning System Using Visible Light and Accelerometer," *J. Lightw. Technol.*, vol. 32, no. 19, pp. 3306–3316, Oct 2014.

[21] M. Kashef, M. Abdallah, K. Qaraqe, and M. Uysal, "The Impact of Location Errors on Achievable Rates in OFDM-based Multi-user Visible Light Communication Systems," in *2014 3rd International Workshop in Optical Wireless Communications (IWOW)*, Sept 2014, pp. 65–69.

[22] A. Papoulis, *Probability, Random Variables and Stochastic Processes*, 2nd ed. McGraw-Hill Inc., 1984.

[23] P. P. Williamson, D. P. Mays, G. A. Asmerom, and Y. Yang, "Revisiting the classical occupancy problem," *The American Statistician*,

vol. 63, no. 4, pp. 356–360, 2009. [Online]. Available: http://www.jstor.org/stable/25652315

[24] B. Almeroth, A. Fehske, G. Fettweis, and E. Zimmermann, "Analytical Interference Models for the Downlink of a Cellular Mobile Network," in *2011 IEEE GLOBECOM Workshops (GC Wkshps)*, Dec 2011, pp. 739–743.

[25] C. Chen, D. Basnayaka, and H. Haas, "Downlink Performance of Optical Attocell Networks," *J. Lightw. Technol.*, vol. PP, no. 99, pp. 1–1, 2015.

Interference Mitigation for Indoor Optical Attocell Networks using Angle Diversity Receiver

Zhe Chen, *Student Member, IEEE*, Dushyantha A. Basnayaka, *Member, IEEE*, Xiping Wu, *Member, IEEE* and Harald Haas, *Member, IEEE*

***Abstract*—In this paper, interference mitigation techniques based on an angle diversity receiver (ADR) are studied for optical attocell networks. ADRs consist of multiple photodiodes (PDs), and require appropriate signal combining schemes in order to mitigate inter-cell interference (ICI) in optical attocell networks. Therefore, four signal combining schemes namely select best combining (SBC), equal gain combining (EGC), maximum ratio combining (MRC) and optimum combining (OPC) are investigated. In order to further mitigate the ICI, a novel double-source cell configuration with two transmission modes is also proposed. Results show that the systems with ADRs significantly outperform the systems with single-PD receivers in terms of signal-to-interference-plus-noise-ratio (SINR) performance. It is also shown that double-source cell configurations provide over 20 dB SINR improvement over conventional single-source cell configurations. Two transmission modes are proposed for double source cell configurations, and a criteria for selecting the modes in order to further enhance the system performance in different deployments is also proposed. Furthermore, in order to theoretically analyse the performance of optical attocell networks with ADRs, analytical models for different scenarios including line-of-sight (LOS) and non-line-of-sight (NLOS) propagation are proposed, and the accuracy of the proposed analytical model is validated by Monte-Carlo simulations.**

***Index Terms*—visible light communication; optical attocell network; angle diversity receiver; signal combining schemes; double-source cell configuration; theoretical analysis.**

I. Introduction

In recent years, data traffic has increased exponentially. According to the latest Cisco Visual Networking Index (VNI), overall mobile data traffic is expected to increase to 24.3 exabytes per month by 2019 [1]. In order to alleviate the congestive data traffic in existing radio frequency (RF) system, visible light communication (VLC) technology has emerged as a promising alternative [2]. Recent research shows that VLC can achieve high data rates [3], [4]. In particular, a single-colour light-emitting diode (LED) can achieve transmission speeds of 3 Gbps [5]. Compared with RF communication, VLC operates at an unregulated part of the electromagnetic spectrum and is intrinsically safe to be used in electromagnetic interference (EMI) sensitive environments [6], such as aircraft, hospitals and oil refineries.

Harald Haas, and Dushyantha Basnayaka acknowledge support from the Engineering and Physical Sciences Research Council (EPSRC) under Established Career Fellowship grant EP/K008757/1.

The authors are with the Institute for Digital Communications, Li-Fi R&D Centre, School of Engineering, The University of Edinburgh, UK. (e-mail: z.chen@ed.ac.uk; d.basnayaka@ed.ac.uk; xiping.wu@ed.ac.uk; h.haas@ed.ac.uk)

Cellular networks achieve higher area spectral efficiency (ASE) by efficient frequency reuse. In a typical cellular network, the minimum distance between any two access points (APs) is strictly limited to avoid strong inter-cell interference (ICI). In RF, femtocell has the minimum cell size of 10 m [7]. Since the radiation of an RF APs are typically omni-directional, ICI increases as cell size decreases. In VLC, since light beams from LEDs are intrinsically directional, and the coverage of LEDs is confined, the size of optical cells can be much smaller than the size of RF cells [8]. As a result, optical APs can be installed much densely without causing strong ICI in comparison with RF counterparts. Therefore, an optical cell size in the order of 1 m is typically achievable. In comparison with RF femtocell networks, optical cellular networks can achieve better bandwidth reuse and higher ASE [9]. In a typical indoor scenario, each lighting fixture is regarded as an AP and networks consist of multiple light fixtures are usually referred to as optical attocell networks.

Even though optical attocell networks have been shown to have several advantages over conventional RF communication networks, their performance is still limited by ICI especially at cell edge area. In order to mitigate ICI, several methods have been investigated. The concepts of fractional frequency reuse (FFR) and joint transmission (JT) were introduced in [11] and [12], respectively. The results show an improvement in term of spectral efficiency and the signal quality of cell edge users. In [13], space division multiple access (SDMA) scheme using an angle diversity transmitter was proposed. This method mitigates ICI by generating more concentrated light beams to different users.

In this study, novel ICI mitigation techniques based on angle diversity receivers (ADRs) are proposed. The ADR in the proposed technology consists of multiple narrow field-of-view (FOV) photodiodes (PDs) with different orientations. In [14]–[17], a single link from an optical transmitter to an ADR is investigated. The results show an improvement in terms of signal-to-noise ratio (SNR), transmission speed and coverage. To the best knowledge of the authors, the current article is the first paper that uses ADR to achieve low ICI in optical attocell networks. In this paper, four different signal combining schemes namely select best combining (SBC), equal gain combining (EGC), maximum ratio combining (MRC) and optimum combining (OPC), are studied for ADRs in optical attocell networks. Moreover, a novel double-source cell configuration with two transmission modes is designed to improve the signal-to-interference-plus-noise-ratio (SINR) performance. A criteria for selecting the modes in different

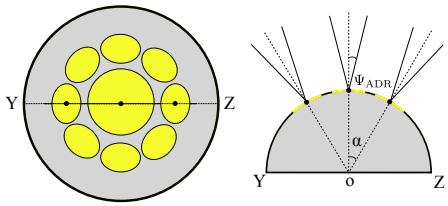

Fig. 1: The shape of an ADR (9 PDs).

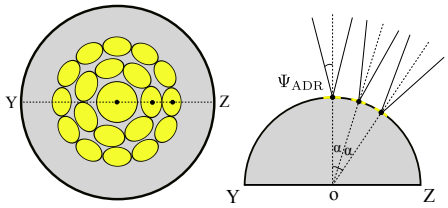

Fig. 2: The shape of an ADR (20 PDs).

deployment scenarios are also proposed. Finally, an analytical framework of evaluating the performance of ADRs in hexagonal optical attocell networks is also introduced. It is further shown that the analytical results accurately predict and evaluate the performance of optical attocell networks.

The remainder of this paper is organised as follows: the system model is introduced in Section II. Four different signal combining schemes for ADRs are discussed in Section III. The concept of the optical double-source cell is introduced in Section IV. Theoretical analysis of an optical attocell network is presented in Section V. The results and discussions are presented in Section VI. Finally, in Section VII, conclusions are given.

II. System Model

A. Optical Receivers

In this study, three types of optical receivers are considered in optical attocell networks. The first type is a single-PD receiver with only one upward-pointing PD with a FOV of Ψ_{single}. The second type is an ADR with 9 PDs. As shown in Fig. 1, this ADR consists of an upward-pointing PD which is surrounded by a ring of 8 PDs. The third type is an ADR with 20 PDs as shown in Fig. 2. This ADR has an upward-pointing PD and two rings PDs. The number of PDs in each ring is 7 and 12, respectively. Each PD on an ADR has identical FOV, Ψ_{ADR}. In addition, as shown in Fig. 1 and Fig. 2, α is defined as the tilted angle between the neighbouring rings. The tilted angle, α is designed so that the overlap between the coverage area of each PD is minimised without yielding black spots. As a result, the ADR has a strong ablity to separate different light sources. For a fair comparison, the overall coverage area of each optical receiver is assumed to be identical. The coverage area of a single-PD receiver (S1) and the coverage area of each ADR (S2,S3) are illustrated in Fig. 3.

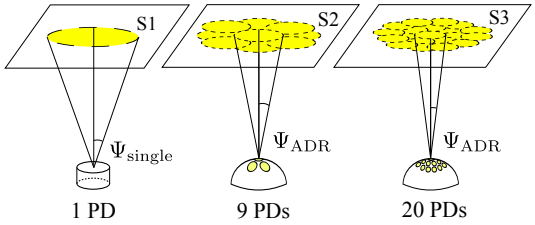

Fig. 3: The coverage area of different types of optical receivers. The overall coverage area of an ADR is the union of the individual coverage areas of each PD on that ADR. The coverage area of the single-PD receiver is defined by the only PD.

In optical attocell networks, the interference in the form of light which is defined in this study as light interference. It can be reduced by increasing the number of PDs on an optical receiver, especially when PDs point to a different directions. The reasons for this are twofold. Firstly, since the overall coverage area of each optical receiver is identical, the optical receiver with more PDs can have a narrower FOV for each PD. A narrow FOV PD can effectively reject the line-of-sight (LOS) interference. Also, due to the dispersive nature of light reflections, a narrow FOV PD can significantly mitigate the non-line-of-sight (NLOS) interference because it collects less light from reflections. Secondly, as the number of individual detector elements on a receiver increases, the granularity of the receiver increases. This results in the better capability of suppressing light interference.

B. Optical Free-space Transmission

In optical attocell networks, lighting fixtures are regarded as APs. The index of an AP is denoted as $a = 1, 2, ..., N_{\mathrm{AP}}$ and N_{AP} is the total number of the APs. Also, the index of PDs on an ADR is denoted as $p = 1, 2, ..., N_{\mathrm{PD}}$ and N_{PD} is the total number of PDs on a receiver. The total received electrical signal sample from PD p is given as [18]:

$$y_p(t) = \tau s_{a_{\mathrm{d}}}(t) \otimes h_{a_{\mathrm{d}},p}(t) + \sum_{a=1, a\neq a_{\mathrm{d}}}^{N_{\mathrm{AP}}} \tau s_a(t) \otimes h_{a,p}(t) + n_{\mathrm{rx}}(t), \quad (1)$$

where τ is the optical-to-electric conversion efficiency; a_{d} is the index of the desired AP; $h(t)$ is the channel impulse response between an AP and a PD and the subscripts of $h(t)$ denotes index of the AP and the PD, respectively; $s(t)$ is the sample transmitted by an AP and the subscript of $s(t)$ denotes the index of the AP; the noise sample generated by the receiver circuit are represented as $n_{\mathrm{rx}}(t)$.

Assuming that the symbol duration of the system is much longer than the duration of channel impulse response, (1) can be expressed as:

$$y_p(t) = \tau s_{a_{\mathrm{d}}}(t) H_{a_{\mathrm{d}},p} + \sum_{a=1, a\neq a_{\mathrm{d}}}^{N_{\mathrm{AP}}} \tau s_a(t) H_{a,p} + n_{\mathrm{rx}}(t), \quad (2)$$

where H is the channel direct current (DC) gain between an AP and a PD, which is $H = \int_{\infty}^{-\infty} h(t)\mathrm{d}t$. The subscripts of H denotes the index of the AP and the PD, respectively.

C. Channel Gain

In this study, both LOS and NLOS paths are considered. The overall channel DC gain is the sum of both LOS component and NLOS components:

$$H = H_{\mathrm{LOS}} + \sum_{l=1}^{N_{\mathrm{ref}}} H_{\mathrm{NLOS}}^{l}, \tag{3}$$

where l is the order of NLOS light reflections; N_{ref} is the total number of light reflections that are taken into account for the NLOS path.

1) LOS Propagation: In LOS links, the channel DC gain can be calculated as follows [18]:

$$H_{\mathrm{LOS}} = \frac{(m+1)A_{\mathrm{eff}}}{2\pi d^2}\cos^m(\phi)\cos(\psi)\mathrm{rect}\left(\frac{\psi}{2\Psi_{\mathrm{fov}}}\right), \tag{4}$$

where d is the distance between an optical transmitter and its corresponding receiver; Ψ_{fov} is the FOV of the optical receiver; m is the Lambertian order of the optical transmitter and is a function of the transmitter half-intensity radiation angle Φ_{tx} as $m = 1/\log_2(\cos(\Phi_{\mathrm{tx}}))$; ϕ is the angle of irradiance; ψ is the angle of light incidence at the receiver; $\mathrm{rect}(\cdot)$ is the rectangular function; the effective signal collection area A_{eff} is given as:

$$A_{\mathrm{eff}} = A_{\mathrm{p}} G \frac{n_{\mathrm{ref}}^2}{\sin^2(\Psi_{\mathrm{fov}})}, \tag{5}$$

where n_{ref} is the refractive index of the receiver optics; A_{p} is the physical area of a PD; G is the signal transmission gain of the optical filter.

2) NLOS Propagation: In NLOS links, the transmitted power reaches the optical receivers through reflections. In order to calculate the NLOS channel gain, all of the reflective surfaces are divided into a number of small reflecting surface elements [19]. Each element of reflective surfaces reflects a fraction of incident light energy on it. Typically, the fraction of the reflected light energy is determined by the reflection coefficient of the surface material. We mathematically model this complex behaviour of light as follows.

A typical NLOS link can be divided into three parts. The first part is the light path from an optical transmitter to the q^{th} reflecting surface element. The optical channel gain for this path can be calculated as:

$$L_{1,q} = \frac{(m+1)\Delta A}{2\pi d_{q,\mathrm{tx}}^2}\cos^m(\phi)\cos(\psi), \tag{6}$$

where ΔA is the area of the reflecting surface element. The distance between the optical transmitter and the q^{th} reflecting surface element is denoted as $d_{q,\mathrm{tx}}$. Equation (6) provides a method to calculate the power distribution on the reflecting walls due to a single-point source. Each reflective element is modelled as a light source which reflects a fraction of the incident light on it. It is assumed that the reflection of light obeys Lambertian radiation patten, and the intensity is determined by the reflective coefficient ρ. Therefore, the power on each reflecting surface element after the l^{th} light reflection can be derived.

In the second part of the NLOS path, the q^{th} reflecting surface element is regarded as a transmitter and the p^{th} reflecting surface element is regarded as a receiver, the optical channel gain between them is described as:

$$L_{l,p} = \sum_{q=1}^{Q} \frac{\rho_q(n+1)\cos^n(\phi)\cos(\theta)\Delta A}{2\pi d_{p,q}^2} L_{l-1,q}, \tag{7}$$

where l represents the number of the light reflections and $d_{p,q}$ is the distance between the reflecting element p and the reflecting element q. The total number of reflecting elements is Q. The reflection coefficient of the reflecting element q is ρ_q; n is the Lambertian order of the reflecting element, which is a function of the reflecting element half-intensity radiation angle θ_{ref} as $n = 1/\log_2(\cos(\theta_{\mathrm{ref}}))$. For most surfaces, $\theta_{\mathrm{ref}} = 60^{\mathrm{o}}$.

The third part of the NLOS link is the light path from the last reflecting elements to an optical receiver. The optical channel gain for this path can be obtained as:

$$H_{\mathrm{NLOS}}^{l} = \sum_{p=1}^{Q} L_{l,p} \frac{\rho_p(n+1)\Delta A}{2\pi d_{\mathrm{rx,p}}^2}\cos^n(\phi)\cos(\psi)\mathrm{rect}\left(\frac{\psi}{\Psi_{\mathrm{fov}}}\right), \tag{8}$$

where $d_{\mathrm{rx,p}}$ is the distance between the q^{th} reflecting surface element and the optical receiver; the reflection coefficient of the reflecting element p is ρ_p.

III. Signal Combining Schemes for ADR

In this section, four signal combining schemes for ADRs, namely SBC, EGC, MRC and OPC are described. Similar to RF [20], it is assumed that a user chooses the desired AP that provides the strongest signal strength:

$$a_{\mathrm{d}} = \underset{a}{\mathrm{argmax}} \sum_{p=1}^{N_{\mathrm{PD}}} \left|H_{a,p}\right|^2. \tag{9}$$

The ADR combines the received signals from its PDs. According to (1), the received electrical signal sample is given as:

$$z(t) = \sum_{p=1}^{N_{\mathrm{PD}}} w_p y_p(t). \tag{10}$$

SINR is an important metric to evaluate the link quality and capacity in optical attocell networks. According to [18], the SINR of the desired user after signal combining is given by:

$$\gamma = \frac{\left(\sum_{p=1}^{N_{\mathrm{PD}}} \tau P_{\mathrm{tx}} w_p H_{a_{\mathrm{d}},p}\right)^2}{\sum_{p=1}^{N_{\mathrm{PD}}} w_p^2 N_0 B + \sum_{a=1,a\neq a_{\mathrm{d}}}^{N_{\mathrm{AP}}} \left(\tau P_{\mathrm{tx}} \sum_{p=1}^{N_{\mathrm{PD}}} w_p H_{a,p}\right)^2}, \tag{11}$$

where w_p is the weight of PD p; N_0 is the additive white Gaussian noise (AWGN) power spectral density; B is the

communication bandwidth; $P_{\rm tx}$ is the transmission power of an optical AP which is defined as:

$$P_{\rm tx} = \lim_{T\to\infty} \sqrt{\frac{1}{2T}\int_{-T}^{T} (s(t)-\bar{s})^2 {\rm d}t}, \tag{12}$$

where $\bar{s}$ is given by:

$$\bar{s} = \lim_{T\to\infty} \frac{1}{2T}\int_{-T}^{T} s(t){\rm d}t. \tag{13}$$

If $N_{\rm PD}$ is set to 1, (11) represents the SINR of a single-PD receiver.

In different combining schemes, the weights are evaluated differently, and requires the knowledge of channel state information (CSI) at the ADR. In this study, CSI is assumed as channel DC gain, H, and usually ADR acquires CSI through pilot sequences.

A. SBC scheme

In SBC, the PD has the highest received SNR is selected. All information from other PDs are discarded. The index of the desired PD is determined by:

$$p_{\rm d} = \underset{p}{\rm argmax} \frac{\left(\tau P_{\rm tx} H_{a_{\rm d},p}\right)^2}{N_0 B}. \tag{14}$$

The weight of PDs is:

$$w_p = \begin{cases} 1 & p = p_{\rm d} \\ 0 & \text{otherwise.} \end{cases} \tag{15}$$

According to (14), only the knowledge of CSI from the desired cell to a user is required. The knowledge of CSI from the other interfering APs to the user is unnecessary. In terms of the circuit design, a switch is required for selecting the signals from the desired PD.

B. EGC scheme

The EGC simply combines signals from all PDs with equal weights, which is $w_p = 1$.

The EGC requires only a simple adder for the combining circuit. No knowledge of CSI from any AP to a user is required for signal combining. Since optical power from multiple PDs is added up, the received optical power using EGC is higher than the optical power using SBC. However, as the signal from each PD is equally weighted, the interference cannot be suppressed effectively which could result in poor overall SINR performance.

C. MRC scheme

In MRC, weight w_p, is proportional to the SNR on each PD, which is:

$$w_p = \frac{\left(\tau P_{\rm tx} H_{a_{\rm d},p}\right)^2}{N_0 B}. \tag{16}$$

Similar to SBC, MRC only requires the knowledge of CSI from the desired cell to a user. For circuit design, a multiplier and an adder are necessary for combining the received signals. With proper weight on each PD, the MRC should boost the signal component and attenuates the interference and noise components which would result in a high overall SINR.

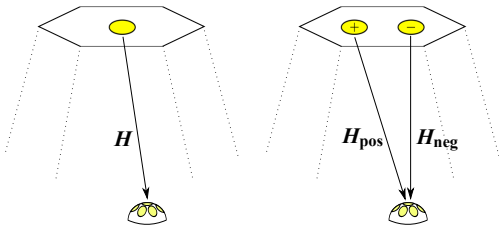

Fig. 4: The layout of a conventional optical cell and a double-source optical cell. $H_{\rm pos}$ is the channel gain between the positive AP and a PD; $H_{\rm neg}$ is the channel gain between the negative AP and a PD; ΔH denotes the difference between $H_{\rm pos}$ and $H_{\rm neg}$.

D. OPC scheme

If there is no interference components, MRC can provide the optimised SNR [21]. However, in the proposed optical attocell network, both LOS and NLOS interference components from the neighbouring APs can be received. The correlation between interference terms at different PDs significantly affects the performance of MRC. As a consequence, OPC is developed. OPC was initially used in RF scenario [21] and is adopted for optical attocell network. It mitigates the ICI by considering an interference-plus-noise correlation matrix which can significantly suppress the correlated interference. In OPC, weights are calculated as:

$$\mathbf{w} = \xi \mathbf{R}_{nn}^{-1} \mathbf{u}_{a_{\rm d}}, \tag{17}$$

where the signals received from the desired AP $a_{\rm d}$ is $\mathbf{u}_{a_{\rm d}} = [\tau P_{\rm tx} H_{a_{\rm d},1}, \tau P_{\rm tx} H_{a_{\rm d},2}, \cdots, \tau P_{\rm tx} H_{a_{\rm d},N_{\rm PD}}]^T$; and a vector with the different weight is represented as $\mathbf{w} = [w_1, w_2, \cdots, w_{N_{\rm PD}}]^T$; ξ is a scaling factor; the interference-plus-noise correlation matrix, $\mathbf{R}_{nn}$, is given by:

$$\mathbf{R}_{nn} = N_0 B \mathbf{I} + \sum_{a\neq a_{\rm d}} \left[\mathbf{u}_a \mathbf{u}_a^T\right]. \tag{18}$$

In (18), $\mathbf{I}$ is the identity matrix and $\mathbf{u}_a$ is the signals received from AP a: $\mathbf{u}_a = [\tau P_{\rm tx} H_{a,1}, \tau P_{\rm tx} H_{a,2}, \cdots, \tau P_{\rm tx} H_{a,N_{\rm PD}}]^T$.

Compared with MRC, OPC not only requires the knowledge of CSI from the desired cell to a user, but also the knowledge of CSI from all other interfering cells to the user in order to estimate the interference-plus-noise correlation matrix. However, by exploiting the correlation of interference received from each PD, OPC can effectively suppress the correlated interference and this is expected to achieve better SINR performance compared with MRC.

IV. Double-source Optical Cell

The existing optical attocell has a single AP at each cell centre. In this section, we increase the number of optical transmitters in each cell and propose a novel double-source cell configuration to further improve the performance of ADRs. As shown in Fig. 4, in each double-source cell, there are two

APs which are termed as the positive AP and the negative AP. The time domain signal transmitted by the positive AP and the negative AP are denoted as $s_{\rm pos}(t)$ and $s_{\rm neg}(t)$, respectively. The dynamic range of them is from 0 to $s_{\rm H}$. Two data transmission modes, mode A and mode B, are defined in double-source cell configuration.

A. Mode A

In mode A, the relationship between $s_{\rm pos}(t)$ and $s_{\rm neg}(t)$ is represented as:

$$s_{\rm neg}(t) = s_{\rm H} - s_{\rm pos}(t). \tag{19}$$

According to (12), the transmission power of the positive AP and the negative AP is obtained as:

$$\mathrm{P}_{\rm tx,pos} = \sqrt{\mathrm{E}\left[(s_{\rm pos}(t) - \mathrm{E}[s_{\rm pos}(t)])^2\right]}, \tag{20}$$

$$\begin{aligned}\mathrm{P}_{\rm tx,neg} &= \sqrt{\mathrm{E}\left[(s_{\rm neg}(t) - \mathrm{E}[s_{\rm neg}(t)])^2\right]} \\ &= \sqrt{\mathrm{E}\left[(s_{\rm H} - s_{\rm pos}(t) - \mathrm{E}[s_{\rm H} - s_{\rm pos}(t)])^2\right]} \\ &= \sqrt{\mathrm{E}\left[(s_{\rm pos}(t) - \mathrm{E}[s_{\rm pos}(t)])^2\right]}. \end{aligned} \tag{21}$$

Since the transmission power of the positive AP and the negative AP is the same, it is simply denoted as $\mathrm{P}_{\rm tx}$. Furthermore, the transmit power, $\mathrm{P}_{\rm tx}$ is assumed to be the same for all APs. For a single optical cell, the received optical signal at a PD is represented as:

$$s_{\rm sum}(t) = s_{\rm pos}(t)H_{\rm pos} + s_{\rm neg}(t)H_{\rm neg}. \tag{22}$$

Therefore, the received optical power at a PD is:

$$\begin{aligned}\mathrm{P}_{\rm rx} &= \sqrt{\mathrm{E}\left[(s_{\rm sum}(t) - \mathrm{E}[s_{\rm sum}(t)])^2\right]} \\ &= \sqrt{\mathrm{E}\left[(s_{\rm pos}(t) - \mathrm{E}[s_{\rm pos}(t)])^2\right]}\,|H_{\rm pos} - H_{\rm neg}| \\ &= \mathrm{P}_{\rm tx}\Delta H, \end{aligned} \tag{23}$$

where $H_{\rm pos}$ is the channel gain between the positive AP and a PD. $H_{\rm neg}$ is the channel gain between the negative AP and a PD; ΔH denotes the difference between $H_{\rm pos}$ and $H_{\rm neg}$.

It can be observed from (23) that the received signal power is scaled by the channel gain difference, ΔH. Generally, the desired cell is close to a receiver and the interfering cells are much farther. As illustrated in Fig. 5, a receiver is underneath its desired cell and the channel gain difference ΔH of a PD is large. This is because, the PD has little chance to simultaneously receive LOS signals from the two APs due to the narrow FOV. Therefore, only one of $H_{\rm pos}$, and $H_{\rm neg}$ appears as LOS channel gain in (22). Since the difference between LOS and NLOS channel gain is significant, the received optical signal is enhanced. It is also shown in Fig. 5 that, when a receiver is far from an interfering cell, the channel gain, $H_{\rm pos}$ and $H_{\rm neg}$, are both NLOS. The difference between them is small which means the received interference is attenuated. Hence, this configuration can effectively boost the signal from the desired cell and suppress the interference. Moreover, the double-source cell configuration is easy to implement, since the signal from the negative AP is simply an inverted version of the signal from the positive AP. A practical differential LED driver for double-source cell configuration has been made and achieved high energy efficiency [22].

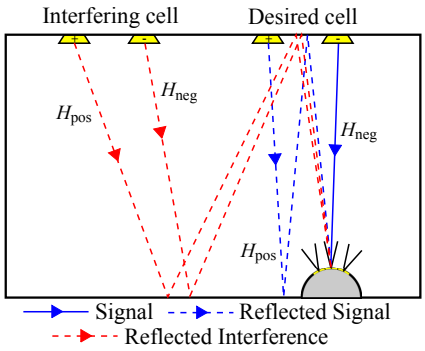

Fig. 5: The benefit of implementing a double-source cell configuration.

B. Mode B

Transmission mode A can effectively suppress interference. However, mode A requires an optical receiver that has the ability to separate the signals from the positive and negative APs in the desired cell. If a receiver cannot distinguish them, the SINR performance of it will be significantly degraded, especially at cell centre. In order to facilitate the receivers that cannot distinguish the signals from the positive and negative APs in their desired cells, another transmission mode, mode B, is proposed. In mode B, the relationship between $s_{\rm neg}(t)$ and $s_{\rm pos}(t)$ is represented as:

$$s_{\rm neg}(t) = s_{\rm pos}(t). \tag{24}$$

This means both APs transmit identical signals which is similar to the conventional single-source cell configuration. In order to optimise the system performance in double-source cell configuration, a criteria for transmission modes selection is necessary. Simulations and discussions on this criteria are presented in Sec. VI.

V. Performance Analysis

In this section, an analytical framework for analysing the system performance in optical attocell networks is presented. For simplicity, only the desired AP and the interfering APs in the vicinity are considered. Also, each optical cell is assumed to be hexagonal.

A. Simplified NLOS Propagation Model

Firstly, a simplification of the NLOS model is required. In the conventional model, high-order reflections are taken into account and this significantly increases the computational complexity. However, this is unnecessary in an optical attocell network. As illustrated in Fig. 6, the FOV of the optical receiver is designed to be narrow enough to block the LOS

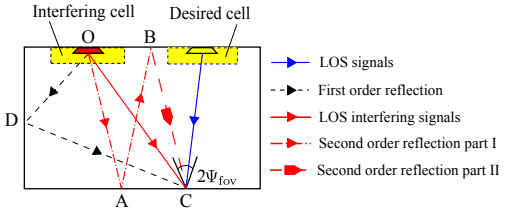

Fig. 6: The propagation model in optical attocell network.

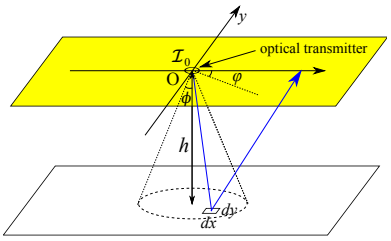

Fig. 7: The conventional propagation model for second order reflection part I. Blue line represents one of the second order reflection paths.

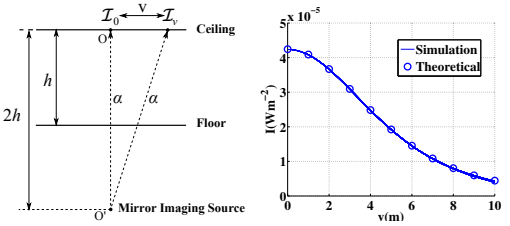

(a) Simplified reflection model. (b) Reflected optical power density at horizontal different distances.

Fig. 8: The simplified propagation model for second order reflection part I.

interference ($O \rightarrow C$) from cells in the vicinity. Furthermore, the narrow FOV optical receiver also blocks the first-order reflections ($O \rightarrow D \rightarrow C$) which are reflected by walls. Second-order reflections are the only dominant inter-cell interference occurred because the other high-order reflections attenuates significantly and thus are negligible. Hence, only the second-order reflection ($O \rightarrow A \rightarrow B \rightarrow C$) is assumed in the simplified model. Usually, the propagation path of the second order reflection can be divided into two parts as part I ($O \rightarrow A \rightarrow B$) and part II ($B \rightarrow C$).

1) Second Order Reflection Part I: For this path, light signals are considered to be transmitted from an optical transmitter at point O on the ceiling, reflected by the floor and transmitted back to the ceiling (see Fig. 7). The optical power density of the reflected light at point O, $\mathcal{I}_0$, has the maximum value and can be presented as:

$$\mathcal{I}_0 = \frac{C(m+1)(n+1)}{4\pi^2 h^{-(m+n+2)}} \iint_{\text{floor}} \frac{dxdy}{(x^2+y^2+h^2)^{(m+n+6)/2}}. \tag{25}$$

Here, x, y in (25) can be switched by ϕ, φ, respectively. The mathematical relationship between them is as follows:

$$\begin{cases} x = h\tan(\phi)\cos(\varphi) \\ y = h\tan(\phi)\sin(\varphi), \end{cases} \tag{26}$$

where ϕ is the angle of irradiance and φ is the azimuth angle. Then, the intensity density at point O can be calculated as closed-form:

$$\begin{aligned} \mathcal{I}_0 &= \frac{C(m+1)(n+1)}{4\pi^2 h^4} \int_0^{2\pi} \int_0^{\pi/2} \cos(\phi)^{m+n+6} J d\phi d\varphi \\ &= \frac{C(m+1)(n+1)}{2\pi h^2 (m+n+4)}, \end{aligned} \tag{27}$$

where the coefficient $C = \rho_{\text{floor}}\rho_{\text{ceiling}}P_{\text{tx}}$; and the reflection coefficient of the floor and ceiling are ρ_{floor} and ρ_{ceiling}, respectively; also, J is the Jacobian determinant of the co-ordinate conversion which can be represented as:

$$J = \det\left(\begin{bmatrix} \frac{\partial x}{\partial \phi} \frac{\partial x}{\partial \varphi} \\ \frac{\partial y}{\partial \phi} \frac{\partial y}{\partial \varphi} \end{bmatrix} \right). \tag{28}$$

In the simplified model, $\mathcal{I}_0$ is used to estimate the optical power density at other points on the ceiling. Since light transmission is isotropic, two points on the ceiling have the same optical power density when their distances to O are the same. Hence, for an arbitrary point on the ceiling, optical power density attenuates according to its horizontal distance to point O. The trend of attenuation is approximated by a model, as illustrated in Fig. 8(a). It is assumed that the optical power emits from a mirror imaging source O' and the distance between them is $2h$. At point O, the optical power intensity is assumed to be the same as in the conventional model. The attenuation factor is defined as α. Hence, at an arbitrary point on the ceiling, the optical power density can be derived as:

$$\mathcal{I}_v = \mathcal{I}_0 \left(\frac{2h}{\sqrt{v^2+4h^2}} \right)^{\alpha} \tag{29}$$

where v is the horizontal distance from an arbitrary point to point O. The attenuation factor, α, is chosen to minimise the difference between the proposed simplified model and the conventional model. In this study, the transmitter semi-angle is chosen to be 60^o and α is set as 4.8 accordingly. Fig. 8(b) shows that there is a close match between the simplified model and conventional model. In the simplified model, the optical power density of an arbitrary point on the ceiling, $\mathcal{I}_v$, can be calculated in closed-form using (29). As a result, the simplified model significantly reduces the computational complexity in comparison with the conventional model.

2) Second Order Reflection Part II: For this path, the reflected light from the ceiling is transmitted to an optical receiver, as shown in Fig. 9. Due to the limitation of the receiver FOV, only the reflected light in the grey area on the ceiling can be captured by the receiver. For simplicity,

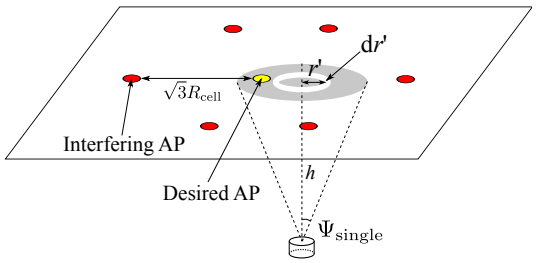

Fig. 9: The simplified propagation model for second order reflection part II. The light intensity in grey area is assumed to be identical.

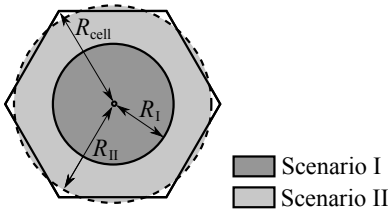

Fig. 10: The region of scenario I and scenario II for analysing a conventional single-PD receiver. The region of scenario I is a circle with a radius of R_{I}. The region of scenario II is a circle ring.

the optical power intensity of the reflected light in grey area is assumed to be constant. In a typical 7-cell optical attocell network, NLOS interference is generated by the six APs in the vicinity . The distance between an interfering AP to the desired cell centre is $\sqrt{3}R_{\text{cell}}$. Hence, the total received NLOS interference is:

$$\begin{aligned}\mathcal{I}_{\text{NLOS}}(\Psi_{\text{single}}) &= 6\left[\int_0^{h\tan(\Psi_{\text{single}})} \tau\mathcal{I}_v 2\pi r' H(r')\mathrm{d}r'\right]^2 \\ &= 6\left[\tau\mathcal{I}_v A_{\text{eff}}\sin^2(\Psi_{\text{single}})\right]^2\Big|_{v=\sqrt{3}R_{\text{cell}}}.\end{aligned} \tag{30}$$

With the simplified assumption of NLOS path II, the entire NLOS interference in the vicinity can be calculated as closed-form by (30).

B. SINR Statistic of Conventional Single-PD Receiver

The service quality in optical attocell networks is determined by the statistic of received SINR. In this study, the distribution, especially the cumulative distribution function (CDF) of the SINR is derived to evaluate the performance of optical attocell networks. The simplified NLOS propagation model is applied in the evaluation since general analysis of SINR performance in optical attocell networks is difficult. According to the position of active users, the statistic analysis of a single-PD receiver can be separated into the analysis of two scenarios, scenario I and scenario II, as shown in Fig. 10. For simplicity, the boundary of scenario I and II is approximated as a circle. The area of the approximated circle is equivalent to that of the original region, where $R_{\text{II}} \approx 0.91R_{\text{cell}}$.

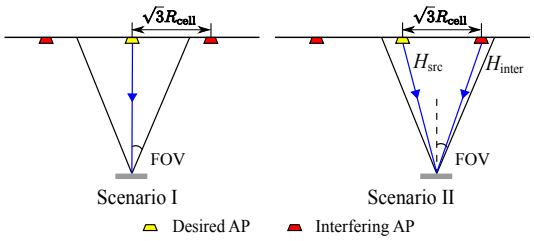

Fig. 11: The layout of scenario I and scenario II.

1) Scenario I: As shown in Fig. 10, users are uniformly distributed at cell centre. There is no LOS interference from the optical cells in the vicinity (see Fig. 11). The horizontal distance between an active user and its desired cell centre is defined as r. The probability density function (PDF) of r is given as:

$$f_{\text{I}}(r) = \frac{2r}{R_{\text{I}}^2}, \quad (0 \le r \le R_{\text{I}}) \tag{31}$$

where R_{I} is the radius of the circular region of scenario I. By considering the geometry relationship between the parameters: $d = h/\cos(\phi), \cos(\phi) = h/\sqrt{h^2+r^2}, \psi = \phi$, (4) can be expressed as:

$$H(r, \Psi_{\text{single}}) = \frac{(m+1)A_{\text{eff}}(\Psi_{\text{single}})}{2\pi h^2}\left(\frac{h}{\sqrt{h^2+r^2}}\right)^{m+3}, \tag{32}$$

where Ψ_{single} is the FOV of a single-PD receiver. Assuming that an attocell network is an interference limited system, the SINR can be represented as:

$$\gamma(r) = \frac{\left(\tau P_{\text{tx}} H(r, \Psi_{\text{single}})\right)^2}{\mathcal{I}_{\text{NLOS}}(\Psi_{\text{single}}) + N_0 B} \approx \frac{\left(\tau P_{\text{tx}} H(r, \Psi_{\text{single}})\right)^2}{\mathcal{I}_{\text{NLOS}}(\Psi_{\text{single}})}. \tag{33}$$

The PDF of SINR for scenario I is given as:

$$f_{\text{I}}(\gamma) = \begin{cases} \dfrac{h^2}{(m+3)R_{\text{I}}^2}\gamma_0^{\frac{1}{m+3}}\gamma^{-\frac{m+4}{m+3}} & \gamma_{\text{I}} \le \gamma \le \gamma_0 \\ 0 & \text{otherwise,} \end{cases} \tag{34}$$

where γ_0 is the maximum SINR at the cell centre ($r = 0$), which can be derived as:

$$\gamma_0 = \frac{\left(\tau P_{\text{tx}} H(0, \Psi_{\text{single}})\right)^2}{\mathcal{I}_{\text{NLOS}}(\Psi_{\text{single}})}; \tag{35}$$

and γ_{I} is the minimum SINR at the boundary of the region of scenario I ($r = R_{\text{I}}$):

$$\gamma_{\text{I}} = \frac{\left(\tau P_{\text{tx}} H(R_{\text{I}}, \Psi_{\text{single}})\right)^2}{\mathcal{I}_{\text{NLOS}}(\Psi_{\text{single}})}. \tag{36}$$

The closed-form CDF of the SINR for the scenario I is:

$$F_{\mathrm{I}}(\gamma)=\begin{cases}0 & \gamma<\gamma_{\mathrm{I}}\\ \frac{h^2}{R_{\mathrm{I}}^2}\gamma_0^{\frac{1}{m+3}}\left(\gamma_{\mathrm{I}}^{-\frac{1}{m+3}}-\gamma^{-\frac{1}{m+3}}\right) & \gamma_{\mathrm{I}}\le\gamma\le\gamma_0\\ 1 & \gamma>\gamma_0.\end{cases} \tag{37}$$

2) Scenario II: As shown in Fig. 10, users are uniformly distributed at cell edge. LOS interference from the neighbouring cell can be received (see Fig. 11). The PDF of r in scenario II can be derived as:

$$f_{\mathrm{II}}(r)=\frac{2r}{R_{\mathrm{II}}^2-R_{\mathrm{I}}^2},\quad (R_{\mathrm{I}}\le r\le R_{\mathrm{II}}), \tag{38}$$

where R_{II} is the outer radius of the region of scenario II.

In this scenario, NLOS interference components and noise are assumed to be negligible. This is because the magnitude of the LOS interference component is a few orders higher then the NLOS interference components and noise. Hence, the SINR of the system can be approximated as:

$$\gamma(r)=\frac{\left(\tau P_{\mathrm{tx}}H_{\mathrm{src}}(r)\right)^2}{\left(\tau P_{\mathrm{tx}}H_{\mathrm{inter}}(r)\right)^2}\approx\left(\frac{h^2+\tilde{r}^2}{h^2+(\sqrt{3}R_{\mathrm{cell}}-r)^2}\right)^{-(m+3)}, \tag{39}$$

where $H_{\mathrm{src}}(r)$ is the link from desired AP to optical receiver; $H_{\mathrm{inter}}(r)$ is the link from interfering AP to optical receiver; $\tilde{r}=\sqrt{3}R_{\mathrm{cell}}-(R_{\mathrm{I}}+R_{\mathrm{II}})/2$. The PDF of the SINR for the scenario II is:

$$f_{\mathrm{II}}(\gamma)=\begin{cases}\frac{h^2+\tilde{r}^2}{(m+3)(R_{\mathrm{II}}^2-R_{\mathrm{I}}^2)}\gamma^{-\frac{m+2}{m+3}} & 1\le\gamma\le\gamma_{\mathrm{I}}'\\ 0 & \text{otherwise,}\end{cases} \tag{40}$$

and the CDF of the SINR for the scenario II is:

$$F_{\mathrm{II}}(\gamma)=\begin{cases}0 & \gamma<1\\ \frac{h^2+\tilde{r}}{R_{\mathrm{II}}^2-R_{\mathrm{I}}^2}\left(-1+\gamma^{\frac{1}{m+3}}\right) & 1\le\gamma\le\gamma_{\mathrm{I}}'\\ 1 & \gamma>\gamma_{\mathrm{I}}',\end{cases} \tag{41}$$

and γ_{I}' is also the SINR that exists at the boundary of region I ($r=R_{\mathrm{I}}$). Unlike (36), γ' represents the SINR of an optical receiver that captures the LOS interference from the AP in the vicinity. The difference between (36) and (42) is due to the cut-off effect of receiver FOV. γ_{I}' is derived as:

$$\gamma_{\mathrm{I}}'=\left(\frac{h^2+\tilde{r}^2}{h^2+(\sqrt{3}R_{\mathrm{cell}}-R_{\mathrm{I}})^2}\right)^{-(m+3)}. \tag{42}$$

3) Overall Theoretical Performance: Similar to the derivation for scenario I and scenario II, the SINR CDF of a single-PD receiver in optical attocell networks can be derived. The PDF of r is given as:

$$f_{\mathrm{overall}}(r)=\frac{2r}{R_{\mathrm{II}}^2},\quad (0\le r\le R_{\mathrm{II}}). \tag{43}$$

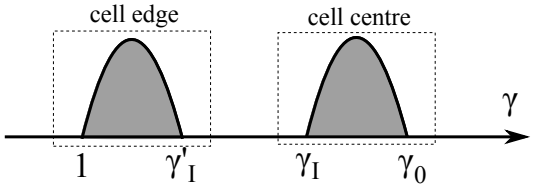

Fig. 12: The bimodal distribution of the SINR PDF of a single-PD receiver.

Similar to (34) and (40), the PDF of SINR γ can be derived:

$$f_{\mathrm{overall}}(\gamma)=\begin{cases}\frac{h^2+\tilde{r}^2}{(m+3)R_{\mathrm{II}}^2}\gamma^{-\frac{m+2}{m+3}} & 1\le\gamma\le\gamma_{\mathrm{I}}'\\ \frac{h^2}{(m+3)R_{\mathrm{II}}^2}\gamma_0^{\frac{1}{m+3}}\gamma^{-\frac{m+4}{m+3}} & \gamma_{\mathrm{I}}\le\gamma\le\gamma_0\\ 0 & \text{otherwise,}\end{cases} \tag{44}$$

where $\gamma_{\mathrm{I}}>\gamma_{\mathrm{I}}'$. It is notable that the PDF of SINR γ, follows bimodal distribution (see Fig. 12). The PDF of SINR consists of two regions, high SINR and low SINR regions. The high SINR region corresponds to scenario I (cell centre). In cell centre, the limited FOV of an PD can reject the LOS interference from neighbouring cells which means only NLOS interference can be captured. This results in a high received SINR. The low SINR region corresponds to scenario II (cell edge). Strong LOS ICI at cell edge results in low received SINR. It is notable that there is a sharp separation between the low and high SINR regions. This is because of the cut-off effect stemmed from the FOV-limited optical receiver. According to (34) and (40), the PDF can then be represented as:

$$f_{\mathrm{overall}}(\gamma)=\begin{cases}\frac{R_{\mathrm{II}}^2-R_{\mathrm{I}}^2}{R_{\mathrm{II}}^2}f_{\mathrm{II}}(\gamma) & 1\le\gamma\le\gamma'\\ \frac{R_{\mathrm{I}}^2}{R_{\mathrm{II}}^2}f_{\mathrm{I}}(\gamma) & \gamma_{\mathrm{I}}\le\gamma\le\gamma_0\\ 0 & \text{otherwise.}\end{cases} \tag{45}$$

The CDF of SINR γ_{dB} can then be generated as:

$$\begin{aligned}F_{\mathrm{overall}}(\gamma)&=\int_{-\infty}^{\gamma}f_{\mathrm{overall}}(\gamma)\mathrm{d}\gamma\\ &=\int_{-\infty}^{\gamma}\frac{R_{\mathrm{I}}^2}{R_{\mathrm{II}}^2}f_{\mathrm{I}}(\gamma)+\frac{R_{\mathrm{II}}^2-R_{\mathrm{I}}^2}{R_{\mathrm{II}}^2}f_{\mathrm{II}}(\gamma)\mathrm{d}\gamma\\ &=\frac{R_{\mathrm{I}}^2}{R_{\mathrm{II}}^2}F_{\mathrm{I}}(\gamma)+\frac{R_{\mathrm{II}}^2-R_{\mathrm{I}}^2}{R_{\mathrm{II}}^2}F_{\mathrm{II}}(\gamma).\end{aligned} \tag{46}$$

The SINR performance of a single-PD receiver via numerical simulation and theoretical analysis are shown in Fig. 13. The theoretical results show a close match to the simulation results which verifies the accuracy of the theoretical model.

C. SINR Statistics of Angle Diversity Receiver

The theoretical tools developed for analysing single-PD receivers can be generalised to ADRs. For simplicity, it is assumed that each PD on an ADR points to a different

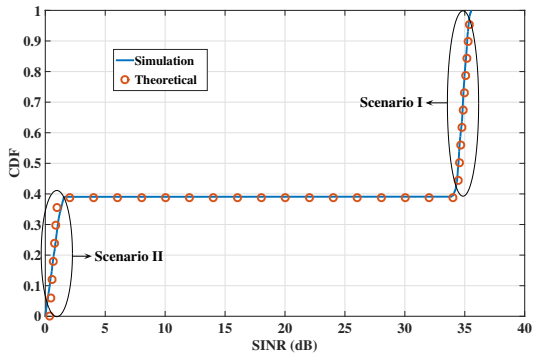

Fig. 13: The CDF of the received SINR when conventional single-PD receivers are used. Solid line represents the simulation result and round marker represents theoretical results.

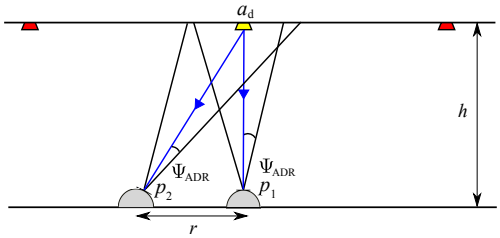

Fig. 14: The generalisation of scenario I. The desire AP a_{d} is represented in yellow; the interfering APs are represented in red.

direction and there is no overlap and black spot between the aperture of each PD. This means that one PD can establish at most one LOS link with a desired AP.

1) SBC: As shown in Fig. 14, an user in cell centre selects the upward pointing PD, p_1 to achieve the best SINR performance. Similar to (33), the SINR of an user can be derived as:

$$\gamma_{\mathrm{SBC,centre}}(r) = \frac{\left(\tau P_{\mathrm{tx}} H(r, \Psi_{\mathrm{ADR}})\right)^2}{\mathcal{I}_{\mathrm{NLOS}}(\Psi_{\mathrm{ADR}})}, \tag{47}$$

where Ψ_{ADR} is the FOV of PDs on an ADR; $\mathcal{I}_{\mathrm{NLOS}}(\Psi_{\mathrm{ADR}})$ is the NLOS interference received by p_1. An user at the cell edge selects PD, p_2 to achieve the best SINR, and the SINR of the user is:

$$\gamma_{\mathrm{SBC,edge}}(r) = \frac{\left(\tau P_{\mathrm{tx}} H(r, \Psi_{\mathrm{ADR}})\right)^2}{\mathcal{I}'_{\mathrm{NLOS}}(\Psi_{\mathrm{ADR}})}, \tag{48}$$

where $\mathcal{I}'_{\mathrm{NLOS}}$ is the NLOS interference received by p_2. According to [23], when p_1 and p_2 have identical FOV, $\mathcal{I}_{\mathrm{NLOS}}(\Psi_{\mathrm{ADR}}) = \mathcal{I}'_{\mathrm{NLOS}}(\Psi_{\mathrm{ADR}})$. This means SINR of the optical receiver can be represented by (47) in both cell centre and cell egde area. Therefore, the PDF of SINR, γ can be approximated as:

$$f_{\mathrm{SBC}}(\gamma) = \begin{cases} \dfrac{h^2 (\gamma_{0,\mathrm{SBC}})^{\frac{1}{m+3}}}{(m+3) R_{\mathrm{II}}^2} \gamma^{-\frac{m+4}{m+3}} & \gamma_{\mathrm{II,SBC}} \le \gamma \le \gamma_{0,\mathrm{SBC}} \\ 0 & \text{otherwise,} \end{cases} \tag{49}$$

where $\gamma_{0,\mathrm{SBC}}$ is the SINR at $r = 0$:

$$\gamma_{0,\mathrm{SBC}} = \frac{\left(\tau P_{\mathrm{tx}} H(0, \Psi_{\mathrm{ADR}})\right)^2}{\mathcal{I}_{\mathrm{NLOS}}(\Psi_{\mathrm{ADR}})}, \tag{50}$$

and $\gamma_{\mathrm{II,SBC}}$ is the SINR at $r = R_{\mathrm{II}}$:

$$\gamma_{\mathrm{II,SBC}} = \frac{\left(\tau P_{\mathrm{tx}} H(R_{\mathrm{II}}, \Psi_{\mathrm{ADR}})\right)^2}{\mathcal{I}_{\mathrm{NLOS}}(\Psi_{\mathrm{ADR}})}. \tag{51}$$

The CDF of the SINR for the SBC is:

$$F_{\mathrm{SBC}}(\gamma_{\mathrm{dB}}) = \begin{cases} 0 & \gamma < \gamma_{\mathrm{II,SBC}} \\ \dfrac{h^2}{R_{\mathrm{II}}^2} \gamma_{0,\mathrm{SBC}}^{\frac{1}{m+3}} \left(\gamma_{\mathrm{II,SBC}}^{-\frac{1}{m+3}} - \gamma^{-\frac{1}{m+3}} \right) & \\ & \gamma_{\mathrm{II,SBC}} \le \gamma \le \gamma_{0,\mathrm{SBC}} \\ 1 & \gamma > \gamma_{0,\mathrm{SBC}}, \end{cases} \tag{52}$$

2) EGC: In cell centres, the received signal of an user using EGC is similar to that of SBC. This is because PDs point to different directions and only one of them can receive the LOS signal from the desired cell. However, since the weights of all PDs are identical, the received NLOS interference is scale with the number of PDs on the receiver. Therefore, the SINR can be approximated as:

$$\gamma_{\mathrm{EGC,centre}}(r) = \frac{\left(\tau P_{\mathrm{tx}} H(r, \Psi_{\mathrm{ADR}})\right)^2}{M^2 \mathcal{I}_{\mathrm{NLOS}}(\Psi_{\mathrm{ADR}})}. \tag{53}$$

The SINR of cell edge users is similar to (39):

$$\gamma_{\mathrm{EGC,edge}}(r) = \frac{\left(\tau P_{\mathrm{tx}} H_{\mathrm{src}}(r, \Psi_{\mathrm{ADR}})\right)^2}{\left(\tau P_{\mathrm{tx}} H_{\mathrm{inter}}(r, \Psi_{\mathrm{ADR}})\right)^2}. \tag{54}$$

Similar to the derivation in Sec.V-B, the CDF of SINR, γ in EGC can be approximated as:

$$F_{\mathrm{EGC}}(\gamma) = \frac{R_{\mathrm{I}}^2}{R_{\mathrm{II}}^2} F_{\mathrm{EGC,centre}}(\gamma) + \frac{R_{\mathrm{II}}^2 - R_{\mathrm{I}}^2}{R_{\mathrm{II}}^2} F_{\mathrm{EGC,edge}}(\gamma), \tag{55}$$

where $F_{\mathrm{EGC,edge}}(\gamma) = F_{\mathrm{II}}(\gamma)$ and $F_{\mathrm{EGC,centre}}(\gamma)$ is:

$$F_{\mathrm{EGC,centre}}(\gamma) = \begin{cases} 0 & \gamma < \gamma_{\mathrm{I,EGC}} \\ \dfrac{h^2}{R_{\mathrm{I}}^2} \gamma_{0,\mathrm{EGC}}^{\frac{1}{m+3}} \left(\gamma_{\mathrm{I,EGC}}^{-\frac{1}{m+3}} - \gamma^{-\frac{1}{m+3}} \right) & \\ & \gamma_{\mathrm{I,EGC}} \le \gamma \le \gamma_{0,\mathrm{EGC}} \\ 1 & \gamma > \gamma_{0,\mathrm{EGC}}, \end{cases} \tag{56}$$

Here, $\gamma_{0,\mathrm{EGC}}$ is the SINR at the cell centre ($r = 0$):

$$\gamma_{0,\mathrm{EGC}} = \frac{\left(\tau P_{\mathrm{tx}} H(0, \Psi_{\mathrm{single}})\right)^2}{M^2 \mathcal{I}_{\mathrm{NLOS}}(\Psi_{\mathrm{ADR}})}; \tag{57}$$

and $\gamma_{\mathrm{I,EGC}}$ is the SINR at the boundary of scenario I ($r = R_{\mathrm{I}}$):

$$\gamma_{\mathrm{I,EGC}} = \frac{\left(\tau P_{\mathrm{tx}} H(R_{\mathrm{I}}, \Psi_{\mathrm{single}})\right)^2}{M^2 \mathcal{I}_{\mathrm{NLOS}}(\Psi_{\mathrm{ADR}})}. \tag{58}$$

3) MRC: In MRC, the received optical power from all PDs contributes to SINR performance. The different weight will be allocated to different PDs according to their SINR. Therefore, the SINR of a user when using MRC can be represented as:

$$\gamma_{\mathrm{MRC}} = \frac{\left(\tau P_{\mathrm{tx}} \sum_{p=1}^{N_{\mathrm{PD}}} w_p H_{a_{\mathrm{d}},p}\right)^2}{\mathcal{I}_{\mathrm{NLOS,MRC}}}, \tag{59}$$

where $\mathcal{I}_{\mathrm{NLOS,MRC}}$ is NLOS interference component when MRC is used. According to the assumption that only one of the PD can establish LOS link to the source AP, it can be concluded that:

$$w_{p_{\mathrm{d}}} \gg w_{p \neq p_{\mathrm{d}}}. \tag{60}$$

The LOS links have the highest SINR, and thus contributes the most to the received signal. Therefore, (59) can be approximated as:

$$\begin{aligned}\gamma_{\mathrm{MRC}}(r) &\approx \frac{\left(\tau P_{\mathrm{tx}} w_{p_{\mathrm{d}}} H(r, \Psi_{\mathrm{ADR}})\right)^2}{w_{p_{\mathrm{d}}}^2 \mathcal{I}_{\mathrm{NLOS}}(\Psi_{\mathrm{ADR}})} \\ &= \frac{\left(\tau P_{\mathrm{tx}} H(r, \Psi_{\mathrm{ADR}})\right)^2}{\mathcal{I}_{\mathrm{NLOS}}(\Psi_{\mathrm{ADR}})}.\end{aligned} \tag{61}$$

After the approximation, (61) and (47) are identical. Hence, the CDF of the SINR for MRC is: $F_{\mathrm{MRC}}(\gamma) = F_{\mathrm{SBC}}(\gamma)$.

4) OPC: OPC mitigates the NLOS ICI by exploiting CSI of NLOS interference. The SINR of OPC is:

$$\gamma_{\mathrm{OPC}} = \frac{\left(\sum_{p=1}^{N_{\mathrm{PD}}} \tau w_p P_{\mathrm{tx}} H_{a_{\mathrm{d}},p}\right)^2}{\mathcal{I}_{\mathrm{NLOS,OPC}} + \sum_{p=1}^{N_{\mathrm{PD}}} w_p^2 N_0 B}, \tag{62}$$

where $\mathcal{I}_{\mathrm{NLOS,OPC}}$ is the NLOS interference component of OPC. The SINR of OPC can be further approximated as:

$$\gamma_{\mathrm{OPC}}(r) = \frac{\left(\tau P_{\mathrm{tx}} w_{p_{\mathrm{d}}} H(r, \Psi_{\mathrm{ADR}})\right)^2}{\mathcal{I}_{\mathrm{NLOS,OPC}} + \sum_{p=1}^{N_{\mathrm{PD}}} w_p^2 N_0 B}. \tag{63}$$

The proof of (63) is provided in Appendix A. However, it is difficult to directly derive the CDF of the OPC, based on (63). Since the NLOS interference component can be suppressed in OPC scheme, the upper bound of the OPC is considered:

$$\gamma_{\mathrm{OPC,UB}}(r) = \frac{\left(\tau P_{\mathrm{tx}} H(r, \Psi_{\mathrm{ADR}})\right)^2}{N_0 B} > \gamma_{\mathrm{OPC}}(r). \tag{64}$$

The proof of (64) is provided in Appendix A. The CDF of SINR for the OPC upper bound, $F_{\mathrm{OPC,UB}}(\gamma)$ is:

$$F_{\mathrm{OPC,UB}}(\gamma) = \begin{cases} 0 & \gamma < \gamma_{\mathrm{II,OPC}} \\ \frac{h^2}{R_{\mathrm{II}}^2} \gamma_{0,\mathrm{OPC}}^{\frac{1}{m+3}} \left(\gamma_{\mathrm{II,OPC}}^{-\frac{1}{m+3}} - \gamma^{-\frac{1}{m+3}}\right) & \gamma_{\mathrm{II,OPC}} \leq \gamma \leq \gamma_{0,\mathrm{OPC}} \\ 1 & \gamma > \gamma_{0,\mathrm{OPC}}, \end{cases} \tag{65}$$

where $\gamma_{\mathrm{II,OPC}}$ can be represented as:

$$\gamma_{\mathrm{II,OPC}} = \frac{\left(\tau P_{\mathrm{tx}} H(R_{\mathrm{II}}, \Psi_{\mathrm{ADR}})\right)^2}{N_0 B}, \tag{66}$$

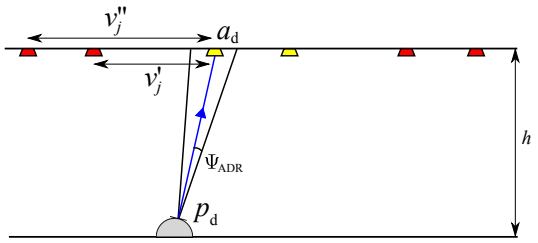

Fig. 15: The illustration of using SBC in double source cell configuration.

and $\gamma_{0,\mathrm{OPC}}$ can be represented as:

$$\gamma_{0,\mathrm{OPC}} = \frac{\left(\tau P_{\mathrm{tx}} H(0, \Psi_{\mathrm{ADR}})\right)^2}{N_0 B}. \tag{67}$$

D. SINR Statistics of Double-source Cell Configuration

In double-source cell configuration, the distance between two APs in the same cell is designed in such a way that no PD on an ADR can simultaneously receive LOS light signals from the two APs in the desired cell. In this section, SINR performance of ADR in double-source cell configuration using mode A is analysed. Since positive and negative APs are close to their cell centre, the LOS channel gain of them is calculated by (32).

1) SBC: As illustrated in Fig. 15, the ADR using SBC choose one AP to establish LOS link. Similar to (47), the SINR of a user can be approximated as:

$$\gamma_{\mathrm{SBC}}^{\mathrm{double}}(r) = \frac{\left(\frac{1}{2} P_{\mathrm{tx}} \tau H(r, \Psi_{\mathrm{ADR}})\right)^2}{\mathcal{I}_{\mathrm{NLOS,SBC}}^{\mathrm{double}}(\Psi_{\mathrm{ADR}})}. \tag{68}$$

According to (23) and (30), the total NLOS interference, $\mathcal{I}_{\mathrm{NLOS,SBC}}^{\mathrm{double}}(\Psi_{\mathrm{ADR}})$, using SBC in double-source cell configuration is derived as:

$$\mathcal{I}_{\mathrm{NLOS,SBC}}^{\mathrm{double}}(\Psi_{\mathrm{ADR}}) = A_{\mathrm{eff}}^2 \tau^2 \sin^2(\Psi_{\mathrm{ADR}}) \sum_j \left| I_{v_j'} - I_{v_j''} \right|^2, \tag{69}$$

where j is the index of interfering optical cells; v_j' represents the distance from the desired AP to a positive AP in interfering cell j; v_j'' represents the distance from the desired AP to a negative AP in interfering cell j. The CDF of SINR for SBC in double-source cell configuration can be derived using a method similar to the analysis of single-source cell configuration in Sec. V-B.

2) MRC: As illustrated in Fig. 16, ADR using MRC can establish two LOS links with both positive and negative APs. The SINR of an active user can therefore be calculated as:

$$\gamma_{\mathrm{MRC}}^{\mathrm{double}} = \frac{\left(\frac{1}{2} \tau P_{\mathrm{tx}} \left(w_{p_{\mathrm{pos}}} H_{a_{\mathrm{pos}},p_{\mathrm{pos}}} + w_{p_{\mathrm{neg}}} H_{a_{\mathrm{neg}},p_{\mathrm{neg}}}\right)\right)^2}{\mathcal{I}_{\mathrm{NLOS,MRC}}^{\mathrm{double}}(\Psi_{\mathrm{ADR}})}, \tag{70}$$

where $\mathcal{I}_{\mathrm{NLOS,MRC}}^{\mathrm{double}}(\Psi_{\mathrm{ADR}})$ is the power of NLOS interference in double-source cell configuration when MRC is used. Since

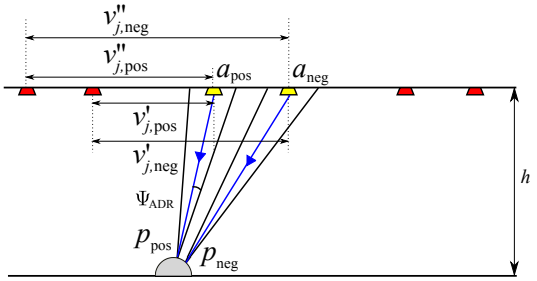

Fig. 16: The MRC scheme in double source cell configuration.

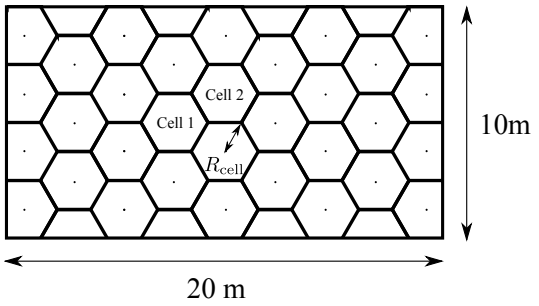

Fig. 17: The layout of a $20 \times 10 \times 4$ m room implementing an optical attocel network. Two optical APs are denoted as Cell 1 and Cell 2.

the desired positive and negative APs are close to each other and the transmission power of them is the same, the relationship between the channel gain $H_{a_{\text{pos}},p_{\text{pos}}}$ and $H_{a_{\text{neg}},p_{\text{neg}}}$ is:

$$H_{a_{\text{pos}},p_{\text{pos}}} \approx H_{a_{\text{neg}},p_{\text{neg}}}. \tag{71}$$

According to (16) and (71), it can be derived that the relationship between the weight of PDs is:

$$w_{p_{\text{pos}}} \approx w_{p_{\text{neg}}}. \tag{72}$$

To this end, (70) can be approximated as:

$$\gamma_{\text{MRC,double}}(r) \approx \frac{\left(\tau P_{\text{tx}} H(r, \Psi_{\text{ADR}})\right)^2}{\mathcal{I}'^{\text{double}}_{\text{NLOS,MRC}}(\Psi_{\text{ADR}})}, \tag{73}$$

where $\mathcal{I}'^{\text{double}}_{\text{NLOS,MRC}}(\Psi_{\text{ADR}})$ can be derived from (23) and (30) that:

$$\mathcal{I}'^{\text{double}}_{\text{NLOS,MRC}}(\Psi_{\text{ADR}}) = A_{\text{eff}}^2 \tau^2 \sin^2(\Psi_{\text{ADR}}) \times \sum_j \left(\left| \mathcal{I}_{v'_{j,\text{pos}}} - \mathcal{I}_{v''_{j,\text{pos}}} \right| + \left| \mathcal{I}_{v'_{j,\text{neg}}} - \mathcal{I}_{v''_{j,\text{neg}}} \right| \right)^2, \tag{74}$$

where $v'_{j,\text{pos}}$ is the horizontal distance between a positive AP in interfering cell j and the positive AP in the desired cell; $v'_{j,\text{neg}}$ is the horizontal distance between a positive AP in the interfering cell j and the negative AP in the desired cell; $v''_{j,\text{pos}}$ is the horizontal distance between a negative AP in interfering cell j and the positive AP in the desired cell; $v''_{j,\text{neg}}$ is the horizontal distance between a negative AP in the interfering cell j and the negative AP in the desired cell.

3) OPC: Similar to MRC, the LOS signals of OPC are captured by two PDs that can establish LOS links with desired APs. Therefore, the SINR of OPC in double-source cell configuration is:

$$\gamma^{\text{double}}_{\text{OPC}} = \frac{\left(\frac{1}{2}\tau P_{\text{tx}} \left(w_{p_{\text{pos}}} H_{a_{\text{pos}},p_{\text{pos}}} + w_{p_{\text{neg}}} H_{a_{\text{neg}},p_{\text{neg}}}\right)\right)^2}{\mathcal{I}^{\text{double}}_{\text{NLOS,OPC}} + \sum_{p=1}^{N_{\text{PD}}} w_p^2 N_0 B}, \tag{75}$$

where $\mathcal{I}^{\text{double}}_{\text{NLOS,OPC}}$ is the NLOS interference component of OPC. The SINR of OPC in double-source cell configuration can be approximated as:

$$\gamma^{\text{double}}_{\text{OPC}}(r) \approx \frac{\left(\frac{1}{2}\tau P_{\text{tx}} \left(w_{p_{\text{pos}}} + w_{p_{\text{neg}}}\right) H(r, \Psi_{\text{ADR}})\right)^2}{\mathcal{I}^{\text{double}}_{\text{NLOS,OPC}} + \sum_{p=1}^{N_{\text{PD}}} w_p^2 N_0 B}. \tag{76}$$

However, it is difficult to derive the CDF of the OPC based on (76). Since the NLOS interference from other cells can be suppressed by OPC, the upper bound of the OPC in double-source cell configuration is considered:

$$\gamma^{\text{double}}_{\text{OPC,UB}}(r) = \frac{\left(\tau P_{\text{tx}} H(r, \Psi_{\text{ADR}})\right)^2}{2 N_0 B} > \gamma^{\text{double}}_{\text{OPC}}(r). \tag{77}$$

The proof of (77) is provided in Appendix B. By comparing (64) and (77), it is notable that the noise level is doubled when double-source configuration is used. This is because that two PDs in an ADR are used to receive LOS signals which doubles the noise from amplifier circuit. Therefore, when double-source cell configuration is used, the SINR performance of OPC is expected to be degraded by 3 dB.

VI. Results and Discussions

In this section, analytical and simulated results obtained from Monte-Carlo simulation are compared and discussed. As illustrated in Fig. 17, computer simulations are performed for a $20 \times 10 \times 4$ m room, and up to fourth-order reflections are considered. As a baseline system, the performance of a single-PD receiver is evaluated. The FOV of the single-PD receiver, Ψ_{single} is set as 22^{o}. For the ADR with 9 PDs, α and Ψ_{ADR} are set as 8.5^{o} and 15.5^{o}, respectively. For the ADR with 20 PDs, α and Ψ_{ADR} are set as 6^{o} and 10.5^{o}, respectively. In the double source cell configuration, when a 9-PD receiver is used, the distance between positive and negative APs is set as 0.7 m. When a 20-PD receiver is used, the distance is set as 0.5 m. The reflection coefficients of the walls, the ceiling, and the floor are 0.8, 0.8 and 0.2, respectively [24]. For fairness, the optical transmission power of the AP in the conventional single-source cell configuration is 1 W, and the optical transmission power of the APs in the double-source cell

TABLE I: Simulation Parameters

Radius of an optical cell, R_{cell}	1.5 m
Responsivity, τ	1 A/W
The gain of the optical filter, G	1
Refractive index, n	1.5
Transmitter half-intensity radiation angle, θ_{tx}	60°
The physical area of a PD, A_{p}	5 mm^2
Modulation Bandwidth, B	20 MHz
AWGN spectral density, N_0	1×10^{-21}A/Hz

configuration is set as 0.5 W, which is half of the transmission power of an AP in single-source configuration. This guarantees the combined optical power of an AP pair equal to the optical transmission power of the AP in a conventional cell. Other simulation parameters are given in Table I. For the theoretical results, a seven-cell configuration is assumed and the other parameters are identical.

A. Convention Single-source Cell Configuration

Fig. 18 shows the SINR performance for the single-source cell configuration when an ADR of 9 PDs is used. Similar to single-PD receiver, the SINR CDF of 9-PD ADR with EGC also has bimodal characteristic. The reason is that, the EGC ADR combines the received light signals with the same weight and cannot suppress the LOS ICI at cell edge like single PD receiver. The theoretical result in (55) accurately captures the SINR performance trends of EGC receiver with some exceptions like the 6 dB gaps in some parts of the curves. This is because, in the numerical simulation, LOS signal might be captured by two different PDs simultaneously at some positions which doubles the received optical power.

The SINR performance of 9-PD ADR with SBC is significantly better than a single-PD receiver. This is because, the SBC chooses the PD that provides the highest channel gain. Due to the narrow FOV, this PD is free from LOS interference. This means the SBC can successfully avoid LOS ICI at cell edges. From (30), it is notable that the NLOS interference decreases as the FOV of a PD decreases. Since the FOV of the selected PD is narrower than the single-PD receiver, the NLOS interference is significantly mitigated compared to the single-PD receiver. Also, numerical results closely match the theoretical results in (52), which proves the accuracy of the model.

The performance of the MRC is, as expected, nearly identical to the SBC. Due to the diffusive NLOS propagation paths, the interference signals received by each PD are correlated and the MRC is unable to suppress this interference. Therefore, the performance of the MRC is not optimal.

As shown in Fig. 18, the OPC has the best SINR performance among all signal combining schemes. By exploiting the interference-plus-noise correlation matrix, the OPC can generate the best weights for the ADR. These weights can effectively suppress the correlated NLOS interfering signals. Results show that OPC achieves over 20 dB improvement over SBC and MRC. The theoretical upper bound for the SINR performance of OPC in (65) also closely comparable to the simulated SINR performance.

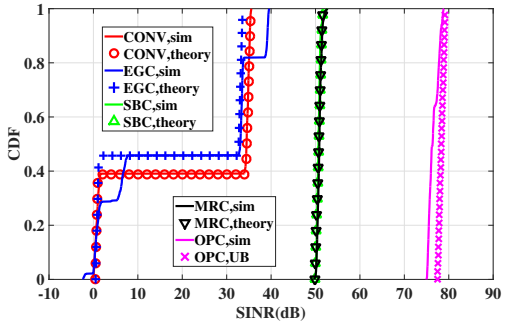

Fig. 18: The CDF of the achieved SINR at 9-PD ADR in conventional single-source cell configuration with different signal combining schemes.

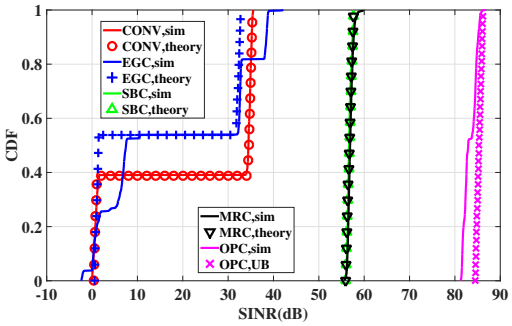

Fig. 19: The CDF of the achieved SINR at 20-PD ADR in conventional single-source cell configuration with different signal combining schemes.

Fig. 19 shows the SINR performance for a single-source cell configuration with an ADR of 20 PDs. The SINR performance trend of EGC is similar to the performance of the previous scenario in Fig. 18. This is because, the overall coverage area of the ADR remains unchanged when the number of receiver elements increases. In SBC and MRC, the SINR performance of 20-PD ADR has a 5 dB improvement over 9-PD ADR. This is because each PD on the 20-PD ADR has a narrower FOV. A narrower FOV means less NLOS interference is captured. Therefore, the overall SINR performance improves. In OPC, interference from other cells are significantly suppressed. The main factor affects the system performance is the magnitude of the received desired power. Since the receiver elements of 20-PD ADR have a narrower FOV and higher concentration gain than the PDs in 9-PD ADR, the 20-PD ADR can receive stronger light signals. Therefore, usually 20-PD ADR performs better than 9-PD ADR when OPC is used.

In summary, in single-source cell configuration, OPC exhibits the best post combining SINR performance in comparison with other signal combining schemes. However, OPC requires the knowledge of CSI not only from the desired cell

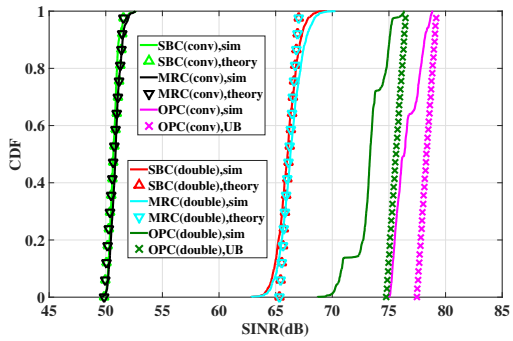

Fig. 20: The CDF of the achieved SINR at a 9-PD ADR when different signal combining schemes are implemented. The results of conventional single-source and double-source cell configurations are denoted by 'conv' and 'double', respectively.

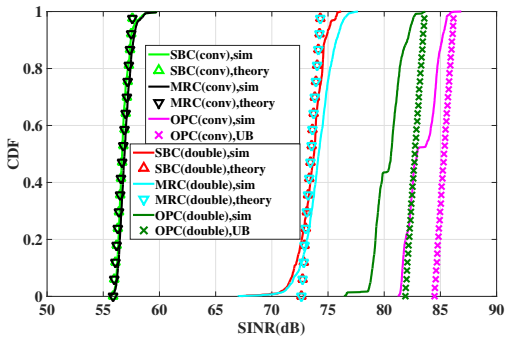

Fig. 21: The CDF of the achieved SINR at a 20-PD ADR when different signal combining schemes are implemented. The results of conventional single-source and double-source cell configurations are denoted by 'conv' and 'double', respectively.

but also from all other interfering cells. Compared with the OPC, SBC and MRC also achieve better SINR performance by simply using the knowledge of CSI from the desired cell.

B. Double-Source Cell Configuration

In this section, the performance of the SBC, MRC, and OPC are evaluated in mode A double-source cell configuration.

Fig. 20 shows the SINR performance for both the single-source and the double-source cell configurations with 9 PDs ADRs. In SBC, the SINR performance improves significantly when double-source cell configuration is implemented. This is because the NLOS interference has been significantly mitigated when two sources in the interfering cells combines destructively at the ADR. Also, there is a close match between the numerical results and analytical SINR results. For MRC, the SINR performance is nearly identical to the SINR performance of SBC. This result is also comparable to the theoretical result. It can also be observed that the post combining SINR performance of OPC in double-source cell is 3 dB weaker than the SINR performance in single-source cell. This is also consistent with the theoretical analysis. Usually, two signals coming from double-source cell are captured by two PDs. Since two PDs are required for OPC to capture light signals in double-source cell, the total noise power is doubled compared with a single-source cell.

Fig. 21 shows the SINR performance for both a single-source cell and a double-source cell configurations with a 20 PDs. The SINR performance trends similar to 9 PDs ADR scenario. For each signal combining scheme, at least 5 dB SINR improvement can be obtained by 20-PD receiver. This is also consistent with the results in single-source cell.

In double-source cell configuration, an important observation is that the SINR performance of SBC and MRC is close to the SINR performance of OPC, which can approach the performance of ICI free system. Compared with OPC, SBC and MRC require less knowledge of CSI. Hence, it is suitable to implement in a practical system.

C. Transmission Mode Selection in Double-source Cell

Although double-source cell configuration using mode A shows a significant improvement, it may not be optimal in all scenarios. In practical optical attocell cell networks, several factors may affect the performance of mode A: a) due to the limitation of hardware, only a suboptimal signal combining scheme, such as EGC, can be applied to an optical receiver; b) active users equipped with single-PD receiver will experience significant signal attenuation in cell centre; c) when user density is low, only a few APs are active which means the ICI is significantly low and the system can be regarded as a noise-limited system. In order to address these issues, transmission mode B is used as a complementary transmission mode for double-source attocell networks. In order to determine a selection criteria for the transmission modes, two cases are studied. One case is the interference-limited case. As illustrated in Fig. 17, only the desired cell (cell 1) and one interfering cell (cell 2) are activated in the room. Only the performance in the desired cell is evaluated. The other case is the noise-limited case. In this case, only one cell (cell 1) in the room is activated and evaluated.

Fig. 22 shows the SINR performance in cell 1 when one neighbouring interfering cell is active. In the single-PD receiver case, mode B achieves better performance. This is because single-PD receiver can not separate the signals from the positive AP and the negative AP. This results in a significant attenuation of the received signal power, especially in cell centre. The performance of EGC is similar to the single-PD receiver. As the EGC combines the signals from both positive and negative APs, the system performance degrades. In SBC and MRC, the SINR performance of mode A outperforms mode B since mode A can effectively mitigate ICI. In OPC, there is no difference between mode A and B. This is because OPC can effectively collect light energy and suppress correlated ICI by adjusting the weights for each PD.

Fig. 23 shows the CDF of SNR in cell 1 when no neighbouring cell is activated. For single-PD receiver and EGC, there

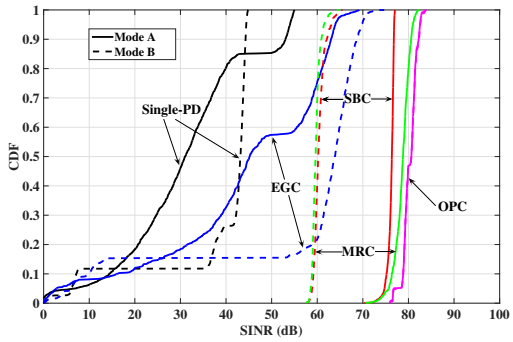

Fig. 22: The CDF of the achieved SINR in cell 1 when only one neighbouring cell is active. 20-PD ADR is used as optical receiver. The results of mode A are represented as solid lines and the results of mode B are represented as dash lines.

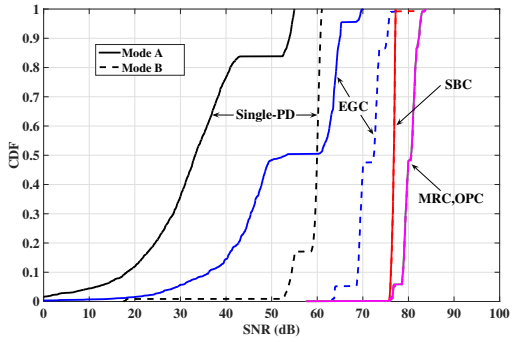

Fig. 23: The CDF of the achieved SNR in cell 1 when no neighbouring cell is active. 20-PD ADR is used as optical receiver. The results of mode A are represented by solid lines and the results of mode B are represented by dash lines.

TABLE II: The Criteria of Transmission Modes Selection.

	Single-PD	EGC	SBC	MRC	OPC
Interference	B	B	A	A	A or B
No Interference	B	B	A or B	A or B	A or B

is a significant improvement when mode B is used. This is because mode B can boost the received signal power of a user. For SBC, since only one of the PD can be set up data link, the performance of the mode A and mode B is the same. For MRC, SNR performance of transmission mode A and transmission mode B is identical since the energy from both APs can be captured in both modes. Lastly, the SINR performance of OPC is identical to the SINR performance of MRC since there is no ICI. The criteria for selecting transmission modes in double-source cell configuration is listed in Table II.

VII. Conclusion

This paper investigates interference mitigation techniques for indoor optical attocell networks with ADRs. Four different signal combining schemes, namely SBC, EGC, MRC and OPC are proposed and evaluated. The performance of ADR is also comprehensively compared with conventional single-PD receivers. A novel double-source cell configuration is proposed for ADR which can further mitigate ICI. Results show that an ADR outperforms a single-PD receiver in terms of the SINR performance. In particular, ADR using OPC performs the best which approaches the performance of interference-free systems. However, OPC requires the knowledge of CSI from all optical APs in the network. In comparison, MRC and SBC can also provide better performance than single-PD receiver and only the knowledge of CSI from the desired cell is required. Results also show that, SBC and MRC can achieve better SINR performance in mode A double-source cell configuration than in single-source cell configuration. Mode B can provide better performance when single-PD receiver or ADR with EGC are used in double-source cell configuration. The criteria for selecting transmission modes in double-source attocell networks is determined. Moreover, according to the proposed analytical framework, the theoretical performance of optical attocell networks with ADRs is derived as closed-form. There is a close match between the numerical and theoretical results which proves the accuracy of the analytical model.

Appendix

A. The Proof of (63) and (64)

$$\gamma_{\mathrm{OPC}} = \frac{\tau^2 P_{\mathrm{tx}}^2 \Big(w_{p_{\mathrm{d}}} H_{a_{\mathrm{d}},p_{\mathrm{d}}} + \sum\limits_{p \neq p_{\mathrm{d}}} w_p H_{a_{\mathrm{d}},p} \Big)^2}{\mathcal{I}_{\mathrm{NLOS,OPC}} + \sum_{p=1}^{N_{\mathrm{PD}}} w_p^2 N_0 B}. \tag{78}$$

The magnitude of the LOS channel is a few order larger than the NLOS channel. Since only the desired PD a_{d} can establish LOS link with the desired AP:

$$H_{a_{\mathrm{d}},p_{\mathrm{d}}} \gg H_{a_{\mathrm{d}},p}. \quad (p \neq p_{\mathrm{d}}) \tag{79}$$

The SINR of OPC can be approximated as:

$$\begin{aligned}
\gamma_{\mathrm{OPC}}(r) &\approx \frac{\Big(\tau P_{\mathrm{tx}} w_{p_{\mathrm{d}}} H(r, \Psi_{\mathrm{ADR}}) \Big)^2}{\mathcal{I}_{\mathrm{NLOS,OPC}} + \sum_{p=1}^{N_{\mathrm{PD}}} w_p^2 N_0 B} \\
&= \frac{\Big(\tau P_{\mathrm{tx}} w_{p_{\mathrm{d}}} H(r, \Psi_{\mathrm{ADR}}) \Big)^2}{\mathcal{I}_{\mathrm{NLOS,OPC}} + \sum\limits_{p \neq p_{\mathrm{d}}} w_p^2 N_0 B + w_{p_{\mathrm{d}}}^2 N_0 B} \\
&< \frac{\Big(\tau P_{\mathrm{tx}} w_{p_{\mathrm{d}}} H(r, \Psi_{\mathrm{ADR}}) \Big)^2}{w_{p_{\mathrm{d}}}^2 N_0 B} \\
&= \frac{\Big(\tau P_{\mathrm{tx}} H(r, \Psi_{\mathrm{ADR}}) \Big)^2}{N_0 B} = \gamma_{\mathrm{OPC,UB}}(r).
\end{aligned} \tag{80}$$

B. The Proof of (77)

$$\gamma_{\mathrm{OPC}}^{\mathrm{double}}(r) = \frac{\left(\frac{1}{2}\tau P_{\mathrm{tx}}\left(w_{p_{\mathrm{pos}}} + w_{p_{\mathrm{neg}}}\right) H(r, \Psi_{\mathrm{ADR}})\right)^2}{\mathcal{I}_{\mathrm{NLOS,OPC}}^{\mathrm{double}} + \sum_{p=1}^{N_{\mathrm{PD}}} w_p^2 N_0 B} < \frac{\left(\frac{1}{2}\tau P_{\mathrm{tx}}\left(w_{p_{\mathrm{pos}}} + w_{p_{\mathrm{neg}}}\right) H(r, \Psi_{\mathrm{ADR}})\right)^2}{\left(w_{p_{\mathrm{pos}}}^2 + w_{p_{\mathrm{neg}}}^2\right) N_0 B} \tag{81}$$

Since

$$\frac{(w_{p_{\mathrm{pos}}} + w_{p_{\mathrm{neg}}})^2}{w_{p_{\mathrm{pos}}}^2 + w_{p_{\mathrm{neg}}}^2} \leq 2, \tag{82}$$

the SINR of the double source cell configuration is:

$$\gamma_{\mathrm{OPC}}^{\mathrm{double}}(r) < \frac{\left(\tau P_{\mathrm{tx}} H(r, \Psi_{\mathrm{ADR}})\right)^2}{2 N_0 B} = \gamma_{\mathrm{OPC,UB}}^{\mathrm{double}}(r). \tag{83}$$

REFERENCES

[1] Cisco Visual Networking Index, "Global Mobile Data Traffic Forecast Update, 2014-2019," White Paper, Feb. 2015. [Online]. Available: http://www.cisco.com/c/en/us/solutions/collateral/service-provider/visual-networking-index-vni/white_paper_c11-520862.html

[2] H. Elgala, R. Mesleh, and H. Haas, "Indoor Optical Wireless Communication: Potential and State-of-the-Art," *IEEE Commun. Mag.*, vol. 49, no. 9, pp. 56–62, Sep. 2011.

[3] A. M. Khalid, G. Cossu, R. Corsini, P. Choudhury, and E. Ciaramella, "1-Gb/s Transmission over a Phosphorescent White LED by Using Rate-adaptive Discrete Multitone Modulation," *IEEE Photon. J.*, vol. 4, no. 5, pp. 1465–1473, Oct 2012.

[4] G. Cossu, A. Wajahat, R. Corsini, and E. Ciaramella, "5.6 Gbit/s Downlink and 1.5 Gbit/s Uplink Optical Wireless Transmission at Indoor Distances," in *2014 European Conference on Optical Communication (ECOC)*, Sep 2014, pp. 1–3.

[5] D. Tsonev, H. Chun, S. Rajbhandari, J. McKendry, S. Videv, E. Gu, M. Haji, S. Watson, A. Kelly, G. Faulkner, M. Dawson, H. Haas, and D. O'Brien, "A 3-Gb/s Single-LED OFDM-Based Wireless VLC Link Using a Gallium Nitride μLED," *IEEE Photon. Technol. Lett.*, vol. 26, no. 7, pp. 637–640, Apr. 2014.

[6] S. Hussain, M. Abdallah, and K. Qaraqe, "Hybrid Radio-visible Light Downlink Performance in RF Sensitive Indoor Environments," in *2014 6th International Symposium on Communications, Control and Signal Processing (ISCCSP)*, May 2014, pp. 81–84.

[7] J. T. J. Penttinen, *The Telecommunications Handbook: Engineering Guidelines for Fixed, Mobile and Satellite Systems*, 2015.

[8] T. Borogovac, M. Rahaim, and J. B. Carruthers, "Spotlighting for Visible Light Communications and Illumination," in *IEEE Global Communications Conference (GLOBECOM 2010) Workshops*, 6-10 Dec 2010, pp. 1077–1081.

[9] I. Stefan, H. Burchardt, and H. Haas, "Area Spectral Efficiency Performance Comparison between VLC and RF Femtocell Networks," in *IEEE International Conference on Communications (ICC)*, Budapest, Hungary, Jun. 9–13 2013, pp. 1–5.

[10] X. Bao, X. Zhu, T. Song, and Y. Ou, "Protocol Design and Capacity Analysis in Hybrid Network of Visible Light Communication and OFDMA Systems," *IEEE Trans. Veh. Technol.*, vol. 63, no. 4, pp. 1770–1778, May 2014.

[11] C. Chen, N. Serafimovski, and H. Haas, "Fractional frequency reuse in optical wireless cellular networks," in *Personal Indoor and Mobile Radio Communications (PIMRC), 2013 IEEE 24th International Symposium on*, Sept 2013, pp. 3594–3598.

[12] C. Chen, D. Tsonev, and H. Haas, "Joint transmission in indoor visible light communication downlink cellular networks," in *Globecom Workshops (GC Wkshps), 2013 IEEE*, Dec 2013, pp. 1127–1132.

[13] Z. Chen and H. Haas, "Space Division Multiple Access in Visible LightCommunications," in *IEEE ICC 2015 - Optical Networks and Systems (ICC'15 ONS)*, London, UK, Jun. 2015.

[14] J. Carruthers and J. Kahn, "Angle Diversity for Nondirected Wireless Infrared Communication," in *1998 IEEE International Conference on Communications, 1998. ICC 98. Conference Record.*, vol. 3, Jun 1998, pp. 1665–1670 vol.3.

[15] Y. Alqudah and M. Kavehrad, "Optimum Order of Angle Diversity with Equal-gain Combining Receivers for Broad-band Indoor Optical Wireless Communications," *IEEE Trans. Veh. Technol.*, vol. 53, no. 1, pp. 94–105, Jan 2004.

[16] H. L. Minh, D. O'Brien, G. Faulkner, O. Bouchet, M. Wolf, L. Grobe, and J. Li, "A 1.25-Gb/s Indoor Cellular Optical Wireless Communications Demonstrator," *IEEE Photon. Technol. Lett.*, vol. 22, no. 21, pp. 1598–1600, Nov 2010.

[17] M. Alresheedi and J. Elmirghani, "Performance Evaluation of 5 Gbit/s and 10 Gbit/s Mobile Optical Wireless Systems Employing Beam Angle and Power Adaptation with Diversity Receivers," *IEEE J. Sel. Areas Commun.*, vol. 29, no. 6, pp. 1328–1340, June 2011.

[18] J. M. Kahn and J. R. Barry, "Wireless Infrared Communications," *Proc. IEEE*, vol. 85, no. 2, pp. 265–298, Feb. 1997.

[19] J. Barry, J. Kahn, W. Krause, E. Lee, and D. Messerschmitt, "Simulation of Multipath Impulse Response for Indoor Wireless Optical Channels," *IEEE J. Sel. Areas Commun*, vol. 11, no. 3, pp. 367–379, Apr. 1993.

[20] S. Vasudevan, K. Papagiannaki, C. Diot, J. Kurose, and D. Towsley, "Facilitating Access Point Selection in IEEE 802.11 Wireless Networks," in *Proc. ACM Fifth SIGCOMM Conf. Internet Measurement (IMC)*, 2005, pp. 293–298.

[21] J. Winters, "Optimum Combining in Digital Mobile Radio with Cochannel Interference," *IEEE J. Sel. Areas Commun.*, vol. SAC-2, no. 4, pp. 528–539, Jul. 1984.

[22] A. Jalajakumari, K. Cameron, D. Tsonev, H. Haas, and R. Henderson, "An Energy Efficient High-speed Digital LED Driver for Visible Light Communications," in *IEEE International Conference on Communications, 2015 (ICC '15)*, Jun 2015.

[23] R. H. Simons and A. Bean, *Lighting Engineering: Applied Calculations*. Architectural Press, 2008.

[24] F. E. Alsaadi and J. M. H. Elmirghani, "Mobile MC-CDMA Optical wireless System Employing an Adaptive Multibeam Transmitter and Diversity Receivers in a Real Indoor Environment," in *In the Proceeding of the IEEE International Conference on Communications (ICC 08)*, May 19–23, 2008, pp. 5196–5203.

Angle diversity for an Indoor Cellular Visible Light Communication System

Zhe Chen, Nikola Serafimovski and Harald Haas
Institute for Digital Communications
Li-Fi R&D Centre
School of Engineering
The University of Edinburgh
EH9 3JL, Edinburgh, UK
{z.chen, n.serafimovski, h.haas}@ed.ac.uk

***Abstract*—In this paper, we investigate the benefits of an angle diversity receiver (ADR) in an indoor cellular optical wireless communications (OWC) network. As the ADR consists of multiple photodiodes (PDs), a proper signal combining scheme is essential to optimise the system performance. Therefore, three different combination schemes, the equal gain combining (EGC), the select best combining (SBC) and the maximum ratio combining (MRC), are investigated. The results indicate that the ADR significantly outperforms the single-PD receiver in terms of both signal to interference plus noise ratio (SINR) and area spectral efficiency (ASE). In particular, the ADR implementing the MRC scheme achieves the best performance, where over 40 dB SINR improvement is attained compared to the single-PD receiver.**

***Index Terms*—angle diversity receiver; visible light communication; access points; cellular communication**

I. Introduction

In order to alleviate the looming spectrum crisis, visible light communication (VLC) has emerged as a supplement to traditional radio frequency (RF) techniques [1]. VLC uses light-emitting diodes (LEDs) for transmission and photodiodes (PDs) for detection. Due to the physical nature of LEDs and PDs, intensity modulation and direct detection (IM/DD) must be used to realise a VLC system. Recent research shows that a VLC system can achieve communication speeds of over 3 Gbps from a single colour LED [2]. Moreover, VLC systems operate in the entirely unregulated electromagnetic spectrum and are therefore: a) safe to use in electromagnetic interference (EMI) sensitive environments; b) not subject to spectrum licensing for communication purposes.

An indoor cellular optical wireless configuration is investigated in this work. This enables high data density by harnessing the frequency reuse gains available to small cell systems. Indeed, optical cells can be considerably smaller than RF cells due to the limited coverage and interference protection by solid objects [3]. An indoor optical cellular system can have small cell sizes with little, if any, inter-cell interference. This facilitates higher bandwidth reuse and therefore higher data density. In an indoor optical wireless scenario, each LED array in a room serves as an optical access point (AP). We refer to this type of the optical cellular network as an optical *attocell* network [4]. In optical *attocell* network, optical orthogonal frequency division multiple access (O-OFDMA) can be used as the multiple access technique, since it allows for a flexible allocation of communication resources to every user in a network.

In previous work, an optical cellular VLC system using multiple laser sources and multiple detectors is shown to provide a wide coverage area and high data rates [5]. Unfortunately, this configuration requires precise alignment and mobile user tracking, which makes it difficult to implement for practical purposes. An indoor optical orthogonal frequency division multiplexing (O-OFDM) based cellular system that achieves high throughput by frequency reuse is proposed in [6]. However, the proposed system is designed specially for an aircraft cabin and fixed frequency reuse is sub-optimal with respect to interference coordination.

In this study, we use angle diversity receivers (ADRs) to address the issue of interference coordination as well as frequency reuse in an indoor cellular system. An ADR consists of multiple narrow-field-of-view (FOV) PDs, which, when combined, result in the same FOV and coverage area as the FOV of a single-PD receiver [7]. These narrow-FOV PDs can be selected or combined to minimize co-channel interference. Therefore, three combining schemes, the select best combining (SBC), the equal gain combining (EGC) and the maximum ratio combining (MRC) are proposed. As a result, the ADR that uses the proposed schemes significantly outperforms the single-PD receiver in an optical cellular system.

The remainder of this paper is organised as follows, the system model is introduced in Section II. The single-PD receiver scenario is introduced in Section III. The scenario of the ADR scenarios are discussed in Section IV. The simulation results are presented in Section V. Finally, Section VI concludes the paper.

II. System Model

A. Channel model

In this work, a line-of-sight (LOS) optical channel is assumed. The channel DC gain is defined as follows [8]:

$$H = \begin{cases} \dfrac{(m+1)A_{\mathrm{p}}T_s(\theta)\mathrm{g}(\theta)}{2\pi d^2}\cos^m(\phi)\cos(\theta), & \theta \le \Theta_c \\ 0, & \theta > \Theta_c \end{cases}, \quad (1)$$

978-1-4799-4482-8/14/$31.00 ©2014 IEEE

where d is the distance from a transmitter to an optical receiver; A_{p} is the physical area of the optical receiver; Θ_c is the FOV of the optical receiver; m is the Lambertian index which is a function of the half-intensity radiation angle $\theta_{1/2}$ as $m = 1/\log_2(\cos(\theta_{1/2}))$; $T_s(\theta)$ is the gain of the optical filter; ϕ is the angle of irradiance; θ is the angle of light incidence at the receiver; the concentrator gain $\mathrm{g}(\theta)$ is given as:

$$\mathrm{g}(\theta) = \begin{cases} \dfrac{n^2}{\sin^2(\Theta_c)}, & 0 \le \theta \le \Theta_c \\ 0, & \theta > \Theta_c \end{cases}, \tag{2}$$

where, n is the reflective index of the receiver optics.

B. Area Spectral Efficiency

Initially, the area spectral efficiency (ASE) is used to evaluate the spectral efficiency of cellular RF systems in [9]. For a cellular VLC system, the ASE is defined as the sum of the user throughput per unit bandwidth per unit area, which can be expressed as:

$$\mathrm{ASE} = \sum_{k=1}^{K} \frac{C_k}{BA}, \tag{3}$$

where k is the user index, K is the total number active users, A is the area of the room, B is the modulation bandwidth of an AP and the Shannon channel capacity for user k is defined as:

$$C_k = B_k \log_2(1 + \gamma_k), \tag{4}$$

where B_k is the allocated bandwidth to user k and γ_k is the electrical signal to interference plus noise ratio (SINR) at the receiver of the user k.

III. Single-PD Receiver Scenario

In this study, the system performance of the single-PD receiver scenario is set as a baseline to evaluate the system performance of ADR scenarios. In the single-PD receiver scenario, each user in the VLC *attocell* network is equipped with a single-PD receiver to collect optical signals.

In order to maximize the SINR of each user in this system, a source AP needs to be selected out of candidate APs for each user. The source AP of user k, $b_{\mathrm{src}}^{(k)}$, can be chosen as:

$$b_{\mathrm{src}}^{(k)} = \arg\max_{b} \left(\gamma_{(b,k)}\right). \tag{5}$$

where, b is the index of the AP. The $\gamma_{(b,k)}$ is the SINR of the user k that establish a link with AP b, which can be expressed as:

$$\gamma_{(b,k)} = \frac{\left(rP_{\mathrm{t}}H_{(b,k)}\right)^2}{\left(N_0 B + \sum_{b' \in \mathcal{B}_{\mathrm{inter}}^{(b,k)}} \left(rP_{\mathrm{t}}H_{(b',k)}\right)^2\right)} \tag{6}$$

where r is the optical to electric conversion efficiency; P_{t} is the average electric power of an LED array; $H_{(b,k)}$ is the channel attenuation between user k and AP b; $\sum_{b' \in \mathcal{B}_{\mathrm{inter}}^{(b,k)}} \left(rP_{\mathrm{t}}H_{(b',k)}\right)^2$ represents the electrical interference power and $\mathcal{B}_{\mathrm{inter}}^{(b,k)}$ is the set of the interfering APs for user k according to the selected AP b; N_0 is the noise spectral density. Note, that there is no frequency selective fading in a VLC system such as the proposed one as the PD area is much larger than the wavelength of the optical signal. It is, therefore, assumed that all AP exhibit similar frequency responses which are determined by the electrical and optical components used.

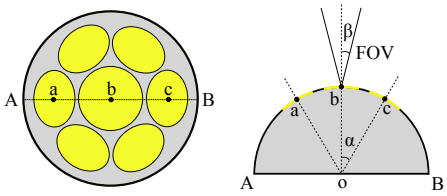

Fig. 1. The shape of an ADR

Proportional fair scheduling is assumed, which means that the available bandwidth of the AP is shared equally across all users that are connected to that particular AP. The bandwidth per user is then:

$$B_k = \frac{B}{N_{\mathrm{sub}}} \left\lfloor \frac{N_{\mathrm{sub}}}{N_k} \right\rfloor, \tag{7}$$

where N_{sub} is the total number of subcarriers of an AP, N_k is the number of users that are served by the same AP which serves user k, $\lfloor \cdot \rfloor$ denotes the floor function.

Finally, the average ASE can be calculated as:

$$\mathrm{ASE}_{\mathrm{CR}} = \sum_{k=1}^{K} \frac{B_k \log_2\left(1 + \gamma_{(b_{\mathrm{src}}^{(k)},k)}\right)}{BA}. \tag{8}$$

IV. ADR Scenarios

In this scenario, each user in the VLC *attocell* network is equipped with an ADR which consists of 7 PDs attached to a semi-sphere base. One of the PDs is located at the top of the base and the other six are located symmetrically along the side of the base, as shown in Fig. 1. Each PD on the receiver has the same FOV and β denotes the half-angle of the FOV. In addition, α is defined as the angle between the direction of the central PD and the direction of the outermost PD.

Unlike a single-PD receiver, the direction of each PD on an ADR varies which can significantly affect the system performance. Therefore, it is of vital importance to carefully choose a fair metric to compare the performance between an ADR scenario and a single-PD receiver scenario. In this study, we constrain the FOV of the ADR to be the same as the FOV of the single-PD receiver. Indeed, the overall coverage area of the ADR is equivalent to the coverage of the single-PD receiver. The FOV area of an ADR (S1) and that of a single-PD receiver (S2) are presented in Fig. 2.

A. SBC scheme

The SBC scheme is originally proposed in [7] and is adapted for an optical *attocell* network. Each user terminal selects one PD to establish a link with its source AP. The source AP, $b_{\mathrm{src}}^{(k)}$, and destination PD, $s_{\mathrm{des}}^{(k)}$, are chosen to maximize the SINR:

$$\left(b_{\mathrm{src}}^{(k)}, s_{\mathrm{des}}^{(k)}\right) = \arg\max_{b, s_k} \left(\gamma_{(b,s_k)}\right), \tag{9}$$

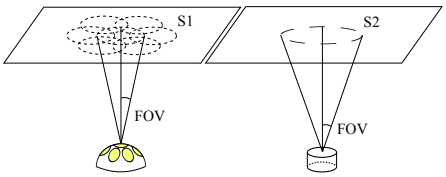

Fig. 2. The coverage area of an ADR and a single-PD receiver on the ceiling. The overall coverage area of the ADR is the union of the individual coverage areas of each PD on that ADR. The coverage area of the single-PD receiver is defined only by the single PD.

where s_k is the PD index of user k and $\gamma_{(b,s_k)}$ is the SINR of the link between AP b and PD s_k, which can be expressed as:

$$\gamma_{(b,s_k)} = \frac{\left(rP_{\mathrm{t}}H_{(b,s_k)}\right)^2}{N_0B + \sum_{b' \in \mathcal{B}_{\mathrm{inter}}^{(b,s_k)}} \left(rP_{\mathrm{t}}H_{(b',s_k)}\right)^2}. \quad (10)$$

The method of bandwidth allocation is identical to the one in the single-PD receiver scenario and the ASE can be represented as:

$$\mathrm{ASE}_{\mathrm{SB}} = \sum_{k=1}^{K} \frac{B_k \log_2\left(1 + \gamma_{(b_{\mathrm{src}}^{(k)}, s_{\mathrm{des}}^{(k)})}\right)}{BA}. \quad (11)$$

In the SBC scheme, an ADR only considers the signal from the PD with the highest SINR. That means it requires a dedicated circuit to continuously monitor the SINR on each PD. Moreover, a fast switch is also needed for receiving the signal from the selected PD. Since the PD with the highest SINR is selected, the ADR can attain a high overall SINR. However, since only one PD is used at a time, the gain of combining signals from different PDs might not be well exploited in this scheme.

B. EGC scheme

The EGC is a scheme that exploits the gain of combining signals from different PDs on an ADR. For each user, the signals on each PD are combined with equal weights. To optimize the SINR performance of each user, an suitable source AP, $b_{\mathrm{src}}^{(k)}$ is chosen:

$$b_{\mathrm{src}}^{(k)} = \arg\max_{b} \left(\gamma_{(b,k)}\right), \quad (12)$$

where $\gamma_{(b,k)}$ is the SINR of the link between AP b and user k, which can be expressed as:

$$\gamma_{(b,k)} = \frac{\left(\sum_{s_k=1}^{S} rP_{\mathrm{t}}H_{(b,s_k)}\right)^2}{SN_0B + \sum_{s_k=1}^{S} \sum_{b' \in \mathcal{B}_{\mathrm{inter}}^{(b,s_k)}} \left(rP_{\mathrm{t}}H_{(b',s_k)}\right)^2} \quad (13)$$

where S is the total number of PDs on an ADR, the numerator of (13) represents the total signal power received by all PDs of an ADR; $\sum_{s_k=1}^{S} \sum_{b' \in \mathcal{B}_{\mathrm{inter}}^{(b,s_k)}} \left(rP_{\mathrm{t}}H_{(b',s_k)}\right)^2$ represents the total interference received by all PDs.

The subcarrier allocation is identical to the one in the single-PD receiver scenario and the ASE can be calculated by (8).

The EGC scheme combines the signals on each PD with equal weights, which means that only a simple combiner is required for the combining circuit. Since signals from different PDs are combined together, the received signal power of an ADR implementing the EGC scheme is higher than the one in the SBC scheme. However, since the signal from each PD is equally weighted and combined, the noise and interference may result in a poor overall SINR.

C. MRC scheme

In order to overcome the drawback of the EGC scheme, MRC scheme is proposed to emphasis the signal from the PD with high SINR. The MRC scheme is similar to the EGC scheme except that the weight factors on each PD are proportional to the respective achieved SINR. In the MRC scheme, a suitable source AP, $b_{\mathrm{src}}^{(k)}$ is selected to maximize the SINR performance:

$$b_{\mathrm{src}}^{(k)} = \arg\max_{b} \left(\gamma_{(b,k)}\right), \quad (14)$$

where $\gamma_{(b,k)}$ can be expressed as:

$$\gamma_{(b,k)} = \frac{\left(\sum_{s_k=1}^{S} rP_{\mathrm{t}}w_{(b,s_k)}H_{(b,s_k)}\right)^2}{\sum_{s_k=1}^{S} \left(w_{(b,s_k)}^2 N_0B + \sum_{b' \in \mathcal{B}_{\mathrm{inter}}^{(b,s_k)}} \left(rP_{\mathrm{t}}w_{(b,s_k)}H_{(b',s_k)}\right)^2\right)}, \quad (15)$$

where w_{s_k} is the weight factor of PD s_k, which can be represented as:

$$w_{(b,s_k)} = \frac{\left(rP_{\mathrm{t}}H_{(b,s_k)}\right)^2}{N_0B + \sum_{b' \in \mathcal{B}_{\mathrm{inter}}^{(b,s_k)}} \left(rP_{\mathrm{t}}H_{(b',s_k)}\right)^2}. \quad (16)$$

The subcarrier allocation scheme is the same as the one in the single-PD receiver scenario and the ASE can be calculated by using (8).

Since the weights are generally different and proportional to the SINR of each PD, a sophisticated circuit is required to continuously monitor the SINR on each PD. In addition, compared to the EGC combing scheme, additional multiplication operations are required for the MRC combiner. However, the computational complexity only grows linearly with the number of PDs at the receiver. By using different weight factors for each PD, the MRC scheme will boost the signal component and attenuate the interference and noise components which results in a high overall SINR.

V. Simulation Results

In the simulation, we assume a 19.5 m long, 10.4 m wide, and 4 m high room. All optical APs are placed on the ceiling and all receivers are placed at a desk height of 0.85 m. The radius of each optical cell is assumed to be 1.5 m. Fig. 3 depicts the layout of APs. Two types of ADRs are considered: one of them has an equivalent FOV of 31.5°

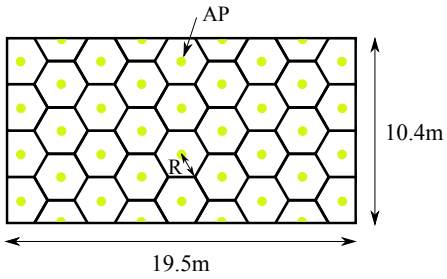

Fig. 3. The layout of APs in the simulation

TABLE I
SIMULATION PARAMETERS

Radius of a cell, R	1.5 m
Optical electricity conversion efficiency, r	0.5 A/W
The gain of the optical filter, $T_s(\theta)$	1
Half-intensity radiation angle, $\theta_{1/2}$	25°
The physical area of a PD, A_p	10 mm^2
The internal reflective index, n	1.5
Transmission Power of an AP, P_t	8.8 W
Modulation Bandwidth, B	20 MHz
Noise spectral density, N_0	10^{-21} A/Hz
The total number of O-OFDMA subcarriers, N_{sub}	2048

($\alpha = 7°, \beta = 25°$); the other one has an equivalent FOV of 48.1° ($\alpha = 25°, \beta = 25°$). In addition, we use the result from the single-PD receiver for comparison assuming two different FOVs (31.5°, 48.1°). The number of O-OFDMA subcarriers is 2048 and full bandwidth reuse is assumed for each AP. Table I shows the simulation parameters.

By varying the position of the optical receiver across all possible locations in the room and estimating the respective achievable SINR, we can determine the cumulative distribution function (CDF) of the SINR for the optical receivers with an equivalent FOV of 48.1°, which is shown in Fig. 4. The single-PD receiver has the worst SINR performance. This indicates that, since the FOV of the PD on the single-PD receiver is large, the single-PD receiver will always receive interference from the APs in the vicinity which dramatically degrades the SINR performance. One important observation is that the ADR implementing the SBC and MRC schemes has an over 40 dB SINR improvement over the single-PD receiver. This is attributed to the structure and the combining scheme of the ADR. The ADR uses narrow-FOV PDs to cover the same FOV as the single-PD receiver. These narrow-FOV PDs provide high concentrator gain and help to reject the co-channel interference. Since the PDs on the ADR point to different directions, some PDs may successfully avoid co-channel interference and some of them may not. Since the optical *attocell* network is an interference limited environment where the interference is several magnitudes higher than the noise [10], the PDs without co-channel interference can achieve significantly higher SINR than the PDs with co-

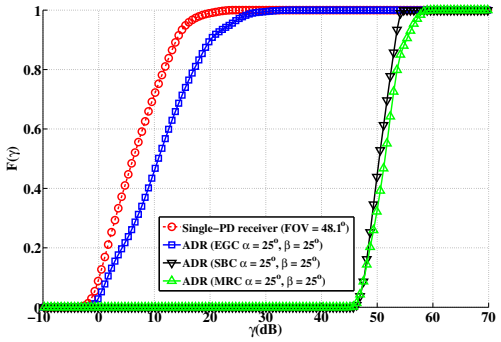

Fig. 4. The CDF of the SINR for single-PD receiver (dash lines) and ADR (solid lines) when the equivalent FOV is 48.1°

channel interference. By implementing the SBC scheme, the ADR can choose the PD with the highest SINR, which is usually the one that is free from co-channel interference. Therefore, the ADR implementing the SBC scheme can achieve a high overall SINR. Compared with the SBC scheme, the MRC scheme proportionally weights and combines the signal on each PD, which effectively boosts the signal and attenuates the interference. As a result, it achieves the best SINR performance. Another observation is that the ADR implementing the EGC scheme has a limited improvement over the single-PD receiver. This corresponds to the fact that some PDs on the ADR suffer from interference. Since the ADR implementing the EGC scheme equally combines the signals from each PD, the interference will not be attenuated which degrades the overall SINR.

Fig. 5 depicts the CDF of the simulation when the equivalent FOV drops to 31.5°. One notable change is that the SINR of the single-PD receiver and the EGC scheme increase dramatically in the high SINR regions. This indicates that the users in some locations, *i.e.*, cell centre, are free from interference. It is also worth emphasising that the MRC scheme again significantly outperforms the SBC scheme compared to the previous scenario. This is because, when α decreases, more PDs on the ADR can receive the signal from the source AP. Therefore, by weighting and combining the signals from multiple PDs, the MRC scheme can achieve a better SINR performance than the SBC scheme which uses the signal from only one PD.

The result of the ASE performance versus the number of active users are presented in Figs. 6 and 7. In general, the ASE increases when the number of active users grows. The reason for this is the increased spatial re-use of the available bandwidth. This means that the reuse gain outweighs the loss due to higher interference in this region of operation.

Since the bandwidth allocation of all scenarios are identical, the ASE performance of different optical receivers only depends on their SINR performance. In general, the optical receiver with a better SINR performance will have a better

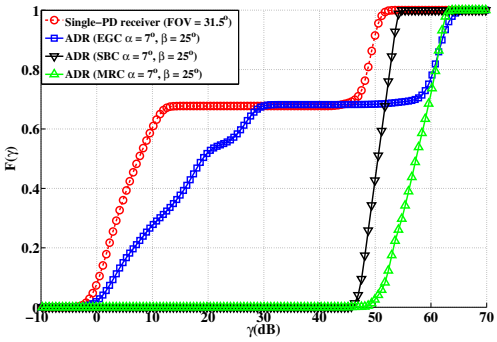

Fig. 5. The CDF of the SINR for single-PD receiver (dash lines) and ADR (solid lines) when the equivalent FOV is $31.5°$

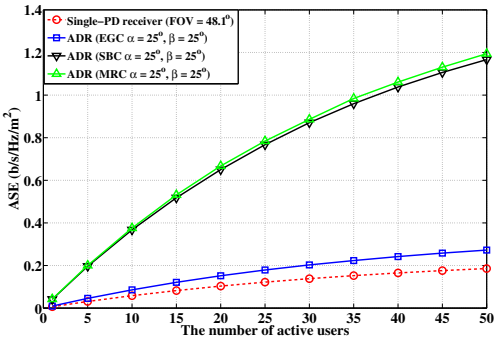

Fig. 6. The area spectral efficiency performance for different receivers (schemes) when the equivalent FOV is $48.1°$.

ASE performance. In Fig. 6 and 7, as expected, the MRC scheme outperforms the other schemes in terms of the ASE performance. In addition, the ASE performance of the single-PD receiver and the ADR implementing the EGC scheme is significantly improved when the equivalent FOV decreases from $48.1°$ to $31.5°$. For the single-PD receiver, the improvement is due to the decrease of the FOV of the PD. A narrower FOV can reject the interference from the other APs and provide a higher gain. For the EGC scheme, the improvement stems from the interference avoidance as well as the gain of combining the signals from multiple PDs.

VI. Conclusion

In this paper, we study the performance of ADR in an indoor cellular VLC system. Three different combining schemes, the SBC, EGC, and MRC schemes are proposed for the ADR and evaluated in comparison with the single-PD receiver. The results reveal that the ADR outperformed the single-PD receiver with regard to the SINR and ASE. In particular, the MRC scheme provides the best performance, where a 40 dB SINR improvement over the single-PD receiver was achieved.

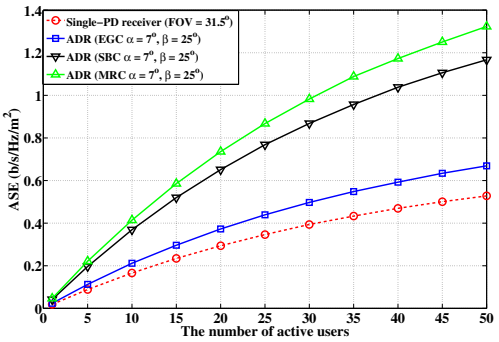

Fig. 7. The area spectral efficiency performance for different receivers (schemes) when the equivalent FOV is $31.5°$.

Compared to the MRC scheme, the SBC scheme is of less complexity but with sub-optimal performance. Finally, the EGC is the simplest combining scheme for implementation but yielded little benefit with respect to the single-PD receiver.

Acknowledgement

We gratefully acknowledge support by the School of Engineering and the Institute for Digital Communications (IDCOM) at the University of Edinburgh for providing a scholarship for this work which is aligned to the Engineering and Physical Sciences Research Council (EPSRC) project EP/K00042X/1.

References

[1] H. Elgala, R. Mesleh, and H. Haas, "Indoor Optical Wireless Communication: Potential and State-of-the-Art," *IEEE Commun. Mag.*, vol. 49, no. 9, pp. 56–62, Sep. 2011, ISSN: 0163-6804.

[2] D. Tsonev, H. Chun, S. Rajbhandari, J. McKendry, S. Videv, E. Gu, M. Haji, S. Watson, A. Kelly, G. Faulkner, M. Dawson, H. Haas, and D. O'Brien, "A 3-Gb/s Single-LED OFDM-based Wireless VLC Link Using a Gallium Nitride μLED," vol. 99 (to appear), p. 4, 2014.

[3] T. Borogovac, M. Rahaim, and J. B. Carruthers, "Spotlighting for Visible Light Communications and Illumination," in *IEEE Global Communications Conference (GLOBECOM 2010) Workshops*, 6-10 Dec 2010, pp. 1077–1081.

[4] H. Haas, "High-speed Wireless Networking Using Visible Light," *SPIE Newsroom*, April 2013. [Online]. Available: http://spie.org/x93593.xml

[5] F. Parand, G. Faulkner, and D. O'Brien, "Cellular Tracked Optical Wireless Demonstration Link," *IEE Proc. Optoelectron*, vol. 150, no. 5, pp. 490–496, 2003.

[6] S. Dimitrov, H. Haas, M. Cappitelli, and M. Olbert, "On the Throughput of an OFDM-based Cellular Optical Wireless System for an Aircraft Cabin," in *Proc. of European Conference on Antennas and Propagation (EuCAP 2011)*, Rome, Italy, 11–15 Apr. 2011, invited Paper.

[7] J. B. Carruthers and J. M. Kahn, "Angle Diversity for Nondirected Wireless Infrared Communication," *IEEE Trans. Commun.*, vol. 48, no. 6, pp. 960–969, Jun. 2000.

[8] J. M. Kahn and J. R. Barry, "Wireless Infrared Communications," *Proc. IEEE*, vol. 85, no. 2, pp. 265–298, Feb. 1997.

[9] M. Alouini and A. Goldsmith, "Area Spectral Efficiency of Cellular Mobile Radio Systems," *IEEE Trans. Veh. Technol.*, vol. 48, no. 4, pp. 1047–1066, 1999.

[10] S. Dimitrov, R. Mesleh, H. Haas, M. Cappitelli, M. Olbert, and E. Bassow, "On the SIR of a Cellular Infrared Optical Wireless System for an Aircraft," *IEEE J. Sel. Areas Commun.*, vol. 27, no. 9, pp. 1623–1638, Dec. 2009.

IEEE ICC 2014 - Optical Networks and Systems

Improving SINR in Indoor Cellular Visible Light Communication Networks

Zhe Chen, Dobroslav Tsonev and Harald Haas

Institute for Digital Communications, Li-Fi R&D Centre, The University of Edinburgh, EH9 3JL, Edinburgh, UK,
Email:{z.chen, d.tsonev, h.haas}@ed.ac.uk

***Abstract*—In this paper, we first investigate the negative impact of light reflections and then introduce an angle diversity receiver (ADR) to mitigate the interference effect resulting from light reflections in an indoor cellular optical wireless communications (OWC) network. As the ADR consists of multiple photodiodes (PDs), a proper signal combining scheme is essential to optimize the system performance. Therefore, four different combining schemes, the select best combining (SBC), the equal gain combining (EGC), the maximum ratio combining (MRC) and the optimum combining (OPC), are investigated. The results indicate that the OPC scheme achieves the best performance among these combination schemes. In particular, when we use a seven-PD ADR as the optical detector, the OPC scheme can significantly suppress the interference signal resulting from light reflections and can achieve a signal to interference plus noise ratio (SINR) performance that is close to the SINR performance of the same configuration that is free of light reflections.**

***Index Terms*—reflection; angle diversity receiver; visible light communication; access points; cellular communication**

I. Introduction

In an attempt to address the looming spectrum crisis, visible light communication (VLC) technology has emerged as a complementary alternative to traditional radio frequency (RF) techniques [1]. Recent research has demonstrated transmission speeds in excess of 3 Gbps from a single colour light-emitting diode (LED) [2]. Unlike RF cellular communication, VLC operates in the entirely unregulated part of the electromagnetic spectrum and is safe to use in critical environments.

A cellular network enables high data density by harnessing the frequency reuse gains available to small-cell systems. Compared to RF cells, optical cells can be considerably smaller due to the limited coverage and interference mitigation induced by solid objects [3]. An indoor optical cellular system can have small cell sizes with little, if any, inter-cell interference. This facilitates higher bandwidth reuse and therefore higher data density than in RF communication. In an indoor optical wireless scenario, each lighting fixture in a room can serve as an optical access point (AP). We refer to an optical cellular layers as an *optical attocell* network [4]. In *optical attocell* network, optical orthogonal frequency division multiple access (O-OFDMA) could be used as the multiple access technique, since it allows for a flexible allocation of communication resources to every user in a network.

In a previous work, an optical cellular VLC system using multiple laser sources and multiple detectors is shown to provide a wide coverage area and high data rates [5]. Unfortunately, only the line-of-sight (LOS) path is considered in this scenario which makes the system model inaccurate. An indoor optical orthogonal frequency division multiplexing (O-OFDM) based cellular system that achieves high throughput through frequency reuse is proposed in [6]. Although the presented study investigates the channel characteristics of non-line-of-sight (NLOS) communication, it is valid only in an aircraft cabin and no method is proposed for mitigating the inter-cell interference signal caused by reflections.

In this study, we investigate the impact of signal reflections on the performance of an optical cellular network in a large-room indoor scenario. Furthermore, we propose the usage of angle diversity receivers (ADRs) to mitigate the inter-cell interference caused by signal reflections. An ADR consists of multiple narrow-field-of-view (FOV) photodiodes (PDs), which, when combined, result in a large-overall-FOV receiver [7],[8]. These narrow-FOV PDs can be selectively combined to minimize the effect of signal interference. Four combining schemes are investigated in this study. The first scheme is termed select best combining (SBC), where each user connects to the most suitable AP through a single PD at the receiver. The second scheme is termed equal gain combining (EGC), where the signals from each PD are combined with equal weights. The third scheme is called maximum ratio combining (MRC), the signals from each PD are combined using different weights and each weight factor is proportional to the signal to interference plus noise ratio (SINR) of the link between each PD and the desired AP. The last scheme is called optimum combining (OPC), where the signals from different PDs are combined with different weights, and the weight factor of each PD is generated by considering the interference-plus-noise correlation matrix which consists of the channel gain factors between all possible APs in the room and all the PDs in a respective receiver.

The remainder of this paper is organised as follows. The channel model is introduced in Section II. Different types of optical receivers are introduced in Section III. The single-PD receiver scenario is introduced in Section IV. The ADR scenarios with one of four different combining schemes are discussed in Section V. The simulation results are presented in Section VI. Finally, Section VII concludes the paper.

II. Channel Model

A. LOS Propagation

In this work, the direct current (DC) gain of a LOS optical channel is defined as follows [9]:

$$H_0 = \frac{(m+1)A_{\text{eff}}}{2\pi d^2}\cos^m(\phi)\cos(\theta)\text{rect}\left(\frac{\theta}{\Theta_{\text{fov}}}\right), \quad (1)$$

978-1-4799-2003-7/14/$31.00 ©2014 IEEE

where d is the distance from a transmitter to an optical receiver; Θ_{fov} is the FOV of the optical receiver; m is the Lambertian index of a transmitter and is a function of the transmitter half-intensity radiation angle θ_{tx} as $m = 1/\log_2(\cos(\theta_{\text{tx}}))$; ϕ is the angle of irradiance; θ is the angle of light incidence at the receiver; rect(x) is an unit step function and the effective signal collection area A_{eff} is given as:

$$A_{\text{eff}} = A_{\text{p}} G \frac{n_{\text{ref}}^2}{\sin^2(\Theta_{\text{fov}})}, \tag{2}$$

where n_{ref} is the refractive index of the receiver optics; A_{p} is the physical area of the optical receiver; G is the gain of the optical filter.

B. NLOS Propagation

Apart from the LOS path, the transmitted power can also reach the receivers through reflections. Common non-smooth reflection surfaces can be modelled by dividing their surface area into a number of small-surface elements [10]. Each of these can be modelled as an optical receiver in order to estimate the amount of light that it collects. With this measure in place, the surface element can then be modelled as a Lambertian transmitter which reemits a fraction of the collected light determined by the reflection coefficient of the surface material. The DC gain of the NLOS path is:

$$H_i = \sum_{q=1}^{Q} \frac{\rho_q (n+1) \cos^n(\phi) \cos(\theta) \Delta A}{2\pi d^2} H_{i-1}, \tag{3}$$

where i represents the number of the light reflections and q is the q^{th} reflecting element, with area ΔA; The total number of reflecting elements is Q. ρ_q is the reflection coefficient of the reflecting element q; n is the Lambertian index of the reflecting element which is a function of reflecting element half-intensity radiation angle θ_{ref} as $n = 1/\log_2(\cos(\theta_{\text{ref}}))$.

Finally, the overall DC gain is the sum of the LOS component and the NLOS components:

$$H = H_0 + \sum_{i=1}^{I} H_i, \tag{4}$$

where up to I reflections are considered in the NLOS path.

III. Optical Receivers

In this study, three types of optical receivers are investigated. The first type is a single-PD receiver with only one upward-pointing PD. The second type is an ADR with three PDs symmetrically attached to a semi-sphere base, as shown in Fig. 1. The third type is an ADR with seven PDs as shown in Fig. 2. Each PD at a single receiver has the same FOV angle, β. In addition, α is defined as the angle between the direction of the central axis of the optical receiver and the direction of each PD placed on the side, as illustrated in Fig. 1 and Fig. 2. M is defined as the number of PDs on an optical receiver.

For a fair comparison, we constrain the overall coverage area of each ADR to be the same as that of the single-PD receiver. The coverage area of each ADR (S2,S3) and the coverage area of a single-PD receiver (S1) are illustrated in Fig. 3. Moreover, we constrain each optical receiver to have the same overall effective area, MA_{eff}, which makes the comparison fair. We believe that the interference of reflected light can be reduced by increasing the number of PDs on an optical receiver, especially when each of the PDs points in a different direction. The reasons are twofold. First, since the overall coverage area of each optical receiver is the same, the optical receiver with more PDs can have a narrower FOV for each PD. Due to the diffusive nature of reflections, a narrow-FOV detector can effectively mitigate the interference because it collects less light from reflections. Second, the more individual detector elements there are in a receiver, the better granularity there is in the effort to separate desired and undesired light components.

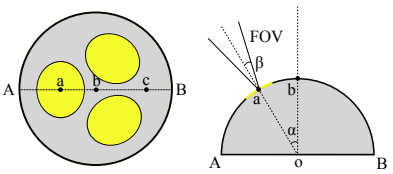

Fig. 1. The shape of an ADR ($M = 3$).

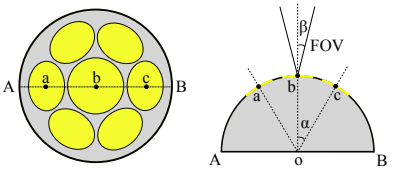

Fig. 2. The shape of an ADR ($M = 7$).

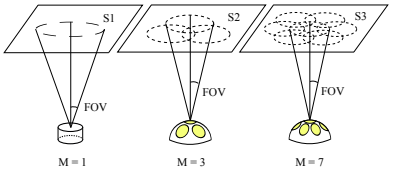

Fig. 3. The coverage area of each type of optical receivers on the ceiling. The overall coverage area of an ADR is the union of the individual coverage areas of each PD on that ADR. The coverage area of the single-PD receiver is defined only by the single PD.

IV. Single-PD scenario ($M = 1$)

In this scenario, each receiver in the *optical attocell* is equipped with a single-PD receiver. In order to maximize the SINR of each user in an optical cellular network, an AP needs to be chosen out of a number of candidate APs for each user. The AP of user k, $b_{\text{src}}^{(k)}$, may be chosen based on the highest achieved SINR:

$$b_{\text{src}}^{(k)} = \arg\max_{b} \left(\gamma_{(b,k)}\right). \tag{5}$$

where, b is the index of the AP, $\gamma_{(b,k)}$ is the SINR of the link between user k and AP b. The SINR can be expressed as:

$$\gamma_{(b,k)} = \frac{\left(rP_{\mathrm{t}}H_{(b,k)}\right)^2}{\left(N_0B + \sum_{b' \in \mathcal{B}_{\text{inter}}^{(b,k)}} \left(rP_{\mathrm{t}}H_{(b',k)}\right)^2\right)}, \quad (6)$$

where r is the responsivity of the PD; P_{t} is the standard deviation of the optical signal transmitted by an AP and is assumed the same for all APs; $H_{(b,k)}$ is the channel attenuation between user k and AP b; $\sum_{b' \in \mathcal{B}_{\text{inter}}^{(b,k)}} \left(rP_{\mathrm{t}}H_{(b',k)}\right)^2$ represents the interference signal from interfering APs; $\mathcal{B}_{\text{inter}}^{(b,k)}$ is the set of the interfering APs with respect to user k; N_0 is the additive white Gaussian noise (AWGN) power spectral density; B is the communication bandwidth.

V. ADR SCENARIOS ($M = 3, 7$)

In this scenario, each user in the *optical attocell* is equipped with an ADR. Different combination techniques for the ADRs are described in the sequel.

A. SBC scheme

The SBC scheme is originally proposed in [8] and is adapted for an *optical attocell* network. Each user terminal selects one PD to establish a link with its source AP. The source AP, $b_{\text{src}}^{(k)}$, and the destination PD, $s_{\text{des}}^{(k)}$, are chosen to maximize the SINR:

$$\left(b_{\text{src}}^{(k)}, s_{\text{des}}^{(k)}\right) = \arg\max_{b,s_k} \left(\gamma_{(b,s_k)}\right), \quad (7)$$

where s_k is the PD index of user k and $\gamma_{(b,s_k)}$ is the SINR of the link between b and s_k, which can be expressed as:

$$\gamma_{(b,s_k)} = \frac{\left(rP_{\mathrm{t}}H_{(b,s_k)}\right)^2}{N_0B + \sum_{b' \in \mathcal{B}_{\text{inter}}^{(b,s_k)}} \left(rP_{\mathrm{t}}H_{(b',s_k)}\right)^2}. \quad (8)$$

In the SBC scheme, an ADR only uses the signal from the PD with the highest SINR. This means that it requires a dedicated circuit to continuously monitor the SINR on each PD. Moreover, a switch is also needed for selecting the signal from the desired PD. Since the PD with the highest SINR is used, the ADR can achieve a high overall SINR.

B. EGC scheme

The EGC is the simplest combination scheme that the signals from each PD are combined with equal weights. It closely resembles the single-PD scenario, but the narrow FOV of the individual components causes interference to be reduced to some extent compared to the single-PD receiver. The way of choosing the most suitable source AP is the same as the method in the single-PD scenario, which is expressed as (5). The SINR can be calculated as:

$$\gamma_{(b,k)} = \frac{\left(\sum_{s_k=1}^{M} rP_{\mathrm{t}}H_{(b,s_k)}\right)^2}{MN_0B + \sum_{s_k=1}^{M} \sum_{b' \in \mathcal{B}_{\text{inter}}^{(b,s_k)}} \left(rP_{\mathrm{t}}H_{(b',s_k)}\right)^2}. \quad (9)$$

The numerator of (9) represents the total signal power received by all PDs of an ADR; $\sum_{s_k=1}^{M} \sum_{b' \in \mathcal{B}_{\text{inter}}^{(b,s_k)}} \left(rP_{\mathrm{t}}H_{(b',s_k)}\right)^2$ represents the total interference received by all PDs.

The EGC scheme requires only a simple adder for the combining circuit. Since optical power from multiple PDs is added up, the received optical power in the EGC scheme is higher than the optical power in the SBC scheme. However, as the signal from each PD is equally weighted, in some situation, the interference cannot be suppressed which could result in a poor overall SINR.

C. MRC scheme

The MRC scheme is similar to the EGC scheme except that the weight factor of each PD is proportional to the SINR it achieves on a given link. In the MRC scheme, the SINR can be expressed as:

$$\gamma_{(b,k)} = \frac{\left(\sum_{s_k=1}^{S} rP_{\mathrm{t}}w_{(b,s_k)}H_{(b,s_k)}\right)^2}{\sum_{s_k=1}^{S} \left(w_{(b,s_k)}^2 N_0B + \sum_{b' \in \mathcal{B}_{\text{inter}}^{(b,s_k)}} \left(rP_{\mathrm{t}}w_{(b,s_k)}H_{(b',s_k)}\right)^2\right)}, \quad (10)$$

where w_{s_k} is the weighting factor of PD s_k applied to the signal received from AP b. It can be calculated as:

$$w_{(b,s_k)} = \frac{\left(rP_{\mathrm{t}}H_{(b,s_k)}\right)^2}{N_0B + \sum_{b' \in \mathcal{B}_{\text{inter}}^{(b,s_k)}} \left(rP_{\mathrm{t}}H_{(b',s_k)}\right)^2}. \quad (11)$$

Since the weight factors are proportional to the SINR that each PD achieved on a given link, a sophisticated circuit is needed to continuously monitor the SINR on each PD. In addition, a multiplier and an adder are necessary for combining the received signals. With proper weight factors on each PD, the MRC scheme should boost the signal component and attenuates the interference and noise components which would result in a high overall SINR.

D. OPC scheme

Assuming the interference at each PD of an ADR is independent, the MRC scheme can provide the highest SINR at the receiver [11]. However, in the proposed high density optical cellular network, the interference signal from the same AP is often present at each of the PDs. The correlation between interference terms at different PDs significantly affects the performance of the MRC scheme. As a consequence, the OPC scheme is developed. The OPC scheme is initially used in RF scenario [11] and is adopted for optical cellular network. It mitigates the inter-cell interference by considering interference-plus-noise correlation matrix which could significantly suppress the correlated interference. In OPC, weights are calculated as:

$$\mathbf{w}_b = a\mathbf{R}_{nn}^{-1}\mathbf{u}_{\text{src}}^b, \quad (12)$$

where $\mathbf{u}_{\text{src}}^b = [rP_{\mathrm{t}}H_{(b,1)}, rP_{\mathrm{t}}H_{(b,2)}, \cdots, rP_{\mathrm{t}}H_{(b,S)}]^T$ is the signal received from the source AP b, a is a constant,

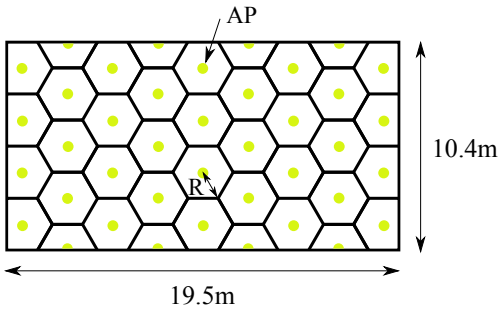

Fig. 4. AP layout in the large room for simulation.

$\mathbf{w}_b = [w_{(b,1)}, w_{(b,2)}, \cdots, w_{(b,S)}]^T$ is a vector which contains the different weight factors, and the interference-plus-noise correlation matrix, $\mathbf{R}_{nn}$, is given by:

$$\mathbf{R}_{nn} = N_0 B \mathbf{I} + \sum_{b' \in \mathcal{B}_{\text{inter}}} \left[\mathbf{u}_{b'} \mathbf{u}_{b'}^T \right]. \quad (13)$$

In (13), $\mathbf{I}$ is the identity matrix and $\mathbf{u}_{b'}$ is the set of interference signal that $\mathbf{u}_{b'} = [rP_t H_{(b',1)}, rP_t H_{(b',2)}, \cdots, rP_t H_{(b',S)}]^T$.

Compared with the MRC scheme, the OPC scheme not only needs a sophisticated circuit to continuously monitor the SINR on each PD, but also needs a complex circuit to calculate the weights according to the interference correlation between each PD. However, by exploiting the correlation of interference between each PD, the OPC scheme can suppress the correlated interference which is expect to achieve a higher SINR performance compared to the MRC scheme.

VI. Simulation Results

In the simulation, we assume a 19.5-m-long, 10.4-m-wide, and 4-m-high room. All optical APs are placed on the ceiling and all receivers are placed at a desk height of 0.85 m pointing upwards. The radius of each optical cell is assumed to be 1.5 m. Fig. 4 depicts the layout of the APs. Two types of ADRs are considered: one of them has three PDs with an equivalent total FOV of 30° ($\alpha = 13°, \beta = 20°$); the other one has seven PDs with an equivalent total FOV of 30° ($\alpha = 16.5°, \beta = 15°$) as well. In addition, we simulate a single-PD receiver with a FOV of 30°. The overall effective area of each optical receiver, MA_{eff}, is assumed to be the same. Therefore, the physical area of the PD on the single-PD receiver is 261 mm^2, the physical area of each PD on the three-PD ADR is 41 mm^2, and the physical area of each PD on the seven-PD ADR is 10 mm^2. The reflection coefficients of the walls, the ceiling, and the floor are 0.8, 0.8 and 0.3, respectively [12]. Table I shows the simulation parameters.

By varying the position of the optical receiver across all possible locations in the room and estimating the respective achievable SINR, we can determine the CDF of the SINR for the single-PD receiver scenario, which is shown in Fig. 5. When no reflections are considered, the distribution of the SINR is split into a high SINR region and a low SINR region. This is because the cellular optical wireless communications (OWC) system is limited by the interference which is several magnitudes higher than the noise [13]. The users in some location near the cell centre, are free from inter-cell interference which means that they can achieve significantly higher SINR than the users near the cell edge. The SINR performance slightly degrades when the first reflection is considered. This is because the first reflection of light can only reach the optical receiver via the walls. Since the room is large and the FOV of the simulated single-PD receiver is narrow, only a user at the edge of the room can receive the interference signal from one reflection. However, when the first two reflections are taken into account, the SINR performance in the high SINR region dramatically decreases. This is because all users can receive the reflected interference signal through the reflection off the ceiling. When the higher-order reflections are considered, the SINR performance degrades slightly. This is because the magnitude of high-order reflected light decays significantly due to the power loss of reflection. Therefore, for the subsequent simulations, only up to four reflections are considered.

Unlike the first-order reflection, the power of the second or higher-order reflected interference signal is spread over the entire ceiling area which means it is impossible to totally eliminate it by properly adjusting the FOV of the receiver.

TABLE I
Simulation Parameters

Radius of a cell, R	1.5 m
Responsivity, r	0.5 A/W
The gain of the optical filter, G	1
Transmitter half-intensity radiation angle, θ_{tx}	25°
Surface half-intensity radiation angle, θ_{ref}	60°
Refractive index, n	1.5
Transmission Power of an AP, P_t	2.2 W
Modulation Bandwidth, B	20 MHz
AWGN spectral density, N_0	2.5×10^{-23} A/Hz

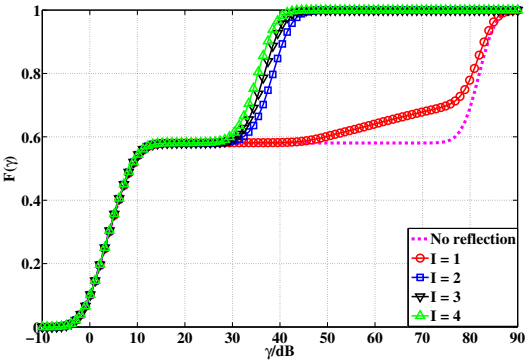

Fig. 5. The CDF of the SINR for the single-PD receiver when the FOV is 30°. No light reflection and different order of reflections ($I = 1, 2, 3, 4$) are considered in this scenario.

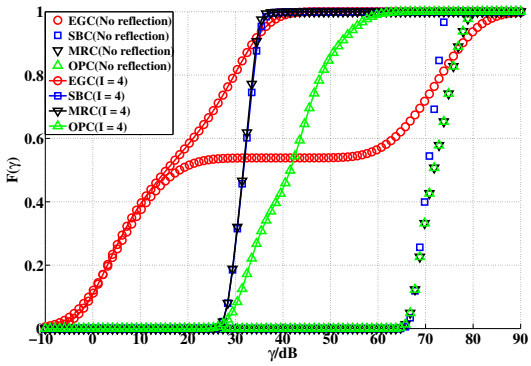

Fig. 6. The CDF of the SINR for the ADR ($M = 3$) when the equivalent FOV is 30°. No reflection and up to fourth-order reflections ($I = 4$) are considered in this scenario.

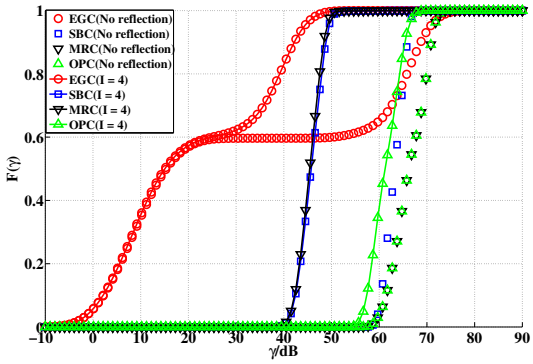

Fig. 7. The CDF of the SINR for the ADR ($M = 7$) when the equivalent FOV is 30°. No reflection and up to fourth-order reflections ($I = 4$) are considered in this scenario.

Furthermore, since the power of the reflected interference signal is proportional to the transmission power of the APs, the reflected interference signal will always constrain the SINR performance especially when high transmission power or a low-noise receiver is used. Therefore, for high SINR performance in an OWC cellular network, it is of vital importance to mitigate the impact of the reflected interference signals.

In order to address this issue, the ADR is introduced. Fig. 6 depicts the SINR performance of the ADR with three PDs. Four different combination techniques are implemented and the two scenarios of no reflection and up to a fourth-order reflection are considered.

When no light reflections are present, the interference signal can only reach the ADR through a LOS path. Since the PDs on the ADR point in different directions, some PDs may successfully avoid inter-cell interference. The EGC scheme equally combines the signal from all PDs, which means the inter-cell interference cannot be attenuated. Therefore, it has the worst SINR performance. Nevertheless, the EGC scheme is able to provide some improvement compared to the single-PD receiver due to the narrower FOV of its receiver elements, which decreases the amount of interference signal that each PD receives. By implementing the SBC scheme, the ADR can choose the PD with the highest SINR, which is usually the one that is free from inter-cell interference. Therefore, the ADR implementing the SBC scheme can achieve a high overall SINR. Compared with the SBC scheme, the MRC scheme and the OPC scheme proportionally weight and combine the received signals on the different PDs, which boosts the desired signal and attenuates the interference. As a result, they can achieve the best SINR performance. One important observation is that the SINR performance of the MRC and the OPC scheme is almost identical and very close to the performance of th SBC. This is because, in the MRC and in the OPC scheme, the PDs affected by LOS inter-cell interference are allocated extremely low weights and, thus, effectively ignored. This means the inter-cell interference hardly affects the overall SINR of the received signal. As the noise at each PD is independent, the results of the MRC scheme and the OPC scheme are practically identical.

When reflections are present, the SINR performance significantly changes. Since the reflected interference signal is spread from the entire ceiling and walls, each PD on the ADR can receive the reflected interference from the same AP. For the EGC scheme, the correlated interference terms are equally added up which significantly increases the interference. Therefore, the EGC scheme has the worst performance which resembles closely the performance of the single-PD receiver. Since no PD can be free from the reflected interference signal, the SBC scheme cannot avoid interference but can only choose the PD with the best local SINR. As no correlated interference is added up, the SINR performance of the SBC scheme outperforms the EGC scheme. The MRC scheme shows no improvement over the SBC scheme. Since the interference signals are correlated in each PD, the magnitude of reflected interference may be improperly amplified by the MRC scheme which does not take into account the correlation between the interference at the different PDs. By using the interference-plus-noise correlation matrix, the OPC scheme can generate the best weights for the ADR. These weights can effectively suppress the correlated interference signal in addition to boosting the amplitude of the desired signal.

When the number of PDs on an ADR is increased to 7, the trend of the SINR performance for the different combination schemes remains the same (see Fig. 7). One notable observation is that all schemes have improved performance for the cases with reflections. In particular, the OPC scheme achieves an SINR performance similar to the SINR performance of the OPC scheme in the scenario without reflections, which suggests that this combining algorithm manages to almost completely suppress the interference from signal reflections. This stems from the fact that more directional PDs on the ADR

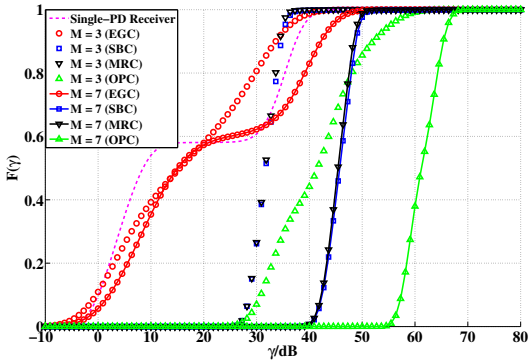

Fig. 8. Comparison of the SINR performance of optical receivers when the equivalent FOV is 30°. Up to fourth-order reflections ($I = 4$) are considered.

can provide additional information about the desired signal as well as about the interference terms which can help to suppress the correlated interference and improve the SINR performance effectively. It is also notable that the no-reflection scenarios in Fig. 7 perform slightly worse than the no-reflection scenarios in Fig. 6. This is because, when there is only one PD on an optical receiver, all effective area of a PD can be used to collect the desired signal. However, when the number of PDs is increased, not all PDs can receive the desired signal due to the narrow FOV characteristic. This means only part of the effective area can be used to collect the desired signal. Since the overall effective area is assumed to be the same for all optical receivers, the received power of the desired signal is attenuated more for the seven-PD receiver than for the three-PD receivers, which results in a worse SINR performance in the no-reflection scenario.

Fig. 8 compares the SINR performance of the two ADR configurations in a four-order reflection scenario. The optical receiver with more PDs can achieve a better SINR performance despite the fact that it receives a smaller portion of the desired signal. Since the equivalent FOV of each optical receiver is the same, when more PDs are on the same optical receiver, each PD will has a smaller FOV which results in a smaller coverage area. Due to the diffusive nature of the reflected light, a smaller area means less reflected interference signal is picked up by each PD. Moreover, a larger number of PDs enables the system to benefit from better receiver diversity by means of the signal combination schemes. As a result, the ADR with more PDs performs better in the scenario with light reflections.

VII. Conclusion

In this paper, the impact of reflected light in an indoor cellular VLC system is investigated. The results show that reflections have a significant impact on the SINR performance of the cellular network. For a narrow-FOV PD, it is interesting to note that higher-order reflections have a stronger negative effect on the SINR than first-order reflections. This is in stark contrast to what is often assumed in the analysis of OWC systems. In order to reduce the impact of the reflected interference signal, ADR is used and four different combining schemes, SBC, EGC, MRC and OPC are investigated. The results demonstrate that a larger number of detector elements in a receiver would improve the efforts to avoid the interference effects caused by signal reflections due to the improved information diversity. It can also be concluded that the correlation between the interference at the different photodetectors significantly affects the performance of the employed combining scheme. It is shown that the OPC performs best as this algorithm successfully manages to evaluate and account for the interference correlation at the different detector elements.

Acknowledgement

We gratefully acknowledge support by the School of Engineering and the Institute for Digital Communications (IDCOM) at the University of Edinburgh for providing a scholarship for this work which is aligned to the Engineering and Physical Sciences Research Council (EPSRC) project EP/K00042X/1.

References

[1] H. Elgala, R. Mesleh, and H. Haas, "Indoor Optical Wireless Communication: Potential and State-of-the-Art," *IEEE Commun. Mag.*, vol. 49, no. 9, pp. 56–62, Sep. 2011, ISSN: 0163-6804.

[2] D. Tsonev, H. Chun, S. Rajbhandari, J. McKendry, S. Videv, E. Gu, M. Haji, S. Watson, A. Kelly, G. Faulkner, M. Dawson, H. Haas, and D. O'Brien, "A 3-Gb/s Single-LED OFDM-based Wireless VLC Link Using a Gallium Nitride μLED," vol. 99 (to appear), p. 4, 2014.

[3] T. Borogovac, M. Rahaim, and J. B. Carruthers, "Spotlighting for Visible Light Communications and Illumination," in *IEEE Global Communications Conference (GLOBECOM 2010) Workshops*, 6-10 Dec 2010, pp. 1077–1081.

[4] H. Haas, "High-speed Wireless Networking Using Visible Light," *SPIE Newsroom*, April 2013. [Online]. Available: http://spie.org/x93593.xml

[5] F. Parand, G. Faulkner, and D. O'Brien, "Cellular Tracked Optical Wireless Demonstration Link," *IEE Proc. Optoelectron*, vol. 150, no. 5, pp. 490–496, 2003.

[6] S. Dimitrov, H. Haas, M. Cappitelli, and M. Olbert, "On the Throughput of an OFDM-based Cellular Optical Wireless System for an Aircraft Cabin," in *Proc. of European Conference on Antennas and Propagation (EuCAP 2011)*, Rome, Italy, 11–15 Apr. 2011, invited Paper.

[7] P. Deng, X. Yuan, M. Kavehrad, M. Zhao, and Y. Zeng, "Off-axis Catadioptric Fisheye Wide Field-of-view Optical Receiver for Free Space Optical Communications," *Optical Engineering*, vol. 51, no. 6, 2012.

[8] J. B. Carruthers and J. M. Kahn, "Angle Diversity for Nondirected Wireless Infrared Communication," *IEEE Trans. Commun.*, vol. 48, no. 6, pp. 960–969, Jun. 2000.

[9] J. M. Kahn and J. R. Barry, "Wireless Infrared Communications," *Proc. IEEE*, vol. 85, no. 2, pp. 265–298, Feb. 1997.

[10] J. Barry, J. Kahn, W. Krause, E. Lee, and D. Messerschmitt, "Simulation of Multipath Impulse Response for Indoor Wireless Optical Channels," *IEEE J. Sel. Areas Commun.*, vol. 11, no. 3, pp. 367–379, Apr. 1993.

[11] J. Winters, "Optimum Combining in Digital Mobile Radio with Cochannel Interference," *IEEE J. Sel. Areas Commun.*, vol. 2, no. 4, pp. 528–539, 1984.

[12] J. Alattar and J. M. H. Elmirghani, "Adaptive Beam Clustering Optical Wireless System for An Indoor Channel," in *IEEE International Conference on Communications, 2007. ICC '07.*, 2007, pp. 2468–2473.

[13] S. Dimitrov, R. Mesleh, H. Haas, M. Cappitelli, M. Olbert, and E. Bassow, "On the SIR of a Cellular Infrared Optical Wireless System for an Aircraft," *IEEE J. Sel. Areas Commun.*, vol. 27, no. 9, pp. 1623–1638, Dec. 2009.

Globecom 2014 - Optical Networks and Systems Symposium

A Novel Double-Source Cell Configuration for Indoor Optical Attocell Networks

Zhe Chen, Dobroslav Tsonev, Harald Haas
Institute for Digital Communications
Li-Fi R&D Centre
School of Engineering
The University of Edinburgh
EH9 3JL, Edinburgh, UK
{z.chen, d.tsonev, h.haas}@ed.ac.uk

***Abstract*—In this paper, a novel double-source cell configuration for indoor optical wireless cellular networks is proposed. In this configuration, each optical cell consists of two access points (APs) which transmit the same information signals, but with opposite polarity. When the optical sequences from the same optical cell are added up, they interfere destructively. This characteristic is beneficial for an angle diversity receiver (ADR) which enables the destructive interference to be exploited in order to reduce inter-cell interference. The results clearly indicate that the double-source cell configuration significantly outperforms the conventional single-source cell configuration when an ADR receiver is used. In this study, four signal combination schemes, the equal gain combining (EGC), select best combining (SBC), maximum ratio combining (MRC) and optimum combining (OPC) are implemented to enhance the performance of the ADR.**

I. Introduction

In recent years, visible light communication (VLC) technology has emerged as a complementary alternative to existing radio frequency (RF) techniques [1]. Transmission speeds of 3 Gbps from a single-colour light-emitting diode (LED) are reported in [2]. Compared with RF communication, VLC operates in an unregulated part of the electromagnetic spectrum and is safe to use in electromagnetic interference (EMI) sensitive environments.

A cellular network can achieve high data density by harnessing the frequency reuse gains. Compared with RF cells, optical cells can be considerably smaller due to the limited coverage of LEDs and the interference mitigation introduced by solid objects [3]. An optical cellular network facilitates higher bandwidth reuse and, therefore, higher data density than in small-cell RF wireless networks. In a typical indoor scenario, each lighting fixture can serve as an access point (AP). We refer to this type of network as an optical *attocell* network. In this network, optical orthogonal frequency division multiplexing (O-OFDM) is a favourable multiple access technique, since it allows the system to give a flexible allocation of communication resources to every user in the network.

In previous research, a simple optical cellular wireless commutation system consisting of multiple LEDs and multiple optical detectors was investigated [4]. The system was shown to provide a wide coverage area at high data rates. However, only the line-of-sight (LOS) path was considered which makes the simulation results inaccurate. Another optical cellular system implementing O-OFDM was investigated in [5]. This optical cellular system achieves high data throughput by exploiting frequency reuse gains. Although that study investigated the channel characteristic of both the LOS and the non-line-of-sight (NLOS) path, the study was limited to an aircraft cabin scenario, and the inter-cell interference becomes a limiting factor for higher system throughput. In order to mitigate the inter-cell interference, an angle diversity receiver (ADR) was introduced in an optical cellular network [6]. An ADR in combination with a proper signal recombination can significantly improve the achievable signal-to-interference-plus-noise-ratio (SINR) in an optical *attocell* network. In [6], only a single AP was considered per optical cell. The current study will demonstrate that there is a better scenario for AP deployment in an optical *attocell*.

In this study, two APs are placed in each optical cell in order to further exploit the spatial diversity introduced by an ADR. These two APs transmit the same information bits but the information signals have opposite polarity. This arrangement is referred to as a double-source cell configuration. Simulation results show that, for each ADR signal-combing scheme, the double-source cell configuration significantly outperforms the conventional single-source cell configuration and a maximum improvement of over 10 dB has been achieved.

The remainder of this paper is organised as follows: the channel model is introduced in Section II. The concepts of the optical double-source cell are introduced in Section III. Four different signal-combing schemes for ADR are discussed in Section IV. The simulation results are presented in Section V. Finally, Section VI concludes this paper.

II. Channel Model

A. LOS Propagation

In an optical *attocell* network, both LOS and NLOS paths need to be considered. In LOS links, the direct current (DC) gain can be accurately calculated as follows [7]:

$$H_0 = \frac{(m+1)A_{\text{eff}}}{2\pi d^2}\cos^m(\phi)\cos(\psi)\text{rect}\left(\frac{\psi}{\Psi_{\text{fov}}}\right), \quad (1)$$

where d is the distance between an optical transmitter and its corresponding receiver; Ψ_{fov} is the field-of-view (FOV) of the optical receiver; m is the Lambertian order of the

978-1-4799-3512-3/14/$31.00 ©2014 IEEE

optical transmitter and is a function of the transmitter half-intensity radiation angle $\Phi_{\rm tx}$ as $m = 1/\log_2(\cos(\Phi_{\rm tx}))$; ϕ is the angle of irradiance; ψ is the angle of light incidence at the receiver; $\mathrm{rect}(\mathrm{x})$ is the rectangular function. The effective signal collection area $A_{\rm eff}$ is given as:

$$A_{\rm eff} = A_{\rm p} G \frac{n_{\rm ref}^2}{\sin^2(\Psi_{\rm fov})}, \tag{2}$$

where $n_{\rm ref}$ is the refractive index of the receiver optics; $A_{\rm p}$ is the physical area of the optical receiver; G is the signal transmission gain of the optical filter.

B. NLOS Propagation

In NLOS links, the transmitted power reaches the optical receivers through reflections. In order to calculate the NLOS channel gain, all of the smooth reflection surfaces are divided into a number of small reflecting surface elements [8]. Each element collects the energy of the light signal incident on its surface and re-emits a fraction of the collected light determined by the reflection coefficient of the surface material.

A NLOS link can be divided into three parts. The first part is the light path from an optical transmitter to the $q^{\rm th}$ reflecting surface element. The optical channel gain for this path can be calculated as:

$$L_{1,q} = \frac{(m+1)\Delta A}{2\pi d_{q,\rm tx}^2} \cos^m(\phi)\cos(\psi), \tag{3}$$

where ΔA is the area of the reflecting surface element. The distance between the optical transmitter and the $q^{\rm th}$ reflecting surface element is denoted as $d_{q,\rm tx}$. Equation (3) enables us to calculate the power distribution on the reflecting walls due to a single-point source. The incident light is absorbed by each reflection element and re-emitted with a Lambertian pattern, and the intensity is determined by the reflection coefficient ρ. Therefore, the power on each reflecting surface element after the $i^{\rm th}$ light reflection can be derived.

Hence, in the second part of the NLOS path, the optical channel gain is described as:

$$L_{i,p} = \sum_{q=1}^{Q} \frac{\rho_q (n+1)\cos^n(\phi)\cos(\theta)\Delta A}{2\pi d_{p,q}^2} L_{i-1,q}, \tag{4}$$

where i represents the number of the light reflections and $d_{p,q}$ is the distance between the reflecting element p and the reflecting element q. The total number of reflecting elements is Q. The reflection coefficient of the reflecting element q is ρ_q; n is the Lambertian order of the reflecting element, which is a function of reflecting element half-intensity radiation angle $\theta_{\rm ref}$ as $n = 1/\log_2(\cos(\theta_{\rm ref}))$. For most surfaces, $\theta_{\rm ref} = 60^{\rm o}$.

The third part of the NLOS link is the light path from the reflecting elements to an optical receiver. The optical channel gain for this path can be represented as:

$$H_i = \sum_{p=1}^{Q} L_{i,p} \frac{\rho_p (n+1)\Delta A}{2\pi d_{\rm rx,p}^2} \cos^n(\phi)\cos(\psi)\mathrm{rect}\left(\frac{\psi}{\Psi_{\rm fov}}\right), \tag{5}$$

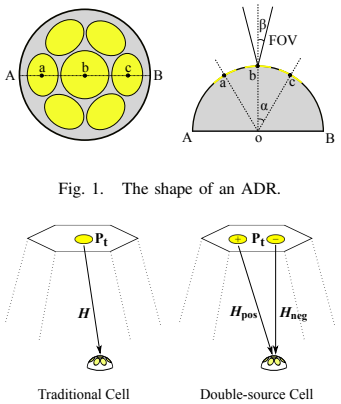

Fig. 1. The shape of an ADR.

Fig. 2. The configuration of a conventional optical cell and a double-source optical cell.

where $d_{\rm rx,p}$ is the distance between the $q^{\rm th}$ reflecting surface element and the optical receiver; the reflection coefficient of the reflecting element p is ρ_p.

Finally, the overall DC gain is the sum of the LOS component and the NLOS components:

$$H = H_0 + \sum_{i=1}^{I} H_i, \tag{6}$$

where up to I reflections are considered in the NLOS path.

III. ADR and the Double-source Optical Cell

In this study, an ADR with seven photodiodes (PDs) as the optical receiver is used, as shown in Fig. 1. Each PD at the ADR has the same FOV angle, β. In addition, α is defined as the angle between the direction of the central axis of the optical receiver and the direction of each PD placed on the side, as shown in Fig. 1.

Conventionally, in an optical *attocell* network, an optical AP is placed at the centre of the optical cell (see Fig. 2). This placement is intuitively reasonable since it can maximise the SINR in the optical cell by keeping the longest distance to the other APs in the vicinity. However, this configuration fails to fully exploit the spatial diversity of the ADR. Therefore, a novel configuration is proposed to improve the performance of the ADR.

As shown in Fig. 2, the new configuration is denoted as a double-source cell configuration. There are two APs in a double-source cell. One is named as the 'Positive AP' and the other one is named as the 'Negative AP'. The distance between the 'Positive AP' and 'Negative AP' is less then the radius of the cell. The 'Positive AP' transmits the signal sequence, $S(t)$, which is the same as the signal sequence that would be transmitted in a conventional cell configuration. The dynamic range of $S(t)$ is from 0 to $S_{\rm H}$. The 'Negative AP' in this cell transmits the signal sequence, $S'(t)$. The relationship between

$S'(t)$ and $S(t)$ is represented as:

$$S'(t) = S_{\mathrm{H}} - S(t). \tag{7}$$

Here, the transmission power of an optical AP is defined as the standard deviation of the optical signal. Therefore, the transmission power of the 'Positive AP' and the 'Negative AP' is represented as:

$$\mathrm{P}_{\mathrm{tx,pos}} = \sqrt{\mathrm{E}\left[(S(t) - \mathrm{E}[S(t)])^2\right]}, \tag{8}$$

$$\begin{aligned}\mathrm{P}_{\mathrm{tx,neg}} &= \sqrt{\mathrm{E}\left[(S'(t) - \mathrm{E}[S'(t)])^2\right]} \\ &= \sqrt{\mathrm{E}\left[(S_{\mathrm{H}} - S(t) - \mathrm{E}[S_{\mathrm{H}} - S(t)])^2\right]} \\ &= \sqrt{\mathrm{E}\left[(S(t) - \mathrm{E}[S(t)])^2\right]}. \end{aligned} \tag{9}$$

Since the transmission power of the 'Positive AP' and the 'Negative AP' is the same, we simply denote them as P_{tx}. P_{tx} is assumed the same for all APs. For one optical cell, the received optical signal is represented as:

$$S_{\mathrm{sum}} = S(t)H_{\mathrm{pos}} + S'(t)H_{\mathrm{neg}}. \tag{10}$$

Therefore, the received power of the information signal is:

$$\begin{aligned}\mathrm{P}_{\mathrm{rx}} &= \sqrt{\mathrm{E}\left[(S_{\mathrm{sum}} - \mathrm{E}[S_{\mathrm{sum}}])^2\right]} \\ &= \sqrt{\mathrm{E}\left[(S(t)(H_{\mathrm{pos}} - H_{\mathrm{neg}}) - \mathrm{E}[S(t)(H_{\mathrm{pos}} - H_{\mathrm{neg}})])^2\right]} \\ &= \sqrt{\mathrm{E}\left[(S(t) - \mathrm{E}[S(t)])^2\right]}\,|H_{\mathrm{pos}} - H_{\mathrm{neg}}| \\ &= \mathrm{P}_{\mathrm{tx}}\Delta H, \end{aligned} \tag{11}$$

where H_{pos} is the channel gain between the 'Positive AP' and the optical receiver and H_{neg} is the channel gain between the 'Negative AP' and the optical receiver; ΔH denotes the difference between H_{pos} and H_{neg}.

The benefit of deploying a double-source cell configuration can be explained by equation (11). The signal power at the receiver end is scaled with ΔH. As illustrated in Fig. 3, when an optical receiver is far from an optical cell, the distance from an optical AP and an optical receiver is significantly larger than the distance between two optical APs. This means the distance between two APs has very little impact on varying the channel gains, H_{pos} and H_{neg}. Therefore, the difference between H_{pos} and H_{neg} is small, which means the received optical signal is attenuated. When the optical receiver is underneath the optical AP, the difference between H_{pos} and H_{neg} is large. This is because, two APs in the same optical cell have little chance to simultaneously establish LOS link with the same PD at the ADR due to the narrow FOV of each PD. Since the difference between LOS and NLOS path is significant, the received optical signal is enhanced. Generally, the desired optical APs are close to an optical receiver and the interference APs are much further from an optical receiver. Hence, this configuration may effectively boost the signal from a source optical AP and attenuate the interference, which results in a better SINR performance. Moreover, the double-source cell configuration is easy to implement, since the signal from the 'Negative AP' is simply an inverted version of the signal from the 'Positive AP'.

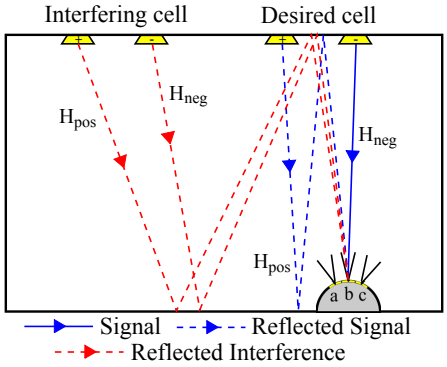

Fig. 3. The optical signal sequence transmitted by the 'Positive AP'.

IV. Signal Combination Schemes for an ADR

In this section, four signal combination techniques for the ADRs, the select best combining (SBC), the equal gain combining (EGC), the maximum ratio combining (MRC) and the optimum combining (OPC) are described. For all schemes, it is assumed that each receiver connects to the closest optical cell in space.

A. SBC scheme

The SBC scheme is originally proposed in [9] and is adapted for an *optical attocell* network. Each user terminal selects one PD on the ADR to establish a link with its source cell. The received SINR can be expressed as:

$$\gamma_{(b,k)} = \frac{\left(rP_{\mathrm{tx}}\Delta H_{(b,s_k)}\right)^2}{N_0 B + \sum_{b'\neq b}\left(rP_{\mathrm{tx}}\Delta H_{(b',s_k)}\right)^2}, \tag{12}$$

where r is the optical-to-electric conversion efficiency; $\Delta H_{(b,s_k)}$ is the channel attenuation between the selected PD s_k and the source optical cell b; N_0 is the additive white Gaussian noise (AWGN) power spectral density; B is the communication bandwidth.

In the SBC scheme, an ADR only uses the signal from the PD with the highest SINR. This means that it requires a dedicated circuit to continuously monitor the SINR on each PD and select the signal from the desired PD. Since the PD with the highest SINR is used, the ADR can achieve a high overall SINR.

B. EGC scheme

The EGC is the simplest combination scheme where the signals from each PD are combined with equal weights. The SINR can be calculated as:

$$\gamma_{(b,k)} = \frac{\left(\sum_{s_k=1}^{M} rP_{\mathrm{tx}}\Delta H_{(b,s_k)}\right)^2}{MN_0 B + \sum_{s_k=1}^{M}\sum_{b'\neq b}\left(rP_{\mathrm{tx}}\Delta H_{(b',s_k)}\right)^2}, \tag{13}$$

where the total number of PDs at the ADR is M.

The EGC scheme requires only a simple adder for the combining circuit. Since signal power from multiple PDs is added up, the received signal power in the EGC scheme is higher than the signal power in the SBC scheme. However, as the signal from each PD is equally weighted, in some scenarios, the interference cannot be suppressed which could result in a poor overall SINR.

C. MRC scheme

The MRC scheme is similar to the EGC scheme except that the weight factor of each PD is proportional to the SINR it achieves on a given link. In the MRC scheme, the received SINR can be expressed as:

$$\gamma_{(b,k)} = \frac{\left(\sum_{s_k=1}^{S} rP_{\mathrm{tx}} w_{(b,s_k)} \Delta H_{(b,s_k)}\right)^2}{\sum_{s_k=1}^{S}\left(w_{(b,s_k)}^2 N_0 B + \sum_{b' \neq b}\left(rP_{\mathrm{tx}} w_{(b,s_k)} \Delta H_{(b',s_k)}\right)^2\right)}, \tag{14}$$

where $w_{(b,s_k)}$ is the weighting factor of PD s_k applied to the signal received from the source optical cell b. It can be calculated as:

$$w_{(b,s_k)} = \frac{\left(rP_{\mathrm{tx}} \Delta H_{(b,s_k)}\right)^2}{N_0 B + \sum_{b' \neq b}\left(rP_{\mathrm{tx}} \Delta H_{(b',s_k)}\right)^2}. \tag{15}$$

Since the weight factors are proportional to the SINR that each PD achieves on a given link, a bespoke circuit is needed to continuously monitor the SINR at each PD. In addition, a multiplier and an adder are necessary for combining the received signals. With proper weight factors for each PD, the MRC scheme boosts the signal component and attenuates the interference and noise components, and this results in a high overall SINR.

D. OPC scheme

Assuming the interference at each PD of an ADR is independent, the MRC scheme can provide the highest SINR at the receiver [10]. However, in the proposed high density optical cellular network, the interference signal from the same AP is often present at each of the PDs. The correlation between the interference terms at the different PDs significantly affects the performance of the MRC scheme. As a consequence, the OPC scheme is developed. The OPC scheme is initially introduced for RF scenario [10] and is later adopted for an optical cellular network. It mitigates the inter-cell interference by taking into account the channel's interference-plus-noise correlation matrix [10]. This could significantly suppress the correlated interference. In OPC, weights are calculated as:

$$\mathbf{w}_b = a\mathbf{R}_{nn}^{-1}\mathbf{u}_{\mathrm{src}}^b, \tag{16}$$

where $\mathbf{u}_{\mathrm{src}}^b = [rP_{\mathrm{tx}}\Delta H_{(b,1)}, rP_{\mathrm{tx}}\Delta H_{(b,2)}, \cdots, rP_{\mathrm{tx}}\Delta H_{(b,S)}]^T$ is the set of signals received from the source optical cell b; a is a constant; $\mathbf{w}_b = [w_{(b,1)}, w_{(b,2)}, \cdots, w_{(b,S)}]^T$ is a vector which contains the different weight factors, and the interference-plus-noise correlation matrix, $\mathbf{R}_{nn}$, is given by:

$$\mathbf{R}_{nn} = N_0 B\mathbf{I} + \sum_{b' \in \mathcal{B}_{\mathrm{inter}}} \left[\mathbf{u}_{\mathrm{b}'}\mathbf{u}_{\mathrm{b}'}^T\right]. \tag{17}$$

where $\mathcal{B}_{\mathrm{inter}}$ is the set of interference optical cells; $\mathbf{I}$ is the identity matrix and $\mathbf{u}_{\mathrm{b}'}$ is the set of interference signals, *i.e.*, $\mathbf{u}_{\mathrm{b}'} = [rP_{\mathrm{tx}}\Delta H_{(b',1)}, rP_{\mathrm{tx}}\Delta H_{(b',2)}, \cdots, rP_{\mathrm{tx}}\Delta H_{(b',S)}]^T$.

Compared with the MRC scheme, the OPC scheme not only needs a circuit to continuously monitor the SINR on each PD, but also requires a circuit to calculate the weights according to the interference correlation between each PD. However, by exploiting the interference correlation between each PD, the OPC scheme can suppress the correlated interference. This technique is expected to achieve a higher SINR performance compared with the MRC scheme.

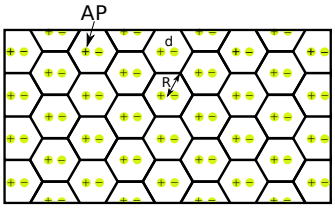

Fig. 4. AP layout in the large room for simulation. '+' denotes the 'Positive AP' and '-' denotes the 'Negative AP'

TABLE I
SIMULATION PARAMETERS

Responsivity, r	0.5 A/W
The gain of the optical filter, G	1
Transmitter half-intensity radiation angle, θ_{tx}	25°
Surface half-intensity radiation angle, θ_{ref}	60°
Refractive index, n	1.5
The area of reflecting elements, ΔA	25cm^2
Modulation Bandwidth, B	20 MHz
AWGN spectral density, N_0	2.5×10^{-23}A/Hz
Number of light reflections, I	4

V. SIMULATION RESULTS

In the simulation, a 20-m-long, 10-m-wide, and 4-m-high room is assumed. In each optical cell, two optical APs are placed on the ceiling and the distance between an optical AP and the optical cell centre is denoted as d, which is varied from 0.1 m to 0.5 m. The layout of the optical APs is depicted in Fig. 4. ADRs are placed at a desk height of 0.85 m pointing upwards. The ADR parameters are $\alpha = 16.5°$ and $\beta = 15°$. The reflection coefficients of the walls, the ceiling, and the floor are 0.8, 0.8 and 0.2, respectively [11]. For fairness, the optical transmission power of the AP in the conventional single-source cell configuration is 2.2 W while the optical transmission power of the APs in the double-source cell configuration is halved, *i.e.*, it is set to 1.1 W to make the combined optical power of an AP pair equal to the optical

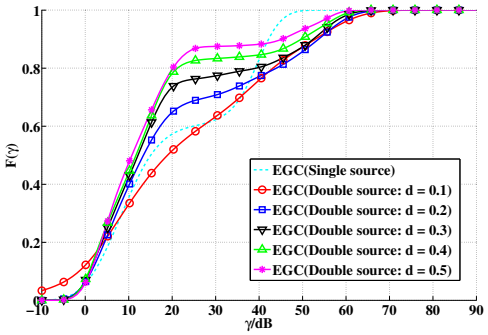

Fig. 5. The CDF of the achieved SINR at the ADR when the double-source cell configuration is implemented. The combination scheme for the ADR is EGC.

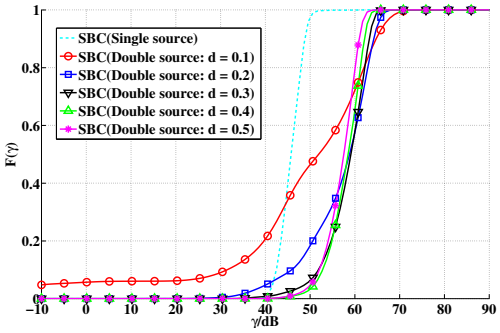

Fig. 6. The CDF of the achieved SINR at the ADR when the double-source cell configuration is implemented. The combination scheme for the ADR is SBC.

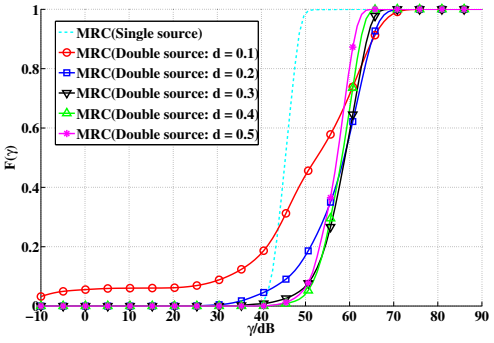

Fig. 7. The CDF of the achieved SINR at the ADR when the double-source cell configuration is implemented. The combination scheme for the ADR is MRC.

transmission power of the AP in the conventional cell. Table I presents the remaining simulation parameters.

By varying the position of the optical receiver across all possible locations in the room and estimating the respective achievable SINR, the cumulative distribution function (CDF) of the SINR for the ADR can be determined. Four signal combination schemes for the ADR are investigated separately to see the effect of the double-source cell configuration on each of them. Also, the conventional cell configuration is simulated as a baseline to evaluate the SINR improvement introduced by the double-source cell configuration.

The SINR performance for the EGC scheme is shown in Fig. 5. When d is 0.1 m, the double-source cell configuration outperforms the conventional cell configuration in terms of SINR. When d increases, the performance of the double-source cell configuration degrades. This is because, when d is large, the distance between the source APs and the interfering APs from the neighbouring cells decreases. This significantly increases the inter-cell interference.

Compared with the EGC scheme, the performance trend of the SBC scheme is different. This is depicted in Fig. 6. When d is small, especially when $d = 0.1$ m, some users inside the optical cell experience a significant SINR drop. This is because, when d is small, the only activated PD may establish LOS links with both of the APs in the source optical cell. Therefore, the channel difference, ΔH, is small and the received optical power decreases which results in a low SINR. When d increases, the double-source cell configuration exhibits an improvement of more than 10 dB over the conventional cell configuration. The reason for this is as follows: when d is large, only one of the APs in the desired cell can establish a LOS link with the activated PD on the optical receiver. Meanwhile, the other AP can only establish a NLOS link to the activated PD due to the narrow FOV of the PD. Therefore, the channel difference, ΔH, would dramatically increase which results in high received signal power.

In Fig. 7, the performance of the MRC scheme is nearly identical to the SBC scheme. This is because the weights on the different received signals are determined according to the SINR achieved at each PD. As a consequence, the signals with low SINR are effectively disregarded. This means that effectively only the strong links contribute to the received signal which is similar to the SBC scheme. Due to the NLOS propagation path, the interference signals are correlated in each PD and the MRC scheme is unable to resolve this correlation. The magnitude of reflected interference may be improperly amplified by the MRC scheme. Therefore, the performance of the MRC scheme is not optimal.

In Fig. 8, when d is small, the performance of the OPC scheme in double-cell scenario is worse than the performance in single-cell scenario. The reason of this is similar to the previous scenarios that ADR cannot exploit the benefit of spatial diversity when 'Positive' and 'Negative' APs are placed too close together. When d increases, the double-source cell configuration provides approximately 2 dB improvement over the conventional cell configuration when the OPC scheme is used. The improvement is not as much as in other schemes, since the OPC scheme has already extensively exploited the channel information by considering the interference-plus-noise correlation matrix. Therefore, the potential for improvement is

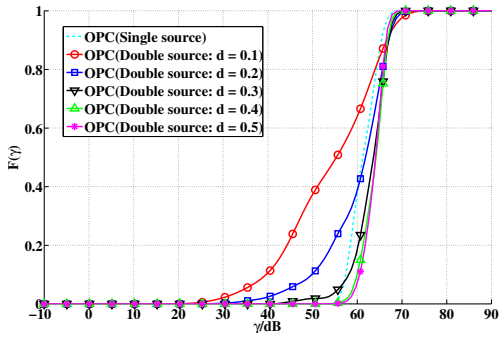

Fig. 8. The CDF of the achieved SINR at the ADR when the double-source cell configuration is implemented. The combination scheme for the ADR is OPC.

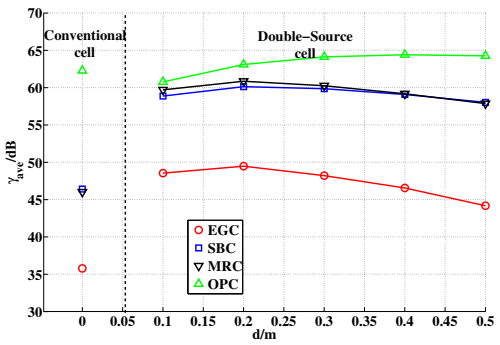

Fig. 9. The average achieved SINR at the ADR when the conventional single-source cell configuration and the double-source cell configuration are considered.

limited.

Finally, a comparison between the average achievable SINR in the conventional cell configuration and in the double-source cell configuration is presented in Fig. 9 for all signal combination schemes. For the EGC scheme, the optimal distance between the 'Positive AP' and the 'Negative AP' is 0.2 m, where an average SINR of 50 dB is achieved. For both the SBC scheme and the MRC scheme, the optimal distance is 0.2 m and the average SINR values are 60 dB and 61 dB respectively. For the OPC scheme, the optimal distance is 0.4 m with an average SINR of 64 dB. For all combination schemes, the double-source cell configuration has a significant improvement over the conventional cell configuration in terms of the achievable average SINR. An important observation is that the SINR performance of the SBC scheme exhibits more than 10 dB SINR improvement for the double-source cell configuration in comparison with the conventional single-source configuration. This means the SBC scheme is very close to the OPC scheme, whose performance can approach the performance of an LOS system which is free from inter-cell interference [6]. Compared with the OPC scheme, the SBC scheme requires less computational complexity and, hence, is very suitable for implementation in an experimental system, and this will be the subject of future work.

VI. Conclusion

In this paper, a novel double-source cell configuration is proposed for improving the SINR performance in an optical *attocell* network. In this configuration, an ADR is used as the optical receiver and four different signal combination schemes, EGC, SBC, MRC and OPC, are investigated. The results clearly demonstrate that the double-source cell configuration significantly improves the SINR performance for all signal combination schemes in comparison with the conventional cell configuration. It is particularly interesting to note that an improvement of more than 10 dB can be obtained for the SBC scheme. This means that, when the double-source cell configuration is implemented, the SBC scheme can approach the performance of a system without inter-cell interference. This result is very promising since the low complexity of the SBC scheme makes it suitable for practical implementation.

Acknowledgement

Professor Haas acknowledges support from the Engineering and Physical Sciences Research Council (EPSRC) under Established Career Fellowship grant EP/K008757/1.

References

[1] H. Elgala, R. Mesleh, and H. Haas, "Indoor Optical Wireless Communication: Potential and State-of-the-Art," *IEEE Commun. Mag.*, vol. 49, no. 9, pp. 56–62, Sep. 2011.

[2] D. Tsonev, H. Chun, S. Rajbhandari, J. J. D. McKendry, S. Videv, E. Gu, M. Haji, S. Watson, A. E. Kelly, G. Faulkner, M. D. Dawson, H. Haas and D. O'Brien, "A 3-Gb/s single-LED OFDM-based wireless VLC link using a Gallium Nitride μLED," *IEEE Photon. Technol. Lett*, vol. 26, no. 7, pp. 637–640, Apr. 2014.

[3] T. Borogovac, M. Rahaim, and J. B. Carruthers, "Spotlighting for Visible Light Communications and Illumination," in *IEEE Global Communications Conference (GLOBECOM 2010) Workshops*, 6-10 Dec 2010, pp. 1077–1081.

[4] B. Ghimire and H. Haas, "Self Organising Interference Coordination in Optical Wireless Networks," *EURASIP Journal on Wireless Communications and Networking*, vol. 1, no. 131, Apr. 2012.

[5] S. Dimitrov, H. Haas, M. Cappitelli, and M. Olbert, "On the Throughput of an OFDM-based Cellular Optical Wireless System for an Aircraft Cabin," in *Proc. of European Conference on Antennas and Propagation (EuCAP 2011)*, Rome, Italy, 11–15 Apr. 2011.

[6] Z. Chen, D. A. Tsonev, and H. Haas, "Improving SINR in Indoor Cellular Visible Light Communication Networks," in *IEEE ICC 2014 - Optical Networks and Systems (ICC'14 ONS)*, Sydney, Australia, Jun. 2014.

[7] J. M. Kahn and J. R. Barry, "Wireless Infrared Communications," *Proceedings of the IEEE*, vol. 85, no. 2, pp. 265–298, Feb. 1997.

[8] J. Barry, J. Kahn, W. Krause, E. Lee, and D. Messerschmitt, "Simulation of Multipath Impulse Response for Indoor Wireless Optical Channels," *IEEE J. Select. Areas Commun.*, vol. 11, no. 3, pp. 367–379, Apr. 1993.

[9] J. B. Carruthers and J. M. Kahn, "Angle Diversity for Nondirected Wireless Infrared Communication," *IEEE Trans. Commun.*, vol. 48, no. 6, pp. 960–969, Jun. 2000.

[10] J. Winters, "Optimum Combining in Digital Mobile Radio with Cochannel Interference," *IEEE J. Select. Areas Commun.*, vol. SAC-2, no. 4, pp. 528–539, Jul. 1984.

[11] F. E. Alsaadi and J. M. H. Elmirghani, "Mobile MC-CDMA Optical wireless System Employing an Adaptive Multibeam Transmitter and Diversity Receivers in a Real Indoor Environment," in *In the Proceeding of the IEEE International Conference on Communications (ICC 08)*, May 19–23, 2008, pp. 5196–5203.

Improved Receivers for Asymmetrically-Clipped Optical OFDM

Zhe Chen, Dobroslav Tsonev and Harald Haas
Institute for Digital Communications
Li-Fi R&D Centre
School of Engineering
The University of Edinburgh
EH9 3JL, Edinburgh, UK
{z.chen, d.tsonev, h.haas}@ed.ac.uk

***Abstract*—In this paper, we propose two novel receiver designs for asymmetrically clipped optical orthogonal frequency division multiplexing (ACO-OFDM). The first one, termed 'Proposed Receiver I', exploits the structure of the clipping noise which improves the power efficiency over the state-of-the-art ACO-OFDM receiver. The second one, termed 'Proposed Receiver II', exploits the benefit of bit error correction which achieves a further improvement over the state-of-the-art ACO-OFDM receiver at the expense of computational complexity.**

***Index Terms*—visible light communication; ACO-OFDM, receiver design**

I. Introduction

To address the looming radio frequency (RF) spectrum crisis, visible light communication (VLC), a complementary to RF, has drawn considerable interest [1]. With the emergence of high-power light-emitting diodes (LEDs) and highly sensitive photodiodes (PDs), VLC systems can operate in the unregulated electromagnetic spectrum where communication speeds of over 3 Gbps from a single light-emitting diode (LED) have been achieved using incoherent light [2]. VLC systems can transmit data through power used for illumination purposes which makes them inherently energy-efficient. In addition, visible light (VL) is safe to use in RF-restricted environments, *i.e.*, hospitals, airplanes, petrochemical plants etc.

Incoherent light sources, such as LEDs assumed in this work, only allow a VLC system to be realised as an intensity modulation and direct detection (IM/DD) system [3]. Since information can only be conveyed in the intensity of an optical signal, a VLC system can employ only unipolar modulation schemes that produce real valued signals. Examples of such modulation schemes are pulse position modulation (PPM), pulse width modulation (PWM) and pulse amplitude modulation (PAM). However, at high data rates, the information signal is affected by inter-symbol interference (ISI) when passing through a dispersive optical channel. Therefore, an advanced modulation technique such as orthogonal frequency division multiplexing (OFDM) is preferred due to its inherent robustness to multi-path propagation. A Hermitian symmetry of OFDM subcarriers in the frequency domain guarantees a real-valued time domain signal. To obtain a non-negative time domain signal, there are two well-known approaches. The first one is termed DC-biased optical orthogonal frequency division multiplexing (DCO-OFDM), where a DC-bias is introduced to transform a bipolar time-domain signal to an unipolar signal [4]. However, in DCO-OFDM, the DC-bias is responsible for a substantial increase in the transmission power. The other approach is termed asymmetrically clipped optical orthogonal frequency division multiplexing (ACO-OFDM), where the power efficiency is improved at the expense of half the spectral efficiency [5], [6].

An ACO-OFDM receiver is initially proposed in [5]. Then, an enhanced ACO-OFDM receiver design is proposed in [7]. This enhanced receiver reduces the additive white Gaussian noise (AWGN) by clipping all negative values in the received signal block. As a result, this receiver achieves a better performance than the previous design in [5]. A further enhanced ACO-OFDM receiver is proposed in [8]. This receiver estimates the position of the positive signal samples and clips the noise samples by exploiting the anti-symmetric characteristic of the time domain signal. However, since the position of the positive samples may be estimated incorrectly, this may result in performance degradations.

In this work, we propose two new ACO-OFDM receiver designs. The first one, termed 'Proposed Receiver I', can amend one more incorrect estimation of the positive samples compared to the state-of-the-art receiver [8]. The second one, termed 'Proposed Receiver II', is inspired by the sub-optimal receiver in [9]. This receiver bit-by-bit adjusts the received signal block of the state-of-the-art receiver and generates a signal block that has the smallest Euclidean distance to the received signal. 'Proposed Receiver I' and 'Proposed Receiver II', respectively, achieve up to 0.5 dB and 1 dB improvement over the state-of-the-art receiver.

The remainder of this paper is organised as follows. Section II presents the channel model and the properties of ACO-OFDM. Section III explains the proposed ACO-OFDM detectors. The computational complexity of the different ACO-OFDM detectors is discussed in Section IV while the simulation results are illustrated in Section V. Finally, Section VI concludes the paper.

II. System Model

A. ACO-OFDM Transmitter

A block diagram of an ACO-OFDM transmitter is illustrated in Fig. 1. The input bits are mapped to complex symbols, $X_{\mathrm{m}}(l)$, by a quadrature amplitude modulation (QAM) modulator. Then, $X_{\mathrm{m}}(l)$ is mapped to form the OFDM frame, $X_{\mathrm{f}}(m)$, $m = 0, ..., N-1$, in accordance with the fast Fourier

978-1-4799-4482-8/14/$31.00 ©2014 IEEE

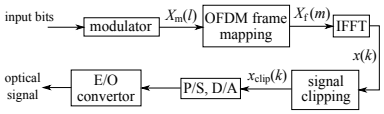

Fig. 1. Block diagram of an ACO-OFDM transmitter. The E/O conversion is considered linear with gain of one.

transform (FFT) size N. In ACO-OFDM, the first half of the odd subcarriers, $X_{\rm f}(m)$, $m = 1, 3, 5, ..., N/2 - 1$ are mapped from the $N/4$ symbols in $X_{\rm f}(l)$, $l = 0, 1, ..., N/4-1$. Meanwhile, the first half of the even subcarriers are set to zero. Then, Hermitian symmetry is imposed on the second half of the OFDM frame:

$$X_{\rm f}(N-m) = X_{\rm f}^{*}(m), \quad m = 1, 2, 3, ..., N/2-1, \qquad (1)$$

where * denotes a complex conjugate.

After performing the inverse fast Fourier transform (IFFT), $X_f(m)$ is converted to a real-valued time domain signal, $x(k)$. The $x(k)$ samples are anti-symmetric within each OFDM frame, where:

$$x(k) = -x(\frac{N}{2}+k), \quad k = 0, 1, ..., N/2-1. \qquad (2)$$

The IM/DD communication system requires a unipolar modulation signal. Therefore, the negative values of $x(k)$ need to be clipped before transmission. As a result, the non-negative signal $x_{\rm clip}(k)$ is obtained. Since the time domain signal block is anti-symmetric, clipping the negative samples does not destroy any information in $x(k)$ [5]. After passing through the parallel-to-serial (P/S), the digital-to-analogue (D/A) and the electrical-to-optical (E/O) converters, the signal is transmitted through the optical channel.

B. Channel Model

Since the optical wireless channel has a relatively small root-mean-square (RMS) delay spread [10], for many practical realisations, the channel can safely be considered as a flat fading channel and, consequently, it can be characterised by an optical path gain, $g_{\rm h(opt)}$. Therefore, the performance of the different ACO-OFDM receivers is evaluated in a flat AWGN channel, where the received electrical signal $\tilde{x}_{\rm rx}(k)$ can be represented as:

$$\tilde{x}_{\rm rx}(k) = r g_{\rm h(opt)} x_{\rm clip}(k) + n(k), \qquad (3)$$

where $n(k)$ is a zero-mean real-valued bipolar AWGN at the receiver end, r is the optoelectronic conversion factor which is assumed to be one.

In this work, the electrical signal-to-noise ratio (SNR), $\text{SNR}_{\rm elec}$, is used to evaluate the performance of different ACO-OFDM receivers. This is defined as:

$$\text{SNR}_{\rm elec} = \frac{E_{\rm b(elec)}}{N_0} \qquad (4)$$

where $N_0/2$ is the two-sided power spectral density of the AWGN. The electrical energy per bit, $E_{\rm b(elec)}$, is defined as:

$$E_{\rm b(elec)} = \frac{P_{\rm elec}}{B\eta} = \frac{\text{E}[z_{\rm elec}^2(s[t])]}{B\eta} \qquad (5)$$

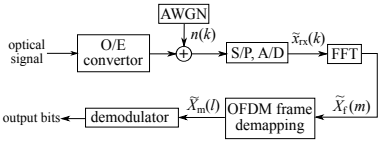

Fig. 2. Block diagram of a 'No Detection' ACO-OFDM receiver.

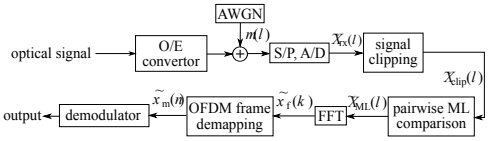

Fig. 3. Block diagram of a 'ML with Clip' ACO-OFDM receiver.

where $\text{E}[\cdot]$ is the statistical expectation, $P_{\rm elec}$ is the average electrical power of the signal, $z_{\rm elec}(s[t])$ is the current signal at the photo diode (PD), B is the signal bandwidth and η is spectral efficiency (bits/s/Hz).

III. Receiver Designs

A. Current ACO-OFDM Receivers

Figure 2 displays the block diagram of an ACO-OFDM receiver design which is initially proposed in [5] and referred to as the 'No Detection' receiver. At the receiver, the input optical signal is converted to an electrical signal by an optical-to-electrical (O/E) converter. The electrical signal is distorted by a zero-mean bipolar AWGN, $n(k)$, which is caused by shot noise and thermal noise at the receiver. After analogue-to-digital (A/D) and serial-to-parallel (S/P) conversion, the electrical signal $\tilde{x}_{\rm rx}(k)$ is obtained. For the 'No Detection' receiver, $\tilde{x}_{\rm rx}(k)$ is simply demodulated in the conventional way for OFDM. The $\tilde{x}_{\rm rx}(k)$ samples are directly passed through an FFT block and converted to the frequency domain signal, $\tilde{X}_{\rm f}(m)$. After OFDM frame demapping, the signal $\tilde{X}_{\rm m}(l)$ is demodulated using a maximum likelihood (ML) M-QAM detector.

To mitigate the AWGN power, an alternative receiver design for ACO-OFDM is proposed in [8]. The receiver termed 'ML with Clip', is illustrated in Fig. 3. This receiver adds two additional processing steps. They are applied to the electrical signal, $\tilde{x}_{\rm rx}(k)$. Firstly, the negative values in $\tilde{x}_{\rm rx}(k)$ are clipped to zero. Then, the clipped signal, $\tilde{x}_{\rm clip}(k)$, is compared pairwise and modified as:

$$\begin{cases} \tilde{x}_{\rm clip}(k) = 0, & \tilde{x}_{\rm clip}(k) \le \tilde{x}_{\rm clip}(k+N/2) \\ \tilde{x}_{\rm clip}(k+N/2) = 0, & \tilde{x}_{\rm clip}(k) > \tilde{x}_{\rm clip}(k+N/2) \end{cases}, \qquad (6)$$

where $k = 0, 1, ..., N/2-1$.

If $\tilde{x}_{\rm clip}(k)$ is greater than $\tilde{x}_{\rm clip}(k+N/2)$, the receiver decides that $\tilde{x}_{\rm clip}(k)$ is the signal sample and $\tilde{x}_{\rm clip}(k+N/2)$ is the noise sample which is set to zero. In contrast, if $\tilde{x}_{\rm clip}(k)$ is less than $\tilde{x}_{\rm clip}(k+N/2)$, then $\tilde{x}_{\rm clip}(k+N/2)$ is the signal sample and $\tilde{x}_{\rm clip}(k)$ is set to zero. If the receiver successfully estimates the position of the signal sample and discards the noise sample, half of the noise power is removed. However, since the noise is

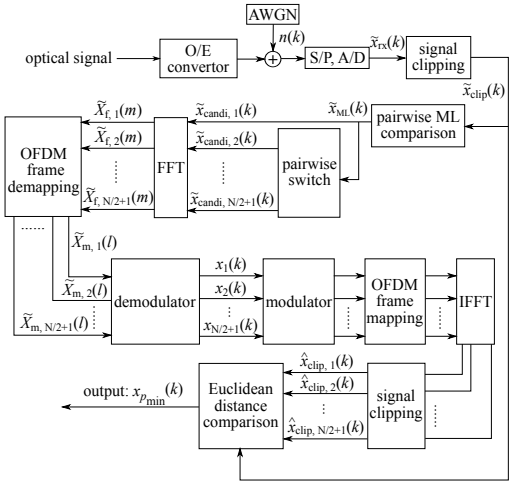

Fig. 4. Block diagram of a 'Proposed Receiver I'.

Gaussian distributed, the amplitude of the noise sample may be higher than the signal sample. In this case, the receiver fails to make the right decision which not only affects the amplitude of the signal sample but reverses the original sign as well. Therefore, this degrades the performance of the 'ML with Clip' receiver.

B. Proposed Receiver I

Since an incorrect decision of the pairwise ML comparison module in the 'ML with Clip' receiver may significantly affect the result of signal decoding, a possibility for improving this receiver design is to increase the probability of an 'ML with Clip' receiver to make a correct decision. Ideally, if we design a receiver that compares every possible combination of the positions of the signal samples and then selects the one that has the smallest Euclidean distance relative to the received signal, it can achieve a similar performance to the receiver that has perfect knowledge of the position of the signal samples. However, the number of all possible position combinations of the signal samples is $2^{N/2}$ which is not practical when the number of the FFT subcarriers, N, is large. Therefore, we propose a new receiver which is of less computational complexity.

The block diagram of 'Proposed Receiver I' is shown in Fig. 4. 'Proposed Receiver I' has the same structure as the 'ML with Clip' receiver before the FFT operation, where the signal, $\tilde{x}_{\text{ML}}(k)$, is obtained as a result of the pairwise ML comparison. Compared to the 'ML with Clip' receiver, the 'Proposed Receiver I' generates another $N/2$ candidates based on $\tilde{x}_{\text{ML}}(k)$ for further comparison. As shown in Fig. 4, the first candidate, $\tilde{x}_{\text{candi,1}}(k)$, is identical to $\tilde{x}_{\text{ML}}(k)$. The rest of the candidates, $\tilde{x}_{\text{candi},p}(k)$, are generated by a pairwise switch module which can be represented as:

$$\begin{aligned}
&\tilde{x}_{\text{candi},p}(p-2) = 0, \\
&\qquad\qquad \text{if } \tilde{x}_{\text{clip}}(p-2) > \tilde{x}_{\text{clip}}(p-2+N/2) \\
&\tilde{x}_{\text{candi},p}(p-2+N/2) = \tilde{x}_{\text{clip}}(p-2+N/2), \\
&\qquad\qquad \text{if } \tilde{x}_{\text{clip}}(p-2) > \tilde{x}_{\text{clip}}(p-2+N/2) \\
&\tilde{x}_{\text{candi},p}(p-2+N/2) = 0, \\
&\qquad\qquad \text{if } \tilde{x}_{\text{clip}}(p-2) \le \tilde{x}_{\text{clip}}(p-2+N/2) \\
&\tilde{x}_{\text{candi},p}(p-2) = \tilde{x}_{\text{clip}}(p-2), \\
&\qquad\qquad \text{if } \tilde{x}_{\text{clip}}(p-2) \le \tilde{x}_{\text{clip}}(p-2+N/2) \\
&\tilde{x}_{\text{candi},p}(k) = \tilde{x}_{\text{ML}}(k), \qquad\qquad \text{otherwise}
\end{aligned} \quad , \quad (7)$$

where $p = 2, 3, ..., N/2+1$. After all candidates are generated, they are passed through the FFT, the OFDM frame demapping and the demodulation stages. This yields a series of candidate output signals, $x_p(k)$, $p = 1, 2, ..., N/2$. In order to choose the most suitable output signal, each $x_p(k)$ is remodulated into an OFDM frame. After the IFFT and the signal clipping operations, we obtain the time-domain unipolar versions of the candidate signals, $\hat{x}_{\text{clip},p}(k)$, $p = 1, 2, ..., N/2$. The Euclidean distances between $\hat{x}_{\text{clip},p}(k)$ and $\tilde{x}_{\text{clip}}(k)$ are calculated and the candidate with the least Euclidean distance measure is determined:

$$p_{\text{min}} = \arg\min_{p} \sum_{k=0}^{N-1} (\hat{x}_{\text{clip},p}(k) - \tilde{x}_{\text{clip}}(k))^2, \quad (8)$$

and the corresponding bit sequence is selected as the output.

Compared to the 'ML with Clip' receiver, the 'Proposed Receiver I' can correct one error from the pairwise ML comparison module by choosing the candidate with the smallest Euclidean distance relative to the received signal. This feature is especially beneficial when the pairwise ML comparison module makes a mistake on a sample with a large absolute value. An incorrect decision on such a sample would significantly enlarge the Euclidean distance between the candidate and the received signal. This means that it is easier for the 'Proposed Receiver I' to detect the error. In addition, the incorrect decision on a sample with a large absolute value has a higher probability to cause bit errors than the incorrect decision on a sample with a small absolute value. Therefore, the 'Proposed Receiver I' is expected to reduce the bit error ratio (BER) compared to the 'ML with Clip' receiver.

C. Proposed Receiver II

Another receiver design, 'Proposed Receiver II', is illustrated in Fig. 5. This receiver design is inspired by the receiver design in [9]. Instead of correcting the errors introduced by the pairwise ML comparison module, the 'Proposed Receiver II' directly fixes the errors in the output bits. The first part of the 'Proposed Receiver II' is the same as the 'ML with Clip' receiver and the output bit stream, $x(k)$, is obtained. When the switch is turned on, $x(k)$ is simultaneously split into two paths. In the first path, the input remains unchanged and is denoted as $x_{\text{u}}(k)$. The bit stream $x_{\text{u}}(k)$ is passed through the four modules: the QAM modulator, the OFDM frame mapping,

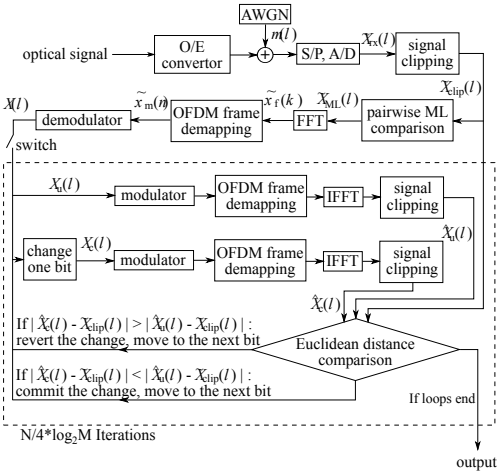

Fig. 5. Block diagram of a 'Proposed Receiver II'.

the IFFT and the signal clipping module. Then, a signal $\hat{x}_{\mathrm{u}}(k)$ is obtained. In the other path, the first bit of the output bit streams, $x(k)$, is changed and the changed signal is denoted as $x_{\mathrm{c}}(k)$. The bit stream $x_{\mathrm{c}}(k)$ is converted to $\hat{x}_{\mathrm{c}}(k)$ by passing through the four modules which is same as in the first path.

The two signals, $\hat{x}_{\mathrm{u}}(k)$ and $\hat{x}_{\mathrm{c}}(k)$, are compared in terms of the Euclidean distance to $\tilde{x}_{\mathrm{clip}}(k)$. The Euclidean distance measure between $\hat{x}_{\mathrm{u}}(k)$ and $\tilde{x}_{\mathrm{clip}}(k)$ is:

$$d_1 = \sum_{k=0}^{N-1} (\hat{x}_{\mathrm{u}}(k) - \tilde{x}_{\mathrm{clip}}(k))^2. \tag{9}$$

The Euclidean distance between $\hat{x}_{\mathrm{c}}(k)$ and $\tilde{x}_{\mathrm{clip}}(k)$ is:

$$d_2 = \sum_{k=0}^{N-1} (\hat{x}_{\mathrm{c}}(k) - \tilde{x}_{\mathrm{clip}}(k))^2. \tag{10}$$

If d_1 is less than d_2, the unchanged signal, $x_{\mathrm{u}}(k)$, becomes the input to the next iteration. However, if d_1 is greater than d_2, the changed signal, $x_{\mathrm{c}}(k)$, becomes the input to the next iteration. For iteration n, the n-th bit of the input is taken into consideration and the processing operations are the same in every iteration. The procedure continues until the last bit of the signal is reached. Finally, the output signal is obtained.

IV. Computational Complexity

In this section, we discuss the computational complexity of the ACO-OFDM receivers. We assume that the computational complexity of the IFFT and the FFT stages is significantly higher than the computational complexity of the other stages in the ACO-OFDM receivers. The computational complexity order of the IFFT and the FFT stages can be denoted as $\mathrm{O}(N \log_2 N)$. Here, $\mathrm{O}(\cdot)$ is a function that describes the equivalent growth rate of a function when the value of N and M tends toward infinity.

Since the 'No Detection' receiver and the pairwise ML receiver includes a single IFFT operations, their order of the computational complexity is $\mathrm{O}(N \log_2 N)$. In the case of 'Proposed Receiver I', as the number of IFFT and FFT operations increases linearly with the number of OFDM subcarriers, the 'Proposed receiver I' has a computational complexity of $\mathrm{O}(N^2 \log_2 N)$. In the case of 'Proposed Receiver II', the number of IFFT and FFT modules increases linearly with not only the number of OFDM subcarriers, N, but with the constellation size M as well. Therefore, 'Proposed Receiver II' has the highest order of the computational complexity which is denoted as $\mathrm{O}\left(N^2 \log_2 N \log_2 M\right)$.

V. Simulation Results

In this section, the performances of 'Proposed Receiver I' and 'Proposed Receiver II' are evaluated. The number of subcarriers per OFDM frame, N, is 64 [10]. The channel attenuation factor, $g_{h(opt)}$, is assumed to be 1 for simplicity. Also, Gray coding is applied in both the modulators and the demodulators for the best BER performance. As a lower performance bound, we use the BER performance of the 'No Detection' receiver, where no AWGN is removed [5]. The 'ML with clip' receiver from [8] is evaluated for comparison purposes. As an upper bound of the performance, an ideal receiver is simulated and denoted as 'Genie Rx with Clip' [8]. This receiver has perfect knowledge of the position of the time domain samples. In all scenarios, we compare the performance of different ACO-OFDM receivers in terms of the electrical SNR, defined in (4) for a BER of up to 10^{-4}.

A. 4-QAM ACO-OFDM

The SNR versus the BER performance of 4-QAM ACO-OFDM is shown in Fig. 6. Among all ACO-OFDM receivers, the 'No Detection' receiver has the worst performance as expected. The 'ML with Clip' receiver exhibits approximately a 1.5 dB SNR improvement over the 'No Detection' receiver for a BER of 10^{-4} since the Gaussian noise is partially suppressed. 'Proposed Receiver I' demonstrates a 0.5 dB SNR improvement over the 'ML with Clip' receiver and a 2 dB SNR improvement over the 'No Detection' receiver for a BER of 10^{-4}. This is because 'Proposed Receiver I' can correct one comparison error made by the comparison module of the 'ML with Clip' receiver. The 'Proposed Receiver II' further improves the BER performance with a 1 dB SNR gain over the 'ML with Clip' receiver and 2.5 dB SNR gain over the 'No Detection' receiver. This is because 'Proposed Receiver II' can correct bit errors caused by the pairwise comparison module. Finally, as expected, the 'Genie Receiver with Clip' achieves a 3-dB improvement over the 'No Detection' Receiver since it can always correctly clip the noise samples which removes half of the Gaussian noise. The presented results clearly indicate that the proposed receivers shift the BER performance of the ACO-OFDM system closer to the upper limit of the BER performance. 'Proposed receiver II', in particular, is only 0.5 dB away from the maximum achievable performance.

B. 16-QAM ACO-OFDM

The SNR versus the BER performance of 16-QAM ACO-OFDM is shown in Fig. 7. Similar to the scenario of

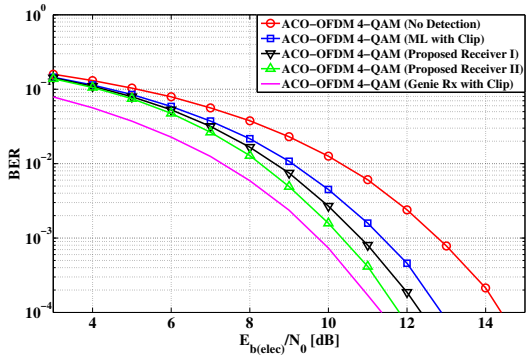

Fig. 6. BER performance for different ACO-OFDM receiver designs in a flat linear AWGN communication channel. (4-QAM).

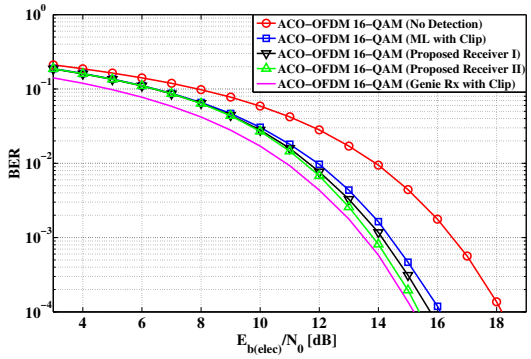

Fig. 7. BER performance for different ACO-OFDM receiver designs in a flat linear AWGN communication channel. (16-QAM).

4-QAM ACO-OFDM, the 'No Detection' receiver has the worst performance among all ACO-OFDM receivers. The 'ML with Clip' receiver demonstrates a 2.1 dB improvement over the 'No Detection' receiver. This improvement is 0.6 dB higher compared to the improvement in 4-QAM ACO-OFDM. This is because a symbol from a larger QAM constellation has a higher average energy when the $E_{\mathrm{b(elec)}}/N_0$ is fixed. Therefore, the power of a time domain sample of 16-QAM is higher than that of 4-QAM which improves the ability of the 'ML with Clip' receiver to correctly estimate the position of a signal sample. Both 'Proposed Receiver I' and 'Proposed Receiver II' outperform the 'ML with Clip' receiver in terms of BER. In particular, the BER performance of 'Proposed Receiver II' is closest to the performance limit, where the difference is only about 0.1 dB.

C. Complexity vs. Performance

According to the previous discussion, we can see a tradeoff between computational complexity and the BER performance for the different ACO-OFDM receivers. 'Proposed Receiver II' has the best performance but also has the highest order of computational complexity, $\mathrm{O}(N^2 \log_2 N \log_2 M)$. With a decreased order of the computational complexity, $\mathrm{O}(N^2 \log_2 N)$, 'Proposed Receiver I' has a slightly decreased BER performance than 'Proposed Receiver II'. With the lowest order of computational complexity, $\mathrm{O}(N \log_2 N)$, the 'ML with Clip' receiver has an even worse performance. In practice, the receivers should be chosen carefully according to the computational capacity of the hardware and the requirement for system performance. In general, 'Proposed Receiver I' strikes the best compromise between complexity and performance.

VI. Conclusion

In this paper, we proposed two new receiver designs for ACO-OFDM. 'Proposed Receiver I' delivers an up to 0.5 dB improvement over the state-of-the-art 'ML with Clip' receiver. 'Proposed Receiver II' delivers an up to 1.0 dB improvement over the 'ML with Clip' receiver, which is only 0.5 dB away from the upper limit of the BER performance. Both 'Proposed Receiver I' and 'Proposed Receiver II' have a higher computational complexity than the 'ML with Clip' receiver. The tradeoff between computational complexity and BER performance needs to be considered when choosing the most suitable ACO-OFDM receiver for a VLC system.

Acknowledgement

We gratefully acknowledge support by the School of Engineering and the Institute for Digital Communications (IDCOM) at the University of Edinburgh for providing a scholarship for this work which is aligned to the Engineering and Physical Sciences Research Council (EPSRC) project EP/K00042X/1.

References

[1] T. Komine and M. Nakagawa, "Fundamental Analysis for Visible–Light Communication System using LED Lights," *IEEE Transactions on Consumer Electronics*, vol. 50, no. 1, pp. 100–107, Feb. 2004.

[2] D. Tsonev, H. Chun, S. Rajbhandari, J. McKendry, S. Videv, E. Gu, M. Haji, S. Watson, A. Kelly, G. Faulkner, M. Dawson, H. Haas, and D. O'Brien, "A 3-Gb/s Single-LED OFDM-based Wireless VLC Link Using a Gallium Nitride μLED," vol. 99 (to appear), p. 4, 2014.

[3] D. Tsonev, S. Sinanović, and H. Haas, "Novel Unipolar Orthogonal Frequency Division Multiplexing (U-OFDM) for Optical Wireless," in *Proc. of the Vehicular Technology Conference (VTC Spring)*, IEEE. Yokohama, Japan: IEEE, May 6–9 2012.

[4] J. M. Kahn and J. R. Barry, "Wireless Infrared Communications," *Proc. IEEE*, vol. 85, no. 2, pp. 265–298, Feb. 1997.

[5] J. Armstrong and A. Lowery, "Power Efficient Optical OFDM," *Electronics Letters*, vol. 42, no. 6, pp. 370–372, Mar. 16, 2006.

[6] J. Armstrong, B. Schmidt, D. Kalra, H. Suraweera, and A. Lowery, "Spc07-4: Performance of asymmetrically clipped optical ofdm in awgn for an intensity modulated direct detection system," in *Global Telecommunications Conference, 2006. GLOBECOM '06. IEEE*, 2006, pp. 1–5.

[7] S. Wilson and J. Armstrong, "Transmitter and receiver methods for improving asymmetrically-clipped optical ofdm," *IEEE Trans. Wireless Commun.*, vol. 8, no. 9, pp. 4561–4567, 2009.

[8] K. Asadzadeh, A. Dabbo, and S. Hranilovic, "Receiver Design for Asymmetrically Clipped Optical OFDM," in *GLOBECOM Workshops (GC Wkshps)*, IEEE. Houston, TX, USA: IEEE, Dec., 5–9 2011, pp. 777–781.

[9] J. Guerreiro, R. Dinis, and P. Montezuma, "Approaching the maximum likelihood performance with nonlinearly distorted ofdm signals," in *2012 IEEE 75th Vehicular Technology Conference (VTC Spring)*, 2012, pp. 1–5.

[10] S. Dimitrov, S. Sinanovic, and H. Haas, "Clipping Noise in OFDM-based Optical Wireless Communication Systems," *IEEE Transactions on Communications (IEEE TCOM)*, vol. 60, no. 4, pp. 1072–1081, Apr. 2012.

IEEE ICC 2015 - Optical Networks and Systems Symposium

Space Division Multiple Access in Visible Light Communications

Zhe Chen, Harald Haas
Institute for Digital Communications
Li-Fi R&D Centre
School of Engineering
The University of Edinburgh
EH9 3JL, Edinburgh, UK
{z.chen, h.haas}@ed.ac.uk

***Abstract*—In this paper, a visible light communication (VLC) system adopting space division multiple access (SDMA) is proposed. In the optical SDMA system, a conventional single-element transmitter is substituted by an angle diversity transmitter which can simultaneously serve multiple active users in different positions. In the simulation, two spatial partition schemes, random grouping and optimal grouping, are implemented which demonstrate the lower bound and the upper bound of the system throughput gain for the optical SDMA system, respectively. The results indicate that the optical SDMA significantly outperforms conventional optical time division multiple access (TDMA). In specific, it has been found that an optical SDMA can achieve over 10 times higher system throughput compared with optical TDMA.**

I. Introduction

Recently, visible light communication (VLC) technology has emerged as a complementary alternative to current radio frequency (RF) techniques [1]. Transmission speeds of 3 Gbps from a single colour light-emitting diode (LED) have been reported in [2]. In contrast to RF communication systems, VLC operates in an entirely unregulated part of the electromagnetic spectrum and is safe to use in the environments sensitive to electromagnetic interference (EMI).

In a multi-user system, time division multiple access (TDMA) is a multiple access scheme which has been widely used. By assigning information for different users to different time slots, all users can be served by using the same communication bandwidth. The throughput of the TDMA system is limited since only one user can be served in a time slot which cannot effectively exploit the common bandwidth resource. In order to overcome the system throughput limitation, a spatial dimension is added to the conventional TDMA system. In RF, a well-known method is space division multiple access (SDMA) [3] which is integrated as a part of 4G communication standard such as LTE and IEEE802.11ac [4]. In SDMA, an antenna array is used as the transmitter and this can simultaneously generate multiple narrow beams according to the positions of the active users. In this way, multiple users can be served within the same time slot.

Although SDMA shows a promising performance in RF, it cannot be directly implemented into VLC. One of the key issues is the transmitter. In RF, directional narrow-beam signals are generated by changing the amplitude and phase of the signals on an antenna array. However, this cannot be realised in VLC because it is an intensity modulation and direct detection (IM/DD) system. In VLC, LEDs have an inherent feature of limited field-of-view (FOV). This feature is perfect for generating directional light beams. Therefore, in optical SDMA, an angle diversity transmitter which consists of multiple directional narrow FOV LED elements is used as the optical transmitter. By turning on different transmitter elements, the angle diversity transmitter can generate narrow light beams of different directions.

In previous work, a simple optical wireless system consisting of multi-beam transmitters and imaging diversity receivers is proposed [5]. Unfortunately, this system fails to support multiple access and the mobility of the system is significantly restricted by the imaging optical receiver. In [6], an optical wireless system adopting SDMA is studied. However, only an uplink scenario is simulated and the SDMA for the downlink is not considered. In [7], a cellular VLC system is proposed which can achieve a high system throughput by exploiting the benefit of frequency reuse and angle diversity receiver. However, the spatial dimension of optical transmitter is not exploited in this scenario.

In this study, optical SDMA is realised by using the angle diversity transmitter which enables parallel transmissions. Simulation results show that a VLC system implementing optical SDMA can significantly outperform the conventional optical TDMA system where a maximum throughput gain of over 10 is obtained.

The remainder of this paper is organised as follows. The system model is given in Section II. The concept of optical TDMA is introduced in Section III. The concept of optical SDMA is introduced in Section IV. A grouping strategy of optical SDMA is given in Section V. The simulation results are presented and discussed in Section VI. Finally, Section VII concludes the paper.

II. System Model

In this study, only the impact of line-of-sight (LOS) paths of the light fixtures is considered. The direct current (DC) gain of the LOS link can be accurately calculated as follows [8]:

$$H_0 = \frac{(m+1)A_{\text{eff}}}{2\pi d^2}\cos^m(\phi)\cos(\psi)\text{rect}\left(\frac{\psi}{\Psi_{\text{fov}}}\right), \quad (1)$$

where d is the distance between an optical transmitter and its corresponding receiver; Ψ_{fov} is the FOV of the optical receiver; m is the Lambertian order of the optical transmitter

978-1-4673-6432-4/15/$31.00 ©2015 IEEE

and is a function of the transmitter half-intensity radiation angle Φ_{tx} as $m = -1/\log_2(\cos(\Phi_{\mathrm{tx}}))$; ϕ is the angle of irradiance; ψ is the angle of light incidence at the receiver; $\mathrm{rect}(\mathrm{x})$ is the unit step function. The effective signal collection area A_{eff} is given as:

$$A_{\mathrm{eff}} = A_{\mathrm{p}} G \frac{n_{\mathrm{ref}}^2}{\sin^2(\Psi_{\mathrm{fov}})}, \tag{2}$$

where n_{ref} is the refractive index of the receiver optics; A_{p} is the physical area of the optical receiver; G is the signal transmission gain of the optical filter.

III. Optical TDMA

In this study, the optical TDMA scenario is set as the baseline for the optical SDMA scenario. In a TDMA scenario, a light fixture is adapted as an optical access point (AP) for the purpose of communication. The light fixture is assumed to be a point source pointing downwards. Since TDMA is assumed in this scenario, the optical AP can only serve one active user in one time slot. The received signal to noise ratio (SNR) of an active user can be expressed as:

$$\gamma_k = \frac{(rH_k P_{\mathrm{tx}})^2}{N_0 B}, \tag{3}$$

where r is the optical-to-electric conversion efficiency; H_k is the channel attenuation between the optical AP and the optical receiver of user k; N_0 is the additive white Gaussian noise (AWGN) power spectral density; and B is the communication bandwidth.

In optical TDMA, each active user shares the same frequency bandwidth by dividing the transmission frames into different time slots of identical length. Therefore, the overall throughput of the optical TDMA system is calculated as:

$$T_{\mathrm{TDMA}} = \frac{1}{K} \sum_{k=1}^{K} B \log_2(1+\gamma_k), \tag{4}$$

where K is the number of the active users.

By using TDMA, users are arbitrarily assigned to different time slots. Since only one user is active at a time slot, there is no mutual interference between users. However, this assignment significantly limits the overall throughput since the bandwidth resource cannot be effectively shared.

IV. Optical SDMA

In order to boost the system throughput, one of the most effective ways is to enable parallel transmissions to multiple users in the same time slot. However, parallel transmissions will introduce multi-user access interference between active users. Therefore, SDMA is introduced. SDMA is a multiple access scheme that supports parallel transmissions to spatially separated users. In order to avoid significant multi-user access interference, the spatial transmission profile of the transmitters and receivers have to be controlled. Angular diversity transmitters are perfectly suited for this purpose.

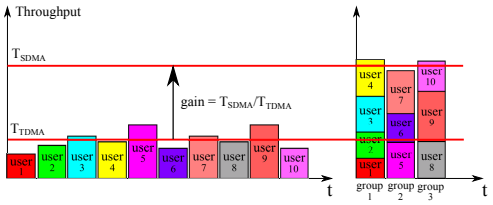

Fig. 1. The example of improving system throughput realised by grouping 10 active users into 3 spatial groups.

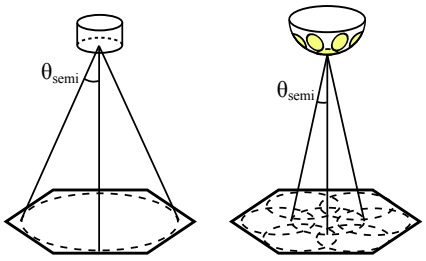

Fig. 2. The layout of the optical TDMA scenario with a conventional single-element optical transmitter (left) and the layout of the optical SDMA scenario with an angle diversity optical transmitter (right).

A. SDMA vs. TDMA

SDMA was initially implemented in RF systems [9]. The mechanism of SDMA is illustrated in Fig. 1. For SDMA, the multiple active users are grouped into one time slot which would otherwise be occupied by only one active user in TDMA. For example, by using TDMA, the optical AP takes four time slots to serve four different users 1,2,3,4 and, in SDMA, this transmission to multiple users can be performed within only one time slot. This provides a large potential improvement in overall throughput. However, grouping has disadvantages: firstly, in order to support parallel and directional transmissions, multi-element transmitters are required; secondly, if users are grouped incorrectly, the multi-user access interference is high so that the data rate of each user in the group will be compromised significantly. To address these issues, an angle diversity transmitter and an optimal spatial grouping strategy are used in the SDMA system. Both techniques are introduced in the following sections.

B. Angle Diversity Transmitter

In RF, a SDMA transmitter is realised by using antenna arrays which could generate multiple narrow beams simultaneously [9]. In order to realise the same function in optical wireless communication, an angle diversity transmitter is required. The layout of an angle diversity transmitter is illustrated in Fig. 2. It consists of multiple narrow beam LEDs attached to a semi-sphere base. These LED arrays can achieve the same coverage area as the conventional optical transmitter in a TDMA scenario. One of the LEDs is located at the top of

the base and others are located symmetrically along the side of the base.

For SDMA in RF, the realisation of transmitters requires multiple RF chains and complex beam-steering algorithms. However, for optical SDMA, since an LED with narrow FOV can generate optical signals with narrow beams, complex algorithms for beamforming can be avoided. The parallel directional transmissions can be realised by turning on the LEDs that cover the areas of different active users.

C. Spatial Grouping

In optical SDMA, users cannot be arbitrarily grouped into different time slots since some users might be spatially close which results in overlapping beams and high multi-user access interference. Therefore, in the absence of adaptive beamforming, a carefully chosen spatial grouping is essential to achieve high throughput in an optical SDMA system.

In arithmetical terms, a spatial grouping is referred to as a partition $\mathcal{P} = \{G_1, G_2, G_3, ...\}$ of the set of the all active users U. Here, G_j represents a spatial group. For the purpose of fairness, all spatial groups are assumed to be mutual exclusive which means that one active user can only belong to one spatial group. Another assumption of spatial partitioning is that all spatial groups should be collectively exhaustive. This means that none of the active users in the system is unserved.

For spatial grouping, not every possible group partition is valid. This occurs when active users in the same group are not spatially separable. In optical SDMA, each LED element on an angle diversity transmitter serves a specific area. If more than one active users are in the area served by the same LED element, these active users cannot be allocated to the same spatial group. Otherwise, it is not possible to serve them simultaneously in only one time slot, which will leave some of the active users unserved.

D. A Performance Evaluation of SDMA Spatial Grouping

For a valid spatial partition $\mathcal{P}_l = \{G_1, G_2, G_3, ..., G_J\}$, the signal-to-interference-plus-noise-ratio (SINR) of active user u_i in spatial group G_j can be expressed as:

$$\gamma_{(u_i,G_j)} = \frac{\left(rP_{\mathrm{tx}}H_{(b,u_i)}\right)^2}{N_0 B + \sum_{b' \in \mathcal{B}_{\mathrm{inter}}^{(b,G_j)}} \left(rP_{\mathrm{tx}}H_{(b',u_i)}\right)^2}, \quad (5)$$

where r is the optical to electric conversion efficiency; P_{tx} is the transmission power of an LED and $H_{(b,u_i)}$ is the channel attenuation between the source LED b and user u_i. $\sum_{b' \in \mathcal{B}_{\mathrm{inter}}^{(b,G_j)}} \left(rP_{\mathrm{tx}}H_{(b',c)}\right)^2$ represents the interference power and $\mathcal{B}_{\mathrm{inter}}^{(b,G_j)}$ is the set of active interfering LEDs which serve the other users in group G_j.

In optical SDMA, each spatial group occupies a time slot. For each time slot, information for multiple active users is transmitted simultaneously. Therefore, the overall throughput of the optical SDMA can be calculated as:

$$T_{\mathrm{SDMA}} = \frac{1}{J}\sum_{j=1}^{J}\sum_{u_i \in G_j} B\log_2(1+\gamma_{(u_i,G_j)}), \quad (6)$$

TABLE I
THE BELL NUMBERS IN TERMS OF A n-ELEMENT SET.

n	1	2	3	4	5
Bell Numbers	1	2	5	15	52
n	6	7	8	9	10
Bell Numbers	203	877	4140	21147	115975

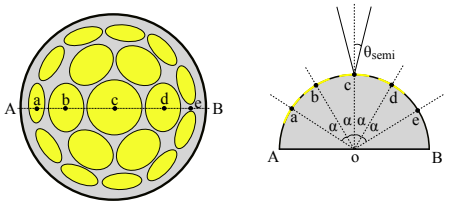

Fig. 3. The shape of a 18-element angle diversity transmitter (N_{Tx} = 18).

where J is the total number of spatial groups. Each spatial group take one time slot for data transmission.

Since different spatial partitions and the relative positions of active users can significantly affect the throughput of the optical SDMA system, a metric to evaluate the performance of optical SDMA is essential. Here, the throughput gain is defined as:

$$x = \frac{T_{\mathrm{SDMA}}}{T_{\mathrm{TDMA}}}. \quad (7)$$

The total number of active users and the position of each active user is identical in both the optical TDMA and the optical SDMA scenario. Therefore, the gain is purely from the implementation of the angle diversity transmitter and spatial grouping strategies.

V. Grouping Strategy

Optimal grouping is a method that determines the best spatial partition by exhaustive search. Firstly, all possible partitions of active users are generated as candidates. Here, Bell number is used to determine the total number of candidates. In combinatorial mathematics, the Bell number represents the number of all possible partitions of an n-element set [10]. The number of all possible spatial partitions for active users of different number are listed in Table I. As the number of active users increases, a steep increase in the number of possible spatial partitions can be observed.

After all candidates are generated, the validation of each candidate is checked in order to guarantee that none of active users is left unserved in each candidate. Then, the invalid candidates are discarded. For each valid partition, the throughput gain is calculated and compared. Finally, the partition with the best throughput gain is chosen as the result. By implementing optimal grouping, the upper bound of the throughput gain for an optical SDMA system can be achieved.

VI. Simulation Results

A. Simulation Parameters

In the simulation, all active users are assumed to be within an hexagonal area with a radius of 3 m. An angle diversity

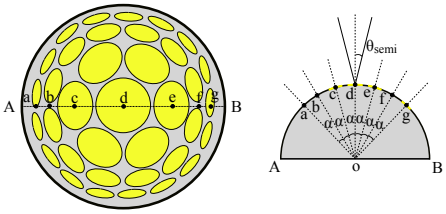

Fig. 4. The shape of a 36-element angle diversity transmitter (N_{Tx} = 36).

TABLE II
SIMULATION PARAMETERS

Responsivity, r	0.5 A/W
The gain of the optical filter, G	1
Refractive index, n	1.5
Modulation Bandwidth, B	20 MHz
AWGN spectral density, N_0	1×10^{-21}A/Hz

transmitter is placed at the centre of the hexagon at a height of 3 m. An angle diversity transmitter consists of several branches. The first branch is the LED at the centre of a semi-sphere. Then, new branches are added as a ring of LEDs with an increasing radius around the central branch. Here, two types of angle diversity transmitters are considered, as illustrated in Fig. 3 and Fig. 4. One has three branches ($N_{\mathrm{tx}} = 18$, $\alpha = 18^{\mathrm{o}}$, $\Phi_{\mathrm{tx}} = 4.5^{\mathrm{o}}$) and the other one has four branches but with narrower FOV for each transmitter element ($N_{\mathrm{tx}} = 36$, $\alpha = 12.9^{\mathrm{o}}$, $\Phi_{\mathrm{tx}} = 3.2^{\mathrm{o}}$). Here, Φ_{tx} is the transmitter half-intensity radiance angle and α is the angle between each neighbouring branches of LEDs. The total number of LEDs of the angle diversity transmitter is represented as N_{tx}. The total number of users in the system is represented as K. In the case of TDMA, a conventional single-element optical transmitter is used. The half-intensity radiance angle of the conventional optical transmitter is assumed to be 45^{o} which guarantees the same equivalent half-intensity radiance angle for all types of optical transmitters. For the purpose of fairness, the transmission power of the conventional optical transmitter is equal to the sum of the transmission power of all LEDs in the angle diversity transmitter. The transmission power of optical transmitter in this study is set as 2 W. Table II shows the other simulation parameters.

B. The Simulation Setups

In total, $10,000$ scenario snapshots are generated for each number of the active users. For each snapshot, the positions of the K active users are generated and these follow a uniform distribution in the hexagon area. By calculating and comparing the system throughput of optical TDMA and SDMA for each snapshot, the cumulative distribution function (CDF) of the throughput gain can be determined. Moreover, random grouping is also considered in the simulation. For random grouping, only a random spatial partition is used in each snapshot. Therefore, the results of the random grouping indicate the lower bound of the system throughput gain.

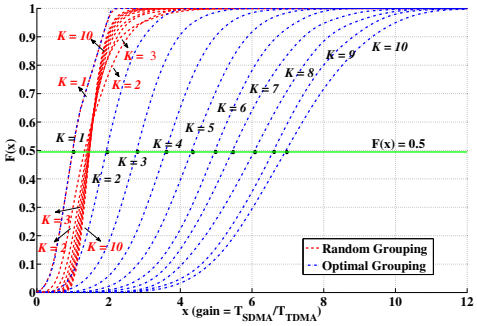

Fig. 5. The CDF of the throughput gains for different number of active users. (N_{tx} = 18).

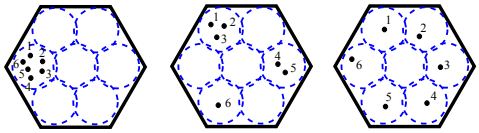

Fig. 6. Three typical relative positions of active users. 1. All active users are close to each other (left). 2. Some of the active users are close to each other (middle). 3. All active users are well-separated (right).

C. Results Analysis

Fig. 5 illustrates the performance of the throughput gain when an 18-element angle diversity transmitter is used. When random grouping is implemented, the overall throughput gain of the system is low. In most of the scenario snapshots, the throughput gains are below 2 and, for some snapshots, the gains are lower than 1 which means, in this case, optical SDMA performs even worse then optical TDMA. Moreover, there is no significant improvement in the throughput gain when the number of the active users K increases. The reason for this is that, for random grouping, active users close to each other may be incorrectly allocated to the same spatial group. This means that these users will experience strong interference which results in a low system throughput.

Compared with the random grouping, the overall throughput gain of the optimal grouping scheme is significantly higher. Also, the dynamic range of the throughput gain is much wider. This is because, for the optimal grouping scheme, the throughput gain mainly depends on the relative position of active users. For example, in Fig. 6, three typical relative positions of active users are illustrated. For the first scenario, all active users are close to each other and within the region that is served by the same transmitter element. The only valid spatial grouping for this scenario is to allocate all active users into six different groups, which is the same as in optical TDMA. Hence, no throughput gain can be achieved. For the second scenario, some of the active users are clustered together. Since there are a maximum of three active users within the area that is served by the same optical transmitter

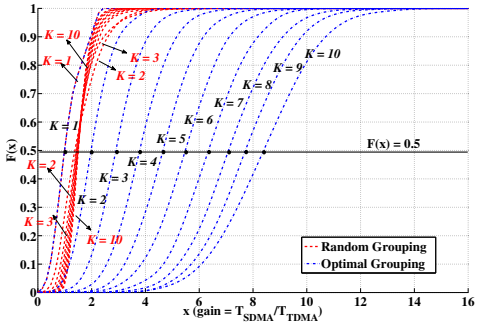

Fig. 7. The CDF of the throughput gains for different number of active users. ($N_{\text{tx}} = 36$).

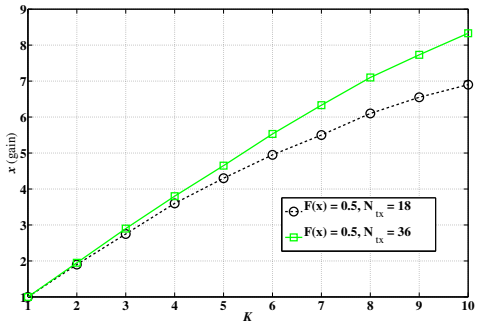

Fig. 8. The comparison of throughput gains when optimal grouping strategy is implemented. The system gains for different number of active users are chosen when $F(x) = 0.5$ in the previous scenarios.

element, at least three groups are required. As a result, the best throughput gain that can be achieved is around two. For the last scenario, each of the active users are well separated. Only one spatial group is required and the best throughput gain can be achieved is around six. As shown in Fig. 5, the overall throughput increases when an optical transmitter serves more active users. This is because, by implementing optimal grouping strategy, interference from the overlapping beams in the same time slot can be significantly mitigated. When the number of active users increases, the angle diversity transmitter can serve more active users simultaneously without introducing significant interference. As a result, the overall system throughput is increased.

Fig. 7 illustrates the performance of the throughput gain when a 36-element angle diversity transmitter is used. The performance trend is similar to the previous scenario where an 18-element angle diversity transmitter is used. A comparison of the optimal grouping scheme between these scenarios is given in Fig. 8. The system gains for different number of active users are compared when $F(x) = 0.5$. The 36-element angle diversity transmitter has a better performance than 18-element angle diversity transmitter when the number of active users is the same. This improvement scales with the number of active users. When more users are served by the angle diversity transmitter, greater improvement can be obtained. This is because a transmitter with more elements can generate narrower light beams to serve multiple active users in parallel. When each of the light beam become narrower, the multi-user access interference between them becomes smaller. Therefore, a higher system throughput can be achieved.

VII. Conclusion

In this paper, a VLC system adopting optical SDMA is proposed. In this system, an angle diversity transmitter is used as the optical transmitter which can serve multiple active users in parallel. The results clearly indicate that the optical SDMA significantly outperforms the optical TDMA in terms of the system throughput. It is particular interesting that, in contrast to optical TDMA, the optical SDMA can achieve a system throughput improvement of over 10 times. This improvement is even higher when an angle diversity transmitter with a larger number of transmitting elements is used. This result is very promising since optical SDMA can significantly increase the system throughput of a VLC system without requiring additional transmission power and bandwidth resource. From an application perspective, the Internet-of-Things will require many different objects to be connected to the internet within one room. The purposed SDMA systems seems to be a very promising candidate for this purpose.

Acknowledgement

Prof. Harald Haas acknowledges support by the UK Engineering and Physical Sciences Research Council (EPSRC) under Grant EP/K008757/1.

References

[1] H. Elgala, R. Mesleh, and H. Haas, "Indoor Optical Wireless Communication: Potential and State-of-the-Art," *IEEE Commun. Mag.*, vol. 49, no. 9, pp. 56–62, Sep. 2011.

[2] D. Tsonev, H. Chun, S. Rajbhandari, J. J. D. McKendry, S. Videv, E. Gu, M. Haji, S. Watson, A. E. Kelly, G. Faulkner, M. D. Dawson, H. Haas and D. O'Brien, "A 3-Gb/s single-LED OFDM-based wireless VLC link using a Gallium Nitride μLED," *IEEE Photon. Technol. Lett*, vol. 26, no. 7, pp. 637–640, Apr. 2014.

[3] A. J. Paulraj and C. B. Papadias, "Space-time processing for wireless communications," *IEEE Signal Process. Mag.*, vol. 14, no. 6, pp. 49–83, Nov. 1997.

[4] I. P802.11, "IEEE802.11ac: The Next Evolution of Wi-Fi Standards," 2012.

[5] P. Djahani and J. M. Kahn, "Analysis of Infrared Wireless Links Employing Multibeam Transmitters and Imaging Diversity Receivers," *IEEE Trans. Commun.*, vol. 48, no. 12, pp. 2077–2088, Dec. 2000.

[6] K. Kawamoto, S. Miyamoto, and S. Sampei, "Spatial division and time division multiple access system based on intensity distribution for hybrid-LOS indoor optical wireless communication," in *1st International Conference on Space Optical Systems and Applications*, Tokyo, Japan, Apr. 4–6, 2009.

[7] Z. Chen, N. Serafimovski, and H. Haas, "Angle diversity for an indoor cellular visible light communication system," in *IEEE 79th Vehicular Technology Conference*, May 2014.

[8] J. M. Kahn and J. R. Barry, "Wireless Infrared Communications," *Proc. IEEE*, vol. 85, no. 2, pp. 265–298, Feb. 1997.

[9] L. Godara, "Application of Antenna Arrays to Mobile Communications. II. Beam-forming and Direction-of-arrival Considerations," *Proc. IEEE*, vol. 85, no. 8, pp. 1195 –1245, Aug. 1997.

[10] N. J. A. Sloane, *A Handbook of Integer Sequences*. Academic Press, NY, 1973.

TuD2.3 (Contributed)
11:30 AM - 11:45 AM

A Simplified Model for Indoor Optical Attocell Networks

Zhe Chen, Harald Haas
Li-Fi R&D Centre, School of Engineering, The University of Edinburgh, EH9 3JL, Edinburgh, UK
Email: {z.chen, h.haas}@ed.ac.uk

***Abstract*—In this paper, a novel model is proposed for estimating non-line-of-sight (NLOS) interference in indoor optical attocell network. The proposed model significantly simplifies the calculation for the NLOS interference. Simulation results verify the accuracy of the model.**

I. Introduction

Recently, there has been great research interest in optical cellular network. Compared with radio frequency (RF) cells, optical cells can be considerably smaller due to the limited coverage area [1]. This facilitates higher bandwidth reuse and therefore higher data density than in RF communication. In an indoor optical wireless scenario, each lighting fixture in a room can serve as an optical access point (AP). This type of optical cellular layers are referred to as an optical attocell network [2].

As the APs in an optical attocell network are close to each other, inter-cell interference between them is inevitable. This issue significantly limits the performance of the system. In an optical attocell network, inter-cell interference consists of two parts: line-of-sight (LOS) and non-line-of-sight (NLOS) interference. In order to mitigate the LOS interference, an angle diversity receiver is introduced in [3]. An angle diversity receiver consists of multiple directional photodiode (PD) with narrow field-of-view (FOV). With the use of signal combining schemes, an angle diversity receiver can significantly improve the system performance by eliminate the effect of LOS interference from the cell in the vicinity without losing the coverage. In terms of NLOS interference, as it can be reflected by wall, even the narrow FOV optical receiver fails to filter it out. Hence, the estimation of the NLOS interference is of significant importance as it is always limits the upper bound of the system performance in optical attocell network.

In previous research, a recursive method for evaluating the light reflection with Lambertian reflector in an indoor free-space optical channel is proposed [4], and referred here to as the conventional model. The model enables accurate analysis of light reflection and the result is validated by experiments. However, this model assumes that each of the smooth reflection surface consists of a large number of Lambertian reflectors which is extremely time consuming for Monte Carlo simulation. A simplified mathematical model is developed in [5]. In that model, NLOS path loss is estimated by a path loss exponent and a shadowing component. Unfortunately, this model is only valid for some particular paths in aircraft cabin.

II. System Model

In this study, a novel simplified model for NLOS propagation is proposed. In the conventional model, high-order reflections are taken in account which significantly increases the computational complexity. However, this is unnecessary in the optical attocell network. As illustrated in Fig. 1(a), the FOV of the optical receiver is designed to be narrow which can mitigate the LOS interference from cells in the vicinity. The narrow FOV optical receiver can also filter the first-order reflection which is reflected by walls. Second-order reflecting light is the predominant one in the inter-cell interference because the high-oder reflecting light attenuates significantly. Hence, only the second-order reflection is assumed in the proposed model. Also, only the desired cell and the interfering cells in the vicinity are considered in the proposed simplified model which is shown in Fig. 1(b).

A. NLOS Path I

The entire propagation path for the proposed simplified model are divided into two parts as: NLOS path I and NLOS path II. For the NLOS path I (see Fig. 2), light signals transmit from an optical transmitter at point O on the ceiling, reflected by the ground and back to the ceiling. In the conventional model, the ground is divided into a number of small elements. Each element collects the energy of the light signal incident on its surface and re-emits a fraction of the collected light determined by the reflection coefficient of the ground. In the simplified model, shown in Fig. 2(a), it is assumed that light is reflected by only two point reflectors S and S'. Since light transmission is isotropic, two points on the ceiling have the same intensity density of the reflected light when their distances to O are identical. Hence, for an arbitrary point on the ceiling, the intensity density can be represented as:

$$I_{r,h} = \frac{0.5 I_{0,h}(h^2+l^2)^{\alpha}}{(h^2+(r+l)^2)^{\alpha}} + \frac{0.5 I_{0,h}(h^2+l^2)^{\alpha}}{(h^2+(r-l)^2)^{\alpha}}, \quad (1)$$

where, r is horizontal separation between a specific point to O and h is the height of the room; l is the horizontal distance between one of the reflectors and point O. This can be represented as: $l = h\tan(\Phi_{\rm tx})$; $I_{0,h}$ represents the light intensity density at point O when the height of the room is h, which can be calculated as close-form:

$$I_{0,h} = \frac{P_{\rm tx}\rho_{\rm floor}\rho_{\rm ceiling}(m+1)(n+1)}{2\pi h^2(m+5)}, \quad (2)$$

where $P_{\rm tx}$ is the power of the optical transmitter; $\rho_{\rm floor}$ and $\rho_{\rm ceiling}$ are the reflecting coefficient of the floor and the ceiling; α is the attenuation factor which is chosen to minimise the difference between the proposed simplified model and the conventional model. Fig. 2(b) shows the estimated values of α at different specific transmitter semi-angles, $\Phi_{\rm tx}$, and three order polynomial is used for interpolation. In this way, α in terms of an arbitrary $\Phi_{\rm tx}$ can be obtained.

978-1-4799-7468-9/15/$31.00 ©2015 IEEE

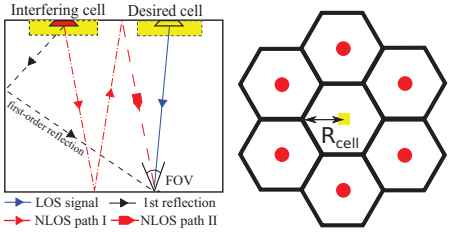

(a) Reflections in optical attocells.(b) Simplified cell configuration.

Fig. 1: An optical attocell network.

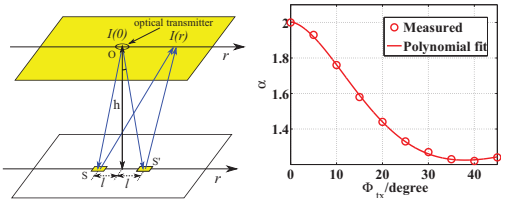

(a) Simplified reflection model. (b) Polynomial fit for α.

Fig. 2: The simplified propagation model for NLOS path I.

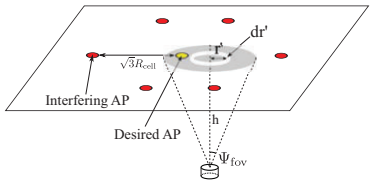

Fig. 3: The simplified propagation model for NLOS path II.

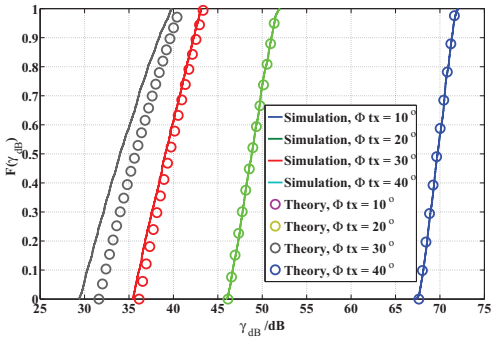

Fig. 4: The CDF of the SINR at the optical receiver in terms of different transmitter semi-angle Φ_{tx}.

B. NLOS Path II

The second part of the NLOS path is the light transmitted from ceiling to an optical receiver (see Fig. 3). Only the reflected light in the grey area on the ceiling can be received by the optical receiver. As the FOV of the optical receiver in the optical attocell network is designed to be small to mitigate inter-cell interference, the variation of the light intensity density in this area is small. Therefore, it is assumed that the intensity density of reflected light at the ceiling is constant which is identical the intensity density at cell centre.

III. Simulation Results and Discussion

The comparison between theoretical model and Monte Carlo simulations of the system signal-to-interference-plus-noise-ratio (SINR) performance is presented in Fig. 4. For numerical simulation, conventional model is used and a $20 \times 10 \times 4$ m room is assumed. The radius of the hexagonal cell is assumed to be scaled with the transmitter semi-angle: $R_{\mathrm{cell}} = h\tan(\Phi_{\mathrm{tx}})$. The FOV of the receiver is designed to be small and can be determined by: $1/2R_{\mathrm{cell}} = h\tan(\Psi_{\mathrm{fov}})$. For simplicity, each of the users is within the area where a LOS link with its desired AP can be established. In terms of the analytical result, the proposed simplified model is assumed and its parameters is consistent with the conventional model.

There is a close agreement between the presented model and the conducted simulation when the transmitter semi-angle of the optical receiver is small. The difference between the result of the Monte Carlo simulation and theoretical model is greater when the transmitter semi-angle is large. This is because, when the transmitter semi-angle is small, the simplified model regresses to the conventional model. When the transmitter semi-angle increases, the accuracy of the model decreases. Fortunately, in an optical attocell network, the cell size and the semi-angle of optical transmitter is designed to be small which can ensure high data density. Hence, the simplified model can accurately estimate the SINR performance in an optical attocell network and significantly reduce the computational complexity in comparison with the conventional model.

IV. Conclusion

In this study, a novel model is proposed for evaluating NLOS interference in an optical attocell network. The novel model significantly reduces the calculation complexity in comparison with the conventional model. Both of the numerical and analytical results of SINR distribution in an optical attocell network are presented. The numerical simulation validates the accuracy of the proposed model.

References

[1] T. Borogovac, M. Rahaim, and J. B. Carruthers, "Spotlighting for Visible Light Communications and Illumination," in *IEEE Global Communications Conference (GLOBECOM 2010) Workshops*, 6-10 Dec 2010, pp. 1077–1081.

[2] H. Haas, "High-speed wireless networking using visible light," SPIE Newsroom, Apr.19 2013.

[3] Z. Chen, N. Serafimovski, and H. Haas, "Angle diversity for an indoor cellular visible light communication system," in *Vehicular Technology Conference (VTC Spring), 2014 IEEE 79th*, May 2014, pp. 1–5.

[4] J. Barry, J. Kahn, W. Krause, E. Lee, and D. Messerschmitt, "Simulation of Multipath Impulse Response for Indoor Wireless Optical Channels," *IEEE J. Select. Areas Commun.*, vol. 11, no. 3, pp. 367–379, Apr. 1993.

[5] S. Dimitrov, R. Mesleh, H. Haas, M. Cappitelli, M. Olbert, and E. Bassow, "On the SIR of a Cellular Infrared Optical Wireless System for an Aircraft," *IEEE Journal on Selected Areas in Communications (IEEE JSAC)*, vol. 27, no. 9, pp. 1623–1638, Dec. 2009.

Workshop on Optical Wireless Communications (OWC 2016)

Space Division Multiple Access in Optical Attocell Networks

Zhe Chen, Dushyantha A. Basnayaka and Harald Haas
Li-Fi R&D Centre, Institute for Digital Communications School of Engineering, The University of Edinburgh, EH9 3JL, Edinburgh, UK Email: {z.chen, d.basnayaka, h.haas}@ed.ac.uk

(Invited Paper)

***Abstract*—In this paper, an optical space division multiple access (SDMA) scheme is proposed for optical attocell networks. In the system, a conventional single-element transmitter in each optical cell is substituted by an angle diversity transmitter which can simultaneously serve multiple active users at different positions. This type of configuration can increase the available bandwidth resource and also mitigate inter-cell interference (ICI) in optical attocell networks. The results indicate that the optical SDMA scheme significantly outperforms the conventional optical time division multiple access (TDMA) scheme. The SDMA schemes is shown to improve the average spectral efficiency of the system by a factor of 26 for a 37-element light-emitting diode (LED) angle diversity transmitter. Finally, the study is extended to account for user position errors. The Monte-Carlo simulation results show that the system is very robust to user position errors.**

***Index Terms*—angle diversity transmitter; visible light communication; space division multiple access; position errors**

I. Introduction

Recently, visible light communication (VLC) technology has emerged as a viable technology to complement conventional radio frequency (RF) systems, and to help alleviate the RF spectrum crunch [1]. One of the key advantages of VLC is that it enables the transformation of conventional lighting infrastructures into high speed optical cellular communication networks. In a typical indoor scenario, each light fixture can act as an access point (AP), and can serve multiple users. This type of network is referred to as an optical attocell networks [2]. Compared with RF cells, optical cells are considerably smaller due to the limited coverage of light-emitting diodes (LEDs) [3]. An optical attocell network facilitates higher frequency reuse and data density than in small-cell RF wireless networks. Recent research shows that an optical attocell network significantly outperforms RF femtocell systems [4], [5].

Typically, time division multiple access (TDMA) is used as a multiple access scheme in a multi-user system. This type of system has two limitations: firstly, only one user can be served in a time slot which is not the optimum transmission strategy for multiple user access; secondly, a transmitter requires to radiate signals omni-directionally to provide full cell coverage. This causes strong inter-cell interference (ICI), especially to cell-edge users. In order to overcome these limitations, a spatial dimension is added to the conventional TDMA system. In RF, space division multiple access (SDMA) is well-known technique [6], and it uses an antenna array at the transmitter to simultaneously generate multiple narrow directional beams which point to the active users. In this way, multiple users can be served within the same time slot.

Although SDMA shows promising performance in RF, it cannot be directly adopted in VLC. One of the key issues is the transmitter. In RF, directional narrow beams are generated by changing the amplitude and phase of the signals transmitted by an antenna array. However, this approach cannot be applied straightforwardly to VLC because VLC uses intensity modulation and direct detection (IM/DD). However, in VLC, LEDs have an inherent feature of a confined field-of-view (FOV). This feature can be exploited for generating directional light beams. Therefore, in optical SDMA, an angle diversity transmitter which consists of multiple narrow FOV LEDs is used as the optical transmitter. By activating different transmitter elements, the angle diversity transmitter can simultaneously serve multiple users at different locations.

Existing approaches to improve the spectral efficiency of VLC networks include a system consisting of multi-beam transmitters and imaging diversity receivers in [7]. Unfortunately, this system fails to support multiple users and their mobility is significantly restricted by the imaging optical receiver. In [8] and [9], an optical attocell network is proposed which can achieve a higher system spectral efficiency by exploiting the benefit of frequency reuse and different ICI mitigation methods. However, to the authors' best knowledge, there is very little published research that exploits the transmitter spatial diversity in a system level. Therefore, in this study, optical SDMA which uses angle diversity transmitters for optical attocell network is proposed.

The remainder of this paper is organised as follows. The propagation model is given in Section II. An optical TDMA system is introduced in Section III. An optical SDMA system is introduced in Section IV. A model of position error is given in Section V. Simulation results are compared and discussed in Section VI. Finally, Section VII concludes the paper.

II. Propagation Model

This study focuses on the downlink transmission of a VLC system. A 7-cell attocell network as shown in Fig. 1 is assumed and the performance of the central cell is considered in order to eliminate cell-edge effects in the simulations. Light fixtures are acting as APs. These APs are assumed to be placed in the ceiling and the optical receivers for all active users are placed at desktop height. In this study, a line-of-sight (LOS) optical channel is assumed. The direct current (DC) gain of the LOS

978-1-4673-8666-1/16/$31.00 ©2016 IEEE

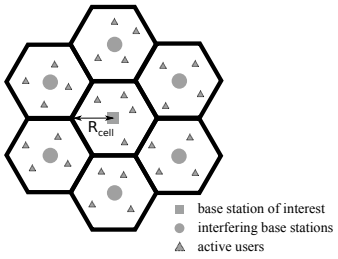

Fig. 1. The layout of a 7-cell optical attocell network.

link can be calculated as follows [10]:

$$H_0 = \frac{(n+1)A_{\text{eff}}}{2\pi d^2}\cos^n(\phi)\cos(\psi)\text{rect}\left(\frac{\psi}{\Psi_{\text{fov}}}\right), \quad (1)$$

where d is the distance between a base station and its corresponding receiver; Ψ_{fov} is the FOV of the optical receiver; n is the Lambertian order of the LED element on the base station; n is also a function of the transmitter half-intensity radiation angle Φ_{tx} as $n = -1/\log_2(\cos(\Phi_{\text{tx}}))$; ϕ is the angle of irradiance; ψ is the angle of light incidence at the receiver; $\text{rect}(\cdot)$ is a unit step function.

III. Optical TDMA

In a typical optical TDMA scenario, a single-element optical transmitter is adapted as a base station. All active users share the same spectrum in their corresponding optical cell. Information for different users is transmitted in different time slots of identical length. In each time slot, only one of the active users can be served. Therefore, the received signal-to-interference-plus-noise-ratio (SINR) of the active user k can be expressed as:

$$\gamma_k = \frac{\left(\tau P_{\text{tx}} H_{(\hat{b},k)}\right)^2}{N_0 B + \sum_{b' \neq \hat{b}} \left(\tau P_{\text{tx}} H_{(b',k)}\right)^2}, \quad (2)$$

where τ is the responsivity of the photodiode (PD); P_{tx} is the optical power transmitted by an AP and is assumed to be the same for all APs; $H_{(\hat{b},k)}$ is the channel attenuation between user k and the desired base station $\hat{b}$; $\sum_{b' \neq \hat{b}} \left(rP_{\text{t}} H_{(b',k)}\right)^2$ represents the interference signal from interfering APs; N_0 is the additive white Gaussian noise (AWGN) power spectral density; B is the optical communication bandwidth.

Assuming a simple Round Robin (RR) scheduler, the spectral efficiency of the optical TDMA scheme is as follows:

$$\Omega_{\text{TDMA}}(k) = \frac{1}{K}\sum_{k=1}^{K}\log_2(1+\gamma_k), \quad (3)$$

where K is the total number of the active users per cell.

The optical TDMA system described here has several disadvantages. On the one hand, users in the system are successively assigned to different time slots. Only one user can be served in each time slot. This strategy significantly limits the overall performance of the system since the available bandwidth cannot be effectively shared and this limit the user data rate granularity. On the other hand, the conventional single-element optical transmitter requires a large half intensity radiation angle to achieve full light and signal coverage. As a consequence, ICI in the system could significantly increase and this will compromise the overall system performance.

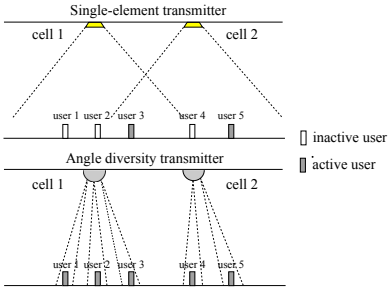

Fig. 2. Single-element versus angle diversity transmitter: the figure on the top illustrates optical TDMA. The figure at the bottom illustrates optical SDMA. Cell 1 and cell 2 are two neighbouring cells in an optical attocell network.

IV. Optical SDMA

A. Angle Diversity Transmitter

In RF, the realisation of narrow beam transmitters requires multiple RF chains and complex beam-steering algorithms. In VLC, by exploiting an angle diversity receiver, narrow beam optical signals can be generated, and complex algorithms for beamforming can be avoided. The parallel directional transmissions can be realised by activating LEDs that cover only the areas occupied by active users. The remaining LEDs not acting as APs generate constant light to provide room illumination. Therefore, an angle diversity transmitter can provide both uniform illumination while communicating to multiple users.

The use of an angle diversity transmitter can effectively mitigate ICI in an optical attocell network. As illustrated in Fig. 2, in a snapshot of an optical TDMA system, user 3 and user 5 are active and are served by APs in cell 1 and cell 2, respectively. Since the transmitter semi-angle for the single-element transmitter is large, both user 3 and user 5 experience high ICI. For the identical snapshot in the optical SDMA system, all users are served by spot beams. Since active LEDs only cover the areas of active users, inter-cell interference can be significantly mitigated.

B. Spatial Grouping

In an optical attocell network, it is assumed that each active user connects to the closest optical access point. In each optical cell, active users are served by different LED elements of the angle diversity transmitter. In optical SDMA, these active users cannot be assigned to arbitrary LED elements since some users might be spatially close to each other which results in overlapping beams and high mutual interference. Therefore, in the absence of adaptive beamforming, a proper spatial grouping strategy is essential to achieve high spectral

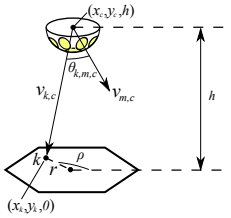

Fig. 3. The geometry of an optical cell.

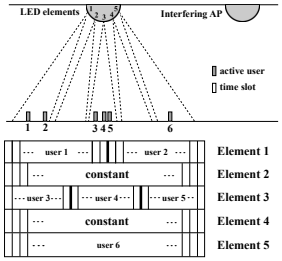

Fig. 4. An example frame of resource allocation in optical SDMA.

efficiency in an optical SDMA system with a fixed grid of beams.

The first step of the spatial grouping strategy is to determine the source LED element for each active user. The geometry of an optical cell is illustrated in Fig. 3. The coordinate of the angle diversity transmitter c is (x_c, y_c, h) and the coordinate of an active user k is $(x_k, y_k, 0)$; $v_{k,c}$ is the vector from the angle diversity transmitter c to the active user k; $v_{m,c}$ is the normal vector of the LED element m on the angle diversity transmitter c; $\theta_{k,m,c}$ is the angle between $v_{k,c}$ and $v_{m,c}$. The source LED element for the active user k is chosen to minimise the angle $\theta_{k,m}$. The index of the source LED element for active user k is given as:

$$I_{k,c} = \min_{m} \theta_{k,m,c}, \quad (c = \hat{c}) \tag{4}$$

where $\hat{c}$ is the desired cell for active user k; $\theta_{k,m,c}$ can be represented as:

$$\theta_{k,m} = \arccos\left(\frac{\overrightarrow{v}_{k,c} \cdot \overrightarrow{v}_{m,c}}{\|\overrightarrow{v}_{k,c}\| \|\overrightarrow{v}_{m,c}\|}\right). \tag{5}$$

The list of active LED elements on the angle diversity transmitter can be obtained after the source LED elements for all active users are determined. In some situations, some active users could be spatially close. As a result, more than one active user could be allocated to a single LED element. In order to serve multiple users with one LED element, it is assumed that TDMA as outlined in Sec. III is used to separate these users.

Finally, an example of resource allocation in optical SDMA is illustrated in Fig. 4. Three LED elements are active. User $1, 2$, are allocated to element 1. These two users equally share the resource using TDMA. User $3, 4, 5$, are allocated to element 3 using TDMA to separate them. User 6 is allocated to element 5. Since there is only one user in that beam, user 6 uses the entire bandwidth continuously, it occupies both time and spectrum exclusively. The other two elements, 2 and 4, are inactive, since no users are required to be served by them. Therefore, these LED elements do not carry intensity modulation (IM) signals and provide constant light output for illumination.

C. Performance Evaluation

In order to evaluate the SINR performance for each active user, interference is a key factor to be considered. In optical SDMA, interference consist of two parts: intra-cell interference and ICI. Intra-cell interference originates from the active LED elements in the desired optical cell. ICI is the interference generated by the active LED elements in other optical cells. Hence, the SINR of active user k can be expressed as:

$$\gamma_k = \frac{\left(\tau P_{\text{tx}} H_{k,m,\hat{c}}\right)^2}{N_0 B + \sum\limits_{m' \neq m} \left(\tau P_{\text{tx}} H_{k,m',\hat{c}}\right)^2 + \sum\limits_{c'} \sum\limits_{\hat{m}} \left(\tau P_{\text{tx}} H_{k,\hat{m},c'}\right)^2}, \tag{6}$$

where τ is the optical to electric conversion efficiency; P_{tx} is the transmission power of an LED; and $H_{k,m,\hat{c}}$ is the channel attenuation between the desired LED element m and an active user k in the desired cell $\hat{c}$. $\sum\limits_{m' \neq m} \left(\tau P_{\text{tx}} H_{k,m'}\right)^2$ represents the intra-cell interference and m' is the index of active LED elements in the desired cell. $\sum\limits_{c'} \sum\limits_{\hat{m}} \left(\tau P_{\text{tx}} H_{k,\hat{m},c'}\right)^2$ represents the ICI; $\hat{m}$ is the index of active LED elements in each interfering cell; c' is the index of the interfering cell.

The spectral efficiency of the optical SDMA scheme can be calculated as:

$$\Omega_{\text{SDMA}} = \sum_{k=1}^{K} \frac{1}{g_k} \log_2(1 + \gamma_k), \tag{7}$$

where g_k is the total number of active uses served by the desired LED element of active user k; K is the total number of active users in an optical cell.

V. The Model of Position Errors

As discussed in the previous section, the spatial grouping strategy depends on the position information of active users. This means that position information is crucial to the operation of the optical SDMA system. However, the position information is not always accurate. The inaccurate position information occurs due to the limitation of positioning hardware and algorithms. When different indoor positioning techniques and devices are used, the position errors vary accordingly [11],[12]. In this section, a simple model for position errors is introduced.

Assume that the Cartesian coordinate of the actual position of an active user k is (x_k, y_k) and its estimated position is (x'_k, y'_k). The relationship between (x_k, y_k) and (x'_k, y'_k) can be represented as:

$$\begin{cases} x'_k = x_k + e_k \\ y'_k = y_k + e'_k \end{cases} \tag{8}$$

where both e_k and e'_k follow a zero-mean normal distribution $\mathcal{N}(0, \sigma_e^2)$ [13]; σ_e is the standard variance. For each active

user, e_k and e'_k are independent and identically distributed. It is notable that the distance between the actual position and the estimated position can be represented as:

$$d_e = \sqrt{(x_k - x'_k)^2 + (y_k - y'_k)^2}. \tag{9}$$

Here, according to [14], d_e follows Rayleigh distribution and the mean value of d_e is:

$$\mathbb{E}[d_e] = \sqrt{\frac{\pi}{2}}\sigma_e. \tag{10}$$

In optical SDMA, user grouping is affected by the position errors. Some users could be allocated to a suboptimal LED element and this results in an increasing intra-cell interference. Therefore, positioning errors could significantly degrade the performance of optical SDMA systems.

VI. Results and Discussions

A. Simulation Setup

In the simulation, both optical TDMA and optical SDMA are considered. The performance of the optical TDMA system is used as a benchmark of the optical SDMA system. For the optical TDMA scenario, the half-intensity radiance angle of the conventional single-element transmitter is assumed to be 60°. For the optical SDMA scenario, three types of angle diversity transmitters are considered. The number of LED elements on each type of angle diversity transmitter is 7, 19 and 37, respectively. For the purpose of fairness, it is ensured that the combined half-intensity radiance angle of all types of angle diversity transmitters is identical to the conventional single-element transmitter. It is also ensured that the total transmission power of all transmitters are the same irrespective of being single or multi-element.

For both scenarios, optical transmitters are placed at the centre of each cell at a height of 3 m. The optical receiver for all active users are assumed to be placed at a desk height of 0.85 m. The radius of each cell is 3 m. The transmission power of an optical access point is set as 2 W. The FOV Φ_{fov}, responsivity τ, and effective area A_{p}, of a PD are 70°, 0.5 A/W and 1 cm^2 respectively. The noise spectral density, N_0 is 1×10^{-21}A/Hz.

B. Spectral Efficiency Performance

The simulation study consists of $100,000$ snapshots of user locations in the 7-cell optical attocell network. For each snapshot, it is ensured that active users are spatially uniformly distributed. The sum spectral efficiencies of all users in the central optical cell of the 7-cell attocell network is calculated. Finally, the average spectral efficiency is obtained as the average of the sum spectral efficiency over all snapshots. The average spectral efficiencies for optical TDMA scheme and optical SDMA scheme are represented as $\overline{\Omega}_{\text{TDMA}}$ and $\overline{\Omega}_{\text{SDMA}}$, respectively. N is denoted as the number of LED elements on each angle diversity transmitter.

Fig. 5 illustrates the average spectral efficiency of the optical SDMA scheme when 7-element angle diversity transmitters are used. It can be observed that the SDMA scheme significantly outperforms TDMA scheme where up to 6 times higher average spectral efficiency can be achieved. The reason is, an angle diversity transmitter can generate narrow directional light beams which can effectively reduce ICI, and in turn increase average spectral efficiency.

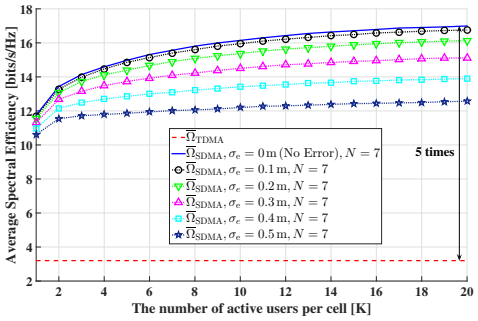

Fig. 5. The average spectral efficiency of optical SDMA scheme. (N = 7)

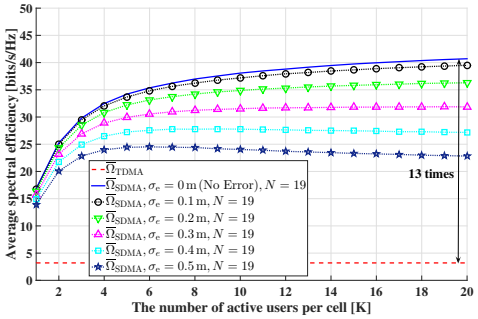

Fig. 6. The average spectral efficiency of optical SDMA scheme. (N = 19)

It is also notable that the average spectral efficiency increases but the increase is saturating as the number of users increases. This is because when the total number of active users is small, the mutual interference between each link is very small. Hence, the average spectral efficiency is scaled with the number of active users. When the total number of active users is large, the number of active LEDs also increases. This will increase ICI which limits the average spectral efficiency.

Fig. 6 illustrates the average spectral efficiency of an optical SDMA system when 19-element angle diversity transmitters are used as the optical transmitters. The trend of the spectral efficiency performance in this scenario is similar to the previous scenario. One notable difference is that, when compared with TDMA, an SDMA system with 19-element angle diversity transmitters can achieve up to 13 times higher average spectral efficiency than the TDMA system. This is because more elements on an optical transmitter enables greater separation of users in the cell which results significantly lower mutual interference between users and better performance. When the number of transmitter elements increases further, the average spectral efficiency of optical SDMA increases

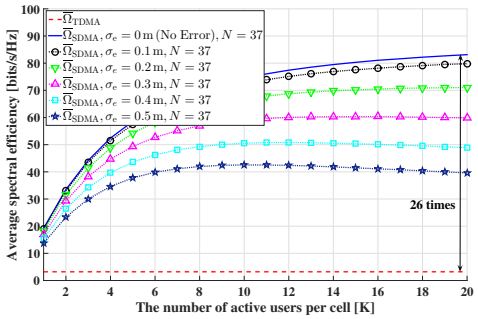

Fig. 7. The average spectral efficiency of optical SDMA scheme. (N = 37)

accordingly. As shown in Fig. 7, an optical SDMA system with 37-element angle diversity transmitters can achieve up to 26 times higher average spectral efficiency than an optical TDMA system.

C. Position Errors

In Fig. 5, when σ_e is 0.1 m, the average spectral efficiency of the SDMA system decreases only by 1.3% compared with the system with perfect position information. When σ_e is increased to 0.2 m, 0.3 m, 0.4 m and 0.5 m, the performance of the SDMA system decreases by 5.0%, 11%, 18% and 26%, respectively. When σ_e is large, the position information for all active users are very inaccurate. As a result, incorrect LED elements in each optical cell are activated. This means active users may not be served by their optimal LED elements and this means additional performance penalty is introduced. Therefore, the overall system performance is degraded significantly if the error of position estimates is large.

Fig. 6 shows the average spectral efficiency of an optical SDMA system with 19-element transmitters. When σ_e are 0.1 m, 0.2 m, 0.3 m, 0.4 m and 0.5 m, the performance of the SDMA system decreases by 3.0%, 11%, 22%, 33% and 44%, respectively, compared with the system with perfect position information. For optical SDMA system using 37-element transmitters (Fig. 7), when σ_e are 0.1 m, 0.2 m, 0.3 m, 0.4 m and 0.5 m, the performance of the SDMA system decreases 4.0%, 14%, 28%, 41% and 52%, respectively, compared with the system with perfect position information. This means that when the number of transmitter elements increases, the SDMA system is more sensitive to the position information of the active users. This is because, when the number of LED elements increases, the service area of each LED element is smaller. As a result, active users may be easily misallocated to the cell in the vicinity when the position information is inaccurate. Therefore, for fixed σ_e, the SDMA systems using more transmitter elements perform worse. It is also notable that the performance of SDMA systems is compromised when σ_e increases. Fortunately, with the use of the-state-of-the-art indoor positioning techniques [12], an average position error of less than 0.25 m can often be achieved in the similar system configuration. This means $\mathbb{E}[d_e] = \sqrt{\frac{\pi}{2}}\sigma_e < 0.25$ m and $\sigma_e < 0.2$ m can be obtained. Therefore, the system average spectral efficiency decreases only by 14%.

VII. Conclusion

In this paper, an optical attocell network adopting optical SDMA is proposed. In this network, an angle diversity transmitter is equipped in each optical cell and it can serve multiple active users simultaneously. With the use of an angle diversity transmitters, the ICI between optical cells can be significantly mitigated. The results clearly indicate that the optical SDMA system significantly outperforms the optical TDMA benchmark system, optical TDMA system. In particular, up to 26 times higher average spectral efficiency can be achieved when the transmitter is equipped with 37 LED elements. Moreover, position errors of active users are considered. Results show that the SDMA system is robust to position errors, and the system performance is only compromised by up to 14% when practical state-of-the-art indoor position techniques are used. The results strongly support the suitability of optical SDMA systems for practical implementations.

Acknowledgement

Professor Haas acknowledges support from the Engineering and Physical Sciences Research Council (EPSRC) under Established Career Fellowship grant EP/K008757/1.

References

[1] H. Elgala, R. Mesleh, and H. Haas, "Indoor Optical Wireless Communication: Potential and State-of-the-Art," *IEEE Commun. Mag.*, vol. 49, no. 9, pp. 56–62, Sep. 2011.

[2] H. Haas, "High-speed Wireless Networking Using Visible Light," SPIE Newsroom, Apr. 19 2013.

[3] T. Borogovac, M. Rahaim, and J. B. Carruthers, "Spotlighting for Visible Light Communications and Illumination," in *IEEE Global Communications Conference (GLOBECOM 2010) Workshops*, 6-10 Dec 2010, pp. 1077–1081.

[4] I. Stefan, H. Burchardt, and H. Haas, "Area Spectral Efficiency Performance Comparison between VLC and RF Femtocell Networks," in *IEEE International Conference on Communications (ICC)*, Budapest, Hungary, Jun. 9–13 2013, pp. 1–5.

[5] H. Haas, L. Yin, Y. Wang, and C. Chen, "What is lifi?" *Journal of Lightwave Technology*, vol. PP, no. 99, pp. 1–1, 2015.

[6] A. J. Paulraj and C. B. Papadias, "Space-time Processing for Wireless Communications," *IEEE Signal Process. Mag.*, vol. 14, no. 6, pp. 49–83, Nov. 1997.

[7] P. Djahani and J. M. Kahn, "Analysis of Infrared Wireless Links Employing Multibeam Transmitters and Imaging Diversity Receivers," *IEEE Trans. Commun.*, vol. 48, no. 12, pp. 2077–2088, Dec. 2000.

[8] Z. Chen, N. Serafimovski, and H. Haas, "Angle diversity for an Indoor Cellular Visible Light Communication System," in *IEEE 79th Vehicular Technology Conference*, May 2014.

[9] C. Chen, N. Serafimovski, and H. Haas, "Fractional frequency reuse in optical wireless cellular networks," in *2013 IEEE 24th International Symposium on Personal Indoor and Mobile Radio Communications (PIMRC)*, Sept 2013, pp. 3594–3598.

[10] J. M. Kahn and J. R. Barry, "Wireless Infrared Communications," *Proc. IEEE*, vol. 85, no. 2, pp. 265–298, Feb. 1997.

[11] M. geun Moon and S. il Choi, "Indoor Position Estimation Using Image Sensor Based on VLC," in *2014 International Conference on Advanced Technologies for Communications (ATC)*, Oct 2014, pp. 11–14.

[12] M. Yasir, S. Ho, and B. Vellambi, "Indoor Positioning System Using Visible Light and Accelerometer," *J. Lightw. Technol.*, vol. 32, no. 19, pp. 3306–3316, Oct 2014.

[13] M. Kashef, M. Abdallah, K. Qaraqe, and M. Uysal, "The Impact of Location Errors on Achievable Rates in OFDM-based Multi-user Visible Light Communication Systems," in *2014 3rd International Workshop in Optical Wireless Communications (IWOW)*, Sept 2014, pp. 65–69.

[14] A. Papoulis, *Probability, Random Variables and Stochastic Processes*, 2nd ed. McGraw-Hill Inc., 1984.

Bibliography

[1] J. Kahn and J. Barry, "Wireless Infrared Communications," *Proceedings of the IEEE*, vol. 85, pp. 265–298, Feb 1997.

[2] Cisco Visual Networking Index, "Global Mobile Data Traffic Forecast Update, 2014-2019," White Paper, Feb. 2015.

[3] X. Zhang and B. Ottersten, "Performance Analysis of V-BLAST Structure with Channel Estimation Errors," in *4th IEEE Workshop on Signal Process. Adv. in Wireless Commun. (SPAWC)*, pp. 487–491, June 2003.

[4] A. Goldsmith, S. Jafar, N. Jindal, and S. Vishwanath, "Capacity limits of MIMO channels," *IEEE J. Sel. Areas Commun.*, vol. 21, pp. 684–702, June 2003.

[5] L. Zheng and D. Tse, "Diversity and Multiplexing: a Fundamental Tradeoff in Multiple-antenna Channels," *IEEE Trans. Inf. Theory*, vol. 49, pp. 1073–1096, May 2003.

[6] Z. Zhou and B. Vucetic, "MIMO Systems with Adaptive Modulation," in *Proc. of the 59th Vehicular Technology Conference (VTC 04)*, vol. 2, (Milan, Italy), pp. 765–769, 17–19 May 2004.

[7] Y. J. Zhang and K. Letaief, "Adaptive Resource Allocation for Multiaccess MIMO/OFDM Systems with Matched Filtering," *IEEE Transactions on Communications*, vol. 53, pp. 1810–1816, Nov. 2005.

[8] T. Yoo and A. Goldsmith, "Capacity and Power Allocation for Fading MIMO Channels With Channel Estimation Error," *IEEE Trans. Inf. Theory*, vol. 52, pp. 2203 –2214, May 2006.

[9] X. Zhang, D. Palomar, and B. Ottersten, "Statistically Robust Design of Linear MIMO Transceivers," *IEEE Trans. on Signal Process.*, vol. 56, pp. 3678 –3689, Aug. 2008.

[10] P. Yang, Y. Xiao, Y. Yi, L. Li, Q. Tang, and S. Li, "Simplified Adaptive Spatial Modulation for Limited-Feedback MIMO Systems," *IEEE Trans. Veh. Technol.*, vol. PP, no. 99, p. 1, 2013. (Early Access Article).

[11] J. Zhang, Y. Wang, L. Ding, and N. Zhang, "Bit Error Probability of Spatial Modulation over Measured Indoor Channels," *IEEE Trans. on Wireless Commun.*, vol. 13, pp. 1380–1387, March 2014.

[12] L. Yan, Z. Wenan, and S. Junde, "An Adaptive Subcarrier, Bit and Power Allocation Algorithm for Multicell OFDM Systems," in *Proc. of the Canadian Conference on Electrical and Computer Engineering (CCECE)*, vol. 3, (Montreal, Canada), pp. 1531–1534, IEEE, May 4–7, 2003.

[13] L. Wang and C. Tellambura, "A Simplified Clipping and Filtering Technique for PAR Reduction in OFDM Systems," *IEEE Signal Processing Letters*, vol. 12, pp. 453–456, June 2005.

[14] G. Song and Y. G. Li, "Cross-Layer Optimization for OFDM Wireless Networks Part II: Algorithm Development," *IEEE Transactions on Wireless Communications*, vol. 4, pp. 625–634, Mar. 2005.

[15] L. Ying, Z. Yang, and W. Jibo, "An Ordering Interpolation-based QR Decomposition Algorithm for V-BLAST OFDM Systems with Two Transmit Antennas," in *Proc. 6th International Conference on ITS Telecommunications*, pp. 366–369, 2006.

[16] T. Pratt, N. Jones, L. Smee, and M. Torrey, "OFDM Link Performance with Companding for PAPR Reduction in the Presence of Non-linear Amplification," *IEEE Transactions on Broadcasting*, vol. 52, no. 2, pp. 261–267, 2006.

[17] S. Weinstein and P. Ebert, "Data Transmission by Frequency-Division Multiplexing Using the Discrete Fourier Transform," *IEEE Trans. Commun. Technol.*, vol. 19, pp. 628–634, October 1971.

[18] R. v. Nee and R. Prasad, *OFDM for Wireless Multimedia Communications*. Norwood, MA, USA: Artech House, Inc., 1st ed., 2000.

[19] L. Hanzo, H. Haas, S. Imre, D. O'Brien, M. Rupp, and L. Gyongyosi, "Wireless myths, realities, and futures: From 3g/4g to optical and quantum wireless," *Proc. IEEE*, vol. 100, pp. 1853–1888, May 2012.

[20] D. Cabric, M. Chen, D. Sobel, J. Yang, and R. Brodersen, "Future Wireless Systems: UWB, 60GHz, and Cognitive Radios," in *In the Proceeding of the IEEE Conference*

on Custom Integrated Circuits, (San Jose, California, USA), pp. 793–796, Sept. 18–21, 2005.

[21] Z. Pi and F. Khan, "An Introduction to Millimeter-wave Mobile Broadband Systems," *IEEE Commun. Mag.*, vol. 49, pp. 101–107, June 2011.

[22] T. Rappaport, S. Sun, R. Mayzus, H. Zhao, Y. Azar, K. Wang, G. Wong, J. Schulz, M. Samimi, and F. Gutierrez, "Millimeter Wave Mobile Communications for 5G Cellular: It Will Work!," *IEEE Access*, vol. 1, pp. 335–349, 2013.

[23] W. Keusgen, A. Kortke, M. Peter, and R. Weiler, "A Highly Flexible Digital Radio Testbed and 60 GHz Application Examples," in *Proc. of European Microwave Conference (EuMC)*, (Nuernberg, Germany), pp. 740–743, Oct. 6–10 2013.

[24] N. Valliappan, A. Lozano, and R. Heath, "Antenna Subset Modulation for Secure Millimeter-Wave Wireless Communication," *IEEE Trans. on Commun.*, vol. 61, pp. 3231–3245, August 2013.

[25] T. Rappaport, F. Gutierrez, E. Ben-Dor, J. Murdock, Y. Qiao, and J. Tamir, "Broadband Millimeter-Wave Propagation Measurements and Models Using Adaptive-Beam Antennas for Outdoor Urban Cellular Communications," *IEEE Trans. Antennas Propag.*, vol. 61, pp. 1850–1859, April 2013.

[26] M. Wolf and D. Kress, "Short-Range Wireless Infrared Transmission: The Link Budget Compared to RF," *IEEE Wireless Communication Magazine*, vol. 10, pp. 8–14, Apr. 2003.

[27] G. Yun and M. Kavehrad, "Indoor Infrared Wireless Communications Using Spot Diffusing and Fly-Eye Receivers," in *The Canadian Journal of Electrical and Computer Engineering*, vol. 18, Oct. 1993.

[28] P. Barna and S. Schlanger, "Fundamentals of the Infrared Physical Layer," January 2004.

[29] "Infrared Data Communication According to IrDA Standard, Part 1: Physical Layer," Tech. Rep. 82513, Vishay Semiconductors, September 2006. Rev. 1.4.

[30] J. B. Carruthers and J. M. Kahn, "Multiple-subcarrier Modulation for Nondirected Wireless Infrared Communication," *IEEE Journal on Selected Areas in Communications*, vol. 14, pp. 538–546, Apr. 1996.

[31] J. B. Carruthers and J. M. Kahn, "Modeling of Nondirected Wireless Infrared Channels," *IEEE Transactions on Communications*, vol. 45, pp. 1260–1268, Oct. 1997.

[32] G. W. Marsh and J. M. Kahn, "Channel Reuse Strategies for Indoor Infrared Wireless Communications," *IEEE Trans. Commun.*, vol. 45, pp. 1280–1290, Oct. 1997.

[33] P. Barker and A. C. Boucouvalas, "Performance modeling of the IrDA protocol for infrared wireless communications," vol. 36, no. 12, pp. 113–117, 1998.

[34] M. R. Pakravan, M. Kavehrad, and H. Hashemi, "Indoor Wireless Infrared Channel Characterization by Measurements," *IEEE Transactions on Vehicular Technology*, vol. 50, pp. 1053–1073, July 2001.

[35] A. Azhar, T. Tran, and D. O'Brien, "A Gigabit/s Idoor Wireless Transmission using MIMO-OFDM Visible-Light Communications," *IEEE Photon. Technol. Lett.*, vol. 25, pp. 171–174, Jan.15 2013.

[36] S. Hussain, M. Abdallah, and K. Qaraqe, "Hybrid Radio-visible Light Downlink Performance in RF Sensitive Indoor Environments," in *2014 6th International Symposium on Communications, Control and Signal Processing (ISCCSP)*, pp. 81–84, May 2014.

[37] T. Wang, Y. Sekercioglu, and J. Armstrong, "Analysis of an optical wireless receiver using a hemispherical lens with application in mimo visible light communications," *Journal of Lightwave Technology*, vol. 31, pp. 1744–1754, June 2013.

[38] L. Zeng, D. O'Brien, H. Minh, G. Faulkner, K. Lee, D. Jung, Y. Oh, and E. T. Won, "High Data Rate Multiple Input Multiple Output (MIMO) Optical Wireless Communications Using White LED Lighting," *IEEE J. Sel. Areas Commun.*, vol. 27, pp. 1654–1662, Dec. 2009.

[39] A. M. Khalid, G. Cossu, R. Corsini, P. Choudhury, and E. Ciaramella, "1-Gb/s Transmission over a Phosphorescent White LED by Using Rate-adaptive Discrete Multitone Modulation," *IEEE Photon. J.*, vol. 4, pp. 1465–1473, Oct 2012.

[40] D. Tsonev, H. Chun, S. Rajbhandari, J. McKendry, S. Videv, E. Gu, M. Haji, S. Watson, A. Kelly, G. Faulkner, M. Dawson, H. Haas, and D. O'Brien, "A 3-Gb/s Single-LED OFDM-Based Wireless VLC Link Using a Gallium Nitride μLED," *IEEE Photon. Technol. Lett.*, vol. 26, pp. 637–640, Apr. 2014.

[41] H. Chun, S. Rajbhandari, G. Faulkner, D. Tsonev, E. Xie, J. McKendry, E. Gu, M. Dawson, D. C. O'Brien, and H. Haas, "LED based Wavelength Division Multiplexed 10 Gb/s Visible Light Communications," *Journal of Lightwave Technology*, vol. PP, no. 99, pp. 1–1, 2016.

[42] G. M. J. Z. K.-W. S. B. Slimane, *Fundamentals of Mobile Data Networks*. Cambridge Press, 2016.

[43] J. G. Andrews, "Interference Cancellation for Cellular Systems: A Contemporary Overview," *IEEE Wireless Communications Magazine*, vol. 12, pp. 19–29, April 2005.

[44] S. Ali and V. Leung, "Dynamic frequency allocation in fractional frequency reused ofdma networks," *IEEE Transactions on Wireless Communications*, vol. 8, pp. 4286 –4295, august 2009.

[45] W. Choi and J. G. Andrews, "Downlink Performance and Capacity of Distributed Antenna Systems in a Multicell Environment," *IEEE Transactions on Wireless Communications*, vol. 6, pp. 69–73, Jan. 2007.

[46] S.-M. Cheng, S.-Y. Lien, F.-S. Chu, and K.-C. Chen, "On exploiting cognitive radio to mitigate interference in macro/femto heterogeneous networks," *IEEE Wireless Communications*, vol. 18, pp. 40 –47, June 2011.

[47] S. Ortiz, "The Wireless Industry Begins to Embrace Femtocells," *Computer*, vol. 41, pp. 14–17, July 2008.

[48] V. Chandrasekhar, J. Andrews, and A. Gatherer, "Femtocell Networks: A Survey," *IEEE Commun. Mag.*, vol. 46, no. 9, pp. 59–67, 2008.

[49] P. Pinto, A. Giorgetti, M. Win, and M. Chiani, "A stochastic geometry approach to coexistence in heterogeneous wireless networks," *IEEE Journal on Selected Areas in Communications*, vol. 27, pp. 1268 –1282, september 2009.

[50] D. Lopez-Perez, I. Guvenc, G. de la Roche, M. Kountouris, T. Quek, and J. Zhang, "Enhanced intercell interference coordination challenges in heterogeneous networks," *IEEE Wireless Communications*, vol. 18, pp. 22 –30, June 2011.

[51] Q. Ye, B. Rong, Y. Chen, M. Al-Shalash, C. Caramanis, and J. Andrews, "User Association for Load Balancing in Heterogeneous Cellular Networks," *IEEE Transactions on Wireless Communications*, vol. 12, no. 6, pp. 2706–2716, 2013.

[52] M. N. Khan, *Understanding LED Illumination*. CRC Press, 2013.

[53] T. Kamalakis, J. Walewski, G. Ntogari, and G. Mileounis, "Empirical Volterra-Series Modeling of Commercial Light-Emitting Diodes," *J. Lightw. Technol.*, vol. 29, pp. 2146–2155, July 2011.

[54] T. Komine and M. Nakagawa, "Fundamental analysis for visible-light communication system using LED lights," *IEEE Transactions on Consumer Electronics*, vol. 50, pp. 100–107, Feb. 2004.

[55] H. Haas, "High-speed Wireless Networking Using Visible Light." SPIE Newsroom, Apr. 19 2013.

[56] I. Stefan, H. Burchardt, and H. Haas, "Area Spectral Efficiency Performance Comparison between VLC and RF Femtocell Networks," in *IEEE International Conference on Communications (ICC)*, (Budapest, Hungary), pp. 1–5, June 9–13 2013.

[57] B. Ghimire and H. Haas, "Self-organising Interference Coordination in Optical Wireless Networks," *EURASIP Journal on Wireless Communications and Networking*, vol. 2012, no. 1, pp. 1–15, 2012.

[58] C. Chen, D. Tsonev, and H. Haas, "Joint transmission in indoor visible light communication downlink cellular networks," in *Globecom Workshops (GC Wkshps), 2013 IEEE*, pp. 1127–1132, Dec 2013.

[59] C. Chen, S. Videv, D. Tsonev, and H. Haas, "Fractional frequency reuse in dco-ofdm-based optical attocell networks," *J. Lightw. Technol.*, vol. 33, pp. 3986–4000, Oct 2015.

[60] Z. Chen and H. Haas, "A simplified model for indoor optical attocell networks," in *2015 IEEE Summer Topicals Meeting Series (SUM)*, pp. 167–168, July 2015.

[61] Z. Chen, N. Serafimovski, and H. Haas, "Angle diversity for an Indoor Cellular Visible Light Communication System," in *IEEE 79th Vehicular Technology Conference*, May 2014.

[62] Z. Chen, D. A. Tsonev, and H. Haas, "Improving SINR in Indoor Cellular Visible Light Communication Networks," in *IEEE ICC 2014 - Optical Networks and Systems (ICC'14 ONS)*, (Sydney, Australia), June 2014.

[63] Z. Chen, D. Tsonev, and H. Haas, "A Novel Double-source Cell Configuration for Indoor Optical Attocell Networks," in *2014 IEEE Global Communications Conference*, pp. 2125–2130, Dec 2014.

[64] Z. Chen and H. Haas, "Space Division Multiple Access in Visible LightCommunications," in *IEEE ICC 2015 - Optical Networks and Systems (ICC'15 ONS)*, (London, UK), June 2015.

[65] Z. Chen, D. A. Basnayaka, and H. Haas, "Space Division Multiple Access in Optical Attocell Networks," in *2016 IEEE Wireless Communications and Networking Conference*, pp. 1–5, April 2016.

[66] H. Elgala, *A Study on the Impact of Nonlinear Characteristics of LEDs on Optical OFDM*. PhD thesis, University of Edinburgh, 2010.

[67] G. Holzmann and B. Pehrson, *The Early History Of Data Networks*. IEEE Computer Society Press, Nov. 1994.

[68] A. G. Bell, "Selenium and the Photophone," *Nature*, vol. 22, pp. 500–503, 1880.

[69] M. I. Nathan, W. P. Dumke, G. Burns, F. H. Dill, and G. Lasher, "Stimulated Emission of Radiation From GaAs p?n Junctions," *Applied Physics Letters*, vol. 1, no. 3, pp. 62–64, 1962.

[70] R. N. Hall, G. E. Fenner, J. D. Kingsley, T. J. Soltys, and R. O. Carlson, "Coherent Light Emission from GaAs Junctions," *Phys. Rev. Lett.*, vol. 9, pp. 366–369, Nov., 1 1962.

[71] F. R. Gfeller and U. Bapst, "Wireless In-House Data Communication Via Diffuse Infrared Radiation," *Proc. IEEE*, vol. 67, pp. 1474–1486, Nov. 1979.

[72] J. R. Barry, *Wireless Infrared Communications*, vol. 280. Springer, 1994.

[73] J. B. Carruthers and J. M. Kahn, "Modeling of Nondirected Wireless Infrared Channels," in *In the Proceeding of the IEEE Conference on Communications.: Converging Technologies for Tomorrow's Applications*, vol. 2, (Dallas, TX, USA), pp. 1227–1231, June 23–27, 1996.

[74] T. Komine and M. Nakagawa, "Integrated System of White LED Visible-light Communication and Power-line Communication," in *The 13th IEEE International Symposium*

on Personal, Indoor and Mobile Radio Communications, 2002, vol. 4, pp. 1762–1766 vol.4, Sept 2002.

[75] T. Komine and M. Nagawa, "Integrated System of White LED Visible-Light Communication and Power-Line Communication," *IEEE Trans. on Consum. Electron.*, vol. 49, pp. 71–79, Feb. 2003.

[76] J. Fakidis, D. Tsonev, and H. Haas, "A comparison between dco-ofdma and synchronous one-dimensional ocdma for optical wireless communications," in *2013 IEEE 24th Annual International Symposium on Personal, Indoor, and Mobile Radio Communications (PIMRC)*, pp. 3605–3609, Sept 2013.

[77] O. Gonzalez, J. A. Martin-Gonzalez, E. Poves, F. J. Lopez-Hernandez, and R. Perez-Jimenez, "Adaptive code-division multiple-access system for communications over indoor wireless optical channels based on random optical codes," *IET Optoelectronics*, vol. 3, pp. 187–196, August 2009.

[78] H. Elgala, R. Mesleh, and H. Haas, "Indoor Optical Wireless Communication: Potential and State-of-the-Art," *IEEE Commun. Mag.*, vol. 49, pp. 56–62, Sept. 2011.

[79] "IEEE Standard for Local and Metropolitan Area Networks, Part 15.7: Short-Range Wireless Optical Communication Using Visible Light." IEEE Std. 802.15.7, 2011.

[80] IEEE, "IEEE 802.15 WPANTM 15.7 Revision: Short-Range Optical Wireless Communications Task Group (TG 7r1)." IEEE Std. 802.15.7, 2014.

[81] J. G. Proakis, *Digital Communications*. McGraw–Hill, 1995.

[82] A. Alshamali and B. Quza, "Performance of Spatial Modulation in Correlated and Uncorrelated Nakagami Fading Channel," *Journal of Commun.*, vol. 4, pp. 170–174, Apr. 2009.

[83] E. Basar, U. Aygolu, E. Panayirci, and H. V. Poor, "New Trellis Code Design for Spatial Modulation," *IEEE Trans. on Wireless Commun.*, vol. 10, pp. 2670 – 2680, Aug. 2011.

[84] B. Choi and L. Hanzo, "Optimum Mode-Switching-Assisted Constant-Power Single- and Multicarrier Adaptive Modulation," *IEEE Transactions on Vehicular Technology*, vol. 52, pp. 536–560, May 2003.

[85] A. Jalajakumari, K. Cameron, D. Tsonev, H. Haas, and R. Henderson, "An Energy Efficient High-speed Digital LED Driver for Visible Light Communications," in *IEEE International Conference on Communications, 2015 (ICC '15)*, Jun 2015.

[86] Y. Tanaka, T. Komine, S. Haruyama, and M. Nakagawa, "Indoor Visible Communication Utilizing Plural White LEDs as Lighting," in *Proc. of the* 12^{th} *IEEE International Symposium on Personal, Indoor and Mobile Radio Communications*, vol. 2, (San Diego, CA, USA), pp. 81–85, Sept. 30–Oct. 3, 2001.

[87] M. Dyble, N. Narendran, A. Bierman, and T. Klein, "Impact of dimming white LEDs: Chromaticity shifts due to different dimming method," in *Proc. of SPIE 5941, 5th International Conference on Solid State Lighting*, (Bellingham, WA), pp. 291–299, 2005.

[88] L. Zeng, H. Minh, D. O'Brien, G. Faulkner, K. Lee, D. Jung, and Y. Oh, "Equalisation for High-speed Visible Light Communications Using White LEDs," in *Proc. 6th International Symposium on Communication Systems, Networks and Digital Signal Processing CSNDSP 2008*, (Graz, Austria), pp. 170–173, 23–25 July 2008.

[89] K. D. Langer, J. Vucic, C. Kottke, L. F. del Rosal, S. Nerreter, and J. Walewski, "Advances and prospects in high-speed information broadcast using phosphorescent white-light leds," in *Proc. 11th International Conference on Transparent Optical Networks*, (Island of So Miguel, Azores, Portugal), p. 6 pages, IEEE, June 28–July 2, 2009.

[90] G. Cossu, A. M. Khalid, P. Choudhury, R. Corsini, and E. Ciaramella, "3.4 Gbit/s visible optical wireless transmission based on RGB LED," *Optics Express*, vol. 20, pp. B501–B506, 2012.

[91] J. Grubor, S. Randel, K. Langer, and J. W. Walewski, "Broadband Information Broadcasting Using LED-Based Interior Lighting," *IEEE J. Lightw. Technol.*, vol. 26, pp. 3883–3892, Dec. 2008.

[92] J. J. D. McKendry, D. Massoubre, S. Zhang, B. R. Rae, R. P. Green, E. Gu, R. K. Henderson, A. E. Kelly and M. D. Dawson, "Visible-light communications using a CMOS-controlled micro-light-emitting-diode array," *J. Lightw. Technol.*, vol. 30, no. 1, pp. 61–67, 2012.

[93] J. J. D. McKendry, R. P. Green, A. E. Kelly, Z. Gong, B. Guilhabert, D. Massoubre, E. Gu and M. D. Dawson, "High-Speed Visible Light Communications Using Individual

Pixels in a Micro Light-Emitting Diode Array," *IEEE Photon. Technol. Lett.*, vol. 22, pp. 1346–1348, Sept. 2010.

[94] J. Wun, C. Lin, W. Chen, J. Sheu, C. Lin, Y. Li, J. Bowers, J. Shi, J. Vinogradov, R. Kruglov, and O. Ziemann, "GaN-Based Miniaturized Cyan Light-Emitting Diodes on a Patterned Sapphire Substrate With Improved Fiber Coupling for Very High-Speed Plastic Optical Fiber Communication," *IEEE Photon. J.*, vol. 4, pp. 1520–1529, Oct. 2012.

[95] S. Rajbhandari, H. Chun, G. Faulkner, K. Cameron, A. V. N. Jalajakumari, R. Henderson, D. Tsonev, M. Ijaz, Z. Chen, H. Haas, E. Xie, J. J. D. McKendry, J. Herrnsdorf, E. Gu, M. D. Dawson, and D. O'Brien, "High-Speed Integrated Visible Light Communication System: Device Constraints and Design Considerations," *IEEE Journal on Selected Areas in Communications*, vol. 33, pp. 1750–1757, Sept 2015.

[96] A. Neumann, J. Wierer, Jr., W. Davis, Y. Ohno, R. Brueck, and J. Tsao, "Four-color Laser White Illuminant Demonstrating High Color-rendering Quality," *OSA Optics Express*, vol. 19, pp. A982–A990, July 2011.

[97] P. Djahani and J. M. Kahn, "Analysis of Infrared Wireless Links Employing Multibeam Transmitters and Imaging Diversity Receivers," *IEEE Trans. Commun.*, vol. 48, pp. 2077–2088, Dec. 2000.

[98] J. Liu, W. Noonpakdee, H. Takano, and S. Shimamoto, "Foundational Analysis of Spatial Optical Wireless Communication Utilizing Image Sensor," in *IEEE International Conference on Imaging Systems and Techniques (IST)*, (Penang, Malaysia), pp. 205–209, May 17–18 2011.

[99] I. Takai, S. Ito, K. Yasutomi, K. Kagawa, M. Andoh, and S. Kawahito, "LED and CMOS Image Sensor Based Optical Wireless Communication System for Automotive Applications," *IEEE Photon. J.*, vol. 5, pp. 6801418–6801418, Oct. 2013.

[100] A. Bauer, J. Hanisch, and E. Ahlswede, "An Effective Single Solar Cell Equivalent Circuit Model for Two or More Solar Cells Connected in Series," *IEEE J. Photovolt.*, vol. 4, pp. 340–347, Jan. 2014.

[101] Z. Wang, D. Tsonev, S. Videv, and H. Haas, "Towards Self-Powered Solar Panel Receiver for Optical Wireless Communication," in *Proc. IEEE Int. Conf. Commun. (ICC)*, (Sydney, NSW), pp. 3348–3353, June 10–14 2014.

[102] Z. Wang, D. Tsonev, S. Videv, and H. Haas, "On the Design of a Solar-Panel Receiver for Optical Wireless Communications with Simultaneous Energy Harvesting," *IEEE J. Sel. Areas Commun.*, vol. PP, no. 99, pp. 1–1, 2015.

[103] S. Schmid, G. Corbellini, S. Mangold, and T. Gross, "An LED-to-LED Visible Light Communication System with Software-based Synchronization," in *IEEE Globecom Workshops (GC Wkshps)*, (Anaheim, CA, USA), pp. 1264–1268, Dec. 3–7 2012.

[104] D. Giustiniano, N. Tippenhauer, and S. Mangold, "Low-complexity Visible Light Networking with LED-to-LED communication," in *IFIP Wireless Days (WD)*, (Dublin, Ireland), pp. 1–8, Nov. 21–23 2012.

[105] R. Mesleh, R. Mehmood, H. Elgala, and H. Haas, "Indoor MIMO Optical Wireless Communication Using Spatial Modulation," in *IEEE International Conference on Communications (ICC)*, (Cape Town, South Africa), pp. 1–5, May 22–27 2010.

[106] Y. Li, M. Safari, R. Henderson, and H. Haas, "Optical OFDM With Single-Photon Avalanche Diode," *IEEE Photonics Technology Letters*, vol. 27, pp. 943–946, May 2015.

[107] N. A. W. Dutton, I. Gyongy, L. Parmesan, S. Gnecchi, N. Calder, B. R. Rae, S. Pellegrini, L. A. Grant, and R. K. Henderson, "A SPAD-Based QVGA Image Sensor for Single-Photon Counting and Quanta Imaging," *IEEE Transactions on Electron Devices*, vol. 63, pp. 189–196, Jan 2016.

[108] S. Cova, M. Ghioni, A. Lacaita, C. Samori, and F. Zappa, "Avalanche PPhotodiode and Quenching Circuits for Single-photon Detection," *OSA Applied Optics*, vol. 35, pp. 1956–1976, Apr. 20 1996.

[109] W. T. Welford and R. Winston, *High Collection Nonimaging Optics*. San Diego: Academic, 1989.

[110] D. Tsonev, S. Sinanović, and H. Haas, "Practical MIMO Capacity for Indoor Optical Wireless Communication with White LEDs," in *Proc. of the Vehicular Technology Conference (VTC Spring)*, (Dresden, Germany), pp. 1–5, IEEE, IEEE, June 2–5 2013.

[111] D. C. O'Brien, S. Quasem, S. Zikic, and G. E. Faulkner, "Multiple Input Multiple Output Systems for Optical Wireless: Challenges and Possibilities," *Proc. SPIE*, September 2006.

[112] X. Ning, R. Winston, and O. J., "Dielectric totally internally reflecting concentrators," *OSA Applied Optics*, vol. 26, pp. 300–305, Jan. 1987.

[113] B. E. A. Saleh and M. C. Teich, *Fundamentals of Photonics*. Wiley Series in Pure and Applied Optics, John Wiley & Sons, Inc., 1 ed., Jan. 1991.

[114] K. Schneider and H. Zimmermann, *Highly Sensitive Optical Receivers*. Springer, 2006.

[115] F. Tavernier and M. Steyaert, *High-Speed Optical Receivers with Integrated Photodiode in Nanoscale CMOS*. Springer, 2011.

[116] J. Barry, J. Kahn, W. Krause, E. Lee, and D. Messerschmitt, "Simulation of multipath impulse response for indoor wireless optical channels," *IEEE J. Select. Areas Commun.*, vol. 11, pp. 367–379, Apr. 1993.

[117] J.-H. Yoo and S.-Y. Jung, "Modeling and analysis of variable ppm for visible light communications," *EURASIP Journal on Wireless Communications and Networking*, vol. 2013, no. 1, p. 134, 2013.

[118] H. Zhu and J. Wang, "Performance Analysis of Chunk-Based Resource Allocation in Multi-Cell OFDMA Systems," *IEEE J. Sel. Areas in Commun.*, vol. 32, pp. 367–375, Feb. 2014.

[119] S. Dissanayake, K. Panta, and J. Armstrong, "A Novel Technique to Simultaneously Transmit ACO-OFDM and DCO-OFDM in IM/DD Systems," in *IEEE GLOBECOM Workshops (GC Wkshps)*, (Houston, TX, USA), pp. 782–786, IEEE, Dec. 5–9 2011.

[120] J. Armstrong and B. J. C. Schmidt, "Comparison of Asymmetrically Clipped Optical OFDM and DC-Biased Optical OFDM in AWGN," *IEEE Commun. Lett.*, vol. 12, pp. 343–345, May 2008.

[121] J. Armstrong, "OFDM for Optical Communications," *Journal of Lightwave Technology*, vol. 27, pp. 189–204, Feb 2009.

[122] K. Asadzadeh, A. Dabbo, and S. Hranilovic, "Receiver Design for Asymmetrically Clipped Optical OFDM," in *GLOBECOM Workshops (GC Wkshps)*, (Houston, TX, USA), pp. 777–781, IEEE, Dec., 5–9 2011.

[123] X. Li, J. Vucic, V. Jungnickel, and J. Armstrong, "On the Capacity of Intensity-Modulated Direct-Detection Systems and the Information Rate of ACO-OFDM for Indoor Optical Wireless Applications," *IEEE Transactions on Communications (IEEE TCOM)*, vol. 60, pp. 799–809, Mar. 2012.

[124] A. A. Abu-Dayya and N. C. Beaulieu, "Outage probabilities of cellular mobile radio systems with multiple Nakagami interferers," *IEEE Transactions on Vehicular Technology*, vol. 40, pp. 757–768, Nov. 1991.

[125] K. Balachandran, S. R. Kadaba, and S. Nanda, "Channel Quality Estimation and Rate Adaptation for Cellular Mobile Radio," *IEEE Journal on Selected Areas in Communications*, vol. 17, pp. 1244–1256, July 1999.

[126] J. G. Andrews, W. Choi, and R. W. Heath Jr., "Overcoming Interference in Spatial Multiplexing MIMO Cellular Networks," *IEEE Wireless Communications Magazine*, vol. 14, pp. 95–104, Dec. 2007.

[127] L. Badia, A. Baiocchi, A. Todini, S. Merlin, S. Pupolin, A. Zanella, and M. Zorzi, "On the Impact of Physical Layer Awareness on Scheduling and Resource Allocation in Broadband Multicellular IEEE 802.16 Systems," *IEEE Wireless Communications*, vol. 14, pp. 36–43, Feb. 2007.

[128] G. Auer, V. Giannini, C. Desset, I. Godor, P. Skillermark, M. Olsson, M. Imran, D. Sabella, M. Gonzalez, O. Blume, and A. Fehske, "How much energy is needed to run a wireless network?," *IEEE Wireless Commun.*, vol. 18, pp. 40–49, October 2011.

[129] H. Claussen, "Future Cellular Networks," in *Proc. of the Wireless Communications and Networking Conference (WCNC)*, (Shanghai, China), Apr.1–4 2012.

[130] H. Dhillon, R. Ganti, F. Baccelli, and J. Andrews, "Modeling and analysis of k-tier downlink heterogeneous cellular networks," *IEEE Journal on Selected Areas in Communications*, vol. 30, pp. 550 –560, april 2012.

[131] L. Godara, "Application of Antenna Arrays to Mobile Communications. II. Beamforming and Direction-of-arrival Considerations," *Proc. IEEE*, vol. 85, pp. 1195 –1245, Aug. 1997.

[132] Z. Chen, N. Serafimovski, and H. Haas, "Angle Diversity for an Indoor Cellular Visible Light Communication System," in *2014 IEEE 79th Vehicular Technology Conference (VTC Spring)*, pp. 1–5, May 2014.

[133] C. Chen, D. A. Basnayaka, and H. Haas, "Downlink Performance of Optical Attocell Networks," *Journal of Lightwave Technology*, vol. 34, pp. 137–156, Jan 2016.

[134] J. Carruthers and J. Kahn, "Angle diversity for nondirected wireless infrared communication," in *Communications, 1998. ICC 98. Conference Record. 1998 IEEE International Conference on*, vol. 3, pp. 1665–1670 vol.3, Jun 1998.

[135] Y. Alqudah and M. Kavehrad, "Optimum order of angle diversity with equal-gain combining receivers for broad-band indoor optical wireless communications," *Vehicular Technology, IEEE Transactions on*, vol. 53, pp. 94–105, Jan 2004.

[136] H. L. Minh, D. O'Brien, G. Faulkner, O. Bouchet, M. Wolf, L. Grobe, and J. Li, "A 1.25-gb/s indoor cellular optical wireless communications demonstrator," *Photonics Technology Letters, IEEE*, vol. 22, pp. 1598–1600, Nov 2010.

[137] M. Alresheedi and J. Elmirghani, "Performance evaluation of 5 gbit/s and 10 gbit/s mobile optical wireless systems employing beam angle and power adaptation with diversity receivers," *Selected Areas in Communications, IEEE Journal on*, vol. 29, pp. 1328–1340, June 2011.

[138] S. Vasudevan, K. Papagiannaki, C. Diot, J. Kurose, and D. Towsley, "Facilitating Access Point Selection in IEEE 802.11 Wireless Networks," in *Proc. ACM Fifth SIGCOMM Conf. Internet Measurement (IMC)*, pp. 293–298, 2005.

[139] T. K. Y. Lo, "Maximum ratio transmission," in *1999 IEEE International Conference on Communications (Cat. No. 99CH36311)*, vol. 2, pp. 1310–1314 vol.2, 1999.

[140] J. Winters, "Optimum Combining in Digital Mobile Radio with Cochannel Interference," *IEEE Journal on Selected Areas in Communication*, vol. SAC-2, pp. 528–539, July 1984.

[141] R. H. Simons and A. Bean, *Lighting Engineering: Applied Calculations*. Architectural Press.

[142] F. E. Alsaadi and J. M. H. Elmirghani, "Mobile MC-CDMA Optical wireless System Employing an Adaptive Multibeam Transmitter and Diversity Receivers in a Real Indoor

Environment," in *In the Proceeding of the IEEE International Conference on Communications (ICC 08)*, pp. 5196–5203, May 19–23, 2008.

[143] A. J. Paulraj and C. B. Papadias, "Space-time Processing for Wireless Communications," *IEEE Signal Process. Mag.*, vol. 14, pp. 49–83, Nov. 1997.

[144] I. P802.11, "IEEE802.11ac: The Next Evolution of Wi-Fi Standards," 2012.

[145] H. Yin and H. Liu, "Performance of Space-division-multiple-access (SDMA) with Scheduling," *IEEE Trans. Wireless Commun.*, vol. 1, pp. 611–618, Oct 2002.

[146] K. Huang, J. Andrews, and R. Heath, "Performance of Orthogonal Beamforming for SDMA with Limited Feedback," *IEEE Trans. Veh. Technol.*, vol. 58, pp. 152–164, Jan 2009.

[147] C. Chen, N. Serafimovski, and H. Haas, "Fractional frequency reuse in optical wireless cellular networks," in *2013 IEEE 24th International Symposium on Personal Indoor and Mobile Radio Communications (PIMRC)*, pp. 3594–3598, Sept 2013.

[148] S.-M. Kim and H.-J. Lee, "Visible light communication based on space-division multiple access optical beamforming," *Chin. Opt. Lett.*, vol. 12, pp. 120601–120601, Dec 2014.

[149] M. geun Moon and S. il Choi, "Indoor Position Estimation Using Image Sensor Based on VLC," in *2014 International Conference on Advanced Technologies for Communications (ATC)*, pp. 11–14, Oct 2014.

[150] M. Yasir, S. Ho, and B. Vellambi, "Indoor Positioning System Using Visible Light and Accelerometer," *J. Lightw. Technol.*, vol. 32, pp. 3306–3316, Oct 2014.

[151] M. Kashef, M. Abdallah, K. Qaraqe, and M. Uysal, "The Impact of Location Errors on Achievable Rates in OFDM-based Multi-user Visible Light Communication Systems," in *2014 3rd International Workshop in Optical Wireless Communications (IWOW)*, pp. 65–69, Sept 2014.

[152] A. Papoulis, *Probability, Random Variables and Stochastic Processes*. McGraw-Hill Inc., 2nd ed., 1984.

[153] P. P. Williamson, D. P. Mays, G. A. Asmerom, and Y. Yang, "Revisiting the classical occupancy problem," *The American Statistician*, vol. 63, no. 4, pp. 356–360, 2009.

[154] B. Almeroth, A. Fehske, G. Fettweis, and E. Zimmermann, "Analytical Interference Models for the Downlink of a Cellular Mobile Network," in *2011 IEEE GLOBECOM Workshops (GC Wkshps)*, pp. 739–743, Dec 2011.